KU LEUVEN

ARENBERG DOCTORAL SCHOOL
Faculty of Engineering Technology

Robust vibration serviceability assessment and design of footbridges under walking loading

Klaus Lievens

Supervisors:
Prof. dr. ir. P. Van den Broeck
Prof. dr. ir. G. Lombaert
Prof. dr. ir. G. De Roeck

Dissertation presented in partial fulfillment of the requirements for the degree of Doctor of Engineering Technology (PhD)

December 2018

Robust vibration serviceability assessment and design of footbridges under walking loading

Klaus LIEVENS

Examination committee:
Prof. dr. ir. D. Pissoort, chair
Prof. dr. ir. P. Van den Broeck, supervisor
Prof. dr. ir. G. Lombaert, supervisor
Prof. dr. ir. G. De Roeck, supervisor
Prof. dr. ir. D. Moens
Dr. ir. B. Peeters (Siemens)
Prof. dr. ir. K. Gryllias
Dr. ir. C. Meinhardt (GERB)

Dissertation presented in partial fulfillment of the requirements for the degree of Doctor of Engineering Technology (PhD)

December 2018

© 2018 KU Leuven – Faculty of Engineering Technology
Uitgegeven in eigen beheer, Klaus Lievens, Gebroeders De Smetstraat 1, B-9000 Ghent (Belgium)

Alle rechten voorbehouden. Niets uit deze uitgave mag worden vermenigvuldigd en/of openbaar gemaakt worden door middel van druk, fotokopie, microfilm, elektronisch of op welke andere wijze ook zonder voorafgaande schriftelijke toestemming van de uitgever.

All rights reserved. No part of the publication may be reproduced in any form by print, photoprint, microfilm, electronic or any other means without written permission from the publisher.

Voorwoord

Men build too many walls and not enough bridges.
J. F. Newton

Met enige voldoening presenteer ik u het werk die voor je ligt. Het sluit een boeiende periode van vijf jaar onderzoek af. Graag zou ik met dit voorwoord een poging willen doen om de mensen te bedanken die een bijzondere bijdrage hebben geleverd bij het tot stand komen hiervan.

Ik dank oprecht mijn promotoren voor de constructieve en aangename samenwerking de voorbije jaren. Jullie zorgden tijdens de vergaderingen steeds voor verrijkende inzichten en een kritische invalshoek die het onderzoek ten goede kwamen. De opmerkingen op de papers en deze tekst heb ik steeds erg gewaardeerd. Ze hielpen het onderzoek beter te verwoorden. Peter Van den Broeck, bedankt voor het vertrouwen dat je me gaf doorheen het onderzoek. Onder jouw begeleiding heb ik me zowel op wetenschappelijk als persoonlijk vlak verder kunnen ontplooien. Geert Lombaert, bedankt voor de talrijke suggesties die het werk mee vorm hebben gegeven en het steeds kritisch beoordelen van tussentijdse resultaten. Door u leerde ik mijn (wetenschappelijke) grens verleggen. Guido De Roeck, bedankt voor de betrokkenheid gedurende dit onderzoek. Het delen van jouw expertise en ervaring heeft onmiskenbaar voor een meerwaarde in dit onderzoek gezorgd.

Naast mijn promotoren wil ik ook de leden van de examencommissie bedanken. David Moens en Bart Peeters, hartelijk bedankt voor jullie inbreng tijdens de tussentijdse vergaderingen en de waardevolle opmerkingen op de tekst. I would also like to thank Konstantinos Gryllias and Christian Meinhardt for their valuable insights and comments on the text. Verder bedank ik Davy Pissoort als voorzitter van de examencommissie en het agentschap voor Innovatie door Wetenschap en Technologie (IWT) voor de financiële ondersteuning van het onderzoek.

De afgelopen jaren had ik het geluk te kunnen werken in een bijzonder aangename werkomgeving. Dan denk ik aan alle (ex-)collega's van zowel de Technologiecluster Bouw in Gent als de (ex-)collega's van de afdeling Bouwmechanica in Leuven. Bedankt iedereen voor de praatjes tijdens de middagpauze, de terrasjes na het werk, de *young researchers evenings*, de jaarlijkse uitstappen en etentjes... In het bijzonder zal ik de speciale momenten van teambuilding met onze onderzoeksgroep koesteren: talrijke meetcampagnes, elk met een bijhorend verhaal, waar hard wordt gewerkt in een gemoedelijke sfeer. Katrien, jouw enthousiasme hiervoor is aanstekelijk.

Wellicht is dit voor velen de laatste bladzijde uit dit boek. Alle begrip daarvoor. Voor diegenen die toch verder durven lezen, wie weet vinden jullie een sprankel inspiratie voor jullie onderzoek.

Dit voorwoord wil ik niet eindigen zonder ook mijn familie en vrienden te bedanken voor hun interesse in het werk. Al weten jullie vaak niet veel meer dan dat mijn onderzoek 'iets met trillingen van bruggen' te maken heeft, de vele momenten van ontspanning hebben zeker bijgedragen voor de nodige rust na het werk. Ma, pa, bedankt voor de vele aangename familiemomenten en voor de onvoorwaardelijke steun die jullie bieden. Lore, jouw verrijkende hersenspinsels helpen me het onderzoek te relativeren. *Grazie*! Voor ontspannende momenten kan ik ook altijd terecht bij mijn vrienden. Ik kijk al uit naar de volgende fietsritten, spel-, fifa-, snooker-avonden, terrasjes, etentjes, weekends weg, reünies...

Margot, ondertussen weet je al meer van TMDs dan dat je wellicht had gewild. Jou dank ik als laatste voor je lieve *zijn* en voor de onvoorwaardelijke steun die je me biedt. Nu dit project ten einde is, kijk ik vol enthousiasme uit naar ons eigen project...

Klaus Lievens
December 2018, Gent

Abstract

The use of high strength materials and advanced calculation methods facilitates the design of slender footbridges, often resulting in low natural frequencies of the structure in the range of the loading frequencies of human-induced excitation. In combination with a low modal damping, these structures are sensitive to human-induced loading. Therefore, a vibration serviceability assessment of structures subjected to human-induced loading has become an important design issue. A reliable response estimation requires a description of both the human-induced loading and the dynamic behaviour of the structure. If the calculated response exceeds a predefined limit for vibration comfort, the installation of vibration mitigation devices such as Tuned Mass Dampers (TMDs) can be desired. However, both the vibration serviceability assessment and the TMD parameter tuning are subject to a high degree of uncertainty since they require an accurate description of human-induced loading and the dynamic behaviour of the structure. Due to these uncertainties, an acceptable behaviour after construction cannot always be guaranteed sometimes resulting in modifications of the structure or the unexpected installation of vibration mitigation devices leading to additional costs.

The innovative approach of this doctoral study is to introduce the concept of robustness in the vibration serviceability assessment and TMD design. The main objective is to design footbridges which are minimally sensitive to the effect of the uncertainties in the modal parameters and to variability in the loading, resulting in safe and cost-effective designs.

A generic methodology for the robust vibration serviceability assessment of footbridges to walking loading is proposed. By considering multiple levels of uncertainty in the modal parameters, a gradual evaluation of the vibration response is performed. Additional variation on the stochastic models for walking loading is also included. It is shown that human-structure interaction effects considerably affect the response and therefore must be considered. It is also indicated how the multi-level assessment provides a measure for the sensitivity

of the response of the footbridge to the effect of uncertainties.

The presented methodology for the robust vibration serviceability assessment is implemented in the TMD design. The TMD design problem is defined as a robust optimisation problem. By minimising a cost function, the TMD mass, stiffness and damping constants are tuned. Design constraints are implemented for operability of the TMD and for vibration serviceability considering uncertainties in the dynamic behaviour of the footbridge. The effect of human-induced walking loading is directly accounted for in the response. The design can be performed for a selected range of uncertainty. If multiple designs are performed at different levels of uncertainty, the sensitivity of the TMD design to the range of uncertainties can be verified. It is concluded that for designs considering a wider range of uncertainty, the total TMD mass increases. However, its performance is ensured with respect to uncertainties. It is also shown that the TMD mass can be strongly reduced in comparison with conventional designs by tuning the TMD mass, stiffness and damping independently from each other.

Beknopte samenvatting

Het gebruik van hoogwaardige materialen en geavanceerde rekentechnieken maakt het ontwerp van slanke constructies mogelijk. Deze structuren worden vaak gekenmerkt door lage eigenfrequenties in de buurt van de belastingsfrequentie van mens-geïnduceerde trillingen. In combinatie met een lage modale demping kan dit leiden tot structuren die gevoelig zijn voor mens-geïnduceerde belasting. Een trillingsbeoordeling bestaat uit een voorspelling van de te verwachten trillingsniveaus die getoetst worden aan vooropgestelde comfortnormen en is vaak een belangrijk criterium in het ontwerp. Een nauwkeurige beschrijving van de belasting en van het dynamisch gedrag van de structuur zijn hiervoor noodzakelijk. Wanneer vooropgestelde niveaus voor trillingscomfort niet worden gehaald, kunnen trillingsreducerende maatregelen worden genomen zoals de installatie van Tuned Mass Dampers (TMDs). Zowel de voorspelling van de respons als het TMD ontwerp is in hoge mate onderworpen aan onzekerheden omdat ze een nauwkeurige beschrijving van de mens-geïnduceerde belasting en een goede kennis van het dynamische gedrag van de structuur vereisen. Deze onzekerheden zorgen ervoor dat een aanvaardbaar gedrag van de constructie niet altijd gegarandeerd kan worden zodat dure aanpassingen aan de structuur of trillingsreducerende maatregelen nodig zijn.

Het innovatieve aspect van dit doctoraatsonderzoek is het introduceren van het concept van robuustheid in de trillingsbeoordeling en het TMD ontwerp voor voetgangersbruggen. De belangrijkste doelstelling is om een robuuste constructie te bekomen die minimaal gevoelig is voor het effect van onzekerheden in de dynamische eigenschappen van de voetgangersbrug en voor het effect van variabiliteit in de belasting. Dit moet leiden tot een veilig en kostenefficiënt ontwerp.

In dit doctoraatsonderzoek is een generieke methodologie voor een robuuste trillingsbeoordeling opgesteld. Verschillende niveaus van onzekerheid in de modale parameters worden aangenomen om trapsgewijs het effect op

de responsbeoordeling na te gaan. Een bijkomende variatie op bestaande stochastische modellen voor het beschrijven van de wandelbelasting wordt ook in rekening gebracht. Het is aangetoond dat de berekende respons aanzienlijk wordt beïnvloed door het effect van mens-structuur interactie en dat deze effecten daarom best worden meegenomen. Daarnaast is aangegeven hoe de voorgestelde graduele analyse gebruikt kan worden om de trillingsgevoeligheid van de brug voor het effect van onzekerheden te beoordelen.

De voorgestelde methode voor de robuuste trillingsbeoordeling wordt ook gebruikt in het robuust ontwerp van TMDs. De parameters van de TMD worden gevonden als oplossing van een robuust optimalisatieprobleem waar de totale TMD kost wordt geminimaliseerd. Hierbij worden randvoorwaarden opgelegd voor zowel het trillingscomfort als voor de werking en praktische uitvoering. Het effect van mens-geïnduceerde belasting wordt rechtstreeks in rekening gebracht in de responsberekening. Ook hier kan het TMD ontwerp worden uitgevoerd voor een vooraf aangenomen bereik van onzekerheden. Wanneer meerdere ontwerpen op verschillende onzekerheidsniveaus onderling worden vergeleken, kan het effect van onzekerheden op het uiteindelijke ontwerp worden nagegaan. Aan de hand van uitgewerkte voorbeelden is aangetoond dat de totale massa van de TMD stijgt wanneer een groter bereik voor de onzekerheden wordt aangenomen. Het voordeel van deze aanpak is dat de werking van de TMD gegarandeerd is in onzekere omstandigheden door in het ontwerp al rekening te houden met het effect van onzekerheden. Bovendien is ook aangetoond dat de totale massa van de TMD kan worden verminderd door de parameters van de TMD onafhankelijk van elkaar af te stemmen, in tegenstelling tot de methode bij conventionele ontwerpen.

List of Symbols

The following list gives an overview of the most commonly adopted acronyms and symbols used throughout the text.

Acronyms

DAF	Dynamic Amplification Factor
DLF	Dynamic Load Factor
DOF	Degree Of Freedom
FE	Finite Element
FEM	Finite Element Model
GRF	Ground Reaction Force
HHI	Human-Human Interaction
HSI	Human-Structure Interaction
MDOF	Multiple Degree Of Freedom
MTMD	Multiple Tuned Mass Dampers
PDF	Probability Density Function
PSD	Power Spectral Density
RBDO	Reliability Based Design Optimisation
RBRDO	Reliability Based Robust Design Optimisation
RDO	Robust Design Optimisation
RMS	Root Mean Square
SDOF	Single Degree Of Freedom
SQP	Sequential Quadratic Programming
TMD	Tuned Mass Damper

Operators, sets and general notational conventions

$\mathbb{C}$	Set of complex numbers

$\mathbb{R}$	Set of real numbers
x	Scalar
$\mathbf{x}$	Vector
$\mathbf{X}$	Matrix
$\nabla\square$	Gradient of function $\square$
$\bar{\square}$	Upper bound of an interval $\square$
$\underline{\square}$	Lower bound of an interval $\square$
$\square^{\mathsf{T}}$	Transpose of a matrix $\square$
$\square^{-1}$	Inverse of a matrix $\square$
$\dot{\square}$	First order time derivative of $\square$
$\ddot{\square}$	Second order time derivative of $\square$
$\hat{\square}$	Variable $\square$ in frequency domain
$\tilde{\square}$	Fuzzy variable $\square$
$\square_{\mathrm{B}}$	Subscript referring to the bridge
$\lvert\square\rvert$	Absolute value of scalar $\square$
$\lVert\square\rVert_n$	n-norm of a vector $\square$

Human-induced vibrations

d	Pedestrian density [persons/m^2]
f_{H}	Human body natural frequency [Hz]
f_s	Step frequency [Hz]
$\bar{f}_s$	Average step frequency [Hz]
G	Body weight [N]
l_s	Step length [m]
n_{H}	Number of persons
$\mathbf{p}_{\mathrm{H}}$	Interaction forces
$\mathbf{p}_{\mathrm{P}}$	Total pedestrian forces
$\mathbf{p}_{\mathrm{S}}$	Walking forces on a rigid surface
T	Time window for response evaluation [s]
T_{cross}	Time to cross the footbridge [s]
T_s	Step period [s]
$\ddot{u}_{\max}(T)$	Instantaneous peak response in time window T [m/s^2]
v_s	Walking speed [m/s]
$\bar{v}_s$	Average free walking speed [m/s]
ξ_{H}	Human body damping ratio [%]
$\xi_{\mathrm{eff},j}$	Effective damping ratio of mode j [-]
$\square_{\mathrm{H}}$	Subscript referring to the human body
$\square_{\mathrm{B}}$	Subscript referring to the empty footbridge
$\square_{\mathrm{HB}}$	Subscript referring to the coupled crowd-structure system

Tuned Mass Damper

$\mathbf{b}$	Vector of parameters describing the structural behaviour
c_{TMD}	TMD damping constant [Ns/m]
k_{TMD}	TMD stiffness constant [N/m]
$\mathbf{l}$	Vector of parameters describing the loading
m_{TMD}	TMD mass [kg]
n_{TMD}	Number of TMDs
$\ddot{u}_{\mathrm{comfort}}$	Acceleration limit for vibration comfort [m/s^2]
$\mathbf{y}$	Vector of decision variables
Δ_{rel}	Relative TMD displacement [m]
Δ_{tol}	Tolerable value of the relative TMD displacement [m]
μ_{TMD}	Mass ratio [-]
ρ_{TMD}	Frequency ratio [-]
ξ_{eff}	Effective damping ratio [-]
ξ^0_{eff}	Effective damping ratio of undamped system with TMD [-]
ξ_{TMD}	TMD damping ratio [-]
f_{TMD}	TMD frequency [Hz]
$\square_{\mathrm{TMD}}$	Subscript referring to TMD parameter

Other scalars, vectors and matrices

$\mathbf{C}$	Damping matrix
f	Frequency [Hz]
f_j	Natural frequency of mode j [Hz]
$f(x)$	Objective function
$g(x)$	Equality constraint function
$h(x)$	Inequality constraint function
i	Imaginary unit $i^2 = -1$
$\mathbf{I}$	Identity matrix
$\mathbf{K}$	Stiffness matrix
$\mathcal{L}$	Lagrangian function
m_j	Modal mass of mode j [kg]
$m_{\mathrm{eq},j}$	Equivalent mass of mode j [kg]
$\mathbf{M}$	Mass matrix
n_{DOF}	Number of degrees of freedom
n_m	Number of modes
$\mathbf{p}$	Vector of forces
p_F	Probability of failure
$\mathbf{S}_{\mathrm{H}}$	Selection matrix for interaction forces with human body
$\mathbf{S}_{\mathrm{p}}$	Selection matrix for forces
$\mathbf{S}_{\mathrm{TMD}}$	Selection matrix for interaction forces with TMD

t	Time
$\mathbf{u}$	Vector of displacements
(x, y, z)	Cartesian coordinates
$\mathbf{z}$	Vector of modal coordinates
α	Level of uncertainty
β_f	Multiplication factor for uncertain natural frequency
β_m	Multiplication factor for uncertain modal mass
β_ξ	Multiplication factor for uncertain modal damping ratio
$\mathbf{\Gamma}$	Diagonal matrix containing the terms $2\xi_j\omega_j$
$\tilde{\Lambda}$	Triangular shaped membership function
$\mu_\square$	Mean value of $\square$
$\mathbf{\Phi}$	Mode shape matrix
ω	Circular frequency [rad/s]
ω_j	Circular natural frequency [rad/s]
$\mathbf{\Omega}^2$	Diagonal matrix containing the terms ω_j^2
$\boldsymbol{\varphi}_j$	Unity normalised mode shape vector of mode j
$\boldsymbol{\phi}_j$	Mass normalised mode shape vector of mode j
$\sigma_\square$	Standard deviation of $\square$
ξ_j	Modal damping ratio of mode j [-]
$\square_j$	Subscript referring to mode j

Contents

Abstract iii

Beknopte samenvatting v

List of Symbols vii

Contents xi

List of Figures xv

List of Tables xxiii

1 Introduction 1

1.1 Problem statement and motivation 1

1.2 State of the art and further needs 2

1.2.1 Vibration serviceability assessment 2

1.2.2 TMD parameter tuning for footbridges 5

1.3 Objectives and main contributions of the research 7

1.4 Organisation of the text 8

2 Human-induced vibrations of footbridges 11

2.1 Dynamic behaviour of footbridges 12

2.1.1 Equations of motion 13
2.1.2 Modal decomposition 14
2.1.3 Dynamic response 15
2.1.4 Modal parameters 17
2.2 Human-induced walking loading 21
2.2.1 Parameters describing the walking loading 22
2.2.2 Single pedestrian force 24
2.2.3 Human-human interaction 29
2.2.4 Human-structure interaction 33
2.3 Response calculation 34
2.3.1 Available design procedures 35
2.3.2 Simulations of continuous flows using detailed load models 36
2.3.3 Simplified method by design guides Sétra and HiVoSS . 41
2.4 Vibration evaluation 46
2.4.1 Characteristic response quantity 46
2.4.2 Vibration comfort scales 49
2.5 Sensitivity of the response to uncertainties 51
2.6 Conclusion 53

3 Robust vibration serviceability assessment of footbridges 55
3.1 Non-deterministic analysis 56
3.1.1 Terminology 56
3.1.2 Probabilistic approach 57
3.1.3 Non-probabilistic approach 59
3.1.4 Robustness 63
3.2 Accounting for uncertain modal parameters 66
3.2.1 Selected approach 66

3.2.2 Membership functions of modal parameters 66
3.2.3 Combining uncertain modal parameters 67
3.3 Accounting for variability in loading 68
3.3.1 Inter- and intra-subject variability 68
3.3.2 Variation on average pedestrian characteristics 70
3.4 Robust response evaluation 72
3.4.1 Nested response calculation 72
3.4.2 Fuzzy response analysis 74
3.5 Sensitivity of the vibration serviceability assessment to selected variations 79
3.5.1 Influence of uncertainty in modal parameters 80
3.5.2 Influence of variability in loading 86
3.6 Conclusion 89

4 Robust vibration serviceability design of TMDs for footbridges 91
4.1 Vibration mitigation for footbridges 92
4.1.1 Modification of the mass 93
4.1.2 Modification of the stiffness 93
4.1.3 Modification of the damping - passive systems 94
4.1.4 Modification of the damping - active systems 102
4.1.5 Modification of the damping - semi-active systems . . . 103
4.2 Design considerations for TMDs 106
4.2.1 Vibration serviceability 106
4.2.2 Operability 107
4.2.3 Positioning 108
4.2.4 Effect of detuning 109
4.3 Robust design optimisation 111
4.3.1 Problem formulation 111

4.3.2 Solution techniques and optimisation algorithms 114
4.4 Robust TMD design 118
4.5 Effect of uncertainties on a conventional and a robust TMD design 123
4.5.1 Effects of detuning for a conventional TMD design . . . 123
4.5.2 Trade-off between cost and robustness in a robust TMD design 128
4.6 Conclusion 132

5 Case study of the Avelgem footbridge 135
5.1 The Avelgem footbridge 135
5.2 Robust vibration serviceability assessment 138
5.2.1 Effect of human-structure interaction on the modal parameters 138
5.2.2 Scenarios for the simulations 139
5.2.3 Discussion 141
5.3 Cost-effective TMD design for the Avelgem footbridge 147
5.3.1 TMD design problem for the Avelgem footbridge 148
5.3.2 Results 150
5.3.3 Evaluation of TMD performance 153
5.4 Conclusion 159

6 Conclusions and recommendations for further research 161
6.1 Main conclusions of the research 162
6.2 Recommendations for further research and valorisation 165

Bibliography 169

Curriculum vitae 193

List of Figures

1.1 Installed TMD for the (a) Van Beethoven footbridge in Mechelen (Belgium, 2013), (b) Phénix footbridge in Charleroi (Belgium, 2014) and (c) Rabo footbridge in Utrecht (the Netherlands, 2016). 5

2.1 Overview of footbridges in Flanders since beginning of 20th century: year of construction and main material of the supporting structure. 12

2.2 Gait cycle for human walking with indication of swinging and stance phases (after [15]). 23

2.3 Walking forces induced in three directions. 23

2.4 Gaussian probability distribution function of (a) step frequency f_s and (b) walking speed v_s: data provided by authors in table 2.2 individually (dashed) and overall combined data (solid). . . . 25

2.5 Continuous walking load for a pedestrian walking at $f_s = 2$ Hz. (a) Vertical loading according to Young [236] (dark –), Bachmann [12] (dark – –), Kerr [103] (light –), Pedersen [152] (light – –) and Brownjohn [26] (dark $\cdots$). (b) Lateral loading according to Bachmann [12] (dark – –) and Ricciardelli [176] (light –). 28

2.6 (a) Single-step force time history following Li et al. [109]. Step-by-step model with left foot (–) and right foot (– –). (b) Continuous walking load as obtained from the step-by-step model of [109] (dark) and according to Young [236] (light). 30

2.7 (a) Kladek relation between pedestrian density and walking speed v_s. (b) Relation between walking speed and step frequency using eq. (2.39) [223] (solid) and using eq. (2.31) and (2.40) [152] with $\gamma = 1.913$ m^2/pers. and $d_{\text{jam}} = 5.4$ pers./m^2 (dashed). 32

2.8 Spatial distribution of single step forces of randomly distributed pedestrians with different characteristics during an arbitrary time interval $[t_{i,k}, t_{i,k} + T_{c,k}]$ with $t_{i,k}$ the time of the i-th start point of one single footstep in the flow simulation of pedestrian k and $T_{c,k}$ the duration of contact of the footstep of the k-th pedestrian. 38

2.9 Human body represented as a SDOF system with indication of interaction force. 39

2.10 Reduction coefficient $a_n G\psi(f_j)$ according to HiVoSS (light –), Sétra (dark –) and after [213, 220] in the design stage (light – –) and the completion stage (dark $\cdots$) for (a) vertical loading, (b) lateral loading. 43

2.11 The Phénix footbridge in Charleroi: (a) Global view, (b), Cross section and (c) Full view of the FEM with beam and shell elements. 44

2.12 Top and side view of the first three modes of the Phénix footbridge as calculated by the FEM. 45

2.13 (a) Acceleration time history of continuous pedestrian traffic (–) with indication of 95th percentile of peak response (– –) and indication of time windows T and shift Δ in the zoom window. (b) PSD of the acceleration response. (c) Absolute value of the autocorrelation function of the acceleration time history. . . . 49

2.14 Reduction coefficient according to HiVoSS [170] for a density d of 0.2 pers./m^2 for the Phénix footbridge. Value at nominal conditions (– –) and considering up to 10% variation on the natural frequency (grey area). 53

3.1 Membership function of (a) a deterministic number, (b) a crisp set or conventional interval and (c) a fuzzy set with triangular membership function. 60

3.2 Joint membership function of two fuzzy variables with indication of discrete intervals according to the (a) short transformation method [81] and (b) grid search with equidistant sampling. . . 62

3.3 Membership function with indication of two selected α-cut sets of (a) the input variables $\tilde{x}_1$, $\tilde{x}_2$ assuming no interaction for the joint membership function and (b) the output function $f(\tilde{x}_1, \tilde{x}_2)$. 63

3.4 (a) Design with high (– –) and low (–) reliability index, (b) robustness versus reliability and (c) less (– –) versus more (–) robust design (after [101]). 65

3.5 Multi-level approach for the multiplication factor at different levels of uncertainty α for (a) natural frequency, (b) modal damping ratio and (c) modal mass. 69

3.6 Joint membership function for uncorrelated values of the uncertain natural frequency, modal damping ratio and modal mass. 69

3.7 Flowchart for the robust vibration serviceability assessment. . . 73

3.8 Top view of the Phénix footbridge with indication of the 15 possible walking paths (–) and the fixed locations for the SDOFs representing the human bodies to account for HSI (×). 76

3.9 Modal projection of the force for the Phénix footbridge considering nominal values of the flow for a pedestrian density of 0.5 pers./m^2 of the (a) first mode, (b) second mode and (c) third mode. 76

3.10 Transfer function for acceleration with input and output point at point P1 for the empty structure (dark) and the coupled crowd-structure system (light). 77

3.11 Response for the Phénix footbridge at point P1 assuming nominal conditions of the flow and no uncertainty in the modal paramters ($\alpha = 1.0$). Response calculated without HSI (dark) and with HSI (light). (a) Acceleration time history and (b) PSD of acceleration response, calculated at point P1. 79

3.12 Dynamic amplification factor for accelerations showing the sensitivity of the response of a SDOF system to uncertainties (a) in the modal damping ratio and (b) in the natural frequency for off-resonance ($f_P/f = 0.4$) and near-resonance ($f_P/f = 1.1$) excitation and considering the nominal value of ξ. 81

3.13 Effect of uncertainties in the natural frequency. (a) Membership function of the overall maximum response at all locations. (b) PSD of acceleration response at point P1 for different levels of uncertainty. (c) Response at point P1 as a function of β_f. (d) Top view of the Phénix footbridge with indication of maximum response for each node for $\alpha = 0.0$. 83

3.14 Effect of uncertainties in the modal damping ratio. (a) Membership function of the overall maximum response at all locations. (b) PSD of acceleration response at point P1 for different levels of uncertainty. (c) Response at point P1 as a function of β_ξ. (d) Top view of the Phénix footbridge with indication of maximum response for each node for $\alpha = 0.0$. . . 84

3.15 Effect of uncertainties in the modal mass. (a) Membership function of the overall maximum response at all locations. (b) PSD of acceleration response at point P1 for different levels of uncertainty. (c) Response at point P1 as a function of β_m. (d) Top view of the Phénix footbridge with indication of maximum response for each node for $\alpha = 0.0$. 86

3.16 (a) Peak response as a function of μ_{f_s} for $\alpha = 1.0$. (b) Membership function of the overall maximum response at all locations accounting for uncertainty in the natural frequency and variation on the average step frequency. (c) PSD of acceleration response at point P1 for different levels of uncertainty α and different values μ_{f_s}. (d) Top view of the Phénix footbridge with indication of maximum response for each node for $\alpha = 0.0$. . . 89

4.1 Tuned Mass Damper ($\square_{\text{TMD}}$) and main structure ($\square_{\text{eq},j}$), considering only the contribution of mode j, as coupled SDOF systems. 95

4.2 Dimensionless frequency response function of the structure without TMD (light –), with undamped TMD ($\rho^*_{\text{TMD}}, \xi_{\text{TMD}} = 0$) (–·) and with TMD with optimal parameters ρ^*_{TMD} and ξ^*_{TMD} (dark –). TMD parameters optimised for (a) displacements using eq. (4.3) (b) accelerations using eq. (4.4) with indication of maximum value (horizontal line). 96

4.3 TMD performance as a function of the TMD mass ratio for different values of the modal damping ratio of the main structure (0%–0.4%–1%, light to dark) and optimal values of the TMD according to eq. (4.3)(–) and eq. (4.4)(– –). (a) Effective damping ratio following eq. (4.6) and (b) ratio of the relative TMD displacement to the static deflection of the structure. 98

4.4 Characteristics of installed TMDs for footbridges as found in literature [34, 40, 126, 210, 211, 232] and comparison with the optimal values according to eq. (4.3) [52] (–) and eq. (4.4) [7, 8, 230] (– –). (a) TMD frequency ratio ρ_{TMD} and (b) TMD damping ratio ξ_{TMD}. 98

4.5 Pendulum Tuned Mass Damper ($\square_p$) and main structure ($\square_{\text{eq},j}$) as coupled SDOF systems. 99

4.6 Viscous dampers: (a) working principle of viscous fluid damper (after [203]) and (b) installation of viscous dampers and TMDs at the London Millennium Bridge (top view, after [46]). 100

4.7 Scheme of (a) Tuned Liquid Column Damper with orifice and (b) Tuned Sloshing Damper with additional damping screens. . 101

4.8 Working principle of (a) electrodynamic inertial mass damper (after [155]) and (b) twin rotor damper (after [16]). 103

4.9 Control schemes for structure (a) without damping device, (b) with passive damper, (c) with active damper and (d) with semi-active damper (based on [196]). 104

4.10 Working principle of (a) controllable fluid damper (after [198]) and (b) friction damper (after [235]). 106

4.11 Effect of detuning on TMD performance given as the ratio of the H_∞-norm for TMD with detuned frequency ratio ρ_{TMD} and with optimal frequency ratio ρ^*_{TMD} according to equation (4.4) for TMD with mass ratio (a) $\mu_{\text{TMD}} = 2\%$ and (b) $\mu_{\text{TMD}} = 5\%$. Effect of structural damping given for $\xi_j = 0.5\%$ (– –), $\xi_j = 1.0\%$ (–) and $\xi_j = 1.5\%$ (–·). 110

4.12 Effect of detuning on TMD performance given as the ratio of the H_∞-norm for TMD with detuned damping ratio ξ_{TMD} and with optimal damping ratio ξ^*_{TMD} according to equation (4.4) for an undamped main system $\xi_j = 0\%$. TMD with mass ratio $\mu_{\text{TMD}} = 2\%$ (–) and $\mu_{\text{TMD}} = 5\%$ (– –). 110

4.13 Conventional TMD design for the Phénix footbridge following eq. (4.4). (a) Effective damping ξ_{eff} and (b) ratio of the relative displacement and static deflection of the footbridge with a modal damping ratio of $\xi_1 = 0.4\%$ for different values of the mass ratio μ_{TMD}. Indication of the minimally required mass ratio μ_{TMD} for different pedestrian densities. 126

4.14 Robust vibration serviceability assessment for the Phénix footbridge with TMD tuned according to equation (4.4). (a) Acceleration response, (b) Relative TMD displacement. Possible range of response for increasing levels of uncertainty for the natural frequency and the modal damping ratio (dark to light) and indication of the response at nominal conditions (×). . . . 128

4.15 Robust vibration serviceability assessment for the Phénix footbridge with TMD tuned for worst case response (a) at $\alpha = 0.0$ considering the largest range of uncertainty, (b) at $\alpha = 0.6$ considering a smaller range of uncertainty, indicated with (–). Possible range of acceleration levels for increasing levels of uncertainty for the natural frequency and the modal damping ratio (dark to light) and indication of the response at nominal conditions (×). 131

4.16 Robust evaluation of the relative TMD displacement for the Phénix footbridge with TMD tuned for worst case response (a) at $\alpha = 0.0$ considering the largest range of uncertainty, (b) at $\alpha = 0.6$ considering a smaller range of uncertainty, indicated with (–). Possible range of relative TMD displacement for increasing levels of uncertainty for the natural frequency and the modal damping ratio (dark to light) and indication of the response at nominal conditions (×). 132

5.1 The Avelgem footbridge: (a) Global views, (b) cross section and (c) full view of the FEM with the bridge deck, arches, tension bars and pillars. 136

5.2 Transfer function for vertical accelerations of the empty structure (dark) and the coupled crowd-structure system for different pedestrian densities (light). Input and output point at the antinode of (a) mode 1 (b) mode 3 (midspan). 140

5.3 Top view of the Avelgem footbridge with indication of the five possible walking paths. 141

5.4 Robust vibration serviceability assessment for the Avelgem footbridge: possible range of the 95th percentile of the instantaneous peak response accounting for variability in the loading and for uncertain modal parameters of the structure, indicated by increasing levels of uncertainty in the natural frequency and modal damping ratio (dark to light) and indication of the response at nominal conditions (×). Comfort criteria according to [9]. Overall maximum of all locations of the bridge deck for different pedestrian densities: (a) considering the contribution of all modes (left bars) and the first mode only (right bars). (b) effect of uncertainties of β_f and β_ξ combined (left bars), β_f only (middle bars) and β_ξ only (right bars). Maximum response along the length of the bridge for (c) 0.2 pers./m^2 and (d) 1.5 pers./m^2. 143

5.5 PSD of the acceleration response at point A assuming nominal conditions ($\beta_f = 1$, $\beta_\xi = 1$ and $\mu_{f_s} = \bar{f}_s$) and considering the contribution of all modes (–) and the first mode only (– –) to the response for a pedestrian density of (a) $d = 0.2$ pers./m^2 and (b) $d = 1.5$ pers./m^2. 145

5.6 Robust vibration serviceability assessment for the Avelgem footbridge for different TMD designs. Possible range of the 95th percentile of the instantaneous peak response accounting for variability in the loading and for β_f and β_ξ combined (left bars), β_f (middle bars) and β_ξ (right bars), indicated by increasing levels of uncertainty in the modal parameters (dark to light) and indication of the response at nominal conditions (×). Comfort criteria according to [9]. (a)-(c) Single TMD (Case A), (d)-(f) Two identical TMDs (Case B), (g)-(i) Two independently tuned TMDs (Case C) and (j)-(l) Two independently but conventionally tuned TMDs (Case D). 156

5.7 Structure with two independently tuned TMDs (Case C) at $\alpha = 0.0$. PSD of the acceleration response at point A assuming nominal conditions ($\beta_f = 1$, $\beta_\xi = 1$ and $\mu_{f_s} = \bar{f}_s$) and considering the contribution of all modes (–) and only the first mode (– –) in the response. PSD for the structure without TMDs (light) and with TMDs (dark) for a pedestrian density of (a) $d = 0.2$ pers./m^2 and (b) $d = 1.5$ pers./m^2. Maximum response along the length of the bridge for different levels of uncertainty for (c) 0.2 pers./m^2 and (d) 1.5 pers./m^2. 158

5.8 Effect of detuned TMD parameters on the maximum response for two independently tuned TMDs (Case C) at $\alpha = 0.0$ (–) and at $\alpha = 1.0$ (– –). Maximum response for a pedestrian density of 0.5 pers./m^2 considering nominal conditions of the flow and no uncertainty in the modal parameters (dark) and worst case value of the response considering variation on the average step frequency and uncertainty in the natural frequency (light). Effect of (a) detuned TMD stiffness (frequency ratio) and (b) detuned TMD damping (ratio). 159

List of Tables

2.1 Modal damping ratios [%] for different types of footbridges according to different authors [9, 12, 70, 71, 97, 170]. 20

2.2 Experimentally identified walking characteristics for N free walking pedestrians according to different authors and aggregate values: step frequency f_s, walking speed v_s and step length l_s. . 25

2.3 Dynamic load factors a_n for vertical and lateral walking loading according to different authors. 27

2.4 Fourier coefficients of the five harmonic components of the vertical single step walking force according to Li et al. [109]. 29

2.5 Walking speed v_s and average step frequency $\bar{f}_s$ for different pedestrian densities using eq. (2.38) [231] and eq. (2.39) [223] respectively. 32

2.6 Overview of human body parameters for different postures. . . 34

2.7 Standard deviation of the step frequency σ_{f_s} for different pedestrian densities. 38

2.8 Modal parameters of the Phénix footbridge. 45

2.9 Response calculation for the Phénix footbridge following HiVoSS [170] for a density d of 0.2 pers./m^2 and 1.0 pers./m^2. 46

2.10 Calculation of the instantaneous peak acceleration for $T = 40$ s, estimated based on the standard deviation of the response (method II). 49

2.11 Categories for vibration comfort and range for 95th percentile of peak accelerations (after [31]). 50

2.12 Effect of uncertain natural frequency on reduction coefficient ψ and maximum response $\ddot{u}_{1,\max}$ for the response calculation for the Phénix footbridge following HiVoSS [170] for a density d of 0.2 pers./m^2. 53

3.1 Selected values for the walking characteristics and human body parameters at nominal conditions of the flow for simulations of moving pedestrian traffic. 71

4.1 Conventional TMD design for the Phénix footbridge. Evaluation of design constraints to obtain the minimally required mass ratio. 126

4.2 Conventional TMD design for the Phénix footbridge. Optimal TMD parameters according to eq. (4.4). Values are derived considering the modified value of the modal parameters accounting for the added mass. 126

4.3 Optimised TMD parameters as a solution of eq. (4.31) for the Phénix footbridge and constraint evaluation at different α-levels. 130

5.1 Modal parameters of the Avelgem footbridge as calculated by the FEM in ANSYS ® [4]. 137

5.2 Results of the FEM of the Avelgem footbridge: 3D view of the first 10 mode shapes. 137

5.3 Effect of human-structure interaction on the modal parameters of the first, third and ninth mode of the Avelgem footbridge. . 139

5.4 Optimised values of the parameters of the four different TMD designs and for the three considered values of the parameter α which defines the range of uncertainties in the modal parameters. 154

5.5 Range of instantaneous peak acceleration of the Avelgem footbridge equipped with two independently tuned TMDs with parameters according to Case C (table 5.4). Evaluation at different α-levels for a density of 0.2 and 0.5 pers./m^2. 157

Chapter 1

Introduction

1.1 Problem statement and motivation

The development of high-strength, lightweight materials and advanced calculation techniques allows architects and engineers to design and build ever more slender structures. Due to the relatively small service loads in the case of structures designed for human occupation, challenging lightweight structures are possible for footbridges, large span floors, stairs or grandstands. The slenderness of these structures often results in low natural frequencies in the range of the loading frequencies of human-induced excitation. In combination with a low modal damping, these structures are sensitive to human-induced loading. Besides the static design ensuring the general stability of the structure, vibration serviceability has become an important design criterion requiring an assessment of the dynamic behaviour of the structure under human-induced loading [250].

For a reliable response estimation, a description of both the relevant human-induced loading and the dynamic behaviour of the structure is required. Currently, detailed models exist to describe human-induced loading corresponding to activities as walking and jumping, even including the interaction effects between pedestrians and between human and structure. In the design stage, the modal parameters describing the dynamic behaviour are often calculated by a finite element model (FEM) based on detailed building plans and architectural drawings. After construction, results from measurements can help to calibrate the FEM.

If the response exceeds a predefined limit for vibration comfort, the installation

of vibration mitigation devices such as Tuned Mass Dampers (TMDs) can be opted. The TMD is determined by its mass, stiffness and damping constant which have to be tuned to the modal parameters of the main structure to obtain an effective reduction.

However, both the vibration serviceability assessment and the performance of the TMD are susceptible to the assumptions made for the human-induced loading and the dynamic behaviour of the structure. Due to these uncertainties, an acceptable behaviour after construction cannot always be guaranteed sometimes requiring structural modifications or the unexpected installation of vibration mitigation devices leading to additional costs. Therefore, a robust approach is proposed to account for the effect of uncertainties in the modal parameters and for variability in the loading. The robustness of the vibration serviceability assessment is obtained by evaluating a range of responses where the effect of uncertainties is accounted for. For the TMD performance, robustness is obtained by ensuring its efficiency (e.g. limits for vibration comfort) under a range of uncertainties considered in its parameter tuning.

1.2 State of the art and further needs

The state of the art of two important aspects of this doctoral research are elaborated in this section. First, an overview of current methods for the vibration serviceability assessment of footbridges under walking loading is given. Both simplified and more detailed methods for the response calculation are considered. Second, widely applied design methods for the (robust) parameter tuning of a TMD for footbridges are discussed. For each aspect, shortcomings with respect to the effect of uncertainties are highlighted.

1.2.1 Vibration serviceability assessment

For footbridges subjected to human-induced loading, many procedures for the vibration serviceability assessment have been proposed in the past. They require a description for the relevant type of human-induced loading and for the dynamic behaviour of the structure. Generally, two types of methods are distinguished for the response calculation. First, simplified methods which are useful tools for designers and architects are proposed. They mostly account for the contribution of only one mode and the simplified loading models do not deal explicitly with the complex behaviour of pedestrian flows. Second, more advanced methods are proposed based on simulations using detailed load models where more realistic walking scenarios are considered. These response calculations are assumed to

be more accurate, however often time consuming. Extensive literature reviews concerning the modelling of the human-induced loading are given in [164, 253].

Amongst the simplified procedures, guidelines such as Sétra [9], HiVoSS [170] or the procedure proposed by Willford and Young [237] are widely applied. Other simplified methods are included in standards as Eurocode 5 [70] and ISO 10137 [97]. For all these methods, resonance is assumed for the loading frequency of the first or the second harmonic component of the walking load coinciding with the natural frequency of a mode of the footbridge. The modal damping ratio is estimated based on experience from similar structures. By upscaling the load models of single pedestrians, the loading of a group of pedestrians crossing a footbridge is represented. A reduction coefficient is applied to evaluate if resonance can occur for the natural frequencies and the expected loading frequencies during normal walking. In [213, 220], an alternative reduction coefficient is proposed accounting for uncertainties in the natural frequency. Other methods such as those proposed in [26, 35, 105, 159] are based on an equivalent spectral load model and explicitly account for variability in the walking characteristics of one pedestrian (intra-subject variability) and for variability of walking characteristics among pedestrians (inter-subject variability). In all these methods, a simplified load model is used and the contribution of only one mode is taken into account in the calculation of the response to human-induced loading. The main advantage of these methods is that no extensive statistical analysis is required but that an equivalent deterministic response calculation is performed. However, for footbridges, modes are often closely spaced [33, 85] and the contribution of several modes must be accounted for in the vibration serviceability assessment. Higher harmonic components of the human-induced loading must be considered as well. Generally, it is recommended to consider all modes with a frequency up to 10 Hz in the response calculation since it is assumed that all harmonic components of the loading up to that frequency have a relevant contribution to the total response [255].

In detailed response calculations, more advanced load models are assumed and all modes with a natural frequency in the range of the loading frequencies are considered to describe the dynamic behaviour of the structure. Response calculations using more advanced models for vertical loading are proposed in [189, 219, 225, 252]. By performing Monte Carlo simulations, more realistic situations of the pedestrian traffic are considered and the response is evaluated statistically. The contribution of multiple modes is accounted for and the walking characteristics of the pedestrians are modelled using a stochastic approach accounting for inter- and intra-subject variability. Two other important aspects to model the crowd can be directly included as well: interaction effects among pedestrians (human-human interaction, HHI) and interaction between

pedestrians and structure (human-structure interaction, HSI). Interaction and synchronisation phenomena among pedestrians are described by HHI models. The general effect is that the average walking velocity decreases for higher pedestrian densities [231]. Recently, Bruno et al. in [27] proposed a framework for a probabilistic approach to model the pedestrian behaviour while crossing a footbridge. In addition to HHI, HSI affects the response as well. A distinction is made between active interaction where the pedestrian behaviour is influenced by the vibrating surface and passive interaction where this is not the case. In vertical direction, mainly passive HSI-effects are expected: the added mass and the added damping effect due to the pedestrian bodies [36, 179, 219, 251]. For lateral vibrations, active HSI can result in synchronisation of the step frequencies with the motion of the structure (the so-called *lock-in* effect) [39, 176].

Besides the walking characteristics, the vibration serviceability assessment also depends on the assumptions made for the dynamic behaviour of the footbridge and it is recommended to account for uncertainties in the modal parameters. In the design stage, the natural frequencies and modes of the footbridge can be calculated by a FEM while for the modal damping, an estimation based on experience with similar structures is required such as the values proposed in [9, 170]. After construction, vibration based system identification and model updating help to calculate more accurately the modal parameters. Relatively small variations of the nominal values of the modal parameters may lead to large changes in the response, however, as illustrated in [110] for a response calculation following the widely applied guideline HiVoSS [170]. Two types of sources of uncertainty are distinguished. The first source of uncertainty is due to a lack of knowledge. For example, small deviations in the assumed material properties or support conditions affect the effective stiffness of the footbridge. The effects are time-invariant. The second source encompasses time-variant uncertainties, such as on the natural frequency and modal damping due to daily or seasonal and environmental changes like temperature or due to long-term degradation. Shifts in the natural frequency and modal damping during the structure's life-time are reported in [89, 113, 136]. In [24, 217], it was found that natural frequencies calculated by a detailed FEM of a structure may be up to 10% off from the actual measured values. Based on long term monitoring, variations of 20% are found in the natural frequency of a stress-ribbon footbridge [197]. In [10], large variations of the modal damping are reported depending on the amplitude of the acceleration.

Up to now, this uncertainty in the modal parameters of the structure is not accounted for in any of the conventional methods for the evaluation of footbridges. Often, only the inter- and intra-subject variability of the pedestrian walking characteristics is considered. An approach for the robust vibration serviceability assessment of footbridges is needed to evaluate the structure's



(a) (b) (c)

Figure 1.1: Installed TMD for the (a) Van Beethoven footbridge in Mechelen (Belgium, 2013), (b) Phénix footbridge in Charleroi (Belgium, 2014) and (c) Rabo footbridge in Utrecht (the Netherlands, 2016).

dynamic behaviour, accounting for both uncertainties in the modal parameters and variability in the loading.

1.2.2 TMD parameter tuning for footbridges

If the vibration levels exceed the threshold for vibration comfort, the installation of a TMD can be considered as a passive vibration control device [34, 128, 129, 253]. The TMD serves as an energy absorber and is characterised by its mass, stiffness and damping constant. The TMD parameters have to be tuned to the modal parameters of the main structure to optimise its performance and to ensure a sufficient supplementary damping. Criteria for vibration serviceability (e.g. response of the main structure) and operability (e.g. TMD movement relative to the bridge deck) must therefore be considered. Figure 1.1 shows some recent examples of TMDs for footbridges. The units are attached to the vibrating bridge deck or can be hidden inside the cross section.

The basic working principle of a TMD is described by Warburton in [227, 228] and by Den Hartog in [52]. The formulae provided by Den Hartog give the optimal values for the stiffness and damping for a given TMD mass to minimise the displacement response of the structure while assuming no modal damping of the main structure. A pure harmonic loading causing resonance with the mode to which the TMD is tuned, is assumed. The expressions by Asami [8] generalise those given in the classical work by Den Hartog for a lowly damped structure. Alternative expressions in case of a damped main structure are presented by Ghosh and Basu in [77] and Tsai in [206]. A similar approach is given by

Asami in [7, 8, 230] where formulae are provided for the TMD parameters by minimising the acceleration response for a damped structure.

A TMD design thus consists of tuning the mass, stiffness and damping to the main structure's dynamic behaviour. A good knowledge of the modal parameters of the structure is important even though it often contains various kinds of uncertainties. A discrepancy between the values of the modal parameters assumed for the design of the TMD, and the actual values adversely affects the performance [98]. This effect of detuning was studied by Rana and Soong [168] and Werkle [233]. Small adjustments to the TMD properties are possible on-site after installation [76].

The conventional approaches for the design of a TMD as presented by Den Hartog [52] or Asami [7, 8] do not consider the effect of uncertainties in the loading, or in the modal parameters of the main system. Several other studies try to optimise the performance of a TMD under uncertain circumstances. Papadimitriou et al. in [149] present a probabilistic TMD design, accounting for an uncertain natural frequency and modal damping ratio. The procedure is illustrated for a harmonic loading and a single degree of freedom (SDOF) system. Similar, Jensen et al. in [98] consider different coefficients of variation to define the ranges of uncertainty in the main system modal parameters. Marano et al. in [119] compare a conventional TMD design with two robust designs (a single and a multi-objective design problem). The analysis showed that the TMD parameters of the conventional and the robust design differ considerably from each other. Zang et al. [246] propose to determine the TMD mass, stiffness and damping by solving a multi-objective optimisation problem to minimise a linear combination of the mean value and the standard deviation of the peak response. An alternative approach is proposed in [120] where all system and loading parameters are modelled as fuzzy numbers. The TMD parameters are assumed to be deterministic and the expected value and variance of the fuzzy output are weighted in the design constraints. In [182], interval-based uncertainty on the TMD parameters is considered to tune the TMD under earthquake excitation. A frequently used simplification is the assumption that the loads are the only uncertain quantity [117]. However, in many problems of structural dynamics, the uncertainty of the system parameters is of the same importance as the uncertainty in the loading [95].

Several TMD designs for footbridges are discussed in literature [32, 129]. In [34], the TMD design is based on the methodology proposed in [14]. Some authors account for the effect of human-induced walking load in their TMD design. Tubino in [211] tunes the TMD parameters considering an estimation of the equivalent spectral model of the pedestrian traffic [159]. A scalar value measuring the efficiency of the TMD is maximised while evaluating the standard deviation of the response. In [38], a solution of multiple TMDs is proposed following [52]

and the performance was tested afterwards considering human-induced loading. Daniel et al. in [48] solve an allocation and sizing problem for multiple TMDs and a multi-mode vibration problem considering the first harmonic of the walking loading. A range of possible step frequencies is considered. A TMD design is elaborated in [214, 222] based on increasing the effective damping as defined in [229]. The response of the footbridge is verified afterwards considering the simplified load models from [9].

For footbridges, TMDs are rarely designed accounting for the combined effect of uncertainties in the main system modal parameters and variability in the (walking) loading. Furthermore, multiple harmonic components of the loading and multiple modes of vibrations determine the response as well. A robust design of a TMD is desired which is characterised by a decreased sensitivity to the effect of uncertain modal parameters while accounting for all human-induced loading aspects.

1.3 Objectives and main contributions of the research

Current methodologies seldom include the effect of uncertainties in the modal parameters of the footbridge in their calculations despite the large effect on the vibration serviceability assessment. When the effect of these uncertainties is not accounted for in the design of a TMD for footbridges, the effective performance of the damping device strongly drops due to detuning effects. This thesis therefore focusses on (1) the development and implementation of an approach for the robust vibration serviceability assessment of footbridges under walking loading and (2) the robust vibration serviceability design of a TMD. The main scientific objectives and original contributions of the research are summarised as follows.

- The effect of both uncertainties in the modal parameters of the structure and variability in the loading on the vibration serviceability assessment is investigated. A generic approach is developed to allow for an evaluation of the effect of uncertainties in the modal parameters. Different levels of uncertainties in the modal parameters of the footbridge are considered for a gradual evaluation of the effect of uncertainties;
- The generic approach is applied for the robust vibration serviceability assessment of footbridges [111]. The response is calculated using simplified load models or based on an advanced load model which simulates flows of pedestrians on the structure. Variability in the walking characteristics

and interaction effects are considered. Robustness of the vibration serviceability assessment is obtained by evaluating a range of instantaneous peak responses that accounts for the effect of uncertainties;

- A methodology for the robust vibration serviceability design of TMDs is proposed. The TMDs are tuned accounting for uncertainties in the modal parameters of the structure and variability in the loading. The robust design ensures performance in uncertain circumstances for a presumed degree of uncertainty. The TMD performance under uncertain circumstances is compared to that of a conventional TMD design;
- An optimisation problem is formulated for the TMD parameter tuning. Considered as the determining factor for the cost of the TMD, the total TMD mass is minimised. Constraints are added to satisfy criteria for vibration serviceability. The problem is solved using gradient-based optimisation algorithms. For different design conditions corresponding to different levels of uncertainty, the TMD parameters are compared, investigating the trade-off between cost and robustness. The effect of human-induced walking loading is directly included in the TMD parameter tuning to ensure performance for different walking scenarios.

1.4 Organisation of the text

Three main parts are considered in the text. In the first part (chapter 2), the general topic of human-induced vibrations of footbridges is introduced focussing on walking loading. In the second part (chapter 3 and 4), an approach for the robust vibration serviceability assessment and the robust design of TMDs for footbridges is elaborated. Third (chapter 5), the proposed methodologies are applied in a case study.

Chapter 1 outlines the problem statement and motivation of the thesis. An overview is given of the state of the art focussing on vibration serviceability assessment of footbridges and the design of TMDs. The main contributions of the work are summarised and the organisation of the thesis is discussed.

Chapter 2 gives an introduction to human-induced vibrations of footbridges. First, the characteristics determining the dynamic behaviour of footbridges are discussed. Second, possible modelling techniques for human-induced walking loading are summarised and widely applied methods for the response calculation are given. Shortcomings in existing procedures for the vibration serviceability assessment regarding the effect of uncertainty in the modal parameters of the structure on the response are indicated.

Chapter 3 presents a generic methodology for the robust vibration serviceability assessment of footbridges. For different types of uncertainty, an appropriate approach is selected to deal with them. It is elaborated how to account for the effect of uncertainties in the modal parameters of the footbridge and for variability in the loading aiming at a robust vibration serviceability assessment of footbridges.

Chapter 4 focusses on the robust vibration serviceability design of TMDs for footbridges. Frequently used vibration mitigation techniques and their design procedures are discussed. Design criteria are formulated and (robust) optimisation techniques are discussed. The chapter ends with the formulation of a TMD design problem accounting for the effect of uncertainties in the modal parameters of the structure and for variability in the loading. The main advantages compared to conventional designs are given.

Chapter 5 applies the presented methodology for the robust vibration serviceability assessment and robust design of TMDs in a case study. A detailed discussion and interpretation is given for the assessment, including the effect of HSI on the response. A comparison is made between TMD designs for different configurations and different ranges of uncertainty. The focus is on investigating the trade-off between cost and robustness.

Chapter 6 summarises the most relevant conclusions of the research and gives recommendations for future research. Further steps for valorisation of the research are indicated as well.

Chapter 2

Human-induced vibrations of footbridges

Nowadays, structures are designed and dimensioned following a factorial design procedure as prescribed for example in the structural Eurocodes [71]. Using a partial factor method, it is to be verified that in all relevant design situations no limit state, ultimate limit state (ULS) or serviceability limit state (SLS), is exceeded. The partial factors are used to account for unfavourable deviations by increasing representative values of the actions and reducing the resistance of the structure. The serviceability limits consist of static design requirements (e.g. structural deflection) and vibration serviceability requirements [70, 71]. Newly built slender footbridges are often characterised by rather low natural frequencies, possibly in the range of the loading frequencies of human-induced excitation. As these light footbridges are generally characterised by a low modal damping, a high sensitivity to human-induced loading can be expected. An evaluation of the dynamic performance is therefore required.

A turning point in the history of research on human-induced vibrations are the incidents at the opening day of two footbridges: the Paris Solférino footbridge in 1999 [63] and the London Millennium bridge in 2000 [46, 47]. Large lateral vibrations are observed due to interaction between the pedestrians and a low frequency lateral mode of the footbridge. These incidents initiated many research teams to investigate the effect of human-induced loading on footbridges, leading to practical guidelines to assess the vibration serviceability of footbridges to human-induced loading such as Sétra [9] and HiVoSS [170].

Today, footbridges become more and more popular as a safe passage crossing

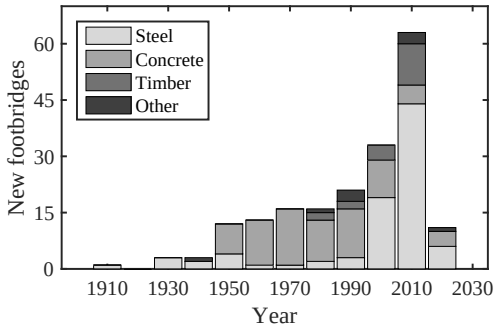

Figure 2.1: Overview of footbridges in Flanders since beginning of 20th century: year of construction and main material of the supporting structure.

motor-, rail- and waterways. A history of all footbridges that have been built in Flanders since the 20th century is given in figure 2.1. As data, the year of construction and main material of more than 200 footbridges in Flanders is provided by [53]. It can be seen from figure 2.1 that the number of newly built footbridges strongly increases in the last decade(s). Whereas concrete footbridges have widely been built in the past, steel structures are strongly gaining popularity more recently. Other footbridges are constructed in timber or masonry or using composite materials.

The present chapter focusses on the dynamic behaviour of footbridges under human-induced walking loading and is organised in five more sections. First, the dynamic behaviour of structures is discussed in section 2.1. Second, a selection of state-of-the-art models for human-induced walking loading is given in section 2.2. In section 2.3, widely applied procedures for the response calculation of footbridges under walking excitation are presented. Next, evaluation criteria for human-induced vibrations are summarised in section 2.4. Finally, it is indicated in section 2.5 how uncertainties in the dynamic behaviour of the structure and variations in the loading can affect the vibration serviceability assessment.

2.1 Dynamic behaviour of footbridges

To assess the vibration serviceability of footbridges, information on both the loading and the dynamic behaviour of the structure is required. This section discusses following topics. First, the equations of motion are given in section 2.1.1. Second, the equation of motion is decomposed to select the

contribution of relevant modes in section 2.1.2. Third, it is indicated how to calculate the vibration response from the equations of motion (section 2.1.3). Fourth, typical values for the modal parameters of footbridges are given in section 2.1.4.

2.1.1 Equations of motion

Using a finite element (FE) formulation, the continuous-time equations of motion for a linear structure, assuming viscous damping, can be written as:

$$\mathbf{M}\ddot{\mathbf{u}}(t) + \mathbf{C}\dot{\mathbf{u}}(t) + \mathbf{K}\mathbf{u}(t) = \mathbf{P}(t) \tag{2.1}$$

with $\mathbf{M}$, $\mathbf{C}$ and $\mathbf{K} \in \mathbb{R}^{n_{\text{dof}} \times n_{\text{dof}}}$ the mass, damping and stiffness matrix, respectively of the structure. $\mathbf{u}$, $\dot{\mathbf{u}}$ and $\ddot{\mathbf{u}}$ are the vectors containing the displacement, velocity and acceleration response, respectively at n_{dof} degrees of freedom (DOF) of the structure. The vector of the forces $\mathbf{P}(t) \in \mathbb{R}^{n_{\text{dof}}}$ corresponding to each DOF of the structure at time t, can be written as the product of a time-variant selection matrix $\mathbf{S}_{\text{p}}(t) \in \mathbb{R}^{n_{\text{dof}} \times n_{\text{p}}}$ and the time history of the forces $\mathbf{p}(t) \in \mathbb{R}^{n_{\text{p}}}$ as follows:

$$\mathbf{P}(t) = \mathbf{S}_{\text{p}}(t)\mathbf{p}(t) \tag{2.2}$$

where n_{p} represents the number of forces. Each column of $\mathbf{S}_{\text{p}}$ gives the spatial distribution of the load time history in the corresponding element of the vector $\mathbf{p}(t)$.

For an undamped system ($\mathbf{C} = \mathbf{0}$) and considering no external forces, the equation of motion is given as follows:

$$\mathbf{M}\ddot{\mathbf{u}}(t) + \mathbf{K}\mathbf{u}(t) = \mathbf{0} \tag{2.3}$$

A solution of the coupled differential equation (2.3) can be written in following form:

$$\mathbf{u}(t) = \varphi \cos(\omega t - \theta) \tag{2.4}$$

A substitution of equation (2.4) in (2.3) results in the eigenvalue problem:

$$\mathbf{K}\boldsymbol{\varphi}_j = \omega_j^2 \mathbf{M}\boldsymbol{\varphi}_j \tag{2.5}$$

for which the eigenvalues ω_j^2 and the eigenvectors $\boldsymbol{\varphi}_j \in \mathbb{R}^{n_{\text{dof}}}$ are the square of the circular natural frequencies $\omega_j[\text{rad/s}] \in \mathbb{R}^{n_{\text{dof}}}$ and the mode shapes, respectively. The mode shapes can be normalised to unity such that $\max|\boldsymbol{\varphi}_j| = 1$ and the modal mass of mode j (m_j) then is defined as $m_j = \boldsymbol{\varphi}_j^T \mathbf{M}\boldsymbol{\varphi}_j$. The mode shapes

can also be normalised to the mass such that $\boldsymbol{\phi}_j^{\mathsf{T}}\mathbf{M}\boldsymbol{\phi}_j = 1$. The relation between the mode shape of mode j, normalised to unity and to the mass then is given as:

$$\boldsymbol{\phi}_j = \frac{1}{\sqrt{m_j}}\boldsymbol{\varphi}_j \tag{2.6}$$

Consequently, the modal mass m_j can be calculated using the maximum component of the mass-normalised modal displacements ϕ_j as:

$$m_j = \frac{1}{\left(\max|\boldsymbol{\phi}_j|\right)^2} \tag{2.7}$$

The mode shapes are orthogonal with respect to the matrices $\mathbf{M}$ and $\mathbf{K}$. In the special case of proportional damping, the mass, stiffness and damping matrix are diagonalised using mass-normalised mode shapes as follows:

$$\begin{aligned}
&\boldsymbol{\Phi}^{\mathsf{T}}\mathbf{M}\boldsymbol{\Phi} = \mathbf{I} \\
&\boldsymbol{\Phi}^{\mathsf{T}}\mathbf{K}\boldsymbol{\Phi} = \boldsymbol{\Omega}^2 \\
&\boldsymbol{\Phi}^{\mathsf{T}}\mathbf{C}\boldsymbol{\Phi} = \boldsymbol{\Gamma}
\end{aligned} \tag{2.8}$$

with $\boldsymbol{\Phi} \in \mathbb{R}^{n_{\text{dof}} \times n_{\text{dof}}}$, the matrix containing the mass-normalised mode shapes, $\mathbf{I} \in \mathbb{R}^{n_{\text{dof}} \times n_{\text{dof}}}$ an identity matrix, $\boldsymbol{\Omega}^2 \in \mathbb{R}^{n_{\text{dof}} \times n_{\text{dof}}}$ the matrix containing on its diagonal the values of ω_j^2 and $\boldsymbol{\Gamma} \in \mathbb{R}^{n_{\text{dof}} \times n_{\text{dof}}}$ also a diagonal matrix with on its diagonal the values of $\{2\xi_j\omega_j\}$ where ξ_j [-] represents the modal damping ratio of mode j.

2.1.2 Modal decomposition

The total (displacement) response $\mathbf{u}(t)$ of the structure can be calculated as a contribution of n_{dof} modes (modal superposition) as:

$$\mathbf{u}(t) = \sum_{j=1}^{n_{\text{dof}}} \boldsymbol{\phi}_j z_j(t) \tag{2.9}$$

with $z_j(t)$ the modal coordinate of mode j so that $\boldsymbol{\phi}_j z_j$ represents the contribution of mode j to the total response. By pre-multiplying equation (2.1) with $\boldsymbol{\Phi}^{\mathsf{T}}$ and considering equation (2.9), the equation of motion (2.1) then becomes:

$$\boldsymbol{\Phi}^{\mathsf{T}}\mathbf{M}\boldsymbol{\Phi}\ddot{\mathbf{z}}(t) + \boldsymbol{\Phi}^{\mathsf{T}}\mathbf{C}\boldsymbol{\Phi}\dot{\mathbf{z}}(t) + \boldsymbol{\Phi}^{\mathsf{T}}\mathbf{K}\boldsymbol{\Phi}\mathbf{z}(t) = \boldsymbol{\Phi}^{\mathsf{T}}\mathbf{S}_{\text{p}}(t)\mathbf{p}(t) \tag{2.10}$$

with $\mathbf{z}(t) \in \mathbb{R}^{n_{\text{dof}}}$ the vector of modal coordinates. Considering the orthogonality properties of the mode shapes $\mathbf{\Phi}$ as defined in equation (2.8), equation (2.10) reads:

$$\mathbf{I}\ddot{\mathbf{z}}(t) + \mathbf{\Gamma}\dot{\mathbf{z}}(t) + \mathbf{\Omega}^2\mathbf{z}(t) = \mathbf{\Phi}^{\mathsf{T}}\mathbf{S}_{\text{p}}(t)\mathbf{p}(t) \tag{2.11}$$

In particular, the equation for a selected mode j can be written as:

$$\ddot{z}_j(t) + 2\xi_j\omega_j\dot{z}_j(t) + \omega_j^2 z_j(t) = \boldsymbol{\phi}_j^{\mathsf{T}}\mathbf{S}_{\text{p}}(t)\mathbf{p}(t) \tag{2.12}$$

Usually, the total response is dominated by only a limited number of relevant modes n_{m} and the number of equations is strongly reduced (modal reduction). In that case, equation (2.11) is used by replacing $\mathbf{z}$, $\mathbf{I}$, $\mathbf{\Gamma}$, $\mathbf{\Omega}$ and $\mathbf{\Phi}$ by $\mathbf{z}_r \in \mathbb{R}^{n_{\text{m}}}$, $\mathbf{I}_r \in \mathbb{R}^{n_{\text{m}} \times n_{\text{m}}}$, $\mathbf{\Gamma}_r \in \mathbb{R}^{n_{\text{m}} \times n_{\text{m}}}$, $\mathbf{\Omega}_r \in \mathbb{R}^{n_{\text{m}} \times n_{\text{m}}}$ and $\mathbf{\Phi}_r \in \mathbb{R}^{n_{\text{dof}} \times n_{\text{m}}}$, respectively.

2.1.3 Dynamic response

Time domain

The decoupled equations of motion (2.11)–(2.12) are now rewritten in state-space form as:

$$\dot{\mathbf{x}}(t) = \mathbf{A}_c\mathbf{x}(t) + \mathbf{B}_c\mathbf{S}_{\text{p}}(t)\mathbf{p}(t) \tag{2.13}$$

with the state vector $\mathbf{x}(t) \in \mathbb{R}^{n_{\text{s}}}$ containing the modal displacements and modal velocities of each mode contributing to the response ($n_{\text{s}} = 2n_{\text{m}}$):

$$\mathbf{x}(t) = \begin{bmatrix} \mathbf{z}_r(t) \\ \dot{\mathbf{z}}_r(t) \end{bmatrix} \tag{2.14}$$

The continuous time system matrices $\mathbf{A}_c \in \mathbb{R}^{n_{\text{s}} \times n_{\text{s}}}$ and $\mathbf{B}_c \in \mathbb{R}^{n_{\text{s}} \times \frac{n_{\text{s}}}{2}}$ are defined as:

$$\mathbf{A}_c = \begin{bmatrix} \mathbf{0} & \mathbf{I}_r \\ -\mathbf{\Omega}_r^2 & -\mathbf{\Gamma}_r \end{bmatrix} \tag{2.15}$$

and

$$\mathbf{B}_c = \begin{bmatrix} \mathbf{0} \\ \mathbf{\Phi}_r^{\mathsf{T}} \end{bmatrix} \tag{2.16}$$

For computational reasons, a time discretisation of equation (2.13) is required:

$$\mathbf{x}_{[k+1]} = \mathbf{A}\mathbf{x}_{[k]} + \mathbf{B}\mathbf{S}_{\text{p}[k]}\mathbf{p}_{[k]} \tag{2.17}$$

with $\square_{[k]} = \square(k\Delta t)$, for $k = 0, 1, ..., N-1$, N the number of steps and Δt the time step. The state matrix $\mathbf{A}$ and input matrix $\mathbf{B}$ are calculated from the continuous time system matrices as follows [114]:

$$\mathbf{A} = e^{\mathbf{A}_c \Delta t} \tag{2.18}$$

$$\mathbf{B} = (\mathbf{A} - \mathbf{I})\mathbf{A}_c^{-1}\mathbf{B}_c \tag{2.19}$$

with $\mathbf{I} \in \mathbb{R}^{n_\mathrm{s} \times n_\mathrm{s}}$ an identity matrix.

Frequency domain

In frequency domain, the uncoupled equation of motion (2.12) reads as:

$$\left[-\omega^2 + 2i\xi_j\omega_j\omega + \omega_j^2\right] \hat{z}_j(\omega) = \boldsymbol{\phi}_j^\mathsf{T} \hat{\mathbf{P}}(\omega) \tag{2.20}$$

with $\hat{z}_j(\omega)$ and $\hat{\mathbf{P}}(\omega)$ the forward Fourier transforms of the modal coordinate $z_j(t)$ of mode j and of the vector of the input force (eq. (2.2)), respectively and i the imaginary unit ($i^2 = -1$). From equation (2.20), the modal coordinate $\hat{z}_j(\omega)$ can be written as:

$$\hat{z}_j(\omega) = \frac{\boldsymbol{\phi}_j^\mathsf{T}}{\left(-\omega^2 + 2i\xi_j\omega_j\omega + \omega_j^2\right)} \hat{\mathbf{P}}(\omega) \tag{2.21}$$

The displacement vector $\hat{\mathbf{u}}(\omega)$ in frequency domain is calculated as the contribution of multiple modes as follows:

$$\begin{aligned} \hat{\mathbf{u}}(\omega) &= \sum_{j=1}^{n_\mathrm{m}} \boldsymbol{\phi}_j \hat{z}_j(\omega) \\ &= \sum_{j=1}^{n_\mathrm{m}} \frac{\boldsymbol{\phi}_j \boldsymbol{\phi}_j^\mathsf{T}}{\left(-\omega^2 + 2i\xi_j\omega_j\omega + \omega_j^2\right)} \hat{\mathbf{P}}(\omega) \\ &= \mathbf{H}_\mathbf{u}(\omega)\hat{\mathbf{P}}(\omega) \end{aligned} \tag{2.22}$$

where $\mathbf{H}_\mathbf{u}(\omega) \in \mathbb{C}^{n_\mathrm{dof} \times n_\mathrm{dof}}$ is the matrix of complex transfer functions, expressed in terms of displacements. An element $\mathbf{H}_{\mathbf{u},lk}(\omega)$ relates the output in DOF l to a harmonic input at DOF k as:

$$\mathbf{H}_{\mathbf{u},lk}(\omega) = \sum_{j=1}^{n_\mathrm{m}} \frac{\boldsymbol{\phi}_j(k)\boldsymbol{\phi}_j(l)}{\left(-\omega^2 + 2i\xi_j\omega_j\omega + \omega_j^2\right)} \tag{2.23}$$

The frequency response function for accelerations can be obtained similar by multiplying equations (2.22) and (2.23) with $-\omega^2$.

2.1.4 Modal parameters

The dynamic behaviour of structures is determined by the modal parameters, i.e. natural frequency, mode shape and modal damping ratio. Focusing on the dynamic behaviour of footbridges, a discussion of each modal characteristic is given below. Afterwards, it is indicated how the parameters can be derived for an equivalent mass-spring-damper system in case of a structure where the modes are well separated in frequency domain and with sufficiently low modal damping.

Natural frequency

The natural frequency f_j [Hz] or circular natural frequency ω_j [rad/s] is a measure for the rhythm of oscillation of a certain mode j of the structure. For slender footbridges, characterised by a low stiffness to mass ratio, the fundamental natural frequency is typically below 5 Hz.

The natural frequencies can either be calculated based on a FEM for example in the design stage or experimentally identified for an existing structure. In this thesis, no further attention is given to methods for the in situ identification of modal parameters but the interested reader is referred to [88, 153, 172].

In [216], the modal parameters of an extensive dataset of footbridges are presented. Generally, the fundamental natural frequency decreases for an increasing span of the footbridge. Compared to the number of vertical bending, lateral bending and torsional modes, only a small number of longitudinal modes is reported.

Modal mass

As already indicated in section 2.1.1, the modal mass is directly related to the structural response through the mass-normalised mode shapes. The modal mass of each mode (equation (2.7)) is a fraction of the total mass engaged in that mode and is inversely proportional to the sensitivity of an excitation of that mode [10]. The modal mass, calculated as $m_j = \boldsymbol{\varphi}_j^T \mathbf{M} \boldsymbol{\varphi}_j$ with the unity-normalised eigenvectors $\boldsymbol{\varphi}_j \in \mathbb{R}^{n_{\text{dof}}}$, can for a two-dimensional (x, y) case of a bridge deck with a mass distribution per unit of area $m(x, y)$, also be written as

$$m_j = \int_S m(x,y) \boldsymbol{\varphi}_j^2(x,y)\, dS \tag{2.24}$$

with S [m^2] the bridge deck surface and $\boldsymbol{\varphi}_j(x, y)$ the mode shape functions normalised to unity. The effect of additional mass on the structure on the modal mass can be investigated similarly and is illustrated in example 2.1. Since the modal mass is related to the bridge (deck) size, its value generally increases for a larger surface, as concluded in [216].

Usually, mass-normalised mode shapes are calculated with a FEM. However, modal masses can also be estimated experimentally using modal data based on a controlled input force (e.g. shaker excitation) [10, 37, 93]. In [25], a methodology is proposed to experimentally estimate the modal mass considering human-induced excitation. It is assumed that the human-induced loading of a single person is repeatable and that only small changes are expected between the force tests in laboratory and in situ. The response of in situ tests is measured and compared to the simulated response using the force measured in laboratory. The modal mass is fitted to obtain good agreements between the build-up of the measured and the simulated response. An accuracy up to 15% is obtained.

Example 2.1. Effect of added mass on modal parameters

To account for additional mass on the structure, for example due to human occupancy, the added modal mass $m_{j,\text{add}}$ is calculated following equation (2.24) with $m(x, y)$ representing the added mass.

Consider a footbridge as a simply supported Bernouilli beam with a length of 30 m, a linear mass of $m(x) = 500$ kg/m and a natural frequency of $f_1 = 2.00$ Hz. The first mode has a sinusoidal shape. The modal mass of the empty footbridge thus equals:

$$m_1 = \int_0^L m(x)\varphi_1^2(x)\,dx = \int_0^{30\ \text{m}} 500\ \text{kg/m}\ \sin(\frac{\pi x}{30})^2\,dx = 7500\ \text{kg}$$

which is half of the total mass of the bridge (500 kg/m $\times$ 30 m = 15000 kg), as expected. The maximum value of the mass-normalised modal displacement according to equation (2.7) equals $\max|\boldsymbol{\phi}_1| = m_1^{-0.5} = 0.0115$.

A supplementary mass of 50 kg/m is now added and that the added modal mass becomes:

$$m_{1,\text{add}} = \int_0^{30\ \text{m}} 50\ \text{kg/m}\ \sin(\frac{\pi x}{30})^2\,dx = 750\ \text{kg}$$

The mass-normalised mode shapes are now rescaled using equation (2.7) for $m_1 + m_{1,\text{add}}$. Consequently, the shifted value of the natural frequency f_1' is

calculated as:

$$f_1' = \sqrt{\frac{m_1}{m_1 + m_{1,\text{add}}}} f_1 = 1.91 \text{ Hz}$$

assuming that the stiffness is not affected by the added mass.

This procedure is applicable for all modes and for all directions (vertical, lateral and longitudinal). To calculate the modified value of the natural frequency, the maximum vector sum of the mass-normalised modal displacements must be used.

Modal damping

The modal damping is a measure for the energy dissipation of structures. It comprehends two components: energy dissipation in the structure itself and energy losses away from the structure [151]. The modal damping is frequently modelled as viscous, moreover assuming proportional damping. Then, for each mode j, a modal damping ratio ξ_j is defined [253].

For footbridges, near-resonance between the walking loading and a mode of the footbridge often occurs. High values of the modal damping are thus beneficial since the structural response highly depends on the modal damping. An as accurate as possible estimation of the modal damping is desirable [253]. An overestimation can lead to an unconservative design of the structure [9].

In the design stage, an estimation of the modal damping ratio is based on experience with similar structures. Suggestions for values are provided by design guides based on in situ identified modal damping ratios. In table 2.1, a range of values is given for different types of structures according to different guidelines. For steel and composite footbridges, the modal damping is generally lower than for concrete or timber footbridges. After construction, the modal damping can be estimated from vibration data [115, 153, 172] or, as suggested by [31], can be obtained by analysis of the free decay response after harmonic excitation at the natural frequency of the considered mode.

From the dataset of footbridges presented in [216], two conclusions are drawn considering the modal damping. First, the modal damping ratio is different for each mode of the structure which can be related to modal deformations (e.g. large modal deformations at the supports imply an increasing interaction with bearings or the supporting structure leading to higher values of the modal damping). Second, a large degree of scatter is found in the identified damping

	Steel	Concrete		Timber	Composite
		Reinforced	Prestressed		
Bachmann [12]	0.2–0.4	0.8–2.0	0.5–1.7	1.5–3.0	0.3–0.6
Eurocode [70, 71]	0.5	1.5	1.0	1.0–1.5	0.5
ISO 10137 [97]	0.5	0.8	0.8	–	0.6
Sétra [9]	0.2–**0.4**	0.8–**1.3**	0.5–**1.0**	1.5–3.0	0.3-**0.6**
HiVoSS [170]	0.2–**0.4**	0.8-**1.3**	0.5–**1.0**	1.0–1.5	0.3–**0.6**

Table 2.1: Modal damping ratios [%] for different types of footbridges according to different authors [9, 12, 70, 71, 97, 170].

ratios for different modes and for different structures. This impedes an accurate estimation of the modal damping ratios before construction.

In literature, it is also reported that the modal damping is a function of the vibration amplitude and increases for larger vibration levels [9, 10, 254]. For these larger amplitudes, higher values are assumed (e.g. 1.0–4.0% for steel and 2.0–7.0% for concrete footbridges [69, 170]).

Equivalent mass-spring-damper system

In case of a structure with natural frequencies well separated in the frequency domain and with sufficiently low damping, the frequency response function in the frequency range around a natural frequency is dominated by the contribution of a single mode, corresponding to that natural frequency. This leads to the following expression for the frequency response function in the frequency range around the jth natural frequency, relating an harmonic load in degree of freedom k to the output in degree of freedom l:

$$\mathbf{H}_{\mathbf{u},lk}(\omega \approx \omega_j) = \frac{\boldsymbol{\phi}_j(k)\boldsymbol{\phi}_j(l)}{\left(-\omega^2 + 2i\xi_j\omega_j\omega + \omega_j^2\right)} \tag{2.25}$$

corresponding to equation (2.23) with only the contribution of mode j. This expression is completely analogous to the frequency response function $\mathbf{H}_{\mathbf{u}}(\omega)$ for a single-degree-of-freedom system with mass m, a natural frequency ω_j and a damping ratio ξ_j:

$$\mathbf{H}_{\mathbf{u}}(\omega) = \frac{1/m}{\left(-\omega^2 + 2i\xi_j\omega_j\omega + \omega_j^2\right)} \tag{2.26}$$

It can be concluded that, under the above mentioned conditions, in the frequency range around the jth natural frequency, the structure can be considered as an

equivalent mass-spring-damper system with the following characteristics:

$$m_{\mathrm{eq},j} = \frac{1}{\boldsymbol{\phi}_j(k)\,\boldsymbol{\phi}_j(l)} \tag{2.27}$$

$$k_{\mathrm{eq},j} = \frac{\omega_j^2}{\boldsymbol{\phi}_j(k)\,\boldsymbol{\phi}_j(l)} \tag{2.28}$$

$$c_{\mathrm{eq},j} = \frac{2\,\xi_j\,\omega_j}{\boldsymbol{\phi}_j(k)\,\boldsymbol{\phi}_j(l)} \tag{2.29}$$

The equivalent mass depends on the position and direction of motion of the force (degree of freedom k) and the position and direction of motion of the receiver (degree of freedom l).

This equivalent SDOF system thus corresponds to a mass-spring-damper system which will have an identical response as the full structure when loaded by the same force and assuming only the contribution of a single mode. The equivalent mass can be used to indicate the direction in which a mode is active. Referring to footbridges, the relevant directions are vertical, lateral en longitudinal. When considering the maximum component of the mass-normalised mode shape $\boldsymbol{\phi}_j$, in these directions, a minimal equivalent mass in direction e can be calculated as:

$$m_{\mathrm{eq},j,\min,e} = \frac{1}{(\max \mid \boldsymbol{\phi}_{j,e} \mid)^2} \tag{2.30}$$

The lower the minimal equivalent mass in a direction, the higher the sensitivity of the mode in that direction. For example, a purely vertical mode, will have zero-valued components in the other directions leading to infinite values of the equivalent mass in these directions, indicating that this mode will have no contribution in these directions. From this definition, it can be seen that if $\max \mid \boldsymbol{\phi}_{j,e} \mid = \max \mid \boldsymbol{\phi}_j \mid$, then $m_{\mathrm{eq},j,\min,e} = m_j$, the modal mass as also defined by equation (2.7).

2.2 Human-induced walking loading

Slender footbridges are often characterised by a natural frequency which may lie in the range of human-induced loading. In order to satisfy the requirements for the vibration serviceability limit state, a vibration serviceability assessment is required. Different types of rhythmic activities can be considered: pedestrian movements (walking, jogging, running, etc.) or other rhythmic activities (on

the spot) such as jumping, bobbing, dancing, etc. [156]. This section focusses on the discussion of the walking loading.

First, the parameters describing the typical walking behaviour are discussed in section 2.2.1. Second, two detailed ways to mathematically describe the walking force induced by a single pedestrian are summarised in section 2.2.2. The effect of interaction among multiple pedestrians (human-human interaction) is discussed in section 2.2.3. In section 2.2.4, interaction effects between the pedestrian (crowd) and the structure are discussed.

2.2.1 Parameters describing the walking loading

Walking cycle

The walking behaviour of a pedestrian is described by its gait cycle, defined by the time between two identical events in the walking pattern. Figure 2.2 shows the typical phases of the walking gait cycle. The starting point of the cycle is usually defined by the heel strike of one foot. Typically, two stance and swing phases are distinguished. The stance phase of one foot is initiated by the heel strike and ends with the toe-off, losing contact with the ground. Then, the foot leaves the ground and transits to the swing phase, characterised by an acceleration and deceleration phase. A typical gait cycle consists of alternating single and double support phases. During the single support phases, one swinging and one stance leg is observed. At the double support phase, contact forces are transmitted between both feet and the ground. The stride length is defined as the distance travelled by one foot (left or right) per gait cycle. Compared to walking loading, the gait cycle of jogging or running loading is characterised by periods without contact between foot and ground.

The force induced by the pedestrian can be split into three components: (1) an up- and downward gravitational force (vertical), (2) a sidewards force perpendicular to the walking direction (lateral) and (3) a smaller component in the direction of walking (longitudinal). A visualisation of the three directions is given in figure 2.3.

Walking characteristics

From figure 2.3, it is clear that the stride length is defined by the distance travelled by two consecutive steps of one foot. For normal walking behaviour, the step length l_s [m] is defined as half of the stride length. The period of time needed for each step is the step period T_s [s] and the pacing rate or step

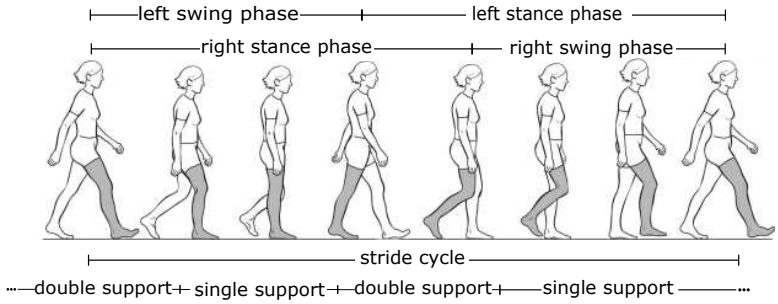

Figure 2.2: Gait cycle for human walking with indication of swinging and stance phases (after [15]).

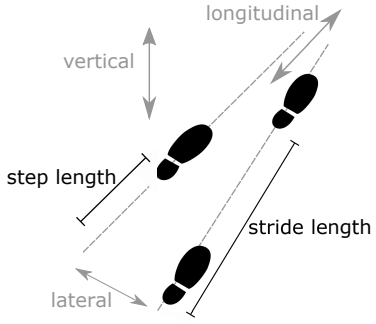

Figure 2.3: Walking forces induced in three directions.

frequency f_s [s^{-1}, Hz] is defined as the number of steps per second. The typical range for the step frequency for normal, unrestricted walking is between 1.5 and 2.5 Hz [12]. The (free) walking speed v_s [m/s] of the pedestrian is the vector-valued velocity in the intended direction of motion. For unrestricted movements of the pedestrian, the vector of the walking speed is oriented towards the walking direction. Following relation links the step frequency f_s, the walking speed v_s and the step length l_s:

$$v_s = \frac{l_s}{T_s} = l_s f_s \tag{2.31}$$

Inter- and intra-subject variability

Experiments to identify the walking characteristics (walking speed v_s, step frequency f_s and step length l_s) have been performed by many researchers. A selection of the results is summarised in table 2.2. The parameters given for each experiment are a statistical interpretation of results of tests with multiple participants. They include the effect of natural variation in the walking pattern of one pedestrian (intra-subject variability) and the effect of variability of walking characteristics among pedestrians (inter-subject variability) [35, 225]. Therefore, probability density functions are derived to statistically describe the walking characteristics. The experimentally obtained mean value and standard deviation of each characteristic are given in table 2.2 according to different authors. A normal distribution is often assumed [255].

To obtain a single value of the walking characteristics, the aggregate mean value μ and standard deviation σ, assuming independent samples j, are calculated following [73] as:

$$\mu = \frac{\sum_j N_j \mu_j}{\sum_j N_j} \tag{2.32}$$

$$\sigma = \sqrt{\frac{\sum_j N_j (\sigma_j^2 + d_j^2)}{\sum_j N_j}} \tag{2.33}$$

with $d_j = \mu_j - \mu$ with j here referring to one of the models in table 2.2. The corresponding aggregate values are in the last row of table 2.2. In figure 2.4, the Gaussian probability distribution functions are plotted for the step frequency f_s and walking speed v_s. A comparison is made between the data provided by each author individually and the calculated aggregate values.

As the results from table 2.2 indicate, variability on the walking characteristics between different experiments is inevitable. An alternative for considering the aggregate values of the walking characteristics, is to consider multiple of the proposed distributions next to each other.

2.2.2 Single pedestrian force

To model the force induced by a single pedestrian in time domain, two approaches are distinguished in literature: (1) the continuous step force model and (2) the single step force model. Below, a discussion of each is given.

Author	f_s [Hz]		v_s [m/s]		l_s [m]		N
	μ_{f_s}	σ_{f_s}	μ_{v_s}	σ_{v_s}	μ_{l_s}	σ_{l_s}	
Kasperksi et al. [102]	1.82	0.12	1.37	0.15	0.75	0.07	251
Petersen [158]	1.75	0.19	1.48	0.18	0.84	0.05	55
Riccardelli et al. [174]	1.84	0.17	1.41	0.22	0.77	0.10	116
Pachi et al. [147]	1.80	0.11	1.30	0.13	0.71	–	800
Niu [141]	1.77	0.15	–	–	0.65	0.07	94
Zivanovic et al. [256]	1.87	0.19	–	–	0.71	0.07	1976
Matsumoto et al. [123, 124]	1.99	0.18	–	–	–	–	505
Toso et al. [205]	1.70	0.19	–	–	–	–	35
Aggregate values	1.86	0.18	1.33	0.16	0.72	0.10	–

Table 2.2: Experimentally identified walking characteristics for N free walking pedestrians according to different authors and aggregate values: step frequency f_s, walking speed v_s and step length l_s.

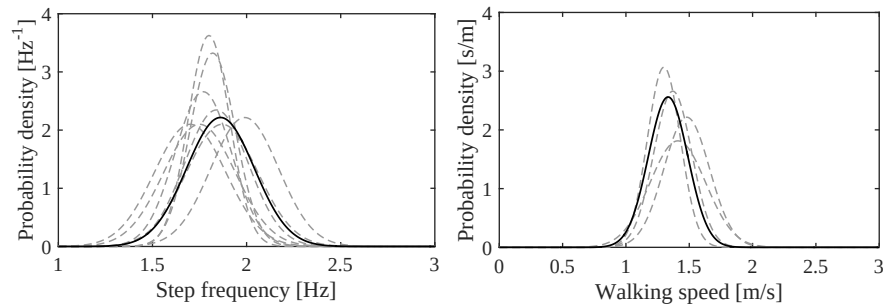

Figure 2.4: Gaussian probability distribution function of (a) step frequency f_s and (b) walking speed v_s: data provided by authors in table 2.2 individually (dashed) and overall combined data (solid).

Continuous walking force

The continuous walking force of a pedestrian is the total force induced by left and right foot for a sequence of steps. Various experiments to identify the time-history of the continuous loading are described in literature [12, 13, 103, 164, 165]. Thereby, ground reaction forces (GRF) induced by left and right foot alternatingly are measured for example using treadmills. Fourier series are fitted to the test results to describe the continuous walking force as a function of the fundamental step frequency f_s [Hz] as:

$$p_s(t) = G + G \sum_{n=1}^{n_h} a_n(f_s) \sin(2\pi n f_s t - \theta_n) \tag{2.34}$$

with $p_s(t)$ [N] the continuous force time history in vertical direction of one pedestrian, G [N] the weight of the pedestrian, $a_n(f_s)$ the dynamic load factor (DLF) of the n-th harmonic component such that $a_n G$ is the Fourier coefficient of the load model and θ_n the phase shift of the n-th harmonic component.

In the early work of Bachmann [12], three harmonic components are proposed for the vertical component of the loading. Kerr [103] and Rainer [165] identified DLFs for the first four harmonic components of the walking loading. An increasing trend of the DLF for the first component (a_1) is observed for higher step frequencies. For other harmonic components, larger variations are found and only mean values are given. A first practical approach has been introduced by Willford et al. [236] who write all DLFs as a function of the step frequency, providing mean and design values. In [12, 176], DLFs are given for the lateral component of the loading. For a broader literature overview of the DLFs, including other types of human-induced loading, the interested reader is referred to [164, 253]. In table 2.3, the DLFs for vertical and lateral walking loading are summarised according to different authors. Values for the phase shift θ_n are rarely given in literature. Generally, following values are assumed for the vertical walking forces: $\theta_1 = 0$, $\theta_2 = \pi/2$ and $\theta_3 = \pi/2$ [12, 216]. In [35], a phase shift of zero is used for all harmonics assuming this as the worst case situation.

Figures 2.5(a) and 2.5(b) show the continuous walking force in vertical and lateral direction, respectively. A comparison is made between the models according to different authors as summarised in table 2.3. The amplitude of the vertical walking force varies around the static weight of the pedestrian. In lateral direction, the mean value of the force equals zero.

Author	Dynamic load factor a_n [-]	Range [Hz]
Vertical walking loading		
Bachmann [12]	a_1 $0.25f_s - 0.1$ $a_{2\to3}$ 0.1; 0.1	$2.0 < f_s < 2.4$
Kerr [103]	a_1 $-0.2649f_s^3 + 1.3206f_s^2 - 1.7597f_s + 0.7613$ $a_{2\to4}$ 0.07; 0.05; 0.05	$1 < f_s < 2.7$
Young [236]	a_1 $0.37(f_s - 0.95) \leq 0.5$ a_2 $0.054 + 0.0044f_s$ a_3 $0.026 + 0.0050f_s$ a_4 $0.010 + 0.0051f_s$	$1 < f_s < 2.8$
Pedersen [152] based on Ellis [68]	a_1 $4.141f_s^5 - 43.382f_s^4 + 181.021f_s^3 - 376.661f_s^2 + 391.845f_s - 163.160$	$1 < f_s < 2.7$
Brownjohn [26]	a_1 $0.37f_s - 0.42$ $a_{2\to6}$ 0.053; 0.042; 0.041; 0.027; 0.018	$1.2 < f_s < 2.4$
Lateral walking loading		
Bachmann [12]	$a_{1\to5}$ 0.039; 0.010; 0.042; 0.012; 0.015	$f_s = 2$ Hz
Ricciardelli et al. [176]	$a_{1\to5}$ 0.040; 0.0077; 0.023; 0.0043; 0.011	$1.2 < f_s < 2.2$

Table 2.3: Dynamic load factors a_n for vertical and lateral walking loading according to different authors.

Single step force

Alternatively, the walking loading can be described from the single step force. By combining the forces induced by left and right foot, and by respecting the duration of contact between foot and ground, the walking loading is obtained. In this way, there is no lack of information to model the phase shifts θ_n in equation (2.34). In literature, the vertical single footstep force is described mathematically in two ways. First, a polynomial approximation of the single footstep force is proposed in [30, 180, 185]. The vertical force due to a single

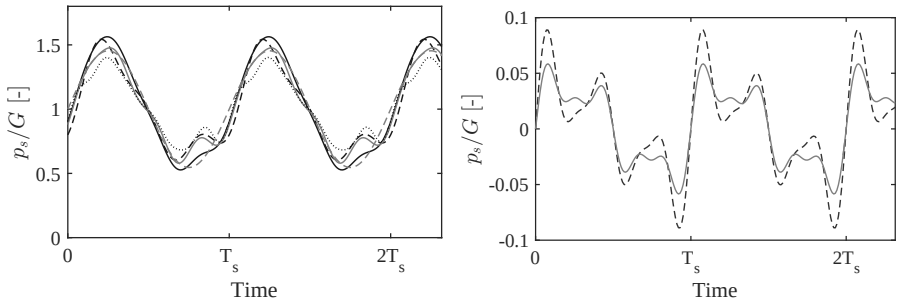

Figure 2.5: Continuous walking load for a pedestrian walking at $f_s = 2$ Hz. (a) Vertical loading according to Young [236] (dark –), Bachmann [12] (dark – –), Kerr [103] (light –), Pedersen [152] (light – –) and Brownjohn [26] (dark $\cdots$). (b) Lateral loading according to Bachmann [12] (dark – –) and Ricciardelli [176] (light –).

step then reads as:

$$\frac{F_s(t)}{G} = \sum_{n=1}^{8} K_n t^n \quad \text{for} \quad 0 \leq t \leq T_c \tag{2.35}$$

with $F_s(t)$ the vertical force [N] of one single footstep at time t, G the weight of the pedestrian [N], K_n the fitting coefficient of the n-th order, as a function of the step frequency f_s and T_c [s] the duration of contact between the foot and the ground. A quadratic approximation is proposed to calculate the duration of contact T_c as a function of f_s [180]. A second method to model the single step force is using a Fourier series as in [109]. The vertical force due to a single footstep of a pedestrian is written as a summation of harmonic components as:

$$\frac{F_s}{G} = \sum_{n=1}^{n_h} a_n(f_s) \sin(\frac{\pi n}{T_c} t) \quad \text{for} \quad 0 \leq t \leq T_c \tag{2.36}$$

with $a_n(f_s)$ the Fourier coefficient of the n-th harmonic component of the generalised load model as a function of the step frequency f_s [Hz]. The model given by Li et al. [109] can be used to calculate the walking force in vertical direction, specifying the values of $a_n(f_s)$. These values are fit to obtain a good correspondence with the continuous load model from Young [236] and are summarised in table 2.4. According to Li [109], the duration of contact between foot and ground is $T_c = T_s/0.76$ based on [64].

a_n	$1.6 \leq f_s \leq 2.32$ Hz	$2.32 \leq f_s \leq 2.40$ Hz
a_1	$-0.0698 f_s + 1.211$	$-0.1784 f_s + 1.463$
a_2	$0.1052 f_s - 0.1284$	$-0.4716 f_s + 1.210$
a_3	$0.3002 f_s - 0.1532$	$-0.0118 f_s + 0.5703$
a_4	$0.0416 f_s - 0.0288$	$-0.2600 f_s + 0.6711$
a_5	$-0.0275 f_s + 0.0608$	$0.0906 f_s - 0.2132$

Table 2.4: Fourier coefficients of the five harmonic components of the vertical single step walking force according to Li et al. [109].

For lateral walking forces, a rectangular force with alternating sign and an amplitude of $0.04G$ is considered in [31]. If synchronisation with one of the modes is considered, a higher factor is proposed [31].

By considering a continuous sequence of forces alternatingly induced by the left and the right foot and respecting the duration of contact, the (continuous) step-by-step walking force is derived from the single step force F_s as follows:

$$\frac{p_s(t)}{G} = \frac{F_s(t)}{G}\,[H(T_c - t)] + \frac{F_s(t - T_s)}{G}\,[H(t - T_s)] \quad \text{for} \quad 0 < t < 2T_s \quad (2.37)$$

with H the Heaviside function. Two terms are distinguished, each representing the contribution of one foot (left and right).

Figure 2.6(a) shows the step-by-step model according to Li [109] as a combination of the forces induced by left and right footstep. A comparison with the obtained continuous step-by-step model as the total force of the left and right footstep forces with the continuous load model according to Young [236] is given in figure 2.6(b).

2.2.3 Human-human interaction

Usually, a vibration serviceability assessment is performed for one or more pedestrian densities d [pers./m^2], going from low (d <1 pers./m^2) to high occupancy ($d \geq$1 pers./m^2). For densities higher than 0.7 pers./m^2, the free movement of the pedestrian is restricted. This means that the behaviour of a pedestrian is influenced by other pedestrians resulting in a decrease of the overall walking speed v_s. These effects of human-human interaction (HHI) are discussed in this section.

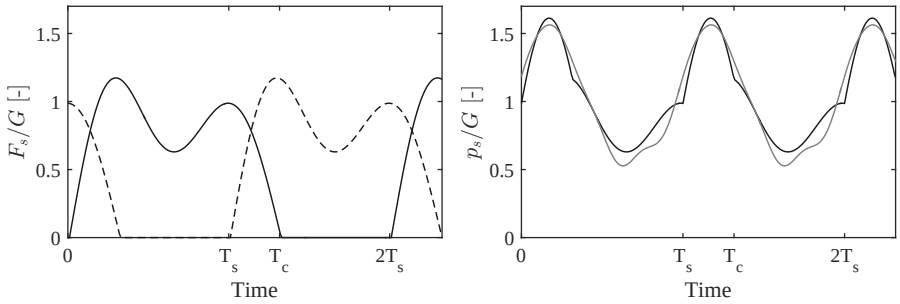

Figure 2.6: (a) Single-step force time history following Li et al. [109]. Step-by-step model with left foot (–) and right foot (– –). (b) Continuous walking load as obtained from the step-by-step model of [109] (dark) and according to Young [236] (light).

Speed-density relation

Two types of models to describe interaction among pedestrians are distinguished. First, microscopic models describe the walking characteristics of each pedestrian in the crowd individually [57, 87]. Second, macroscopic models describe the pedestrian behaviour of the crowd flow as a whole in an analogous way as for fluid flows.

In detailed microscopic models, such as the widely used social force model [86, 87], the behaviour of each pedestrian in a crowd is described individually by calculating the location and velocity of each individual pedestrian. The pedestrian behaviour is governed by a driving force depending on the intention of the pedestrian, an interaction repulsive force due to other pedestrians and a repulsive force due to physical barriers such as borders of the bridge. Venuti et al. in [225] propose a simplified microscopic model. The velocity of each pedestrian consists of two contributions: (1) a desired velocity towards the target point and assuming no interaction and (2) a social velocity that accounts for interaction with other pedestrians within a so-called sensory region.

Alternatively, a macroscopic model such as in [45, 91] is used to link the pedestrian density and average step characteristics (walking velocity v_s and step frequency f_s). A frequently applied model is the Kladek relation by Weidmann [231]. Based on observations, Venuti and Bruno in [223] rewrote this

empirical relation in a more general form as:

$$v_s = \bar{v}_s \left(1 - \exp\left[-\gamma \left(\frac{1}{d} - \frac{1}{d_{\text{jam}}}\right)\right]\right) \tag{2.38}$$

with $\bar{v}_s$ the average free walking speed, γ a fitting coefficient accounting for the travel purpose and d_{jam} the jam density, i.e. the maximum possible density on the structure corresponding to a null speed flow. The jam density generally ranges between 5 and 6 pers./m^2 [223] and depends on the geographic area (intercontinental) and the travel purpose. Equation (2.38) gives the pedestrian speed v_s as a function of the density d. An expression relating the average step frequency $\bar{f}_s$ of the pedestrians to the walking speed v_s was derived from a large set of data from tests in the laboratory [17] and is given by [223] as follows:

$$\bar{f}_s = 2.93 v_s - 1.59 v_s^2 + 0.35 v_s^3 \tag{2.39}$$

The analytical formula proposed by Pedersen et al. in [152] gives the step length as a function of the step frequency based on the results of Wheeler [234] as:

$$l_s(f_s) = 0.2011 f_s^3 - 0.6021 f_s^2 + 0.6462 f_s + 0.2547 \tag{2.40}$$

By combining equations (2.31) and (2.40), an alternative relation between the walking speed and step frequency is obtained. The relations between the pedestrian density and v_s and between v_s and $\bar{f}_s$ are visualised in figure 2.7. A good correspondence of the obtained step frequencies is found between equation (2.39) and equations (2.31) and (2.40) for values of the walking speed in the range of interest, determined by the selected pedestrian densities (see also figure 2.7(b)).

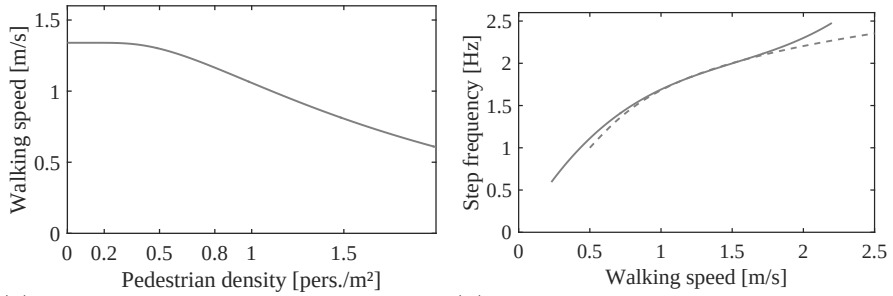

Figure 2.7: (a) Kladek relation between pedestrian density and walking speed v_s. (b) Relation between walking speed and step frequency using eq. (2.39) [223] (solid) and using eq. (2.31) and (2.40) [152] with $\gamma = 1.913$ m^2/pers. and $d_{\text{jam}} = 5.4$ pers./m^2 (dashed).

Example 2.2. Pedestrian speed-density relation

To illustrate the interaction effects among pedestrians, five pedestrian densities are considered: 0.2, 0.5, 0.8, 1.0 and 1.5 pers./m^2. The Kladek relation (2.38) is used with the average free walking speed $\bar{v}_s = 1.34$ m/s, the fitted coefficient for travel purpose $\gamma = 1.913$ m^2/pers. and the jam density $d_{\text{jam}} = 5.4$ pers./m^2 [231]. Values for the walking speed (eq. (2.38)) and average step frequency (eq. (2.39)) for the considered densities are given in table 2.5.

Pedestrian density d [pers./m^2]	0.2	0.5	0.8	1.0	1.5
v_s [m/s]	1.34	1.30	1.17	1.06	0.81
$\bar{f}_s$ [Hz]	1.91	1.89	1.81	1.73	1.51

Table 2.5: Walking speed v_s and average step frequency $\bar{f}_s$ for different pedestrian densities using eq. (2.38) [231] and eq. (2.39) [223] respectively.

Adapted force models

To explicitly account for the effect of human-human interaction in the force models from section 2.2.2, adapted values for dynamic load factors are proposed depending on the pedestrian density. In [156], values for the DLFs are identified for walking, running and other rhythmic activities (jumping). It was concluded that the amplitudes of the harmonics decrease for higher densities. Similar,

Živanović in [252, 255] proposes a Gaussian distribution for the first five DLFs for which the first is related to the step frequency of the pedestrian.

2.2.4 Human-structure interaction

Due to human occupancy, the dynamic behaviour of the footbridge can considerably differ from that of the empty footbridge. Active interaction phenomena occur if the pedestrian behaviour is affected by the vibrating surface (e.g. synchronisation with the bridge motion). If the internal driving term of the pedestrian is identical to the one in case of a rigid surface, passive interaction can occur. These interaction effects between the crowd and the structure can act both in lateral and vertical direction.

In lateral direction, the vibration problems of the Millennium bridge [47, 173] due to the lock-in effect (i.e. the gradually synchronisation of the step frequency and pedestrian motion with the motion of the bridge deck) are a turning point in the research of HSI-effects in lateral direction. Advanced models to account for lateral HSI-effects are proposed such as the inverted pendulum model [39] or the frequency and amplitude dependent lateral force in [96]. A literature review for HSI in lateral direction is given in [224].

In vertical direction, the pedestrian behaviour is less affected by the vibrating surface and mainly passive HSI effects occur. The combined effect of (1) the added damping of human bodies as a mechanical system and (2) the added mass of the pedestrians is expected. Generally, the structural damping increases due to presence of the human bodies [36, 100, 179, 218, 251]. Besides the added mass effect of the human bodies as a static load, a shift in the natural frequency is expected as well. Depending on the ratio of the human body frequency to the natural frequency of the footbridge, an increase [190] or decrease [205] of the natural frequency is observed due to human occupancy. In [219], it was concluded that for natural frequencies of the footbridge below 2 Hz, the pedestrians mainly act as added mass with increased damping effect. For natural frequencies between 2 Hz and 4.5 Hz, HSI-effects are significant resulting in a strong increase of the structural damping. For higher natural frequencies, the increase of the effective structural damping is lower in comparison with natural frequencies in the range of 2–4.5 Hz. The numerical simulations in [219] also show that the structural response may decrease by more than 30% when compared to models where no HSI-effects are accounted for. Multiple approaches to account for the effect of vertical HSI have recently been proposed in literature such as [36, 189, 209, 219, 225].

To mathematically model these vertical HSI-effects, each human body can be modelled as a single or multiple DOF system whose parameters are tuned

Author	Posture	μ_{f_H} [Hz]	σ_{f_H} [Hz]	μ_{ξ_H} [-]	σ_{ξ_H} [-]
Brownjohn [248]	normal standing	5.24	0.40	0.39	0.05
Matsumoto [122]	normal standing	5.7	0.56	0.44	0.07
Van Nimmen [218]	slightly bent legs	3.25	0.32	0.30	0.05
Shahabpoor [188, 189]	normal walking	2.85	0.34	0.295	0.047

Table 2.6: Overview of human body parameters for different postures.

depending on the body posture (standing, sitting, walking, jogging) [2, 121, 122, 188]. This approach is preferred to others where only the added mass of the crowd is considered. If it is assumed that no active interaction takes place, the internal driving forces of the pedestrians remain unaltered when walking on the vibrating footbridge. In this case, the interaction force between the pedestrian and the footbridge is formulated as the sum of the ground reaction force on a rigid surface (see section 2.2.2) and a term resulting from the interaction between the footbridge and the human body as a mechanical system [36, 219], for instance modelled as a SDOF mass-spring-damper system as proposed in [122].

To account for inter-subject variability in the human body parameters, the natural frequency of the human body f_H is sampled from $f_H \sim \mathcal{N}(\mu_{f_H}, \sigma_{f_H})$ [Hz] and the damping ξ_H from $\xi_H \sim \mathcal{N}(\mu_{\xi_H}, \sigma_{\xi_H})$ [–]. In table 2.6, a selection of available data in literature is given for the human body parameters in different postures: normal standing, standing with slightly bent legs, assuming this as representative for an active walking posture, and normal walking.

The impact of vertical (passive) HSI-effects can be considered by including the SDOFs representing the human bodies to the system. In the pseudo moving crowd model of [219], the (walking) forces are moving step-by-step while the SDOFs are distributed uniformly over the bridge deck on their fixed positions according to the pedestrian density to account for the actual spatial distribution of the pedestrians. It was shown in [219] that the pseudo moving crowd model gives results which deviate at most 5% from a model where the SDOFs move with the loads for all densities of 0.2 pers./m^2 and higher.

2.3 Response calculation

For the response calculation, an adequate description of the dynamic behaviour of the footbridge (section 2.1) and the crowd-induced (walking) loading (section 2.2) are required. First, a brief literature review of widely applied methodologies

for the vibration serviceability assessment is given. Then, more attention is given to two methods: a detailed method based on Monte Carlo simulations where the effect of HSI is accounted for and a simplified method according to existing guidelines.

2.3.1 Available design procedures

In articles and design codes, many approaches have been proposed to calculate the response to human-induced walking loading. Reviews of these methods are given in [175, 252]. Generally, a distinction is made between response calculations in time domain and in frequency domain.

Time domain models

Two categories of design procedures for calculations in time domain are found [72]. A first category comprehends simplified procedures where the response for a group of pedestrians is calculated based on superposition of the single pedestrian response. For beam-like footbridges, a simplified formula is proposed in Eurocode 5 [70]. The maximum acceleration depends linearly on the number of pedestrians on the footbridge. Resonance with the first or second harmonic component of the loading is assumed and a reduction coefficient is introduced for natural frequencies which deviate from the expected frequency of walking loading. Alternatively, the improved load model proposed in the ISO 10137 guideline [97] considers six harmonic components of the loading of which the value of the first harmonic increases for higher step frequencies. In the design guides Sétra [9] or HiVoSS [170], a distinction is made between sparse and dense crowds. A dynamic load per unit area is calculated assuming a Gaussian distribution of the step frequencies. The amplitude of the load is reduced by a factor for frequencies away from the normal walking step frequency range. A similar approach is proposed in the UK National Annex to Eurocode 1 [23]. For most of these methods, only one mode is accounted for in the response calculation.

A second category of time domain calculations starts from more detailed load models, eventually including human-human interaction, human-structure interaction, inter- and intra-subject variability, etc. These methods are often based on Monte Carlo simulations. Examples are given in [189, 219, 225, 252]. The contribution of multiple modes to the response can be accounted for. Bruno et al. in [27] propose a probabilistic model for the pedestrian behaviour when crossing a footbridge. A multi-scale approach is used to account for both the

individual pedestrian behaviour (microscopic scale) and the behaviour of groups of pedestrians (intermediate and macroscopic scale).

Frequency domain models

Alternative methods for the response calculation are based on a spectral approach. Brownjohn et al. in [26] calculate the acceleration power spectral density (PSD) based on the PSD of the loading. A Gaussian distribution of step frequencies is considered. Similar, a spectral model for unrestricted pedestrian traffic is proposed by Piccardo et al. in [159] and by Krenk in [105] for resonant and non-resonant loading. The design guideline HiVoSS [170] is based on the spectral load model given by Butz [30]. Caprani in [35] proposes a simple spectral model that is based on a more advanced model accounting for inter- and intra-subject variability.

2.3.2 Simulations of continuous flows using detailed load models

This section describes the methodology how detailed load models can be adopted in the simulation of moving pedestrian traffic. First, it is discussed how the total load can be composed for a predefined pedestrian density considering realistic walking scenarios. Second, it is indicated how the interaction forces between the human bodies and the bridge are transmitted to the structure when HSI effects are considered. Third, the equations of motion are derived for the coupled system of the bridge and the human bodies.

Composition of the total load

Relation (2.31) links the step frequency to the walking speed of each pedestrian. The arrival rate λ [persons/s] is computed as a function of the time that a pedestrian needs to cross the footbridge T_{cross} and the number of pedestrians on the footbridge N (with $N = d \times S$) as:

$$\lambda = \frac{N}{T_{\text{cross}}} \tag{2.41}$$

In the simulations, the arrival times of the individual pedestrians are sampled from a Poisson distribution [123, 145, 251].

Inter-subject variability is considered by modelling the stochastic nature of the walking load. The step frequencies of the pedestrians are sampled from a

Gaussian distribution $f_s \sim \mathcal{N}(\mu_{f_s}, \sigma_{f_s})$ with μ_{f_s} the mean value and σ_{f_s} the standard deviation of the step frequency. The distribution is truncated at 0 Hz to ensure strictly positive step frequencies. An overview of the distribution of step frequencies of the free walking pedestrians is summarised in table 2.2. In order to account for HHI, the mean value μ_{f_s} is taken as the value obtained from equation (2.39) for a given walking speed v_s determined by the pedestrian density d (equation (2.38)). For low densities ($d \leq 1$ pers./m^2), the pedestrian movements are unrestricted while for higher densities ($d > 1$ pers./m^2), the free movement of the pedestrians is restricted and the average speed further decreases which results in a decreased value of the mean step frequency μ_{f_s}. The value of σ_{f_s} also depends on the pedestrian density. A higher level of synchronisation is found for higher densities resulting in a decreased value of σ_{f_s}. In addition to the values in table 2.2, the standard deviation of the step frequency is given as a function of the pedestrian density in table 2.7 according to different authors.

The pedestrian walking speed is determined by the pedestrian density as well (equation (2.38)). At each time step, the longitudinal position of each pedestrian on the footbridge is calculated from the walking speed. For the lateral position of the pedestrian, a uniform distribution covering the width of the bridge is often assumed. In figure 2.8, the spatial distribution of the single step forces is illustrated. An arbitrary time interval $[t_{i,k}, t_{i,k} + T_{c,k}]$ is selected with $t_{i,k}$ the time of the start point of the i-th single footstep of pedestrian k in the simulation. $T_{c,k}$ represents the time duration of contact between foot and ground of the k-th pedestrian.

The total modal load for the flow is found as the superposition of the modal load from the individual pedestrians, respecting the arrival times. For each mode contributing to the response, the time history of the modal load is composed.

Interaction force between human body and the structure

In the equation of motion (2.1), $\mathbf{P}(t)$ represents the total force that is imposed to the structure. This force can refer to different types of excitation such as ambient, shaker or human-induced excitation. As proposed in section 2.2.4, HSI effects can be modelled mathematically considering SDOF systems, representing the human bodies, that are attached to the structure. The total force also includes these additional interaction forces between the human bodies and the bridge. Figure 2.9 shows the transmitted force of a SDOF system that is attached to the main structure.

Author	σ_{f_s} [Hz]	Range of pedestrian density
Synpex [31]	0.10	d <1 pers./m^2
	0.05	$d \geq$1 pers./m^2
Sétra [9]	0.175	d <1 pers./m^2
	0.0	$d \geq$1 pers./m^2
Araújo [6]	0.12	$d = 0.3$ pers./m^2
	0.12	$d = 0.7$ pers./m^2
	0.11	$d = 0.9$ pers./m^2

Table 2.7: Standard deviation of the step frequency σ_{f_s} for different pedestrian densities.

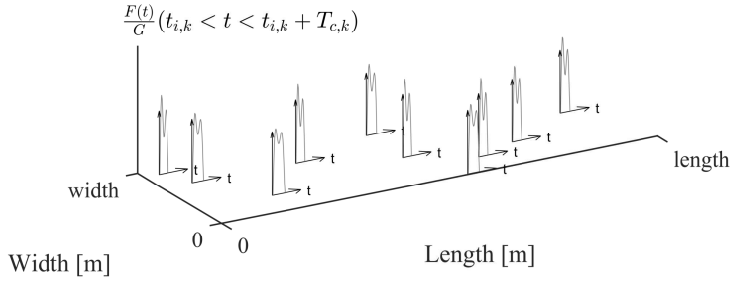

Figure 2.8: Spatial distribution of single step forces of randomly distributed pedestrians with different characteristics during an arbitrary time interval $[t_{i,k}, t_{i,k} + T_{c,k}]$ with $t_{i,k}$ the time of the i-th start point of one single footstep in the flow simulation of pedestrian k and $T_{c,k}$ the duration of contact of the footstep of the k-th pedestrian.

Assuming no active interaction, the interaction force $p_{\mathrm{P},k}$ of pedestrian k with the bridge can be written as:

$$p_{\mathrm{P},k}(t) = p_{s,k}(t) + p_{\mathrm{H},k}(t) \tag{2.42}$$

where $p_{s,k}$ corresponds to the interaction force when walking on a rigid surface (for which the mathematical models are discussed in section 2.2.2) and $p_{\mathrm{H},k}(t)$ corresponds to the change in interaction force due to the mechanical interaction between the human body (modelled as a SDOF) and the bridge as:

$$p_{\mathrm{H},k}(t) = k_{\mathrm{H},k}\left[u_{\mathrm{H},k}(t) - u_{\mathrm{B},k}(t)\right] + c_{\mathrm{H},k}\left[\dot{u}_{\mathrm{H},k}(t) - \dot{u}_{\mathrm{B},k}(t)\right] \tag{2.43}$$

with the subscripts $\square_{\mathrm{H}}$ and $\square_{\mathrm{B}}$ referring to the parameters of the human body and the bridge respectively. $u_{\mathrm{B},k}$ refers to the displacement of the bridge deck

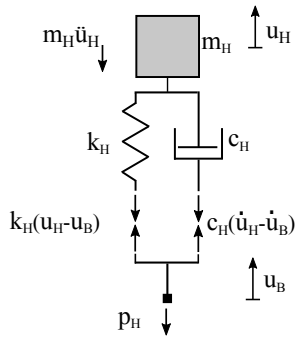

Figure 2.9: Human body represented as a SDOF system with indication of interaction force.

at the DOF of the FEM corresponding to the location of pedestrian k. m_{H} is the pedestrian mass (related to its weight G) and k_{H} and c_{H} are the pedestrian stiffness and pedestrian damping respectively, calculated from the human body natural frequency and damping ratio as follows:

$$k_{\mathrm{H},k} = (2\pi f_{\mathrm{H},k})^2 m_{\mathrm{H},k} \tag{2.44}$$

$$c_{\mathrm{H},k} = 4\pi m_{\mathrm{H},k} f_{\mathrm{H},k} \xi_{\mathrm{H},k} \tag{2.45}$$

These interaction forces can be grouped into a vector $\mathbf{p}_{\mathrm{P}}(t)(= p_s(t)+p_{\mathrm{H}}(t)) \in \mathbb{R}^{n_{\mathrm{H}}}$. n_{H} refers to the number of human bodies. The vector $\mathbf{P}(t)$, collecting all the forces acting on the footbridge, is now formulated as:

$$\mathbf{P}(t) = \mathbf{S}_{\mathrm{H}}(t)\mathbf{p}_{\mathrm{P}}(t) \tag{2.46}$$

where $\mathbf{S}_{\mathrm{H}}(t) \in \mathbb{R}^{n_{\mathrm{dof}} \times n_{\mathrm{H}}}$ is a time-dependent selection matrix (due to the changing positions of the pedestrians on the footbridge) transferring the forces to the corresponding DOFs of the FEM of the bridge. Similar as in equation (2.10), the bridge response at the locations of the pedestrians can be calculated from the modal coordinates and using the selection matrices from eq. (2.46) as:

$$\mathbf{u}_{\mathrm{B}}(t) = \mathbf{S}_{\mathrm{H}}^{\mathsf{T}}(t)\mathbf{\Phi}\mathbf{z}(t)\,, \quad \dot{\mathbf{u}}_{\mathrm{B}}(t) = \mathbf{S}_{\mathrm{H}}^{\mathsf{T}}(t)\mathbf{\Phi}\dot{\mathbf{z}}(t)\,, \quad \ddot{\mathbf{u}}_{\mathrm{B}}(t) = \mathbf{S}_{\mathrm{H}}^{\mathsf{T}}(t)\mathbf{\Phi}\ddot{\mathbf{z}}(t) \tag{2.47}$$

Using these expressions, the force $\mathbf{p}_{\mathrm{P}}(t)$ can be formulated as:

$$\begin{aligned}\mathbf{p}_{\mathrm{P}}(t) = \mathbf{p}_s(t) + \mathbf{K}_{\mathrm{H}}\mathbf{u}_{\mathrm{H}}(t) - \mathbf{K}_{\mathrm{H}}\mathbf{S}_{\mathrm{H}}^{\mathsf{T}}(t)\mathbf{\Phi}\mathbf{z}(t) \\ + \mathbf{C}_{\mathrm{H}}\dot{\mathbf{u}}_{\mathrm{H}}(t) - \mathbf{C}_{\mathrm{H}}\mathbf{S}_{\mathrm{H}}^{\mathsf{T}}(t)\mathbf{\Phi}\dot{\mathbf{z}}(t)\end{aligned} \tag{2.48}$$

with $\mathbf{K}_{\mathrm{H}} = \mathrm{diag}\{k_{\mathrm{H},k}\}$ and $\mathbf{C}_{\mathrm{H}} = \mathrm{diag}\{c_{\mathrm{H},k}\}$.

Equations of motion for the coupled crowd-structure system

The equations of motion of the bridge, expressed in modal coordinates (cfr. eq. (2.11)), are now rewritten accounting for the total force (eq. (2.46) and (2.48)) including additional interaction forces of the human bodies as:

$$\begin{aligned}\mathbf{I}\ddot{\mathbf{z}}(t) + \boldsymbol{\Gamma}\dot{\mathbf{z}}(t) + \boldsymbol{\Omega}^2\mathbf{z}(t) = {} & \boldsymbol{\Phi}^{\mathsf{T}}\mathbf{S}_{\mathrm{H}}(t)\mathbf{p}_s(t) \\ & + \boldsymbol{\Phi}^{\mathsf{T}}\mathbf{S}_{\mathrm{H}}(t)\mathbf{K}_{\mathrm{H}}\mathbf{u}_{\mathrm{H}}(t) - \boldsymbol{\Phi}^{\mathsf{T}}\mathbf{S}_{\mathrm{H}}(t)\mathbf{K}_{\mathrm{H}}\mathbf{S}_{\mathrm{H}}^{\mathsf{T}}(t)\boldsymbol{\Phi}\mathbf{z}(t) \\ & + \boldsymbol{\Phi}^{\mathsf{T}}\mathbf{S}_{\mathrm{H}}(t)\mathbf{C}_{\mathrm{H}}\dot{\mathbf{u}}_{\mathrm{H}}(t) - \boldsymbol{\Phi}^{\mathsf{T}}\mathbf{S}_{\mathrm{H}}(t)\mathbf{C}_{\mathrm{H}}\mathbf{S}_{\mathrm{H}}^{\mathsf{T}}(t)\boldsymbol{\Phi}\dot{\mathbf{z}}(t)\end{aligned} \tag{2.49}$$

After introducing a generalised mass matrix $\bar{\mathbf{M}} \in \mathbb{R}^{n_{\mathrm{dof}} \times n_{\mathrm{dof}}}$, stiffness matrix $\bar{\mathbf{K}} \in \mathbb{R}^{n_{\mathrm{dof}} \times n_{\mathrm{dof}}}$ and damping matrix $\bar{\mathbf{C}} \in \mathbb{R}^{n_{\mathrm{dof}} \times n_{\mathrm{dof}}}$, this equation reads:

$$\begin{aligned}\bar{\mathbf{M}}\ddot{\mathbf{z}}(t) + \bar{\mathbf{C}}\dot{\mathbf{z}}(t) + \bar{\mathbf{K}}\mathbf{z}(t) = {} & \boldsymbol{\Phi}^{\mathsf{T}}\mathbf{S}_{\mathrm{H}}^{\mathsf{T}}(t)\mathbf{p}_s(t) \\ & + \boldsymbol{\Phi}^{\mathsf{T}}\mathbf{S}_{\mathrm{H}}^{\mathsf{T}}(t)\left[\mathbf{K}_{\mathrm{H}}\mathbf{u}_{\mathrm{H}}(t) + \mathbf{C}_{\mathrm{H}}\dot{\mathbf{u}}_{\mathrm{H}}(t)\right]\end{aligned} \tag{2.50}$$

with

$$\bar{\mathbf{M}} = \mathbf{I} \tag{2.51}$$

$$\bar{\mathbf{C}} = \boldsymbol{\Gamma} + \boldsymbol{\Phi}^{\mathsf{T}}\mathbf{S}_{\mathrm{H}}(t)\mathbf{C}_{\mathrm{H}}\mathbf{S}_{\mathrm{H}}^{\mathsf{T}}(t)\boldsymbol{\Phi} \tag{2.52}$$

$$\bar{\mathbf{K}} = \boldsymbol{\Omega}^2 + \boldsymbol{\Phi}^{\mathsf{T}}\mathbf{S}_{\mathrm{H}}(t)\mathbf{K}_{\mathrm{H}}\mathbf{S}_{\mathrm{H}}^{\mathsf{T}}(t)\boldsymbol{\Phi} \tag{2.53}$$

The equation of motion for the masses of the SDOF systems representing the pedestrians can be written as:

$$\begin{aligned}\mathbf{M}_{\mathrm{H}}(t)\ddot{\mathbf{u}}_{\mathrm{H}} + \mathbf{C}_{\mathrm{H}}\left[\dot{\mathbf{u}}_{\mathrm{H}}(t) - \mathbf{S}_{\mathrm{H}}^{\mathsf{T}}(t)\boldsymbol{\Phi}\dot{\mathbf{z}}(t)\right] \\ + \mathbf{K}_{\mathrm{H}}\left[\mathbf{u}_{\mathrm{H}}(t) - \mathbf{S}_{\mathrm{H}}^{\mathsf{T}}(t)\boldsymbol{\Phi}\mathbf{z}(t)\right] = 0\end{aligned} \tag{2.54}$$

All these equations can be combined into

$$\bar{\mathbf{M}}_{\mathrm{TOT}}\begin{bmatrix}\ddot{\mathbf{z}}(t) \\ \ddot{\mathbf{u}}_{\mathrm{H}}(t)\end{bmatrix} + \bar{\mathbf{C}}_{\mathrm{TOT}}\begin{bmatrix}\dot{\mathbf{z}}(t) \\ \dot{\mathbf{u}}_{\mathrm{H}}(t)\end{bmatrix} + \bar{\mathbf{K}}_{\mathrm{TOT}}\begin{bmatrix}\mathbf{z}(t) \\ \mathbf{u}_{\mathrm{H}}(t)\end{bmatrix} = \begin{pmatrix}\boldsymbol{\Phi}^{\mathsf{T}}\mathbf{S}_{\mathrm{H}}(t)\mathbf{p}_s(t) \\ \mathbf{0}\end{pmatrix} \tag{2.55}$$

with $\bar{\mathbf{M}}_{\mathrm{TOT}} \in \mathbb{R}^{\frac{n_{\mathrm{S}}}{2} \times \frac{n_{\mathrm{S}}}{2}}$ the total mass matrix with $n_{\mathrm{S}} = 2(n_{\mathrm{dof}} + n_{\mathrm{H}})$, $\bar{\mathbf{C}}_{\mathrm{TOT}} \in \mathbb{R}^{\frac{n_{\mathrm{S}}}{2} \times \frac{n_{\mathrm{S}}}{2}}$ the total damping matrix and $\bar{\mathbf{K}}_{\mathrm{TOT}} \in \mathbb{R}^{\frac{n_{\mathrm{S}}}{2} \times \frac{n_{\mathrm{S}}}{2}}$, the total stiffness matrix

which are composed as follows:

$$\bar{\mathbf{M}}_{\mathrm{TOT}} = \begin{bmatrix} \bar{\mathbf{M}} & \mathbf{0} \\ \mathbf{0} & \mathbf{M}_{\mathrm{H}} \end{bmatrix} \tag{2.56}$$

$$\bar{\mathbf{C}}_{\mathrm{TOT}} = \begin{bmatrix} \bar{\mathbf{C}} & -\boldsymbol{\Phi}^{\mathsf{T}}\mathbf{S}_{\mathrm{H}}(t)\mathbf{C}_{\mathrm{H}} \\ -\mathbf{C}_{\mathrm{H}}\mathbf{S}_{\mathrm{H}}^{\mathsf{T}}(t)\boldsymbol{\Phi} & \mathbf{C}_{\mathrm{H}} \end{bmatrix} \tag{2.57}$$

$$\bar{\mathbf{K}}_{\mathrm{TOT}} = \begin{bmatrix} \bar{\mathbf{K}} & -\boldsymbol{\Phi}^{\mathsf{T}}\mathbf{S}_{\mathrm{H}}(t)\mathbf{K}_{\mathrm{H}} \\ -\mathbf{K}_{\mathrm{H}}\mathbf{S}_{\mathrm{H}}^{\mathsf{T}}(t)\boldsymbol{\Phi} & \mathbf{K}_{\mathrm{H}} \end{bmatrix} \tag{2.58}$$

with $\mathbf{M}_{\mathrm{H}} = \mathrm{diag}\{m_{\mathrm{H},k}\}$. For the response calculation, the state-space equation reads as:

$$\dot{\mathbf{x}}(t) = \mathbf{A}_c(t)\mathbf{x}(t) + \mathbf{B}_c \begin{pmatrix} \boldsymbol{\Phi}^{\mathsf{T}}\mathbf{S}_{\mathrm{H}}(t)\mathbf{p}_s(t) \\ \mathbf{0} \end{pmatrix} \tag{2.59}$$

with $\mathbf{x}(t) \in \mathbb{R}^{n_{\mathrm{s}}}$ the state vector that contains the modal displacement and modal velocities of all nodes and the displacements and velocities of each human body:

$$\mathbf{x}(t) = \begin{bmatrix} \mathbf{z}(t) \\ \mathbf{u}_{\mathrm{H}}(t) \\ \dot{\mathbf{z}}(t) \\ \dot{\mathbf{u}}_{\mathrm{H}}(t) \end{bmatrix} \tag{2.60}$$

The continuous time system matrices $\mathbf{A}_c(t) \in \mathbb{R}^{n_{\mathrm{s}} \times n_{\mathrm{s}}}$ and $\mathbf{B}_c \in \mathbb{R}^{n_{\mathrm{s}} \times \frac{n_{\mathrm{s}}}{2}}$ are defined as:

$$\mathbf{A}_c(t) = \begin{bmatrix} \mathbf{0} & \mathbf{I} \\ -\bar{\mathbf{M}}_{\mathrm{TOT}}^{-1}\bar{\mathbf{K}}_{\mathrm{TOT}} & -\bar{\mathbf{M}}_{\mathrm{TOT}}^{-1}\bar{\mathbf{C}}_{\mathrm{TOT}} \end{bmatrix} \tag{2.61}$$

and

$$\mathbf{B}_c = \begin{bmatrix} \mathbf{0} \\ \bar{\mathbf{M}}_{\mathrm{TOT}}^{-1} \end{bmatrix} \tag{2.62}$$

For the pseudo moving crowd model [219], it is assumed that the forces $\mathbf{p}_s$ will be moving step-by-step while the SDOFs are distributed uniformly over the bridge deck at their fixed positions. In this case, the matrix $\mathbf{A}_c(t)$ can be considered as time-invariant $\mathbf{A}_c$.

2.3.3 Simplified method by design guides Sétra and HiVoSS

A simplified but practical procedure for the vibration serviceability assessment of footbridges is proposed by design guides Sétra [9] and HiVoSS [170]. The

response is calculated for all modes with a natural frequency below 5 Hz. Resonance with the first or second harmonic of the load is assumed and no interaction forces between human and structure are considered.

The crowd loading is defined as an equivalent deterministic loading. The considered walking load for a single pedestrian is first approximated by a periodic load, representing the first or second harmonic component of the loading. Then, the forces due to a group of N pedestrians are represented in a simplified way by an equivalent uniformly distributed load on the bridge deck. The proposed load model consists of an equivalent number of perfectly synchronised pedestrians N_{eq} that is determined such that the same instantaneous peak response is obtained as by a statistical analysis of simulations of a group of N pedestrians. A distinction is made between sparse and dense pedestrian densities. For low pedestrian densities, the pedestrians are assumed to move independently from each other and a Gaussian distribution of the step frequencies is considered. Based on simulations, it is concluded in [9] that N_{eq} depends on the structural damping ξ_j for these low densities. For higher pedestrian densities, the walking behaviour of the pedestrians is obstructed and the level of synchronisation increases. The higher level of synchronisation results in an increased number of equivalent pedestrians. N_{eq} is found as follows:

$$\begin{aligned} N_{\text{eq}} &= 10.8\sqrt{\xi_j N} \quad \text{for } d < 1\,\text{pers.}/\text{m}^2 \\ N_{\text{eq}} &= 1.85\sqrt{N} \qquad \text{for } d \geq 1\,\text{pers.}/\text{m}^2 \end{aligned} \tag{2.63}$$

The equivalent uniformly distributed load q_{eq} [N/m^2] can act upward or downward and is calculated as:

$$q_{eq} = \frac{N_{eq}}{S} a_n G \psi(f_j) \tag{2.64}$$

with S the surface of the bridge deck walking area, a_n the DLF of the n-th harmonic component of the load and ψ a reduction coefficient that evaluates if resonance can occur between the walking loading and the natural frequency f_j of the bridge. Due to the additional mass of pedestrians, the natural frequency and the modal mass slightly change. The effect can be calculated as proposed in example 2.1. The reduction coefficient ψ therefore depends on the pedestrian density. Values for $a_n G \psi(f_j)$ are given in figure 2.10 for vertical and lateral vibrations. It should be noted that the reduction coefficient is very sensitive to small shifts in the natural frequency. Alternative values for the reduction factor are suggested in [213, 220] where the frequency intervals have been widened to account for uncertainty in the nominal value of the natural frequency (e.g. in the design stage). When uncertainty in the natural frequency can be reduced, for example by performing measurements after completion of the footbridge, the

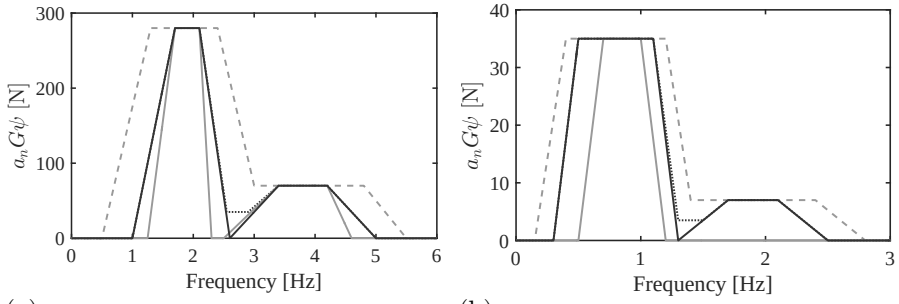

Figure 2.10: Reduction coefficient $a_n G\psi(f_j)$ according to HiVoSS (light –), Sétra (dark –) and after [213, 220] in the design stage (light – –) and the completion stage (dark $\cdots$) for (a) vertical loading, (b) lateral loading.

original intervals are suggested, however with a minimum (non-zero) value for frequencies between the intervals of the first and second harmonic component of the loading (see also figure 2.10).

The modal force F_j is obtained as the projection of the equivalent distributed loading on mode j and can be written as:

$$F_j = q_{eq} \sum_{k=1}^{n_{\text{eff}}} a_{\text{eff},k} \, |\boldsymbol{\phi}_{j,k}| \tag{2.65}$$

with $\boldsymbol{\phi}_j$ the vector containing the mass-normalised modal displacements of the j-th mode for all nodes n_{eff} of the effective bridge deck area A_{eff}, a_{eff} the vector containing the bridge deck area allocated to the corresponding nodes (with $A_{\text{eff}} = \sum_{k=1}^{n_{\text{eff}}} a_{\text{eff},k}$).

Assuming resonance with mode j, the maximum acceleration $\ddot{u}_{j,\max}$ is calculated disregarding the contribution from other modes as follows:

$$\ddot{u}_{j,\max} = \frac{F_j}{2\xi_j} \max |\boldsymbol{\phi}_j| \tag{2.66}$$

with ξ_j the modal damping. Equation (2.66) shows that the final response is very sensitive to the modal damping ξ_j. A good estimation thus is essential for the response calculation. Suggested values are given in table 2.1 and after construction, measurements can be performed for verification. An illustration of the response calculation following the simplified procedure is given in example 2.3.

Example 2.3. Response calculation according to HiVoSS for the Phénix footbridge

The Phénix footbridge is a slender structure with a single span of 38.25 m and a width of 13.35 m and is situated near the railway station of Charleroi, Belgium. The cross section of the bridge consists of three parts. The midspan is a rectangular box of 6.5 m by 1 m with, at both sides, cantilevered tapering I-profiles that are mounted on fixed distances. Stiffeners are interconnecting the I-profiles. The total mass of the footbridge is 242 ton. Figures 2.11(a) and 2.11(b) show a global view of the footbridge and the cross section of the structure, respectively. The bridge is supported by four neoprene bearings. Vertical translations are fixed at all corners while horizontal translations are fixed at one. An additional support is added in the middle of one side of the bridge to avoid lateral movements. A FEM is built in ANSYS [4] (figure 2.11(c)) and consists of 8158 beam elements (Timoshenko beam theory) for the stiffeners and 19392 shell elements (Mindlin-Reissner shell theory) for the steel plates of the box and the tapering I-profiles, resulting in a system with a total of number of 27866 DOFs.

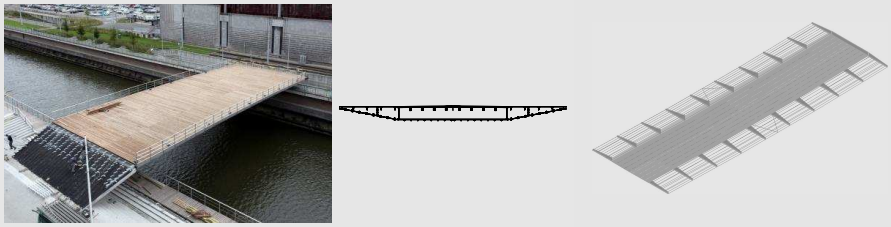

(a) (b) (c)

Figure 2.11: The Phénix footbridge in Charleroi: (a) Global view, (b), Cross section and (c) Full view of the FEM with beam and shell elements.

The dynamic behaviour of the structure is defined by its modal parameters. The mode shapes of the first three modes as calculated by the FEM in ANSYS are given in figure 2.12. The first and second mode are vertical bending modes and the third mode is a torsional mode. The modal parameters are summarised in table 2.8. A modal damping of 0.4% is assumed for all modes as prescribed in [9, 170] for steel footbridges. The modal mass m_j of mode j is calculated using the maximum displacement vector sum of the mass-normalised mode shape $\boldsymbol{\phi}_j$ of the bridge deck in equation (2.7).

j	f_j [Hz]	ξ_j [%]	m_j [ton]
1	1.65	0.4	131.6
2	5.22	0.4	101.1
3	6.15	0.4	23.0

Table 2.8: Modal parameters of the Phénix footbridge.

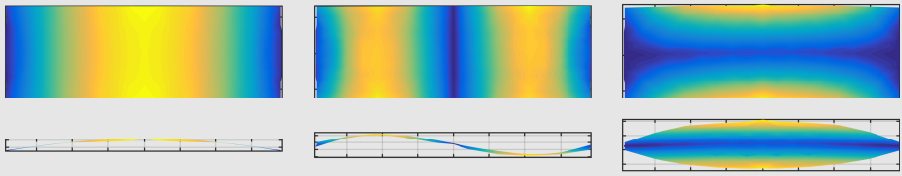

(Mode 1 - $f_1 = 1.65$ Hz) (Mode 2 - $f_2 = 5.22$ Hz) (Mode 3 - $f_3 = 6.15$ Hz)

Figure 2.12: Top and side view of the first three modes of the Phénix footbridge as calculated by the FEM.

The response to walking loading is calculated following the HiVoSS guideline [170]. In this example, the assessment is performed for vertical vibrations of the first mode for a sparse pedestrian density (0.2 pers./m^2) and for a dense crowd (1 pers./m^2).

It is assumed that the bridge deck walking area S is 508 m^2 and the weight of a pedestrian G is 700 N. The results are summarised in table 2.9 for both densities. The modified value of the natural frequency and modal displacement is given accounting for the additional mass effect of the pedestrians. Resonance between the first mode and the first harmonic component of the walking loading is assumed ($a_1 = 0.4$). The value for the reduction coefficient for the density of 1 pers/m^2 is lower than that of 0.2 pers./m^2 since the natural frequency decreases due to the added mass effect and the values of the frequencies are on the increasing slope of the reduction coefficient from figure 2.10(a).

Pedestrian density d [pers./m^2]	0.2 pers./m^2	1.0 pers./m^2
f_1 [Hz]	1.63	1.55
ξ_1 [%]	0.4	0.4
$\max \lvert\phi_{1,\text{vertical}}\rvert$ [$1/\sqrt{\text{kg}}$]	0.0027	0.0026
$N = d \times S$ [persons]	102	508
N_{eq} [persons]	6.89	41.70
a_n [-]	0.4	0.4
$\psi(f_1)$ [-]	0.84	0.66
q_{eq} [N/m^2]	3.20	15.13
F_1 [N]	2.90	13.02
$\ddot{u}_{1,\max}$ [m/s^2]	0.99	4.22

Table 2.9: Response calculation for the Phénix footbridge following HiVoSS [170] for a density d of 0.2 pers./m^2 and 1.0 pers./m^2.

2.4 Vibration evaluation

The response of a footbridge to pedestrian excitation is calculated following simplified methods or by means of detailed simulations of continuous pedestrian traffic. An evaluation of the response consists of selecting a characteristic response quantity and criteria for vibration comfort. Both items are discussed in the present section.

2.4.1 Characteristic response quantity

To evaluate the response, a relevant statistical quantity of interest is selected. In widely used design guides for the vibration serviceability assessment Sétra [9] and HiVoSS [170], the instantaneous peak acceleration in a time window with length T is considered. The peak value with a probability of 95% of non-exceedance ($\ddot{u}_{\max,95}(T)$, corresponding to the 95th percentile of the peak response) is evaluated. Alternatively, in [97], the root mean square (RMS) value of the acceleration response with a time window of 1s is used as a measure. For spectral approaches, the RMS is easily extracted as the square root of the area under the PSD [26].

In the remainder of this thesis, the 95th percentile of the instantaneous peak response is used as evaluation criteria in correspondence with [9, 170]. Assuming a Gaussian distribution of the instantaneous peak values, that value

is approximated as

$$\ddot{u}_{\max,95}(T) \approx \mu_{\ddot{u}_{\max}(T)} + 2\sigma_{\ddot{u}_{\max}(T)} \tag{2.67}$$

with $\mu_{\ddot{u}_{\max}(T)}$ and $\sigma_{\ddot{u}_{\max}(T)}$ the mean value and standard deviation, respectively. As suggested in [9, 170], the length of the time window corresponds to twice the time a pedestrian needs to cross the bridge, T_{cross} ($T = 2 \times T_{\text{cross}}$). It is assumed that the acceleration time history, for example calculated following the procedure from section 2.3.2, is stationary and ergodic. As used for wind engineering or earthquake engineering problems [49], the maximum response thus can be calculated using classical methods for linear random vibration [66, 242]. The mean value and standard deviation of the instantaneous peak value in a time window T are approximated according to [49, 54, 159, 161] as follows.

$$\mu_{\ddot{u}_{\max}(T)} = \left[\sqrt{2\ln(2\nu_e T)} + \frac{0.5772}{\sqrt{2\ln(2\nu_e T)}}\right]\sigma_{\ddot{u}} \tag{2.68}$$

$$\sigma_{\ddot{u}_{\max}(T)} = \left[\frac{1.2}{\sqrt{2\ln(2\nu_e T)}} - \frac{5.4}{13 + (2\ln(2\nu_e T))^{3.2}}\right]\sigma_{\ddot{u}} \tag{2.69}$$

with ν_e the modified expected frequency and $\sigma_{\ddot{u}}$ the standard deviation of the acceleration time history. The modified expected frequency ν_e can be derived from following empirical expression [54]:

$$\nu_e = (1.63q^{0.45} - 0.38)\nu \tag{2.70}$$

with ν [Hz] the expected frequency of the output signal calculated as $\nu = \sqrt{\frac{\lambda_2}{\lambda_0}}$ with $\lambda_i = \int_0^\infty f^i G_{\ddot{u}\ddot{u}}(f)df$ and q a spectral bandwidth parameter. $G_{\ddot{u}\ddot{u}}$ is the one-sided power spectral density function of the acceleration time history. ν thus can be interpreted as the frequency at which most of the energy is concentrated. The spectral bandwidth parameter q can be written as:

$$q = \sqrt{1 - \frac{\lambda_1^2}{\lambda_0\lambda_2}} \tag{2.71}$$

It is verified that the results closely approximate those of the direct peak extraction method for the prediction of human-induced vibrations [112] which is also illustrated in example 2.4. To obtain converged values for the spectral parameters and the peak response, a total simulation time of at least $50 \times T_{\text{cross}}$ is needed. Similar approaches for the evaluation of human-induced vibrations are used in [35, 212].

Example 2.4. Calculation of the instantaneous peak response

This example illustrates the calculation of the instantaneous peak response. First, the peak response is obtained by considering the statistical moments of the maximum values retained from different time windows (method I). Second, equations (2.68) and (2.69) are verified for the response calculation based on the standard deviation of the response (method II). In both cases, the instantaneous peak response is approximated using equation (2.67).

Method I

Consider the acceleration time history of continuous pedestrian traffic in figure 2.13(a). The instantaneous peak response in a time window of 40 s is calculated. For method I, the time history of the acceleration response is subdivided in relevant time windows with length T separated by a time shift Δ to exclude correlation (see detail in figure 2.13(a)). The instantaneous peak values are found as the maximum absolute acceleration in each time window. The mean value and standard deviation of the instantaneous maxima are calculated afterwards. The minimally required simulation time is relatively long to ensure convergence of the values for $\mu_{\ddot{u}_{\max}(T)}$ and $\sigma_{\ddot{u}_{\max}(T)}$. The autocorrelation of the acceleration response is calculated to identify the time lag for which uncorrelated time windows are ensured (see figure 2.13(c)). In this case, a time shift of $\Delta = 8$ s is used corresponding to a correlation lower than 10%. This results in 208 independent samples for the simulation time of 10000 s. The mean value and standard deviation of the instantaneous peak response according to method I equal 0.36 m/s^2 and 0.05 m/s^2 respectively. The standard error of the mean, calculated as $\sigma_{\ddot{u}_{\max}(T)}/\sqrt{(n)}$ with $n = 208$ representing the number of samples, equals 0.003 m/s^2.

Method II

For method II, the one-sided acceleration PSD is calculated using a Gaussian window function (figure 2.13(b)). The spectral parameters and instantaneous peak response are calculated and listed in table 2.10. The obtained instantaneous peak value equals $0.38+2\cdot0.04 = 0.46$ m/s^2 and is also indicated in figure 2.13(a).

An excellent correspondence for the calculated quantities is obtained for this specific example. It has been concluded in [112] that the calculation based on the second order statistics of the response (method II) slightly overestimates the mean value and underestimates the standard deviation of the instantaneous peak value. However, this method is preferred to method I since the computation time is much lower while an accuracy up to 5% is obtained.

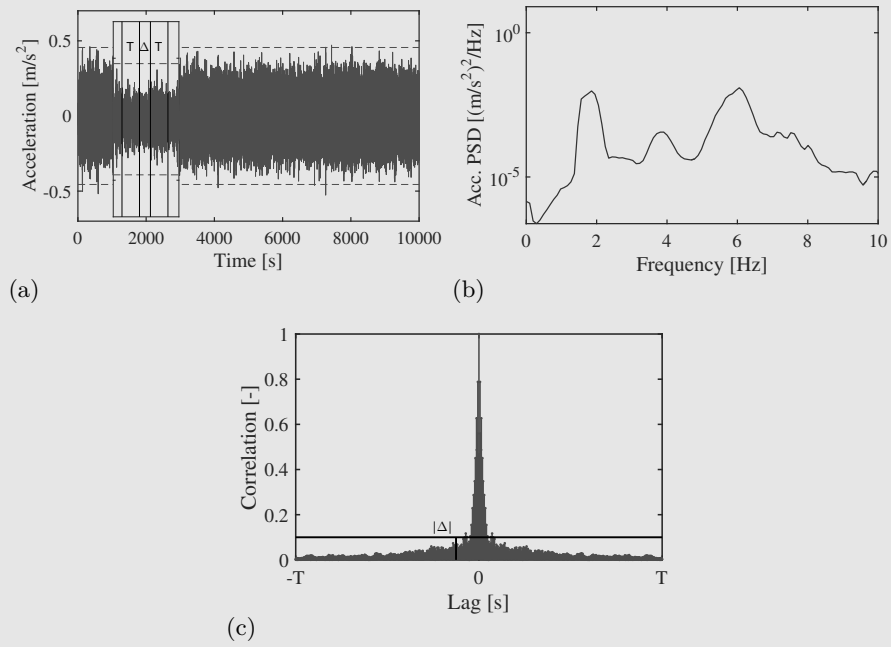

Figure 2.13: (a) Acceleration time history of continuous pedestrian traffic (–) with indication of 95th percentile of peak response (– –) and indication of time windows T and shift Δ in the zoom window. (b) PSD of the acceleration response. (c) Absolute value of the autocorrelation function of the acceleration time history.

Spectral moments	Spectral parameters	Response statistics
$\lambda_0 = 0.01$	$\nu = 4.99$	$\sigma_{\ddot{u}} = \sqrt{\lambda_0} = 0.11$ m/s^2
$\lambda_1 = 0.05$	$\nu_e = 3.57$	$\mu_{\ddot{u}_{\max(T)}} = 0.38$ m/s^2
$\lambda_2 = 0.29$	$q = 0.41$	$\sigma_{\ddot{u}_{\max(T)}} = 0.04$ m/s^2

Table 2.10: Calculation of the instantaneous peak acceleration for $T = 40$ s, estimated based on the standard deviation of the response (method II).

2.4.2 Vibration comfort scales

To define a scale for vibration comfort, human perception is linked to acceleration levels of the footbridge. Parameters influencing the perception of vibration are the body activity (standing, walking, etc.), the duration and intensity

Comfort scale	Vertical [m/s^2]	Horizontal [m/s^2]
maximum	≤ 0.50	≤ 0.10
medium	$0.50 - 1.00$	$0.10 - 0.30$
minimum	$1.00 - 2.50$	$0.30 - 0.80$
unacceptable	> 2.50	> 0.80

Table 2.11: Categories for vibration comfort and range for 95th percentile of peak accelerations (after [31]).

(amplitude) of the vibration, the frequency, the direction (vertical, horizontal), the predictability, etc. [12, 148]. Many studies investigated the human perception of machine-induced vibrations. The results of these studies are valuable to evaluate the acceleration levels. A historical overview of acceptance criteria for (floor) vibrations is given in [139]. General criteria for human perception of (vertical) vibrations are given in [21, 22] as a function of the dominant frequency and a response factor R is defined as a multiplier of the average threshold of human perception ($R = 1$). For outdoor footbridges, a maximum allowed response factor of 64 is proposed in [237]. The response factor R only accounts for the amplitude of the response and not for the duration. The vibration dose value (VDV) can be used alternatively as a quantity that weights the amplitude and the duration of vibrations [237].

In many international standards, a single scalar value for the maximum allowed acceleration is provided. That value may depend on the dominant frequency such as in [20, 146] or be a fixed value independent of the frequency [70]. Similar criteria are given for lateral vibrations. In [31], the pedestrians' opinion to the experienced acceleration levels after crossing a footbridge is questioned. Possible evaluation categories go from imperceptible, over perceptible to (strongly) disturbing. Based on these results, criterion for vibration comfort are defined for vertical and horizontal (lateral and longitudinal) vibrations (see table 2.11). These criteria are useful for an evaluation of the instantaneous peak value and have been adopted in the widely applied guidelines Sétra [9] and HiVoSS [170]. For three classes of vibration comfort (maximum, medium or minimum level of vibration comfort), a range of accelerations is given.

Special attention must be given to the lock-in phenomenon. In [31, 43], it is found that lateral acceleration levels in the interval 0.10–0.15 m/s^2 trigger lateral synchronisation and lock-in. For this reason, Sétra [9] and HiVoSS [170] limit the lateral accelerations to 0.10 m/s^2.

2.5 Sensitivity of the response to uncertainties

The vibration serviceability assessment of footbridges requires an accurate description of the human-induced loading and the dynamic behaviour of the structure. A mathematical model must be selected to describe the walking loading and assumptions are made for the modal parameters of the structure. However, variations in the natural frequency and modal damping are expected to strongly affect the assessment. In this section, various sources of uncertainty are distinguished and the sensitivity of the response to uncertainties in the modal parameters is illustrated. A methodology to account for the effect of these uncertainties will be proposed in chapter 3.

The effective stiffness of the footbridge may be uncertain due to a lack of knowledge on the material properties or the stiffness of the supports resulting in uncertainty in the values of the natural frequency. Assumptions for Young's modulus in the FEM may have a considerable influence on the effective stiffness. Other simplifications causing uncertainty in FE modelling are the possible stiffness effect of railings and the added mass of finishing layers (neglecting a small stiffness component) [24]. Time effects and degradation of the material properties also need to be considered [154]. Young's modulus of concrete increases during the first months after construction. In [130], a footbridge built from composite materials is discussed and it can be readily understood that the creep effects are larger for materials subjected for long time to high temperatures. For bearing supports, the dynamic stiffness with corresponding tolerances can be provided by the producer. The discrepancy between the static and dynamic behaviour of sliding pot bearings is observed for a case study in [221] and it is concluded that the apparent stiffness of the sliding bearings significantly decreases after overcoming an initial friction due to large movements at the supports. Bujňák et al. [28] reported that water dripping through open joints had damaged the bearing details, significantly affecting the dynamic behaviour of the structure. Furthermore, the performance of pot bearing strongly depends on the lubrication condition as observed in [92].

Intensive vibration monitoring of (foot)bridges has also learnt that daily and seasonal temperature and environmental changes affect the natural frequencies [90, 136]. Natural frequencies generally decrease with increasing temperature [58, 154]. Sohn in [194] states that temperature changes not only affect the stiffness but also the support conditions of the bridge. Similarly, Alampalli et al. [3] reported that frozen supports of the bridge resulted in an increased natural frequency. For a concrete slab bridge, Xia et al. [239] found a negative correlation between humidity and natural frequency but a positive correlation between humidity and modal damping. Possible sources of uncertainty for the modal damping are loosely fitted handrails, weak

connections between construction elements, foundation movements, material friction, etc. [78]. Assumptions for the modal damping are based on experience with similar structures. Performing measurements to experimentally identify the modal parameters helps to reduce the level of uncertainty.

Since most commonly used procedures as [9, 170] assume resonance, uncertainties in the modal parameters strongly affect the vibration serviceability assessment. The reduction coefficient to evaluate if resonance can occur with the expected loading frequencies depends on the natural frequency of the footbridge. Example 2.5 shows the sensitivity of the response calculation according to HiVoSS [170] to deviations in the natural frequency.

Example 2.5. Effect of uncertain natural frequency on the response calculation according to HiVoSS

The response calculation according to HiVoSS from example 2.3 is now repeated accounting for uncertainty in the natural frequency. The effect of deviations in the natural frequency on the assessment of vertical vibrations is illustrated for the first mode and a sparse pedestrian density of 0.2 pers./m^2. Up to 10% variation on the nominal value of the natural frequency is considered as proposed in [24, 217].

Table 2.12 summarises the modified values of the reduction coefficient ψ and the maximum acceleration. All other values remain identical as in example 2.3. In this specific case, the value of the natural frequency is on the increasing slope of the reduction coefficient ψ (see figure 2.14) so that the maximum acceleration increases for a higher value of the natural frequency.

A high sensitivity of the response to the effect of uncertainties in the natural frequency is observed. A decrease/increase of 10% for the natural frequency leads in this case to a response decrease/increase of 43%/18%. For other cases, the effect can be larger, e.g. when the natural frequency is in the narrow range between the first and second harmonic component of the loading for which the reduction coefficient is low. Furthermore, it is expected that the vibration serviceability assessment is even more sensitive to uncertainty in the modal damping ratio by equations (2.63) and (2.66).

f_1 [Hz]	$\psi(f_1)$ [-]	$\ddot{u}_{1,\max}$ [m/s^2]
$0.9f_1 = 1.47$	0.48	0.56
$1.0f_1 = 1.63$	0.84	0.99
$1.1f_1 = 1.79$	1.00	1.17

Table 2.12: Effect of uncertain natural frequency on reduction coefficient ψ and maximum response $\ddot{u}_{1,\max}$ for the response calculation for the Phénix footbridge following HiVoSS [170] for a density d of 0.2 pers./m^2.

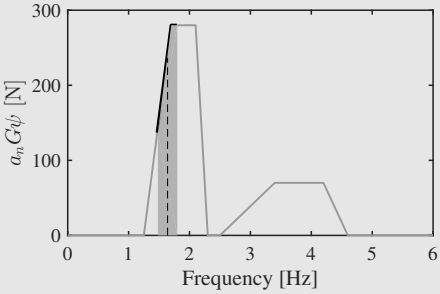

Figure 2.14: Reduction coefficient according to HiVoSS [170] for a density d of 0.2 pers./m^2 for the Phénix footbridge. Value at nominal conditions (– –) and considering up to 10% variation on the natural frequency (grey area).

2.6 Conclusion

For footbridges prone to human-induced vibrations, a response estimation is required to evaluate the dynamic behaviour. In this chapter, attention has been paid to the relevant aspects and assumptions that are needed further in this thesis related to both the dynamic behaviour of the structure and models for human-induced walking loading.

In the design stage, the natural frequencies and modes can be calculated by a FEM. An estimation of the modal damping is required and assumptions are made based on experience with similar structures. After construction, measurements can be performed to verify these calculations. The assumptions made for the modelling and temporary and seasonal variations in the modal parameters cause uncertainty, sometimes resulting in a significant discrepancy between the calculated and actual dynamic behaviour of the footbridge. For frequencies, deviations up to 10% are no exceptions. These uncertainties significantly affect the vibration serviceability assessment.

From the broad overview of models to describe the human-induced walking loading, it is clear that a large number of assumptions has to be made concerning the walking force, the inter- and intra-subject variability effects and concerning interaction phenomena, between pedestrians mutually and between crowd and structure. The assumptions needed for the response calculation are discussed for two selected methodologies: (1) simulations of realistic pedestrian traffic where advanced load models are considered and (2) a simplified and practical procedure frequently used by engineers and designers where HSI effects are disregarded. Following the latter method, it has been illustrated for a case study that a shift in the natural frequency of 10% may result in deviations in the calculated response up to 43%.

Since small deviations in the assumed dynamic behaviour of the footbridge strongly affect the response, a robust approach for the vibration serviceability assessment of footbridges is motivated. In the next chapter, uncertainties in the dynamic behaviour and variations in the loading are accounted for in the evaluation of vibration levels.

Chapter 3

Robust vibration serviceability assessment of footbridges

In the previous chapter, several models for walking loading and procedures for the response calculations which can be applied for the vibration serviceability assessment of footbridges, have been presented. A simplified method, assuming the contribution of only one mode to the response and considering resonance with one harmonic component of the loading, and a detailed method based on simulations of moving pedestrian excitation have been presented. For both, the response strongly depends on the assumed input variables related to the characteristics of the loading and dynamic behaviour of the structure. A comparative study of the response for different loading assumptions in [152] shows a high sensitivity to the stochastic modelling of the pedestrian step frequencies. However, the effect of uncertainties in the modal parameters has not been accounted for. Similarly, a probabilistic evaluation of the behaviour of the traversing pedestrians is considered in [27], but without consideration of uncertainties in the loading or structural parameters.

The objective of this chapter is to elaborate a methodology for the robust vibration serviceability assessment of footbridges. A generic methodology is aimed to account for the effect of uncertainties in the modal parameters. When different degrees of uncertainty are considered, the sensitivity of the response can be gradually evaluated. The procedure allows to account for variability in the loading characteristics as well.

First, different classifications of variation are given in section 3.1 together with an appropriate approach to deal with their effects. Second, a non-probabilistic

approach is selected to deal with uncertainties in the modal parameters of the footbridge (section 3.2). Third, variability in the walking loading is considered and it is indicated how variation on the proposed models from chapter 2 can be accounted for (section 3.3). Section 3.4 then presents the concept for the robust response evaluation based on multiple deterministic calculations. Different degrees of uncertainty are considered in the multi-level evaluation. In section 3.5, the effect of uncertainties in the modal parameters and variations in the walking characteristics on the response of a footbridge is illustrated.

3.1 Non-deterministic analysis

Structural designs are often based on detailed numerical models that rely on the assumptions made for material properties, loading characteristics, modelling simplifications, etc. Often, it is assumed that the input parameters are precisely known leading to a deterministic design. However, the resulting design may be sensitive to small deviations in the design variables. Therefore, non-deterministic designs are performed that deal with randomness in statistical parameters, design variables, measurements, etc. This section first gives the main terminology related to a non-deterministic analysis. Second, methods to deal with the different types of variation are discussed. Probabilistic and non-probabilistic methods are considered. Next, the concept of robustness and criteria to evaluate the robustness of the design are given.

3.1.1 Terminology

Variation is a general term to define randomness. Two main categories of variation are distinguished, each describing different types of randomness [18, 83, 133, 143].

On the one hand, **variability** or aleatory uncertainty, is variation *which is inherent to the modelled physical system or the environment under consideration* [60]. The variation is irreducible and refers to the natural variation of the quantity. Examples are the inherent variability in loading and material properties, humidity, temperature, manufacturing tolerances, etc. Information on the parameter is often available (e.g. defined by a range), however, the exact value cannot be determined. Aleatory uncertainty cannot be excluded. To deal with these non-deterministic variables, a **probabilistic approach** is typically used by assuming probability density functions of the random input variables if statistical parameters of the quantities are known [18, 133] (see section 3.1.2). A stochastic analysis is performed, such as Monte Carlo simulations.

On the other hand, (epistemic) **uncertainty** or vagueness is *a deficiency in any phase or activity of the modelling process due to lack of knowledge* [60]. Epistemic uncertainty can be reduced by increasing the knowledge about the item [29]. These uncertainties can be deterministic but not known [82]. They cover modelling assumptions and approximations, measurement error and inaccuracy, finite element discretisation, etc. If objective probabilistic information is not available [60], for example in the design stage, and only a deterministic value and/or a range of variation is given, non-probabilistic methods are recommended [138]. More specific, a **possibilistic approach** is proposed to deal with these uncertainties (see section 3.1.3). Interval approaches are widely used.

In civil engineering, typical sources of variation are both in the loading (wind, waves, earthquakes, etc.) as well as in structural characteristics (geometry imperfections, material properties as Young's modulus, damping characteristics, presence of cracks in concrete, etc.) [183]. The origin of variations in civil engineering is generally categorised in following five types [29]: (1) time effects (e.g. concrete strength and shrinkage in time or varying load characteristics); (2) statistical limits of the assumptions made for load models or material properties; (3) model errors due to simplifications in the numerical modelling and material behaviour theory; (4) randomness in the deterministic characteristics of variables; (5) human error (e.g. limited construction precision). Most of the variations can be subdivided in one of these five categories. However, none of these categories exclusively contain epistemic or aleatory uncertainties.

The further discussion of both the probabilistic and non-probabilistic approaches in this section is limited to the concepts needed in this thesis.

3.1.2 Probabilistic approach

The probability theory is a popular framework to deal with variations if probabilistic information of the input variables is available and/or if a probabilistic analysis of the output is required [133]. In [67], a profound introduction to the concepts of the probability theory is given. An overview of more recent advances to model structural uncertainties in computational dynamics is given in [195]. The basic concepts of a probabilistic analysis are stated below.

The probability that a variable x lies in the interval $[a, b]$ is calculated from its probability density function (PDF) $f_X(x)$ as follows:

$$\Pr(a \leq x \leq b) = \int_a^b f_X(x)\, dx \tag{3.1}$$

where $\Pr(\cdot)$ denotes the probability that the expression between parenthesis is true. The probability can be interpreted in two ways. First, it represents the frequency that a value occurs or that an event happens for example in repetitive experiments or large scale product design (frequentist perspective). Second, it represents the likelihood that the value occurs, or the likelihood that the value is in a predefined interval (Bayesian perspective). The latter interpretation is more useful in the context of uncertainty analysis.

The PDF of the output quantity of interest is obtained by performing a stochastic analysis of the propagation of uncertainty using the PDFs of the input variable. Usually, statistical moments of the output PDF (expected value, standard deviation, percentiles) or extreme value distributions are of interest to designers. In probability-based structural designs, a predefined reliability is typically targeted [5, 18, 184, 226]. Complementary to the system reliability is the probability of failure p_F, defined as the probability that a system does not satisfy the design criteria, calculated as follows:

$$p_F = \Pr(g(x) \leq 0) = \int_{g(x)\leq 0} f_X(x)\, dx \tag{3.2}$$

with $g(x)$ the performance function of the output. For values of $g(x) \leq 0$, predefined design criteria are not satisfied (failure). This formulation is often used in risk analysis where the risk is defined as the probability (likelihood) that an event will fail, multiplied by a factor representing the consequences of the event.

Practical approximations are often used to calculate the probability of failure such as Monte Carlo simulations or first and second order reliability moments (FORM/SORM) [84]. Many civil engineering applications are designed based on FORM/SORM analysis as prescribed in Eurocode standards. The trustworthiness of high-reliability designs is questionable [133] since the total number of samples must be sufficiently high to obtain a reliable estimate of the failure probability. Advanced methods such as importance sampling are then recommended [184]. Using parallel computing techniques, the calculation time can be strongly reduced.

The main disadvantages of probabilistic methods in engineering are the lack of statistical data for the definition of the PDF, the sensitivity of high reliability designs to small inaccuracies in the PDF, the practical use and verifiability of a very low probability of failure, etc. [67].

3.1.3 Non-probabilistic approach

When no objective probabilistic information of the design parameters is available, non-probabilistic methods can be used. Non-probabilistic methods such as (convex) interval analyses and fuzzy analyses gain popularity to deal with uncertainties. Compared to a probabilistic approach, less information is required for an interval analysis, which is usually the case in the design stage. Values for the lower and upper bound of the interval are required while for probabilistic models, information on the full joint PDF is needed. Below, a selection of non-probabilistic methods needed in this thesis is given. In particular, the concept of fuzzy arithmetic and fuzzy analysis is summarised starting from a classical interval analysis.

Interval analysis

In interval analysis, an uncertain but bounded interval scalar $\mathbf{x}$ is considered as a set of scalars in a continuous range of possible values lying between a lower bound $\underline{x}$ and an upper bound $\bar{x}$ as follows.

$$\mathbf{x} = \{x | (x \in \mathbb{R})(\underline{x} \leq x \leq \bar{x})\} \tag{3.3}$$

Calculations for interval analyses are typically performed using deterministic methods. The deterministic analysis of the discrete values of the uncertain variable x by a performance function $f(x)$ results in an interval of the output $\mathbf{y}$:

$$\mathbf{y} = \{y | (x \in \mathbf{x})(y = f(x))\} \tag{3.4}$$

The bounds of the interval strictly define if the scalar is a member or non-member of the interval. The interval scalar thus can be interpreted as a crisp set. The interval analysis is useful if a possible range of values is known [133]. A worst case design corresponds with an interval analysis where the least favourable value is retained. Performance criteria are satisfied within an acceptable range of uncertainties. The design results in a crisp distinction between acceptable or unacceptable performance.

Fuzzy sets

Fuzzy sets are usually interpreted as an extension of conventional crisp sets (intervals) [132]. In crisp sets, the space is strictly divided in member or non-member samples, defined by the bounds of the interval. In fuzzy sets, a value of membership is assigned to the samples, representing a degree of

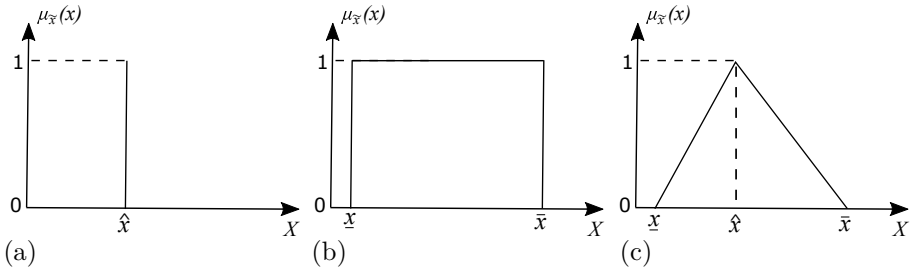

Figure 3.1: Membership function of (a) a deterministic number, (b) a crisp set or conventional interval and (c) a fuzzy set with triangular membership function.

belongingness of the sample to the set. The concept of fuzzy sets was introduced by Zadeh [244, 245]. A fuzzy set $\tilde{x}$ is characterised by its corresponding membership function $\mu_{\tilde{x}}(x)$ for all values of x in the domain X as follows:

$$\tilde{x} = \{(x, \mu_{\tilde{x}}(x))|(x \in X)(\mu_{\tilde{x}}(x) \in [0,1])\} \tag{3.5}$$

The fuzzy set is normalised if all the values of the membership function are in the interval $[0,1]$. For $\mu_{\tilde{x}}(x) = 1$, x is definitely a member of the set and for $\mu_{\tilde{x}}(x) = 0$, x is definitely not a member. More information and applications of the fuzzy arithmetic are found in [60, 83, 133, 135].

A deterministic number can be interpreted as a fuzzy number for which the degree of membership is one for the nominal value $\hat{x}$ and zero for all other values. Similarly, a conventional set (interval) is a fuzzy number for which the degree of membership is the same in the design domain. In figure 3.1, a comparison is given between the fuzzy interpretation of a deterministic number, a crisp set and a fuzzy set with triangular membership function.

Fuzzy analysis

For the practical implementation of fuzzy variables, the membership function is discretised into different values α. For each value, the interval width of the α-cut set is determined by the shape of the membership function. The α-cut set of a fuzzy set $\tilde{x}$ is a set of individuals for which the membership function value is higher than α. For a convex fuzzy set (with closed intervals), the α-cut set $[\tilde{x}]_\alpha$ is defined as:

$$[\tilde{x}]_\alpha = \{x \,|\, \mu_{\tilde{x}}(x) \geq \alpha\} \tag{3.6}$$

The α-cut set strategy is used to define uncertainty intervals for the variable. The value of α refers to a level of uncertainty. The higher α, the higher the level of membership and the more possible the value of the variable. Often, triangular membership functions, denoted as $\tilde{\Lambda}$, are assumed for the fuzzy variable as:

$$\tilde{x} = \tilde{\Lambda}(\hat{x}, \underline{x}, \bar{x}) \tag{3.7}$$

with $\hat{x}$ the nominal value of $\tilde{x}$ and $\underline{x}$ and $\bar{x}$ the lower and upper bound respectively, at the basis ($\alpha = 0.0$). Alternatively, Gaussian shaped membership functions are also frequently used [133].

The evaluation of a function at different α-levels results in a fuzzy set of the output for different levels of uncertainty. In this way, a gradual evaluation of the uncertainties is performed. To construct the membership function of the output, the minimum and maximum value of the objective function must be determined for all values of the α-level intervals considered in the analysis. The fuzzy analysis is transformed to a discrete set of interval problems:

$$\tilde{y} = f(\tilde{x}_1, \tilde{x}_2, \ldots, \tilde{x}_k) \Leftrightarrow [\tilde{y}]_\alpha = f([\tilde{x}_1]_\alpha, [\tilde{x}_2]_\alpha, \ldots, [\tilde{x}_k]_\alpha), \quad \forall \alpha \in [0, 1] \tag{3.8}$$

with f the performance as a function of the fuzzy variables $\tilde{x}_1, \tilde{x}_2, \ldots, \tilde{x}_k$. The values of the membership function of the output are obtained by solving the next constrained optimisation problem:

$$f([\tilde{x}_1]_\alpha, [\tilde{x}_2]_\alpha, \ldots, [\tilde{x}_k]_\alpha) \Leftrightarrow \begin{cases} [\tilde{y}]_\alpha^- = \min(f(x_1, x_2, \ldots, x_k)) \\ [\tilde{y}]_\alpha^+ = \max(f(x_1, x_2, \ldots, x_k)) \end{cases}, \forall x_i \in [\tilde{x}_i]_\alpha \tag{3.9}$$

Different methods to solve the optimisation problem are summarised in [51, 132]. Three types of algorithms are discussed below. (1) A first manner to construct the output membership function are vertex methods [61] which are based on deterministic function evaluations. Two different subtypes are considered. (1i) In the short transformation method (STM) [81], the objective function is evaluated at each α-level for each combination of the lower and upper bound values of the input variables. Only the minimum and maximum possible value of the $[\tilde{x}_i]_\alpha$ interval is considered (see figure 3.2(a)). The total number of function evaluations for the method is $n_\alpha \times 2^{n_x}$ with n_α the number of α-levels and n_x the number of variables. A bad performance for non-monotonic functions is expected because only the extreme values are evaluated at each α-level. (1ii) This can be solved by performing a grid search. Instead of the values at lower and upper bound for each variable, an equidistant sampling is proposed per α-level. For all combinations of the sampled values for the different variables, a dense grid arises for each α-level. The size of the grid decreases for a higher α-level. On each α-level, the grid is formed by j^{n_x} points with j decreasing for higher α-levels. The total number of function evaluations thus equals $\sum_{k=1}^{n_\alpha} j_k^{n_x}$. The number of function evaluation is strongly reduced, however,

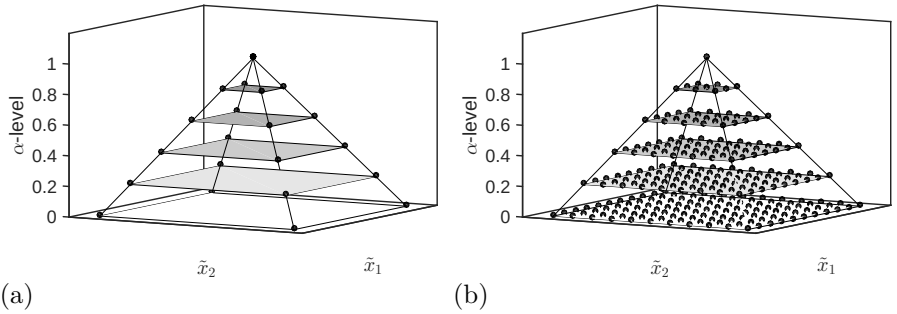

Figure 3.2: Joint membership function of two fuzzy variables with indication of discrete intervals according to the (a) short transformation method [81] and (b) grid search with equidistant sampling.

when the discretisation used at $\alpha = 0.0$, covers the grids of all higher α-levels (figure 3.2(b)). In example 3.1, the working principle and interpretation of such a fuzzy analysis is illustrated. (2) Second, conventional optimisation routines such as genetic algorithms or sequential quadratic programming are used to find the minimum and maximum value at each level. (3) Third, the gradual α-level decreasing (GαD) algorithm [51] is developed to find all local optima for different α-levels in order to obtain the global optimum. The general idea is that search paths are constructed to connect the local minima between different α-levels. Initial search paths starting from the highest α-level are elongated to lower levels or may detect new search paths when partial derivatives of one of the variables become zero and cross the initial path. The advantage of the method is that information is exchanged between different levels.

Example 3.1. Fuzzy analysis

Consider two fuzzy variables, $\tilde{x}_1$ and $\tilde{x}_2$, defined by their triangular membership function as follows:

$$\tilde{x}_1 = \tilde{\Lambda}(2, 0.9, 4) \tag{3.10}$$

$$\tilde{x}_2 = \tilde{\Lambda}(1, 0.5, 1.5) \tag{3.11}$$

A fuzzy analysis of following performance function is evaluated:

$$f(x_1, x_2) = 150 + (x_1 - 9)^3 + 10(x_2 - x_1^2)^2 \tag{3.12}$$

As the input variables are fuzzy numbers, the output is also a fuzzy number. To solve the problem, the grid search method with an equidistant sampling is

selected. No interaction between the two fuzzy input variables is considered here, implying that all combinations of the interval scalars are equally possible. For smoothness of the membership function of the output, a dense discretisation of 200 α-levels is chosen. The membership function of both the fuzzy input variables and the fuzzy output variable is given in figure 3.3.

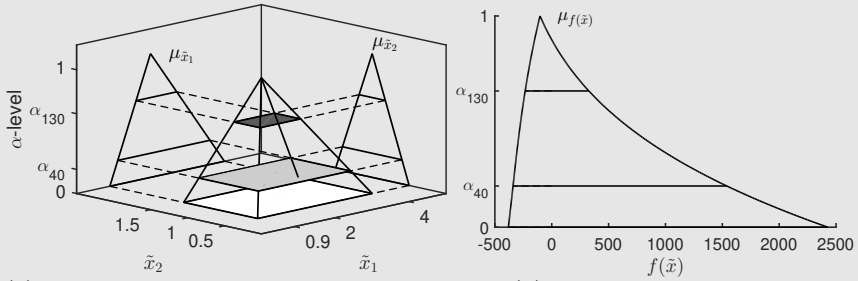

Figure 3.3: Membership function with indication of two selected α-cut sets of (a) the input variables $\tilde{x}_1$, $\tilde{x}_2$ assuming no interaction for the joint membership function and (b) the output function $f(\tilde{x}_1, \tilde{x}_2)$.

3.1.4 Robustness

Robustness in its strict meaning refers to the insensitivity of the design to the effect of uncertainties, within a feasible region [107]. A robust design is characterised by a performance not affected by uncertain conditions [18]. However, the term *robust* is in general frequently used for designs where the effect of uncertainties is accounted for. The concept of robustness was first introduced by Taguchi in the 80s [208]. Knoll and Vogel in [104] define robustness as the ability of a system to satisfy performance in unusual circumstances. Their *survival of the system function* indicates that the obtained performance or design criteria (*the system function*) are preserved (*survival*) in unexpected situations for a predefined period of time. Examples are the resistance of structures to (unexpected) loads, to environmental changes, to human error in construction, etc. Robustness is then interpreted as a measure for the safety of the structure superior to the conventional design criteria. The desired level of robustness depends on the structure's life time but also on the consequences of possible damage and reparation costs. Robustness in this thesis follows this definition [104]. In particular, the vibration comfort of footbridges subject to walking loading (*the system function*) must be guaranteed under uncertainties in the modal parameters and variability in the loading (*survival*).

Many methodologies are developed in engineering applications to evaluate the effect of uncertainties aiming at a robust design. Literature reviews of design methodologies are given in [18, 150, 184, 246]. The approaches for the robust design are mainly classified into two categories: (1) probabilistic and (2) worst case approaches. Below, a summary is given for each of the methods explaining how robustness of the performance can be measured and included in the design.

Measures of robustness for probabilistic methods

In probabilistic approaches, probability density functions for the input variables are assumed representing the likelihood of occurrence. Variation of the output quantity of interest is investigated by uncertainty propagation methods such as Monte Carlo simulation. Different types of measures for robustness are distinguished for these probabilistic methods.

First, a reliability based measure is used for the robustness of the system function by calculating the probability of failure of the design (see equation (3.2)). This reliability index is often determined by the statistical moments of the output function such as the expected value, standard deviation or percentile values [184]. In FORM/SORM analysis, the reliability index is directly used to evaluate the robustness of the system function. In [167], an overview is given of different measures and probability based safety factors to (inversely) calculate the reliability index. In figure 3.4(a), two designs are compared with the same failure domain but a different reliability index. The design with the highest reliability index (lower probability of failure) is characterised by a lower performance at nominal conditions.

Second, the strict interpretation of a robust design can be selected as a measure for robustness. The variance of the output is evaluated, rather than a probability of failure [18]. The difference between a reliability measure and a measure of robustness of the system in its strict meaning (minimal variance) is visualised in figure 3.4(b). Compared to a conventional design, the obtained robust design is much less sensitive to variations or uncertainties in random input parameters. This is illustrated in figure 3.4(c), showing a smaller performance variation for the more robust design. In real-life designs, a trade-off between performance and minimal variance (robustness) is often desired. Therefore, the design is evaluated using a combination of the expected value of the output, as a measure for performance, and the standard deviation, as a measure for robustness [59, 62].

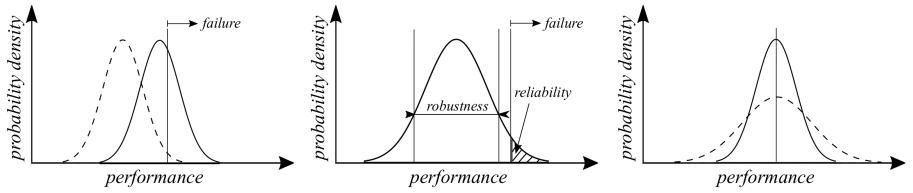

(a) (b) (c)

Figure 3.4: (a) Design with high (– –) and low (–) reliability index, (b) robustness versus reliability and (c) less (– –) versus more (–) robust design (after [101]).

Measures of robustness for non-probabilistic methods

As discussed in section 3.1.3, the uncertain variables are bounded and modelled using intervals or fuzzy sets in non-probabilistic methods. This results in interval fields or ellipsoids for multi-variate problems. Using these (fuzzy) interval methods, alternative measures for robustness must be defined. The width of the membership function of the output can be used to evaluate the robustness of the design [134]. Two other approaches proposed in [62] are discussed below.

First, the combination of uncertainties in the design variables leading to the worst possible output is selected (worst case approach). This requires a sufficiently fine discretisation of the intervals for all uncertain variables (e.g. grid search with equidistant sampling from figure 3.2(b)). This analysis is rather conservative since the worst possible combination of all variables simultaneously is assumed. However, this measure is widely used due to its simplicity. The computational cost of the analysis can be estimated in advance since no convergence of statistical moments is required for a sufficiently large number of samples. By considering different levels of uncertainty (for example corresponding to α-levels of fuzzy sets), the effect of uncertainty can be gradually evaluated assuming the worst case values at each level.

Second, the so-called *corner space* method [62] is a variant for the worst case approach. Tolerance values are considered to define a bounding box around the nominal values of the input variables. The robustness is assessed by evaluating the performance function for the outer values of the box (corners), similar to the short transformation method (figure 3.2(a)). The aim is here to ensure robustness within a feasible range of input variables. The method can only be used for monotonic functions since no intermediate values of the intervals are considered. For more information on this method, the interested reader is referred to [199].

In both of these methods, robustness is not evaluated by explicitly considering the variance of the output but by evaluating the design performance under all uncertain circumstances.

3.2 Accounting for uncertain modal parameters

The vibration serviceability assessment requires information on the modal parameters of the footbridge and the loading. In this section, a generic approach is elaborated to account for uncertainties in the modal parameters. First, an appropriate approach to deal with the non-determinism of the modal parameters is selected. Second, fuzzy intervals are defined for the modal parameters allowing for an evaluation for different degrees of uncertainty. Third, it is indicated how combinations of uncertain modal parameters are dealt with.

3.2.1 Selected approach

Since it is difficult to assume a probability density function for the modal parameters, a non-probabilistic approach is proposed. In [42], variation on the nominal values of the modal parameters is modelled considering tolerance values. This thesis considers the modal parameters similarly as uncertain but bounded parameters. In the proposed approach, the uncertainty in the modal parameters of the footbridge is characterised by a multiplication factor β which is modelled as a convex fuzzy number. This fuzzy number is assumed to lie in an interval for which the minimum and maximum value depends on the membership function $\mu_{\tilde{\beta}}$. The value of the membership function is situated between 0 and 1 and represents a degree of possibility of occurrence rather than a degree of probability. The multi-level analysis is performed by cutting the membership function in multiple α-levels between 0 and 1 and each level corresponding to a different degree of uncertainty. The value $\alpha = 1.0$ refers to the highest possibility of occurrence and corresponds to the analysis with nominal values. For intermediate values of α, the boundaries of these intervals increase linearly for a higher level of uncertainty. This multi-level approach allows assessing the sensitivity of the vibration serviceability assessment to a change in the modal parameters of the structure.

3.2.2 Membership functions of modal parameters

Three multiplication factors are introduced to account for the uncertain modal parameters: β_{f_j}, β_{ξ_j} and β_{m_j} for the natural frequency, the modal damping

ratio and the modal mass, respectively, of mode j. For the sake of simplicity, no uncertainty on the mode shape is considered but only uncertainty on the normalisation is assumed. A multiplication factor is applied to the modal mass m_j rather than to the vector of modal displacements $\boldsymbol{\phi}_j$. Assumptions must be made for the interval bounds of the modal parameters corresponding to the largest level of uncertainty ($\alpha = 0.0$).

For the **natural frequency**, the interval bounds of the multiplication factor correspond to 10% deviation on the nominal value of the natural frequency [24, 217] for the highest level of uncertainty ($\alpha = 0.0$). The nominal values of the natural frequency at the level $\alpha = 1.0$ correspond to the case without uncertainty. The triangular membership function of the multiplication factor for the natural frequency thus reads:

$$\tilde{\beta}_{f_j} = \tilde{\Lambda}(1, 0.9, 1.1) \tag{3.13}$$

Uncertainty in the **modal damping ratio** is modelled similarly although in this case a wider range of uncertainty is considered for the highest level of uncertainty ($\alpha = 0.0$). For steel footbridges, a discrepancy of 50% is reported between the minimum value and the average value of the modal damping ratio in design guides [9, 170]. A similar range of uncertainty is observed in [171, 172] for experimentally identified values and for amplitude dependent damping ratios in [10]. The membership function for the multiplication factor of the modal damping ratio is defined as:

$$\tilde{\beta}_{\xi_j} = \tilde{\Lambda}(1, 0.5, 1.5) \tag{3.14}$$

Little is found in literature on the uncertainty in the **modal mass**. In [25], an accuracy up to 15% is obtained for the experimental identification using human-induced vibrations as input. Therefore, the triangular membership function for the multiplication factor of the modal mass is defined as:

$$\tilde{\beta}_{m_j} = \tilde{\Lambda}(1, 0.85, 1.15) \tag{3.15}$$

The membership functions for the multiplication factors of the modal parameters are visualised in figure 3.5. A grey scale is added to denote the level of uncertainty of the membership function. The lighter the shade of grey, the larger the level of uncertainty considered. A discretisation of the membership functions in six equally spaced α-levels is used. These intervals will be considered in all further analyses in this thesis.

3.2.3 Combining uncertain modal parameters

When the contribution of multiple modes is considered in the calculation, it is assumed that the uncertainties are of a general nature, in a sense that they

affect the natural frequency of all modes in an identical way ($\beta_{f_j} = \beta_f$). A similar argumentation is followed for the modal damping ratio ($\beta_{\xi_j} = \beta_\xi$) and the modal mass ($\beta_{m_j} = \beta_m$). Furthermore, the same level of uncertainty α will be considered for all uncertain modal parameters. Alternatively, different levels of uncertainty for all parameters can be used too, for instance if the uncertainty in the natural frequencies can be reduced after measurements.

The evaluation of the fuzzy intervals for different uncertain variables consists of an optimisation problem in a multidimensional space. For the modal parameters of a footbridge, this results in a three-dimensional space. In figure 3.6, a visualisation is given of the joint membership function of all modal parameters. The centre point of the hypercube corresponds to the situation where the nominal values of the modal parameters are considered ($\alpha = 1.0$). The grey scale holds since the assumption is made that the same α-level holds for all parameters.

3.3 Accounting for variability in loading

Compared to the interval-based approach to deal with uncertainties in the dynamic behaviour of the structure (section 3.2), a different approach is to be followed to account for variability in the loading. In this section, it is indicated how variabilities in the loading characteristics can be accounted for in the presented robust vibration serviceability assessment of footbridges. The focus is on the implementation of variability in the detailed load models for the simulations of moving pedestrian excitation (section 2.3.2). First, assumptions for the pedestrian characteristics are made considering the effect of inter- and intra-subject variability. Second, it is indicated how additional variation on the walking characteristics can be included.

3.3.1 Inter- and intra-subject variability

By simulating moving pedestrian traffic, the pedestrian characteristics (step frequency, trajectory, walking speed) and human body parameters (weight, natural frequency, damping) are sampled from the corresponding distributions to account for inter- and intra-subject variability. Many of these parameters are described by a model in literature (see for example in tables 2.5, 2.6 and 2.7). Below, the nominal conditions of the flow are defined by selecting an appropriate model or values for the walking parameters. These nominal conditions will be assumed in all further analyses in this thesis, unless stated otherwise.

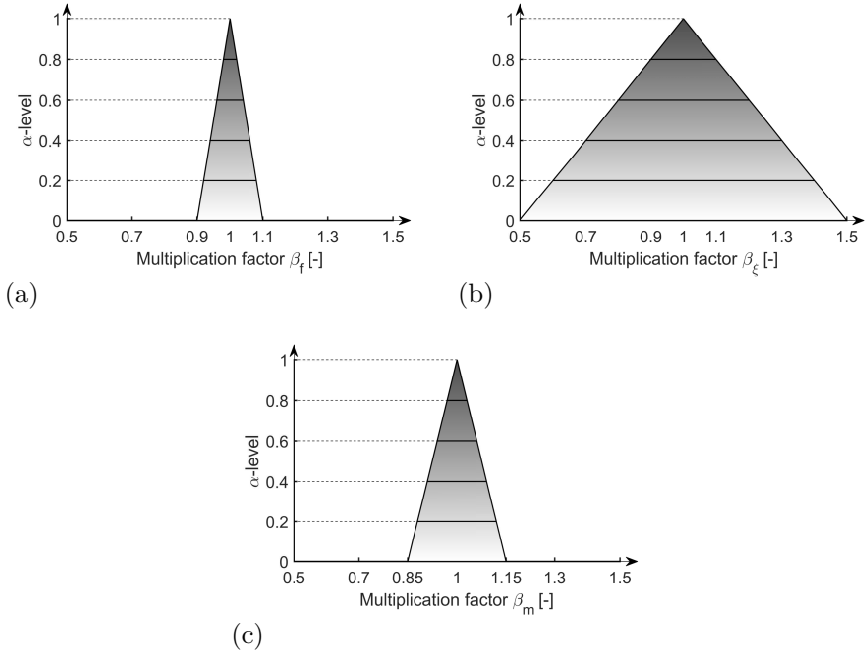

Figure 3.5: Multi-level approach for the multiplication factor at different levels of uncertainty α for (a) natural frequency, (b) modal damping ratio and (c) modal mass.

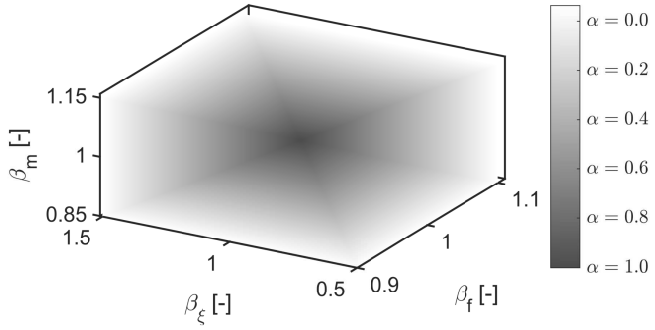

Figure 3.6: Joint membership function for uncorrelated values of the uncertain natural frequency, modal damping ratio and modal mass.

For the pedestrian weight G and walking speed v_s, deterministic values are assumed and no inter-subject variability is considered in line with [152]. The weight of each pedestrian is set to a fixed value of 700 N and the walking velocity is determined by the pedestrian density d using equation (2.38). The step frequency f_s is modelled stochastically assuming a normal distribution with mean value obtained from equation (2.39). Numerical values for the average free walking speed $\bar{v}_s$, the coefficient for travel purpose γ and the jam density d_{jam} are provided in example 2.2. The standard deviation of the step frequency is determined by the density (table 2.7). For σ_{f_s}, the values proposed in [31] are assumed: 0.1 Hz for $d < 1$ pers./m^2 and 0.05 Hz for $d \geq 1$ pers./m^2. The step length l_s depends on the pedestrian step frequency and walking speed and is calculated using equation (2.31). As a consequence, the longitudinal position x of the pedestrian is directly determined by its walking speed and step length (and thus indirectly also by the pedestrian density and step frequency). The lateral position y is sampled from a uniform distribution, covering the width of the bridge w. No intra-subject variability is explicitly considered for the walking characteristics since its effects are mainly covered by the inter-subject variability [219].

To account for human-structure interaction in the response, the pseudo moving crowd model is used [219]. In section 2.3.2, the equations of motion for the coupled crowd-structure system have been derived. The natural frequency and damping ratio of the human body are selected to represent walking postures. The distributions proposed by [219] are selected from table 2.6 to consider inter-subject variability.

A summary of all selected values for the walking characteristics and human body parameters is given in table 3.1 for the nominal conditions of the flow. It is indicated whether the values are used deterministically or modelled in a stochastic way. References to the relevant paragraph(s) or table(s) from the previous chapter 2 are added in the last column.

3.3.2 Variation on average pedestrian characteristics

The walking characteristics provided in section 3.3.1 allow to compose a flow of moving pedestrian traffic accounting for inter-subject variability. One of the models is selected in tables 2.5, 2.6 and 2.7. Alternatively, the vibration serviceability assessment can be performed for combinations of the different models. Such comparative study is performed in [152] considering different models for the pedestrian step frequency, the stride length, the dynamic loading factors and the weight. It is concluded that the response is most sensitive to the assumptions made for the stochastic modelling of the step frequency. For other

Parameter			Type	Value	Reference
Walking characteristics					
Walking speed	v_s	[m/s]	deterministic	eq. (2.38)	table 2.5
Step frequency	$f_s(v_s)$	[Hz]	normal	$\mathcal{N}\left(\bar{f}_s, \sigma_{f_s}\right)$	
	$\bar{f}_s$	[Hz]		eq. (2.39)	table 2.5
	σ_{f_s}	[Hz]		0.10 or 0.05	table 2.7, [31]
Step length	l_s	[m]	defined by f_s and v_s		eq. (2.31)
Longitudinal pos.	x	[m]	defined by v_s and l_s		
Lateral pos.	y	[m]	uniform	$\mathcal{U}(0, w)$	
Human body parameters					
Weight	G	[N]	deterministic	700	fixed value
Natural frequency	f_{H}	[Hz]	normal	$\mathcal{N}(3.25, 0.32)$	table 2.6, [219]
Damping	ξ_{H}	[-]	normal	$\mathcal{N}(0.30, 0.05)$	table 2.6, [219]

Table 3.1: Selected values for the walking characteristics and human body parameters at nominal conditions of the flow for simulations of moving pedestrian traffic.

variables, deterministic values can be used. A procedure that allows accounting for additional variability on the pedestrian step frequency is therefore presented below.

The key aspect of the methodology is that an interval is defined in which the average value of the step frequency can vary. By considering different possible values of the mean step frequency in the interval, a range of responses is obtained. The interval for the mean value of the step frequency μ_{f_s} then is defined as follows:

$$\mu_{f_s} \in [\bar{f}_s - \Delta_{\mu_{f_s}}, \bar{f}_s + \Delta_{\mu_{f_s}}] \tag{3.16}$$

with $\Delta_{\mu_{f_s}}$ the variability considered on the average value of the step frequency. Based on the values of average step frequencies provided in table 2.2, an interval width of 0.2 Hz is chosen for μ_{f_s} such that $\mu_{f_s} \in [\bar{f}_s - 0.1, \bar{f}_s + 0.1]$. The fixed step frequency $f_{s,k}$ of each pedestrian k in the simulation is sampled from a normal distribution for which the mean value is situated in the interval defined in equation (3.16). The walking velocity of pedestrian k is still determined by the pedestrian density through equation (2.38) and remains the same for all pedestrians for the selected density d.

In this thesis, additional variation is only considered for the step frequency as this is the most important walking loading parameter in the response calculation [152]. However, the same approach can be followed for other pedestrian characteristics

or for the human body parameters if HSI is considered. Alternative values defining the distributions of the natural frequency and damping of the human body are summarised in table 2.6.

3.4 Robust response evaluation

The robust vibration serviceability assessment consists of multiple deterministic response calculations for different values of the modal parameters and loading characteristics as summarised in [111]. In this section, it is first discussed how the intervals of the uncertain modal parameters are combined with that of the step frequency. Second, it is indicated how the fuzzy analysis is applied for the response evaluation. For multiple degrees of uncertainty corresponding to different α-levels, the range of responses is calculated.

3.4.1 Nested response calculation

The fuzzy intervals introduced in section 3.2 and the interval for the average step frequency from section 3.3 are used to account for uncertainties in the modal parameters and for variabilities in the walking, respectively. For each pedestrian density, a nested response calculation is performed by considering all possible combinations of the values from each interval. For computational reasons, a discretisation of the intervals is required.

If only variability in the loading is considered (and $\alpha = 1.0$ for the modal parameters), the total number of calculations only depends on the discretisation of the interval for μ_{f_s}. At a lower α-level, the number of calculations depends on the discretisation of the intervals for β_f, β_ξ and β_m. For each possible combination of the values for $\beta_f(\alpha)$, $\beta_\xi(\alpha)$ and $\beta_m(\alpha)$, the response of the bridge to the generated flow is calculated deterministically with each possible value for μ_{f_s}. The response can be calculated for different locations at the bridge and for multiple directions (vertical, lateral, longitudinal). The 95th percentile of the instantaneous peak value is retained.

The flowchart in figure 3.7 illustrates the procedure for the robust vibration serviceability assessment. On the left-hand side, the fuzzy interval approach to account for uncertainty in the modal parameters is visualised. On the right-hand side, assumptions for the loading are made and variability on the average step frequency is considered. The intervals for all parameters are combined, resulting in a large number of deterministic calculations. The robust evaluation then consists of selecting the relevant peak response.

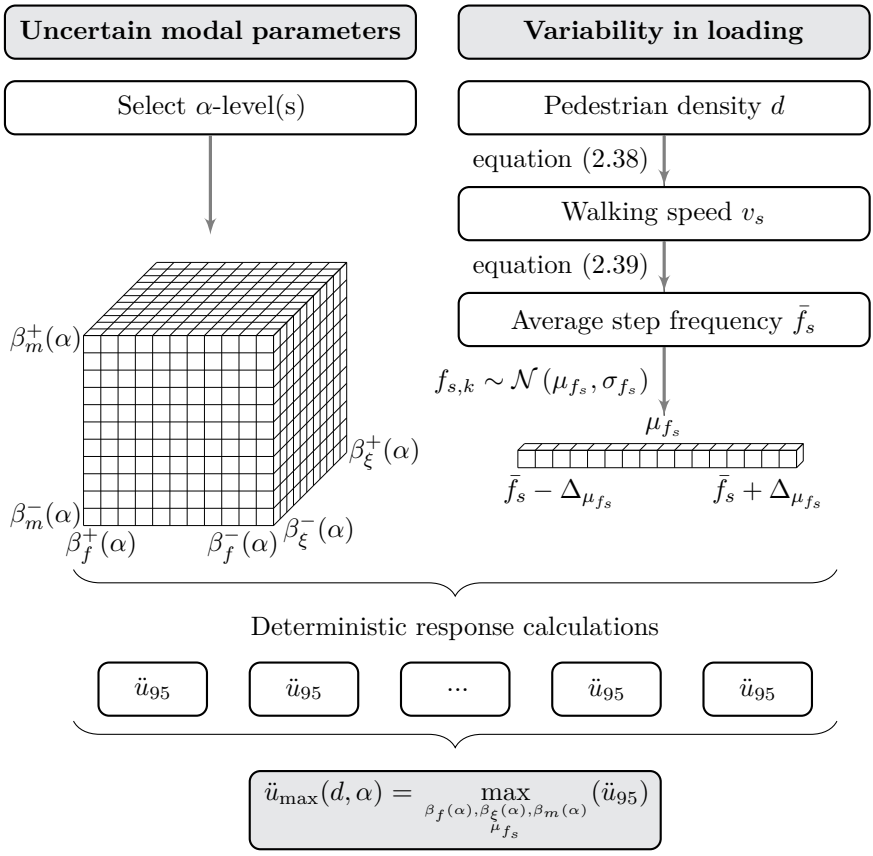

Figure 3.7: Flowchart for the robust vibration serviceability assessment.

It is important that the discretisation of the intervals is sufficiently fine. For the values of the average step frequency, an accuracy up to 0.01 Hz is desired resulting in an interval for μ_{f_s} of 21 values (equation (3.16)). The discretisation of the interval for the natural frequency requires the same accuracy (0.01 Hz) such that a perfect match between the step frequency and the natural frequency is possible (resonance). Depending on the magnitude of the natural frequencies, an appropriate discretisation for β_f must be selected. For the multiplication factors of the modal damping and the modal mass, β_ξ and β_m respectively, a coarser discretisation is proposed.

3.4.2 Fuzzy response analysis

A single representative value must be selected from the large number of responses in the vibration serviceability assessment. A best and worst case approach is followed here to consider the full range of possible values. The discretisation of the membership function in α-levels is useful for a gradual evaluation of the effect of uncertainties in the modal parameters. For a selected pedestrian density d, the best case value $\ddot{u}_{\min}(d,\alpha)$ and the worst case value $\ddot{u}_{\max}(d,\alpha)$ are by definition of the membership function found as:

$$\ddot{u}_{\min}(d,\alpha) = \min_{\substack{\beta_f(\alpha),\beta_\xi(\alpha),\beta_m(\alpha) \\ \mu_{f_s}}} (\ddot{u}_{95}) \tag{3.17}$$

$$\ddot{u}_{\max}(d,\alpha) = \max_{\substack{\beta_f(\alpha),\beta_\xi(\alpha),\beta_m(\alpha) \\ \mu_{f_s}}} (\ddot{u}_{95}) \tag{3.18}$$

As the input variables are modelled as fuzzy numbers, the response is defined by an interval as well. In the special case where the nominal values of the modal parameters ($\alpha = 1.0$) and the nominal conditions of the flow ($\mu_{f_s} = \bar{f}_s$) are considered, the nominal response is found:

$$\ddot{u}_{\text{nom}}(d,1) = \ddot{u}_{95} \quad \begin{matrix} \beta_f(1),\beta_\xi(1),\beta_m(1) \\ \bar{f}_s \end{matrix} \tag{3.19}$$

The range of values obtained between $\ddot{u}_{\min}(d,\alpha)$ and $\ddot{u}_{\max}(d,\alpha)$ for the instantaneous peak response are compared to the vibration comfort criteria from table 2.11. The considered level of uncertainty can be selected based on information for the expected range of uncertainty. In the design stage, when no information is available for the uncertainties in the modal parameters, the largest range corresponding to $\alpha = 0.0$ can be selected for a conservative evaluation. After construction, if measurements are performed to in situ identify the modal parameters, only seasonal variations are expected and a higher α-level can be selected. However, an evaluation for different levels of uncertainty is recommended to gradually evaluate the effect on the response. The multi-level assessment provides a measure for the sensitivity of the response to the effect of uncertainties.

In example 3.2, the evaluation of one of the deterministic calculations is illustrated. It is discussed how the flow is composed and the response is calculated. The effect of HSI on the response is also illustrated.

A similar approach is applicable for a vibration serviceability assessment according to the simplified procedures discussed in section 2.3.3. However, since resonance with one mode of the structure is always considered, no additional

variation on the average step frequency has to be considered. The number of calculations is much smaller since only uncertainty in the modal parameters of the structure has to be considered.

Example 3.2. Evaluation of a deterministic response calculation

In this example, the response is calculated for the Phénix footbridge from example 2.3 considering the nominal values of the modal parameters and nominal situation of the flow. First, the modal load of the flow is composed using the single step force model of Li [109] (see table 2.4) following the procedure discussed in section 2.3.2. Second, the effect of HSI is illustrated by the acceleration transfer function for the coupled crowd-structure system. Third, the response is calculated and the instantaneous peak response is retained. A comparison is made with the response where no HSI-effects are considered.

Composition of the flow

The nominal values for the flow are considered in this example. For the selected pedestrian density of 0.5 pers./m^2, a walking speed v_s of 1.30 m/s and an average step frequency of $\mu_{f_s} = \bar{f}_s = 1.89$ Hz are considered (see table 2.5). A standard deviation of the step frequency σ_{f_s} of 0.10 Hz is assumed since unrestricted pedestrian traffic is considered. The lateral position of the pedestrians is sampled from a uniform distribution covering the width of the bridge. Therefore, 15 equally spaced walking paths are considered as visualised on figure 3.8. In the case where HSI-effects are considered, the pseudo moving force model is used and the human bodies are uniformly distributed at fixed positions on the bridge deck (see also figure 3.8). The distributions for the human body parameters proposed in table 3.1 are assumed. The equations of motion for the coupled crowd-structure system are given in section 2.3.2.

A continuous flow of pedestrian traffic is composed for a period of 10000 s. The modal projection of the force induced by the flow is given in figure 3.9 for the three modes contributing to the response.

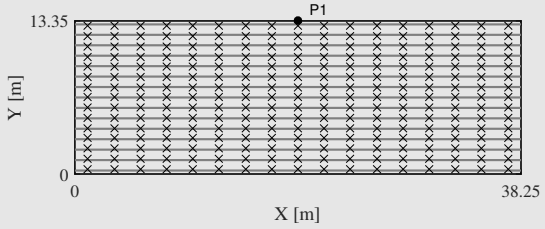

Figure 3.8: Top view of the Phénix footbridge with indication of the 15 possible walking paths (–) and the fixed locations for the SDOFs representing the human bodies to account for HSI (×).

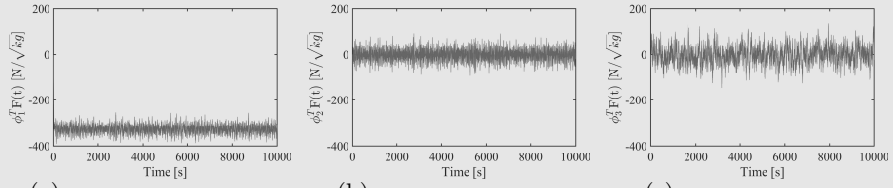

(a) (b) (c)

Figure 3.9: Modal projection of the force for the Phénix footbridge considering nominal values of the flow for a pedestrian density of 0.5 pers./m^2 of the (a) first mode, (b) second mode and (c) third mode.

Effect of human-structure interaction

Passive HSI in vertical direction is now considered as described in section 2.2.4 and 2.3.2. The effect of HSI can be observed in figure 3.10 where the transfer function is given for a vertical input and the vertical output acceleration at the antinode of mode 3 (point P1 in figure 3.8). It can be seen that the natural frequency of the first mode slightly decreases from 1.65 Hz to 1.58 Hz due to the added mass effect. A decrease is observed since the frequency ratio between the human body frequencies and the natural frequencies of the mode is higher than 1 (here: 3.25 Hz/1.65 Hz=1.97). The magnitude of the shift increases for a higher ratio of the added modal mass of the pedestrians to the modal mass. The added modal mass is calculated as in example 2.1 and equals 4.22 ton for a density of 0.5 pers./m^2, resulting in a mass ratio of 4.22/131.6=3.21%. In [216], the effective damping of mode j ($\xi_{\text{eff},j}$) is defined to determine the amplitude of the steady-state response of the coupled crowd-structure system, $\ddot{u}_{\max,\text{HB}}$, as follows:

$$\ddot{u}_{\max,\text{HB}} \sim |\text{H}_{\ddot{\text{u}},\text{HB}}(\omega_{\text{HB},j})| \sim \frac{1}{2\xi_{\text{eff},j} m_j} \tag{3.20}$$

with $H_{\ddot{u},HB}$ the acceleration transfer function and $\omega_{HB,j} = 2\pi f_{HB,j}$ the modified value of the natural frequency of mode j for the coupled crowd-structure system. The maximum response of the crowd-structure system is related to the modal mass of the empty footbridge such that both HSI effects (added mass and added damping) are given by the change in the natural frequency and the effective damping ratio. The latter expresses the change in amplitude of the steady-state response with respect to that of the empty structure and is calculated as follows:

$$\xi_{eff,j} = \frac{|H_{\ddot{u},B}(\omega_{B,j})|}{|H_{\ddot{u},HB}(\omega_{HB,j})|}\xi_j \tag{3.21}$$

with $\square_B$ referring to the parameters considering an empty footbridge.

For the first mode, this results in an effective damping of $\xi_{eff,1} = 0.8\%$. The observed decrease of the natural frequency and the rather low effect for the effective damping correspond to the findings in [219] where it is concluded that for natural frequencies below 2 Hz, the pedestrians mainly act as added mass.

For the second peak (here representing the third mode), again a small effect of the added mass is found resulting in a shifted value of the natural frequency. However, the value now slightly increases (6.15 Hz to 6.24 Hz) for a frequency ratio below unity (3.25/6.15=0.53). A larger effect on the effective damping is observed compared to the first mode ($\xi_{eff,3} = 7.98\%$) since the crowd-structure modal mass ratio is considerably higher (14.7 ton/23.0 ton=63.9% for $d = 0.5$ pers./m^2). These findings also correspond to those in [219].

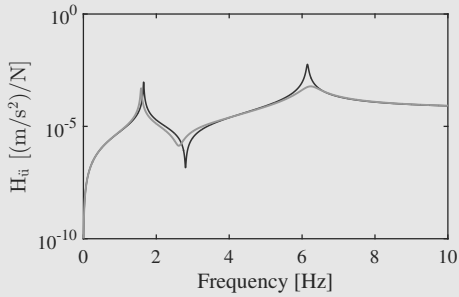

Figure 3.10: Transfer function for acceleration with input and output point at point P1 for the empty structure (dark) and the coupled crowd-structure system (light).

Response calculation

In this example, no additional variability on the walking characteristics is considered and the nominal values of the modal parameters are assumed ($\alpha = 1.0$). The response is calculated at the side of the footbridge at midspan, corresponding to the antinodes of mode 1 and 3 (point P1 in figure 3.8).

The response is first calculated disregarding the effects of HSI. The time history of the acceleration response and the PSD of accelerations are given in figure 3.11. The instantaneous peak response is calculated from equation (2.67)-(2.69) and equals 1.31 m/s^2. The standard deviation of the acceleration time history $\sigma_{\ddot{u}}$ is 0.30 m/s^2. From the PSD in figure 3.11(b), three peaks can clearly be distinguished. The first peak at 1.65 Hz corresponds to the contribution of the first mode (near-resonance with the first harmonic of the walking loading). The second peak at 3.80 Hz represents the contribution due to the second harmonic of the loading (with $\mu_{f_s} = 1.89$ Hz) and the third peak represents the contribution of the third harmonic component of the loading for which (near-)resonance occurs with the third mode (6.15 Hz).

Secondly, HSI-effects are accounted for by considering the human bodies as SDOF systems attached to the structure. The response of the Phénix footbridge accounting for HSI-effects is also given in figure 3.11 (light). HSI results in a strong reduction of the response. The instantaneous peak value now equals 0.47 m/s^2 and the standard deviation of the response is 0.11 m/s^2. The large difference between the maximum accelerations illustrates the importance of HSI. From the acceleration PSD on figure 3.11(b), the following contributions are observed. Compared to the case without HSI, the first peak is now wider and lies between 1.58 Hz and 1.89 Hz and represents the contribution of the average value of the first harmonic component of the loading ($\mu_{f_s} = 1.89$ Hz) and of deviating values ($\sigma_{f_s} = 0.10$ Hz) for which near-resonance occurs with the shifted value of the first natural frequency. The height of the peak is lower due to the increased effective damping for the first mode. The second peak, representing the contribution due to the second harmonic of the loading, is hardly affected by HSI in this case. For that loading frequency, no resonance occurs with one of the modes of the footbridge while HSI effects are characterised by an increased effective damping for frequencies around the natural frequencies of the modes as also apparent from the transfer function presented in figure 3.10. The third peak is found in the range between 5.67 Hz and 6.25 Hz and represents the contribution due to the third harmonic component of the loading causing near-resonance with the third mode. Again, the amplitude of the peak is lower due to the increased effective damping.

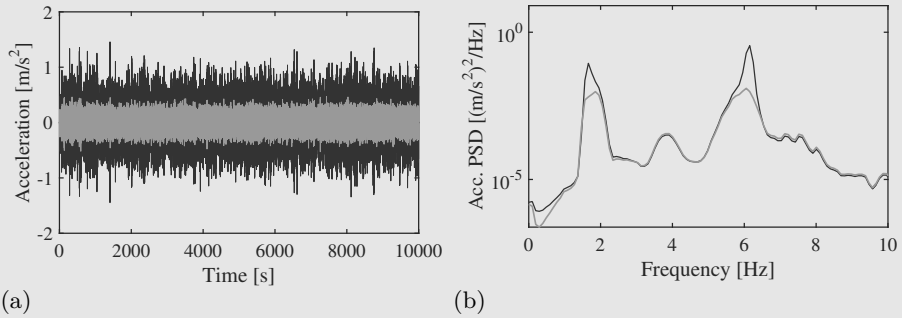

Figure 3.11: Response for the Phénix footbridge at point P1 assuming nominal conditions of the flow and no uncertainty in the modal paramters ($\alpha = 1.0$). Response calculated without HSI (dark) and with HSI (light). (a) Acceleration time history and (b) PSD of acceleration response, calculated at point P1.

3.5 Sensitivity of the vibration serviceability assessment to selected variations

The robust vibration serviceability assessment is performed assuming a realistic range of uncertainties in the modal parameters and considering variability in the average step frequency. By discretising the intervals for the multiplication factors β, modelled as fuzzy numbers (section 3.2), and for the average step frequency μ_{f_s}, a large number of deterministic response calculations is performed. A multi-level assessment is performed to gradually evaluate the effect of uncertainties on the response. This results in a range of responses corresponding to the assumed degrees of uncertainty.

This section first discusses the influence of the selected level of uncertainty on the response. It is investigated how uncertainty in the natural frequency, in the modal damping ratio or in the modal mass affects the response. Second, possible situations for resonance are considered by assuming additional variability on the average step frequency in combination with uncertainty in the natural frequency.

3.5.1 Influence of uncertainty in modal parameters

SDOF system under harmonic excitation

The effect of uncertainty in the modal parameters on the response is first investigated for a SDOF system under perfectly harmonic excitation leading to resonance. A dimensionless dynamic amplification factor (DAF) for the acceleration response of the SDOF system is defined as follows:

$$\mathrm{DAF}\left(\frac{f_\mathrm{P}}{f}\right) = \frac{\left(\frac{f_\mathrm{P}}{f}\right)^2}{\sqrt{\left(1-\left(\frac{f_\mathrm{P}}{f}\right)^2\right)^2 + \left(2\xi\left(\frac{f_\mathrm{P}}{f}\right)\right)^2}} \tag{3.22}$$

with f and ξ the natural frequency and the modal damping ratio, respectively of the SDOF system and f_P the loading frequency.

For a ratio of the loading frequency and the natural frequency close to one, a high amplification factor and dynamic response is found because of resonance (see figure 3.12). When the excitation frequency approaches the natural frequency of the footbridge, a high sensitivity to deviations in the values of the modal damping ratio and the natural frequency is expected. The sensitivity of the DAF for the acceleration response to uncertainties in the modal parameters is evaluated below.

The effect of uncertainty in the modal damping ratio is investigated considering β_ξ from equation (3.14). A nominal value of $\xi = 0.2$ is considered here. From the results in figure 3.12(a), it can be concluded that small deviations in the modal damping ratio strongly affect the response for resonant excitation. For off-resonance excitation, the effect is much smaller. The upper bound of the DAF occurs for values of the modal damping lower than the nominal value. From figure 3.12(a), it can also be concluded that the effect of uncertainties in the modal damping is larger for lower values of the modal damping ratio (upper bound vs lower bound).

The effect of uncertainty in the natural frequency is investigated similarly considering β_f as defined in equation (3.13). The effect is evaluated for off-resonant excitation ($f_\mathrm{P}/f = 0.4$) and near-resonant excitation ($f_\mathrm{P}/f = 1.1$), considering the nominal values of the modal damping ratio. The results are given in figure 3.12(b). A strong sensitivity to uncertainty in the natural frequency is observed for near-resonant excitation, while the effect is much smaller for the off-resonant excitation. That sensitivity to the natural frequency is strongly amplified for lower values of the modal damping ratio, especially for resonant excitation.

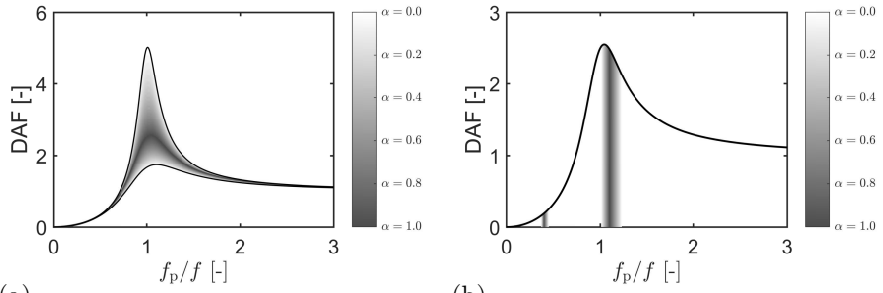

Figure 3.12: Dynamic amplification factor for accelerations showing the sensitivity of the response of a SDOF system to uncertainties (a) in the modal damping ratio and (b) in the natural frequency for off-resonance ($f_P/f = 0.4$) and near-resonance ($f_P/f = 1.1$) excitation and considering the nominal value of ξ.

Footbridge under walking loading

The effect of uncertainty in the modal parameters of the footbridge on the response to human walking loading is now verified for a real case. Therefore, simulations of moving pedestrian traffic are performed for the Phénix footbridge (example 2.3). The procedure for composing the flows and to retain the instantaneous peak response has already been illustrated in example 3.2 considering the nominal flow conditions and modal parameters ($\alpha = 1.0$). In example 3.3, the effect of uncertainties in the modal parameters ($\alpha \leq 1$) on the response is investigated. The multiplication factors for the modal parameters introduced in section 3.2 are considered. The effect is illustrated for the selected pedestrian density of 0.5 pers./m^2 and HSI-effects are considered similarly as in example 3.2.

Example 3.3. Response under uncertain modal parameters

This example investigates how the response of the Phénix footbridge is affected by uncertainty in the natural frequency, in the modal damping ratio and in the modal mass, separately. Simulations of moving pedestrian traffic are considered (section 2.3.2).

Uncertain natural frequency

A triangular membership function is introduced in equation (3.13) for the multiplication factor β_f. Only uncertainty in the natural frequency is accounted

for ($\beta_\xi = 1$ and $\beta_m = 1$) and it is assumed that all modes are simultaneously and equally affected by the multiplication factor. Six α-levels are considered in the analysis and the interval corresponding to $\alpha = 0.0$ is discretised in 21 values. For the pedestrian loading, nominal conditions are assumed (see table 3.1 and example 3.2).

A gradual evaluation of the obtained instantaneous peak values is given in figure 3.13(a) for different degrees of uncertainty in the natural frequency. At the level $\alpha = 1.0$, no uncertainty is considered and the response is given by one single value since no additional variability on the loading characteristics is considered here. To interpret these results, figure 3.13(b) shows the PSD of the acceleration response at the side of the bridge at midspan (point 1 in figure 3.13(d)). The PSD is given for all α-levels to illustrate the effect of uncertainty. For $\alpha = 1.0$, the response is rather low since no resonance occurs between the natural frequency of the first mode ($f_1 = 1.58$ Hz, accounting for the added mass effect due to HSI) and the first harmonic component of the loading ($f_s = 1.89$ Hz). This value corresponds to the frequency of the first peak of the PSD at nominal conditions in figure 3.13(b). For higher levels of uncertainty, a considerable effect on the response is observed (figure 3.13(a)). The effect of the uncertain natural frequency (β_f) on the response at point 1 is indicated in figure 3.13(c). For values of $\beta_f > 1$, (near-)resonance is more expected to occur since the values of the natural frequency f_1 are closer to the step frequency, resulting in a strong sensitivity of the response to the natural frequency. A similar conclusion is made for the SDOF system from figure 3.12(b) (near-resonance). The amplitude of the first peak of the PSD increases in comparison with the nominal case. For $\beta_f < 1$, resonance is not expected to occur. In this particular case, the response is only slightly affected since off-resonance excitation was already the case for $\beta_f = 1$.

Figure 3.13(d) shows the maximum acceleration response at each node of the bridge deck for $\alpha = 0.0$. The colour scale indicates the acceleration amplitudes as a function of the levels for vibration comfort from table 2.11. The maximum accelerations are found near the antinode of the first mode since resonance with that mode occurs in the worst case situation.

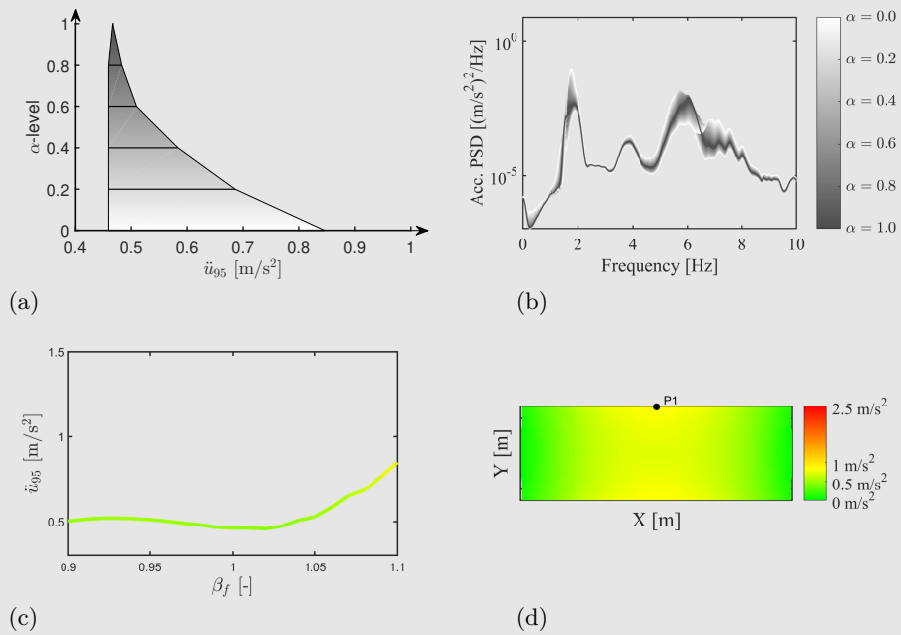

Figure 3.13: Effect of uncertainties in the natural frequency. (a) Membership function of the overall maximum response at all locations. (b) PSD of acceleration response at point P1 for different levels of uncertainty. (c) Response at point P1 as a function of β_f. (d) Top view of the Phénix footbridge with indication of maximum response for each node for $\alpha = 0.0$.

Uncertain modal damping ratio

To account for uncertainty in the modal damping ratio, the triangular membership function for the multiplication factor β_ξ from equation (3.14) is used. Nominal conditions are assumed for the other modal parameters and the pedestrian loading ($\beta_f = 1$ and $\beta_m = 1$, $\mu_{f_s} = 1.89$ Hz). Again, the multiplication factor holds for all modes simultaneously, six α-levels are considered and the interval corresponding to $\alpha = 0.0$ is discretised in 21 values.

In figure 3.14(a), the range of responses for different degrees of uncertainty in the modal damping ratio is summarised. A comparison is made with the case where only uncertainties in the natural frequency are considered (figure 3.13(a)). At the level $\alpha = 1.0$, no uncertainty is considered and the obtained peak response equals the value for the nominal conditions which is the same as in

figure 3.13(a). For higher degrees of uncertainty, the range of responses increases. In this specific case, no resonance occurs and the effect of uncertainty in the modal damping ratio is much smaller when compared to the results considering uncertainty in the natural frequency. The effect of uncertainty in the modal damping ratio can be much larger when resonance occurs as has been illustrated for the SDOF system in figure 3.12(a). However, the total effective damping is mainly determined by the HSI-effects (see example 3.2) which makes that the effect of uncertainty in the modal damping ratio is rather small. From the acceleration PSD on figure 3.14(b), it can also be concluded that uncertainty in the modal damping hardly affects the response. The two contributions at the first peak (for the average loading frequency and for deviating values for which near-resonance occurs with mode 1) can here more clearly be distinguished. Figure 3.14(c) shows the response at point 1 as a function of β_ξ. The maximum response decreases monotonically for a higher modal damping ratio. Figure 3.14(d) shows the overall maximum response for each node of the footbridge considering uncertainty in the modal damping ratio.

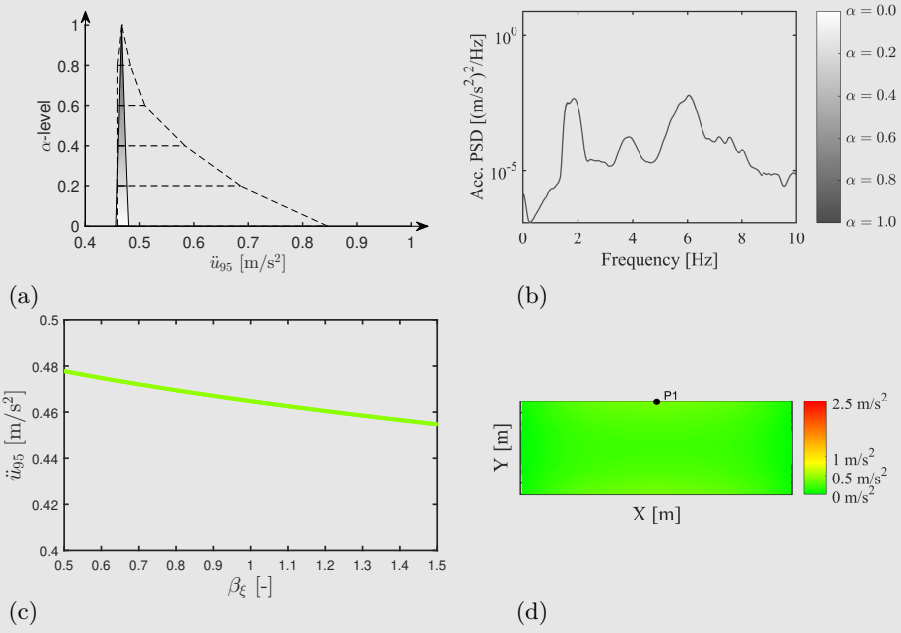

Figure 3.14: Effect of uncertainties in the modal damping ratio. (a) Membership function of the overall maximum response at all locations. (b) PSD of acceleration response at point P1 for different levels of uncertainty. (c) Response at point P1 as a function of β_ξ. (d) Top view of the Phénix footbridge with indication of maximum response for each node for $\alpha = 0.0$.

Uncertain modal mass

The effect of uncertainty in the modal mass is investigated similarly as for the natural frequency and modal damping ratio. The triangular membership function for β_m from equation (3.15) is used and nominal conditions are considered for the other modal parameters and pedestrian loading ($\beta_f = 1$, $\beta_\xi = 1$ and $\mu_{f_s} = 1.89$ Hz). An analogous analysis is performed as for previous cases (β_m holds for all modes simultaneously, the analysis is performed at six α-levels and a discretisation of 21 values at $\alpha = 0.0$ is considered).

The range of responses for different degrees of uncertainty in the modal mass is summarised in figure 3.15(a). Compared to the effect of uncertainty in the natural frequency, only a small sensitivity is observed here. Again, the effect of uncertainties increases for lower α-levels. The small effect of uncertainty in the modal mass is also due to HSI. The ratio of the added modal mass of the crowd to the modal mass slightly changes. In this particular case, the effects are rather small for the considered mass ratio (3.21%, see example 3.2). Resonance cannot occur for the considered values of the natural frequency and the loading frequency. This results in a minor effect of the uncertain modal mass.

The PSD for accelerations, the response at point 1 as a function of the uncertain modal mass and the maximum response per node at $\alpha = 0.0$ is given in figure 3.15(b), (c) and (d) respectively. The rather small effect of the modal mass on the response can be seen as well.

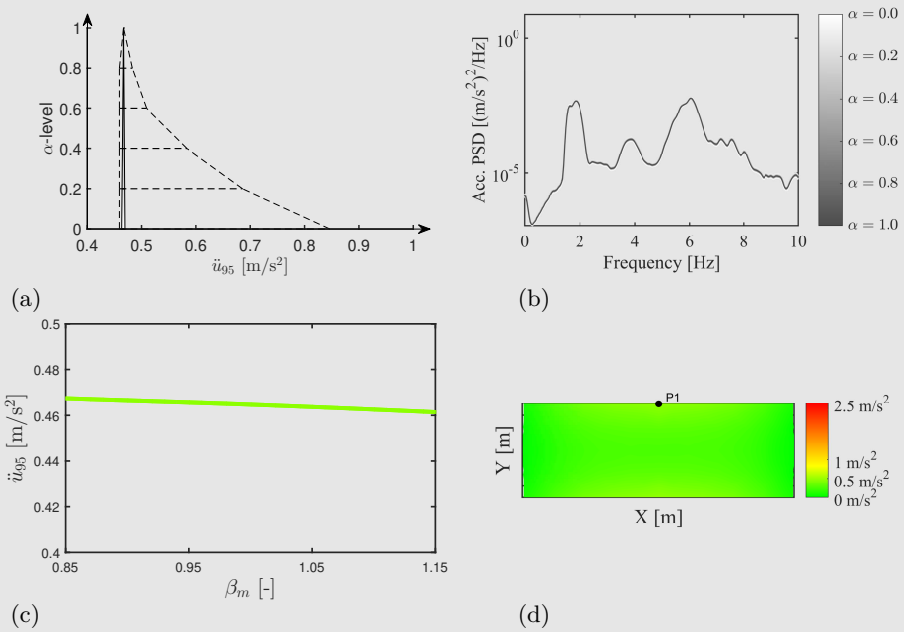

Figure 3.15: Effect of uncertainties in the modal mass. (a) Membership function of the overall maximum response at all locations. (b) PSD of acceleration response at point P1 for different levels of uncertainty. (c) Response at point P1 as a function of β_m. (d) Top view of the Phénix footbridge with indication of maximum response for each node for $\alpha = 0.0$.

3.5.2 Influence of variability in loading

A robust vibration serviceability assessment requires assumptions for both the uncertainty in the modal parameters of the footbridge and variability in the loading. From example 3.3, it follows that the vibration serviceability assessment depends on the fact whether resonance can occur for the loading frequency and the natural frequency of a mode of the footbridge. In this case, small variations in the natural frequency or modal damping can lead to significant deviations in the response. Therefore, it is expected that variability on the average step frequency also strongly affects the response. A similar conclusion has been drawn for the SDOF system. A large sensitivity of the DAF is found for small shifts in the ratio f_P/f (figure 3.12(b)). In example 3.4, the effect of

this variability on the average step frequency on the response is illustrated for the Phénix footbridge.

Example 3.4. Response under variation in average step frequency

The effect of variation on the average step frequency on the response of the Phénix footbridge (see also ex. 2.3) is illustrated in this example. First, the effect of additional variability on the average step frequency is considered. Second, the combined effect of variability on the step frequency and uncertainty in the natural frequency is investigated. All calculations in the example are performed for a pedestrian density d of 0.5 pers./m^2.

Variability on $\mu_{\mathbf{f_s}}$

Variability on the average step frequency is considered as proposed in equation (3.16) considering $\Delta_{\mu_{f_s}} = 0.1$ Hz. The range for μ_{f_s} is discretised in 21 values. The nominal values are considered for the modal parameters, corresponding to the level of uncertainty $\alpha = 1.0$: $\beta_f = 1$, $\beta_\xi = 1$ and $\beta_m = 1$.

Figure 3.16(a) shows the overall maximum response of the bridge deck as a function of the average step frequency. In this specific case, an increasing peak response is observed for both an increasing and decreasing value of μ_{f_s}, which is explained as follows. For values of $\mu_{f_s} < \bar{f}_s$, resonance can occur for the range of average step frequencies and the natural frequency of the first mode resulting in higher values of the peak response. Resonance can also occur for the range of the third harmonic loading component and the natural frequency of the second mode. On the contrary, for $\mu_{f_s} > \bar{f}_s$, resonance with the third harmonic component of the loading and the third mode of the footbridge can occur, resulting in higher response values as well. Furthermore, the amplitude of the third harmonic component of the single step forces increases for higher step frequencies (see table 2.4).

Variation on $\mu_{\mathbf{f_s}}$ in combination with an uncertain natural frequency

The occurrence of resonance for the expected range of the loading frequencies and the natural frequencies is determining for the response. Therefore, the combined effect of uncertainty in the natural frequency and variability on the average step frequency is investigated. The membership function for β_f in equation (3.13) and the interval for μ_{f_s} defined in equation (3.16) are considered. The nominal values for the modal damping ratio and modal mass are assumed ($\beta_\xi = 1$ and $\beta_m = 1$).

The results are summarised in figure 3.16(b). At the level $\alpha = 1.0$, a range of responses is now found corresponding to the range from figure 3.16(a). For

higher levels of uncertainty, the range of responses increases considerably when compared to the case where no additional variation on the step frequency is considered. The maximum instantaneous peak value strongly increases for lower α-levels. At $\alpha = 0.0$, the maximum possible value is even three times higher than its minimum value. The reason for the strong increase of the response is that for some of the combinations of the average step frequency and the uncertain natural frequency, pure resonance occurs ($\mu_{f_s} = \beta_f \times f_1$). In the previous example 3.3, it is observed that the potential for resonance for values of the uncertain natural frequency increases, although, pure resonance has not been reached for the proposed intervals. The PSDs of the acceleration response for all combinations made are given in figure 3.16(c). For higher levels of uncertainty, the frequency of the first peak changes when compared to the nominal situation. For some combinations, its amplitude increases strongly, however, since resonance can occur.

Figure 3.13(d) shows the maximum acceleration response at each node of the bridge deck for $\alpha = 0.0$ with the same colour scale as used in the previous example 3.3. Again, the maximum response is found at the points around the antinodes of mode 1 and 3.

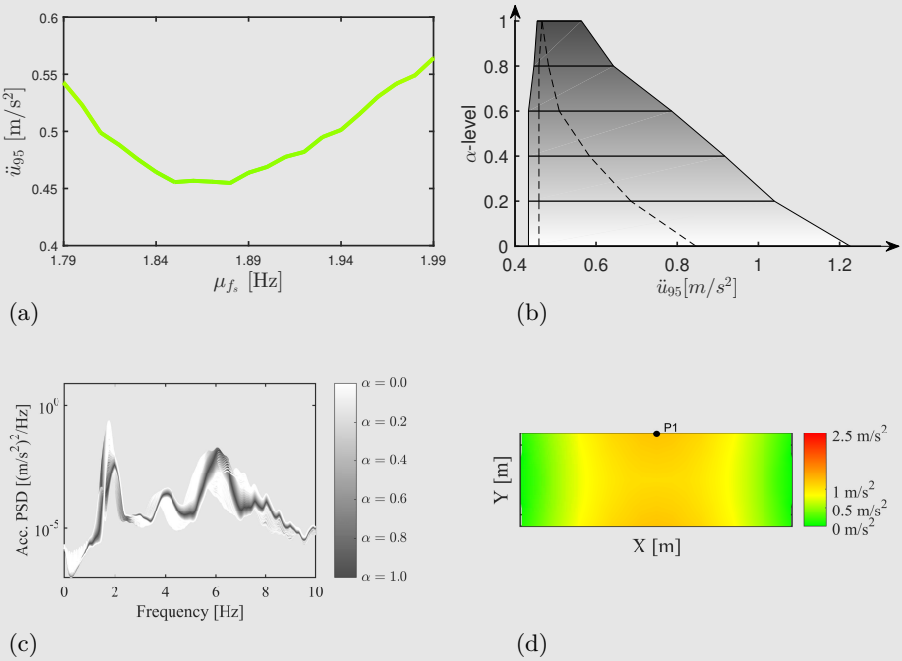

Figure 3.16: (a) Peak response as a function of μ_{f_s} for $\alpha = 1.0$. (b) Membership function of the overall maximum response at all locations accounting for uncertainty in the natural frequency and variation on the average step frequency. (c) PSD of acceleration response at point P1 for different levels of uncertainty α and different values μ_{f_s}. (d) Top view of the Phénix footbridge with indication of maximum response for each node for $\alpha = 0.0$.

3.6 Conclusion

The methodology for the robust vibration serviceability assessment allows to evaluate the vertical response of footbridges under uncertainties. The procedure is applied for walking loading but can be extended for other loading types since it is generic. The effect of uncertainties in the modal parameters is accounted for using multiplication factors which are modelled as fuzzy numbers. It is clear that the assumed range of uncertainty defining the membership function is important for the assessment. The benefit of that approach is that by considering different levels of uncertainty in the analysis, each corresponding to

a degree of membership, the methodology enables to investigate the sensitivity of the response to the effect of uncertainties. Rather than evaluating one single value, a range of responses is tested to criteria for vibration comfort. For the loading, simulations of moving pedestrian traffic are performed using the detailed stochastic models for the walking characteristics from chapter 2, including passive HSI effects in vertical direction. Inter-subject variability is considered for the human body parameters and for the step frequencies. It is illustrated that HSI strongly affects the response calculation, leading to a beneficial effect on the acceleration amplitudes. The occurrence of resonance is generally the most determining aspect for the assessment. An additional variability on the step frequency is therefore considered by defining an interval in which the mean value can vary. In addition, a similar approach can be used for other parameters of the walking loading or for the human body parameters accounting for HSI. To further improve the currently used load model, it is recommended to also include a model for HSI effects in lateral direction (lock-in).

The effect of uncertainties in the dynamic behaviour of a structure has first been illustrated for a SDOF system under perfectly harmonic loading. For near-resonant excitation, uncertainty in the natural frequency and modal damping strongly affects the response while for off-resonance excitation, the effect is much smaller. Second, the effect of uncertainty in the modal parameters and variability in the loading has been investigated for the Phénix footbridge considering simulations of moving pedestrian traffic and assuming a detailed load model. For this specific case, uncertainty in the natural frequency and variation on the average step frequency strongly affects the response since both variables are important for the occurrence of resonance. The effect of uncertainty in the modal damping and modal mass is much smaller in this case since no resonance occurs for nominal conditions of the loading.

Chapter 4

Robust vibration serviceability design of TMDs for footbridges

For footbridges subjected to human-induced vibrations, resonance between harmonic walking loading and one or multiple modes of the footbridge can lead to significant vibration levels. If unacceptable vibration levels are expected, vibration mitigation measures can be implemented in the design. A frequently applied solution is the installation of a Tuned Mass Damper (TMD). Its parameters are generally tuned to one specific mode of the footbridge. A good prior knowledge of the modal parameters is therefore required since small deviations in the natural frequencies can lead to detuning of the device resulting in a reduced performance.

This chapter aims at developing a methodology for the robust design of vibration mitigation devices for footbridges. The main objective is the parameter tuning of TMDs accounting for the effect of uncertainties in the modal parameters of the footbridge. The effect of the human-induced walking loading is considered as well in the methodology for the TMD tuning and additional variability in the walking characteristics is accounted for. The procedure for the robust vibration serviceability assessment of footbridges from chapter 3 is therefore considered.

The chapter is organised as follows. First, a general overview of vibration mitigation measures for footbridges is given in section 4.1. A distinction is made between structural modifications and devices that can be installed in/on the structure. Second, in section 4.2, the main design aspects for TMDs are

given. Conditions for operability and performance are of major interest and the importance of detuning effects is pointed out. In section 4.3, different strategies for robust optimisation problems are defined. Several formulations of the optimisation problem are given and it is indicated how the effect of uncertainties is included. A selection of algorithms is provided to solve the optimisation problem. In section 4.4, the problem of the robust TMD parameter tuning as proposed in this doctoral research is given. Finally, in section 4.5, the effect of uncertainties on the TMD performance is illustrated for two applications. First, the effect of detuning is discussed for a conventional design. Second, a robust design is elaborated directly accounting for the effect of uncertainties in the TMD performance.

4.1 Vibration mitigation for footbridges

If comfort criteria for vibration serviceability are not satisfied, vibration mitigation measures are needed. Three ways to reduce vibrations are given in [31]. First, the mass of the footbridge can be adapted. Second, natural frequencies in the range of human-induced loading are avoided by stiffening the structure [40]. Third, additional damping devices can be considered as vibration mitigation measure.

By adapting the mass or stiffness of the structure, the footbridge is designed such that the natural frequency is beyond the range of human-induced loading frequencies. However, if resonance cannot be avoided, the modal damping ratio can be augmented by adding damping devices to the structure. Modifications of structural stiffness can only be considered in the design stage while an increase of the modal damping ratio is the most recommended approach after construction [31]. A global overview of techniques for structural vibration control is given in [230].

This section summarises possible measures for vibration mitigation of footbridges. First, the modification of the mass is discussed in section 4.1.1. Second, the modification of the structural stiffness and its effect on the natural frequency is given in section 4.1.2. Then, three sections are given discussing techniques for the modification of the modal damping: passive vibration control in section 4.1.3, active vibration control in section 4.1.4 and semi-active control in section 4.1.5.

4.1.1 Modification of the mass

By increasing the mass of the footbridge, for example by adding a concrete layer, the sensitivity of the structure to human-induced loading decreases since more energy is required for the excitation of the higher modal mass [31]. However, its effect on the natural frequency must be considered as well. If the added mass layer brings no additional stiffness, this results in a decrease of the natural frequency. Depending on the values of the natural frequency of the original structure, the values may fall in or out the range of human-induced loading frequencies.

A so-called *mass-tuning* strategy is proposed for footbridges in [116] aiming at a change in the natural frequency of the footbridge rather than an increase of the modal mass. For two case studies, the response is evaluated following conventional design guides [9, 170] as summarised in section 2.3.3. By adding mass to the structure, the natural frequency and consequently the reduction coefficient decreases resulting in a lower response. However, the presented method is very sensitive to the effect of uncertainties in the natural frequencies. Measurements are therefore recommended to experimentally identify the natural frequencies.

4.1.2 Modification of the stiffness

Modifications to the structural stiffness directly aim at changing the natural frequency of the footbridge to avoid resonance with one of the harmonic load components. Although the effect of added mass on the natural frequencies is similar, the main focus is now not on increasing the modal mass of the footbridge. Adding mass can be considered after construction while modifications of the structural stiffness are rather impractical after construction. Therefore, this approach can be considered in the design stage.

Some examples to adapt the structural stiffness in the design stage are given in [31]. The bending stiffness can be increased by changing the size of structural elements such as the height and thickness of steel box girders. The overall bridge deck stiffness can be further increased by including the handrail as a structural element or by considering a continuous (concrete) deck, rather than separated panels that are connected with a finishing layer on top. For lateral vibrations, an increase of the bridge deck width or the positioning of cables laterally to the deck increase the lateral stiffness.

4.1.3 Modification of the damping - passive systems

Passive damping systems reduce vibrations of the structure by energy dissipation for example due to friction or deformation of (viscous) fluids [196]. The passive damping device is activated by the main structure's movements such that no external energy supply is required. Below, an overview is given of passive damping devices for vibration control of footbridges. Much attention is paid to the discussion of the (TMD) since this type of damper is of main interest in this thesis. A linear behaviour of the damper characteristics is therefore assumed. The working principle of other solutions is briefly discussed but references are given for further information. In addition, some designs where non-linearities are considered in the tuning of passive damping systems are given. An elaborated general overview of solution techniques for (passive) vibration control for footbridges and floors is provided in [214, 230].

Tuned Mass Damper (TMD)

A TMD is a passive vibration absorber consisting of a mass that is attached to the footbridge with springs and damper elements [230]. When the TMD starts oscillating relative to its main structure, the counteracting force reduces the response and energy is dissipated by the damper element. For an optimal reduction of the response, the frequency and the damping of the TMD must be tuned to the modal parameters of the footbridge. As a result, the TMD is only effective in a narrow frequency range, around the natural frequency of the mode at which the TMD is tuned. Compared to other vibration mitigation devices, the costs for the installation and maintenance of the TMD are relatively low [138, 240].

Since resonance with the mode at which the TMD is tuned is assumed, the contributions from other modes can be disregarded and the footbridge equipped with TMD can be simplified as two coupled SDOF systems (see figure 4.1). For a TMD attached in degree of freedom l (indicating the position of the TMD as well as the direction in which the TMD is active), the equivalent mass $m_{\mathrm{eq},j}$ following equation (2.27) is calculated as:

$$m_{\mathrm{eq},j} = \frac{1}{\mid \boldsymbol{\phi}_j(l) \mid^2} \tag{4.1}$$

The equivalent stiffness $k_{\mathrm{eq},j}$ and equivalent damping $c_{\mathrm{eq},j}$ for mode j of the footbridge without TMD then are given as in equations (2.28) and (2.29). For the TMD, the SDOF parameters are the TMD mass m_{TMD}, stiffness k_{TMD} and damping c_{TMD}. The dimensionless mass ratio μ_{TMD}, frequency ratio ρ_{TMD} and

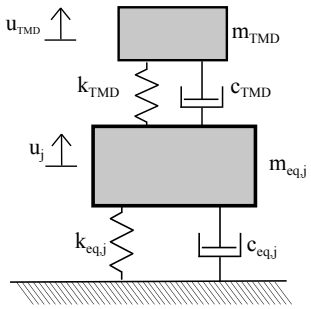

Figure 4.1: Tuned Mass Damper ($\square_{\text{TMD}}$) and main structure ($\square_{\text{eq},j}$), considering only the contribution of mode j, as coupled SDOF systems.

damping ratio ξ_{TMD} of the TMD are defined as follows:

$$\mu_{\text{TMD}} = \frac{m_{\text{TMD}}}{m_{\text{eq},j}} \qquad \rho_{\text{TMD}} = \frac{f_{\text{TMD}}}{f_j} \qquad \xi_{\text{TMD}} = \frac{c_{\text{TMD}}}{4\pi m_{\text{TMD}} f_{\text{TMD}}} \tag{4.2}$$

If in equation (4.1) $\mid \boldsymbol{\phi}_j(l) \mid = \max(\mid \boldsymbol{\phi}_j \mid)$, this will lead to the lowest value of the equivalent mass and thus to the optimal location of the TMD since the highest mass ratio μ_{TMD} can be obtained for a given TMD mass. In this case, the equivalent mass equals the modal mass $m_{\text{eq},j} = m_j$.

In the classical work by Den Hartog [52], the stiffness and the damping of the TMD are determined for a given mass ratio by minimising the maximum displacement response of an undamped main structure, corresponding to the infinity norm ($\text{H}_{u,\infty}$) of the dimensionless frequency response function. Expressions for the optimal frequency ratio ρ^*_{TMD}, optimal damping ratio ξ^*_{TMD} and the minimised maximum value of the dimensionless displacement response $\text{H}^*_{u,\infty}$ are given as:

$$\begin{gathered} \rho^*_{\text{TMD}} = \frac{1}{1+\mu_{\text{TMD}}}; \qquad \xi^*_{\text{TMD}} = \sqrt{\frac{3\mu_{\text{TMD}}}{8(1+\mu_{\text{TMD}})}}; \\ \text{H}^*_{u,\infty} = \left\| \frac{u_j}{u_{j,\text{ref}}} \right\|_\infty = \sqrt{\frac{2+\mu_{\text{TMD}}}{\mu_{\text{TMD}}}} \end{gathered} \tag{4.3}$$

with $u_{j,\text{ref}}$ corresponding to the static deflection of the structure $u_{j,\text{stat}}$ due to a force with amplitude $F_{0,j}$ ($u_{j,\text{stat}} = F_{0,j}/k_{\text{eq},j}$). A harmonic loading causing resonance with the mode at which the TMD is tuned is considered. The expressions by Asami [8] generalise those given by Den Hartog for a lowly damped structure. Alternative expressions in case of a damped main

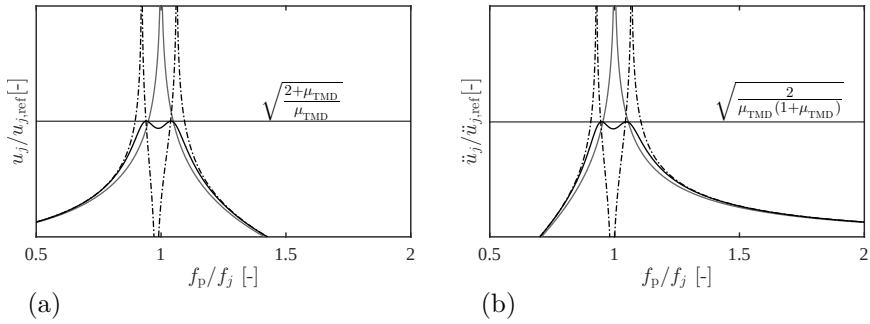

Figure 4.2: Dimensionless frequency response function of the structure without TMD (light –), with undamped TMD ($\rho^*_{\mathrm{TMD}}, \xi_{\mathrm{TMD}} = 0$) (–·) and with TMD with optimal parameters ρ^*_{TMD} and ξ^*_{TMD} (dark –). TMD parameters optimised for (a) displacements using eq. (4.3) (b) accelerations using eq. (4.4) with indication of maximum value (horizontal line).

structure are presented by Ghosh and Basu in [77]. The dimensionless frequency response function for the SDOF system with TMD is given in figure 4.2(a) as a function of the loading frequency f_P normalised to the natural frequency of the main structure. A comparison is made between the structure without TMD, with undamped TMD ($\rho^*_{\mathrm{TMD}}, \xi_{\mathrm{TMD}} = 0$) and with TMD with optimal parameters ($\rho^*_{\mathrm{TMD}}, \xi^*_{\mathrm{TMD}}$). For the structure with TMD, two peaks are observed, corresponding to the natural frequencies of the resulting 2DOF system. For the optimally tuned TMD, the height of the peaks is the same.

Since the criteria for vibration comfort for footbridges are formulated in terms of acceleration levels, the TMD parameters are tuned to obtain a minimal acceleration response. Formulae for the optimal frequency ratio ρ^*_{TMD}, optimal damping ratio ξ^*_{TMD} and the minimised ratio between the maximum acceleration and a reference acceleration level $\ddot{u}_{j,\mathrm{ref}}$ ($= F_{0,j}/m_{\mathrm{eq},j}$), $\mathrm{H}^*_{\ddot{u},\infty}$, are provided in [7, 8, 230]. The following formulae minimise the acceleration response assuming no modal damping of the main structure:

$$\rho^*_{\mathrm{TMD}} = \sqrt{\frac{1}{1+\mu_{\mathrm{TMD}}}}; \qquad \xi^*_{\mathrm{TMD}} = \sqrt{\frac{3\mu_{\mathrm{TMD}}}{8(1+\mu_{\mathrm{TMD}})}}\sqrt{1+\frac{27}{32}\mu_{\mathrm{TMD}}};$$
$$\mathrm{H}^*_{\ddot{u},\infty} = \left\| \frac{\ddot{u}_j}{\ddot{u}_{j,\mathrm{ref}}} \right\|_\infty = \sqrt{\frac{2}{\mu_{\mathrm{TMD}}(1+\mu_{\mathrm{TMD}})}} \tag{4.4}$$

Figure 4.2(b) shows the frequency response function for the structure equipped with a TMD designed for minimal accelerations. TMDs for footbridges are often

tuned using one of the above presented formulae as elaborated in [34, 38, 128]. The TMD performance is evaluated based on a targeted effective damping ratio [214, 230] representing the damping of the equivalent system of the coupled SDOFs [106]. The maximum steady-state amplitude is used to define the damping of the equivalent system. For the undamped system ($\xi_j = 0$) equipped with TMD, the relation between the effective damping ξ^0_{eff} and the height of the peak, given in equations (4.3) and (4.4), is given as:

$$\|\square\|_\infty = \frac{1}{2\xi^0_{\text{eff}}} \tag{4.5}$$

with $\square$ referring to the dimensionless response from equation (4.3) or (4.4). For lowly damped footbridges ($\xi_j < 0.02$), the total effective damping ξ_{eff} can be approximated as the sum of the modal damping ratio of the main structure and the effective damping of an undamped structure with optimally damped TMD [106, 229]:

$$\xi_{\text{eff}} = \xi_j + \xi^0_{\text{eff}} \tag{4.6}$$

The minimal required mass ratio μ_{TMD} is obtained for a desired effective damping ratio by combining equations (4.5) and (4.6) with eq. (4.3) or (4.4). Next, the optimal frequency and damping ratio are calculated from equations (4.3) and (4.4) to design the TMD. In figure 4.3(a), a practical design graph is given to determine the TMD mass ratio based on the effective damping. It can be seen that the effective damping ratio increases for a higher mass ratio μ_{TMD} and that a higher mass ratio is required for a lower modal damping ratio of the main structure. In addition to the evaluation of acceleration criteria, the displacement of the TMD relative to the structure, Δ_{rel}, is of interest as well. Figure 4.3(b) shows the ratio of the relative TMD displacement to the static deflection, calculated by considering the TMD and the footbridge as coupled SDOF systems, as a function of the mass ratio. It can be seen that smaller relative TMD displacements are found for structures with a high modal damping ratio and for TMDs with a higher mass ratio.

In figure 4.4, an overview is given of the characteristics ρ_{TMD} and ξ_{TMD} of installed TMDs for footbridges as reported in literature. The optimal values according to equations (4.3) or (4.4) are also given. It can be seen that for most of the cases, the TMD frequency ratio and damping ratio closely follow the relations given by Den Hartog [52] (eq. (4.3)).

The response of a footbridge equipped with TMD can also be evaluated considering the contributions of multiple modes and a more advanced load model instead of a perfectly harmonic loading. Furthermore, a multiple TMD (MTMD) design can be opted where the frequencies of the different TMDs are distributed to cover a broader frequency range around the natural frequency

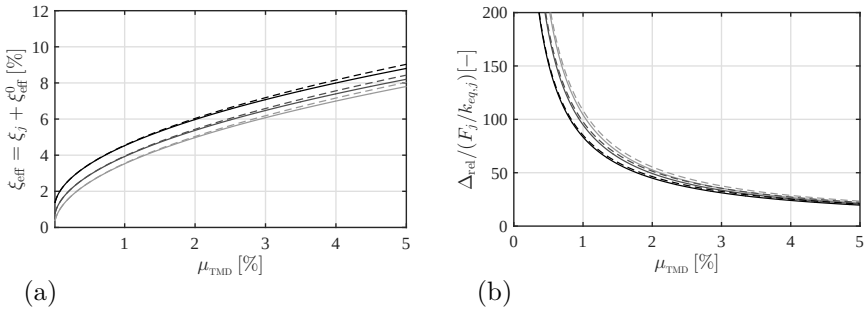

Figure 4.3: TMD performance as a function of the TMD mass ratio for different values of the modal damping ratio of the main structure (0%–0.4%–1%, light to dark) and optimal values of the TMD according to eq. (4.3)(–) and eq. (4.4)(– –). (a) Effective damping ratio following eq. (4.6) and (b) ratio of the relative TMD displacement to the static deflection of the structure.

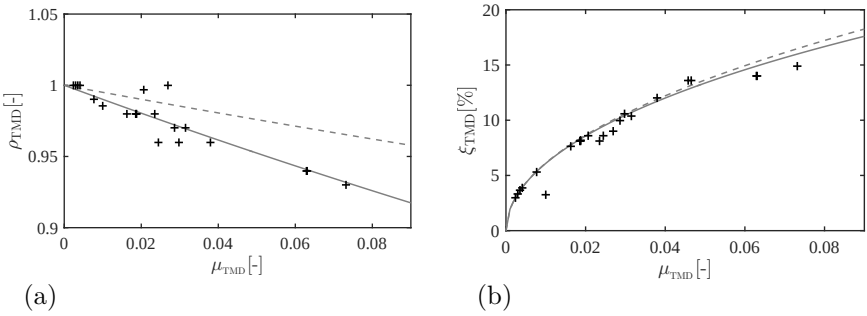

Figure 4.4: Characteristics of installed TMDs for footbridges as found in literature [34, 40, 126, 210, 211, 232] and comparison with the optimal values according to eq. (4.3) [52] (–) and eq. (4.4) [7, 8, 230] (– –). (a) TMD frequency ratio ρ_{TMD} and (b) TMD damping ratio ξ_{TMD}.

of the mode to which the TMDs are tuned [178, 241]. The interested reader is referred to [1, 108] where design strategies for MTMDs are discussed.

Pendulum Tuned Mass Damper (PTMD)

Pendulum TMDs are mostly used to reduce horizontal vibrations of footbridges and towers. A mass is connected to a cable or rod which is fixed to the main structure. The damping is provided by viscous damping devices or by friction.

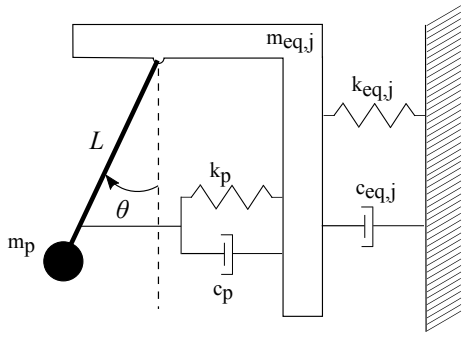

Figure 4.5: Pendulum Tuned Mass Damper ($\square_p$) and main structure ($\square_{\mathrm{eq},j}$) as coupled SDOF systems.

The principle of the PTMD as an equivalent SDOF system is visualised in figure 4.5. The PTMD generates a force in opposite direction of the main structure motion. The main advantage is that the frequency of the pendulum can be retuned by modifying the length of the cable accounting for the dynamic stiffness of the TMD [79]. The PTMD is often used in high-rise buildings under wind loading. In [187], a PTMD is designed for floor vibrations by modelling the pendulum as an equivalent SDOF system. PTMDs have also been installed at the London Millennium Bridge to reduce lateral vibrations [46].

Viscous (Fluid) Damper

In viscous dampers, vibration energy is dissipated through the motion of a piston in a cylinder with a viscous fluid [196] (see figure 4.6(a)). The piston is usually installed between a point of the bridge deck and a fixed point at the ground or between two points of the bridge. Often, the concept of fluid orificing is applied such that energy dissipation is obtained by volume variation of the fluid through the motion of the piston. The efficiency of the viscous damper depends on the relative velocity between both ends of the piston [85].

At the London Millennium bridge, a total of 37 viscous dampers are installed to reduce horizontal vibrations [46]. Some of them are connected between the ground and the deck, others connect the deck and the V-shaped pylons (see figure 4.6(b)). For the first lateral mode, an effective damping of 15-20% is targeted.

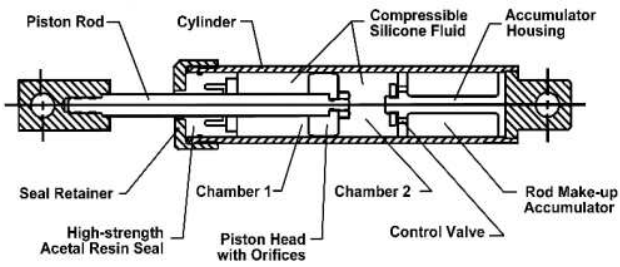

(a)

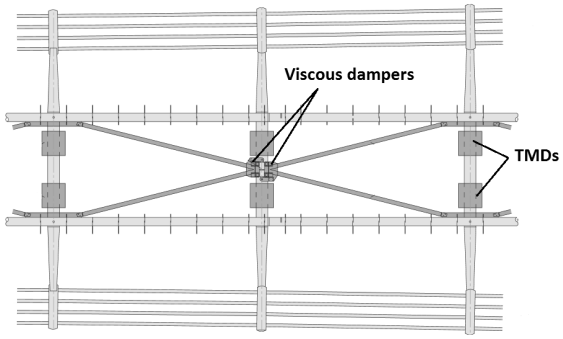

(b)

Figure 4.6: Viscous dampers: (a) working principle of viscous fluid damper (after [203]) and (b) installation of viscous dampers and TMDs at the London Millennium Bridge (top view, after [46]).

Tuned Liquid Dampers (TLD)

The working principle of TLDs is similar to that of TMDs but now, the mass is replaced by a body filled with liquid, usually water [85, 196]. The main advantages of TLDs are the low installation and maintenance costs and the easy tuning of the frequency. Nevertheless, the response of the damper can be highly non-linear. Two types of TLDs are distinguished.

First, a Tuned Liquid Column Damper (TLCD) is characterised by a U-shaped tube filled with water (figure 4.7(a)). The resultant force from the movements of the water reduces the response of the main structure [79]. A control valve or an orifice plate can be added in the horizontal tube to tune the damping [85]. Solutions for optimal values of the TLCD are given in [191, 238].

Second, a Tuned Sloshing Damper (TSD) consists of a tank filled with a liquid

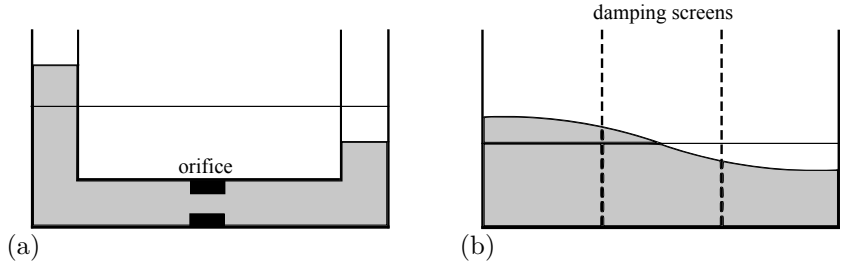

Figure 4.7: Scheme of (a) Tuned Liquid Column Damper with orifice and (b) Tuned Sloshing Damper with additional damping screens.

(figure 4.7(b)). The height of the liquid in the tank is determined such that the sloshing frequency of the liquid is tuned to the natural frequency of the main system [200]. Energy is dissipated by friction of the liquid and the tank. Additional screens can be installed in the tank to increase the damping ratio.

Non-linear passive damping systems

For the passive damping systems considered until now, it is assumed that the relation between the damping force and the relative velocity between main structure and damping device is linear [160, 177]. For viscous damping systems, it is therefore assumed that the viscosity of the fluid remains unaltered under temperature fluctuations or during the expected life time. However, non-linear behaviour of the damper can be expected e.g. for higher vibration amplitudes [75], especially for systems where damping is obtained by friction [177]. In [249], the effect of both a non-linear stiffness and damping of the absorber is investigated. A viscous power law damping is considered for the TMD design in [177] while Gatti in [75] assumes a cubic stiffness non-linearity. A generalisation of Den Hartog's method is applied for the parameter tuning of non-linear vibration absorbers in [55]. From the sensitivity study, it is concluded that the robustness of the non-linear damper can be improved by increasing the mass ratio. An extensive overview of non-linear passive damping systems is given in [94].

A non-linear TMD is designed to reduce vibrations of footbridges under walking loading in [160]. The obtained non-linear damping force results from a drag force of a plate immersed in water. The magnitude of the force is related to the square of the velocity. An in situ validation of the system shows good agreements with numerical simulations and the system ensures an effective response reduction.

4.1.4 Modification of the damping - active systems

To improve the efficiency of passive vibration control systems, (additional) forces can be generated by an active control system. Based on real-time input from the excitation and/or the response of the structure, the counteracting force is regulated. Generally, three steps are distinguished for active vibration control [106, 196]. First, sensors provide information about the external excitation (feedforward algorithm, inner loop), the structural response (feedback algorithm, outer loop) or both (feedforward and feedback). For footbridges subjected to human-induced vibrations, it is impossible to measure the pedestrian forces. Therefore, only systems with feedback control are applicable. Second, a controller is implemented to process the measured data and to calculate the output force. Third, power-supplied actuators are needed to generate the calculated force for the actual response mitigation. The principle of active vibration control and a comparison with passive damping systems are given schematically in figure 4.9.

The main advantage is that active dampers are able to guarantee a desired performance under a broader range of operation conditions and can be applied for various types of structures [41]. However, the implementation of an active damping system often is rather expensive since the installation costs, energy supply and maintenance costs must be considered. Furthermore, rather large actuators are needed to generate sufficiently large forces [65]. Literature reviews of active vibration control for civil engineering structures are given in [41, 74, 196]. Below, two types of active dampers that can be used to reduce footbridge vibrations are briefly discussed: the inertial mass damper and the twin rotor damper.

Inertial Mass Damper (IMD)

Inertial mass dampers (IMD) are similar to conventional TMDs, however, the generated forces are not initiated by the motion of the main structure but are typically induced by an actuator through accelerating the mass of the damper device [56]. The mass can be moving in a magnetic field and can be attached to the main structure with spring and damping elements. Figure 4.8(a) shows the basic working principle of an electrodynamic IMD where the inertial mass is accelerated through adapting the control voltage.

The design of an active IMD for an indoor walkway subjected to human-induced loading is discussed in [155]. A methodology is proposed to find the optimal location for a predefined number of actuators and to determine the control algorithm. Direct velocity feedback is used based on multiple inputs from

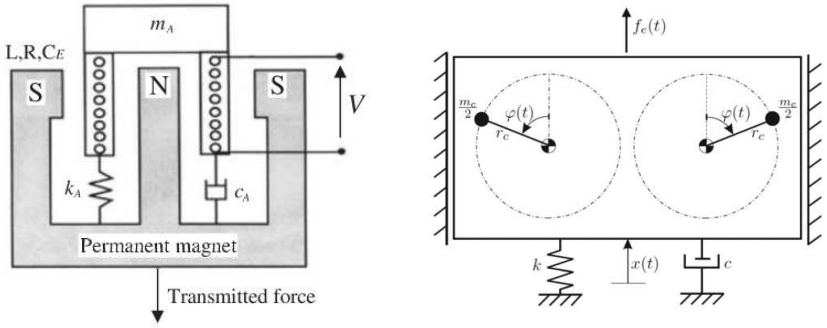

(a) (b)

Figure 4.8: Working principle of (a) electrodynamic inertial mass damper (after [155]) and (b) twin rotor damper (after [16]).

accelerometers. In [40], a commercial shaker is used as active damping system for a footbridge with an acceleration feedback algorithm. Its effectiveness has been proven for walking, running and jumping.

Twin Rotor Damper (TRD)

The twin rotor damper (TRD) consists of two masses, rotating in opposite directions with a mostly constant angular velocity [16]. The resultant centrifugal force is the counteracting force. By regulating the phase shift between the motion of the rotor and the motion of the main structure, the damping force is adjusted. The principle of the TRD is visualised in figure 4.8(b). In [181], a TRD is used to reduce lateral vibrations of footbridges to human-induced loading. If a threshold for displacement (or acceleration) of the bridge deck is exceeded, the rotor motion is initiated. The angular speed or rotor acceleration is used as input variable for the control algorithm. With a small mass ratio (0.48%), an equivalent viscous damping of 5.6% is obtained. The system can also be used to reduce vertical vibrations, but in this case additional power supply is required for the lifting and slowing down of the masses.

4.1.5 Modification of the damping - semi-active systems

In semi-active control systems, the advantages of both passive systems (reliability and robustness) and active systems (adaptability) are combined [41, 198]. The

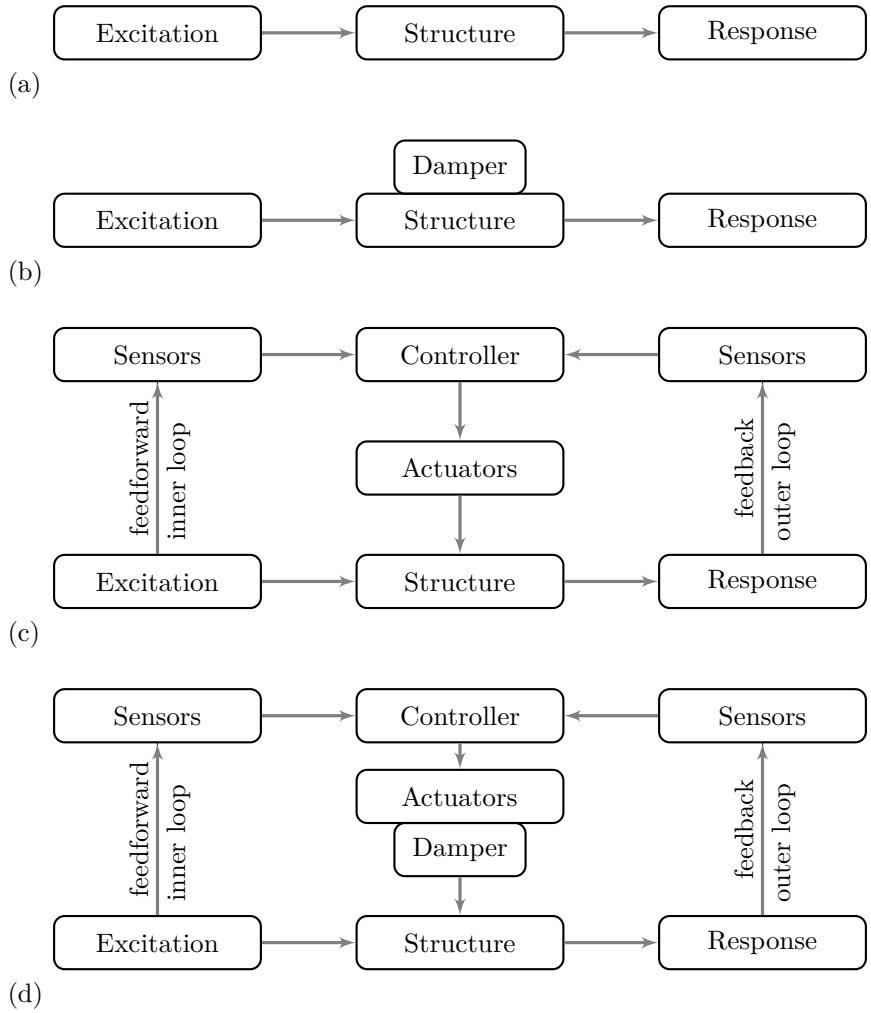

Figure 4.9: Control schemes for structure (a) without damping device, (b) with passive damper, (c) with active damper and (d) with semi-active damper (based on [196]).

semi-active systems consist of sensors, a control computer, an actuator and a passive damping device. The working principle of semi-active dampers is similar to that of active systems. However, now the actuator adjusts the properties of the passive damper [65] (see also figure 4.9(d)). The required energy supply for semi-active systems is much less compared to active systems and can be provided by batteries [196], resulting in lower operational costs [41, 186, 198]. The working of controllable fluid dampers and semi-active TMDs is briefly discussed here.

Controllable fluid dampers

For this type of semi-active dampers, either electrorheological fluids (ER) or magnetorheological (MR) fluids are used [198]. Under an electric (ER) or magnetic field (MR), the fluid turns into a semi-solid with controllable yield strength properties. Alternatively, a controllable valve can be used to alter the flow resistance in the damper [198]. The advantage of the systems is that only the piston is the moving part of the system. MR fluids are preferred to ER fluids since the required power supply is much lower, the temperature working range is larger and they are less sensitive to impurities in the fluid [196]. A more detailed overview of the working principle and applications is given in [196, 230]. The working principle of an ER or MR damper is visualised in figure 4.10(a).

Semi-active TMD

The working of a semi-active TMD is similar to its passive variant. However, semi-active TMDs are characterised by the ability to change their stiffness or damping constants [198]. In this way, variations in the natural frequency or modal damping are considered in the transmitted force. In [186], a semi-active PTMD is designed to reduce vibrations of a floor under human-induced loading. A magnetorheological device is used for the damping. Furthermore, the effect of human-structure interaction on the performance of the damper is investigated. A semi-active friction damper (see figure 4.10(b)) is designed for a footbridge in [235]. Piezoelectric actuators are used to regulate the friction and thus the damping of the device as a reaction to changes in the natural frequency. Compared to a passive system, a mass reduction of 50% is obtained.

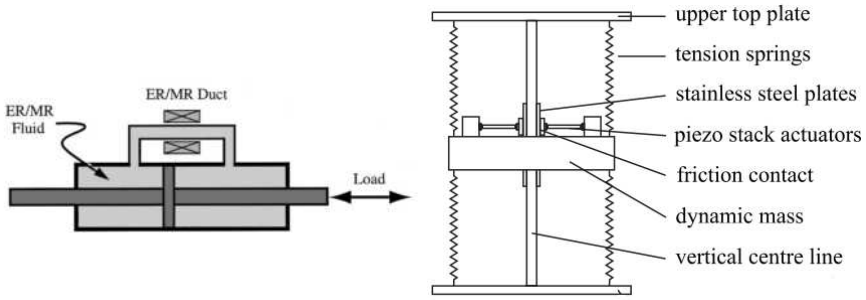

Figure 4.10: Working principle of (a) controllable fluid damper (after [198]) and (b) friction damper (after [235]).

4.2 Design considerations for TMDs

This thesis further focusses on the implementation of TMDs for the vibration mitigation of footbridges subjected to human-induced walking loading. The basic working principles and conventional designs strategies of a TMD have already been summarised in section 4.1.3. This section discusses design considerations for TMDs starting from criteria for vibration serviceability. Next, criteria for operability are considered, including the relative displacement of the TMD and the feasibility to manufacture the TMD mass, spring and damping components. Then, the relation between the TMD performance and its position is discussed. Afterwards, detuning effects on the TMD performance are considered.

4.2.1 Vibration serviceability

A TMD is installed to reduce the vibration levels in a narrow frequency range around the natural frequency of the selected mode. In the specific case of footbridges, this range often corresponds to the range of frequencies of human-induced loading. The design procedures proposed in section 4.1.3 therefore minimise the absolute peak value of the frequency response function (H_∞-norm) since the walking excitation can be considered as a narrowband random process [25, 26, 162]. The effective damping of the coupled structure-TMD system, related to the height of the peak, then holds as a performance parameter. Alternatively, for wideband excitation, the total energy can be minimised (H_2-norm) corresponding to the area under the frequency response function. Criteria for vibration comfort are implemented, usually referring to the acceleration

response. Suggested values for vibration comfort have been summarised in table 2.11. The design consist of finding the minimally required mass ratio for which the desired reduction or response level is obtained. The TMD design strategy followed in [222] directly accounts for the effect of human-induced loading. The minimally required mass ratio is obtained from the effective damping ratio, written as a function of the response calculated according to Sétra [9] or HiVoSS [170] and a predefined threshold level for vibration comfort. Afterwards, the TMD efficiency is verified considering detailed simulations of moving pedestrian traffic. Similar, an equivalent spectral model of the loading is used for the TMD parameter tuning in [211]. For a selected mass ratio, the TMD frequency ratio and damping ratio are tuned by maximising an efficiency factor that rates the acceleration response of a structure without and with TMD. Constraints are added for the maximum allowed acceleration.

4.2.2 Operability

The mass of the TMD is much lower than the modal mass of the main structure. Typically, a mass ratio of the TMD between 1 and 5% is used for footbridges [31]. This results in large displacements of the mass of the TMD in comparison with the main structure's displacements. The TMD movements are restricted to a limited working space (for example when installed inside the bridge deck) and a maximum stroke specified by the manufacturer. By increasing the TMD mass ratio and/or damping ratio, the relative displacement can be limited [230] (see also figure 4.3(b)). For the range of commercially available TMDs given in [126], an amplitude of 40 mm is considered. However, for large mass ratios, local strengthening of the structure can be required and a general stability check must be performed. This problem can be avoided by splitting the TMD into multiple (smaller) units on different locations of the footbridge. Smaller mass ratios again lead to higher relative displacements [230]. For example, the TMD designed in [34] is split into six units for structural reasons and each unit is placed between two transverse beams of the bridge.

Next, practical limitations for the manufacturing of the TMD components need to be considered. A relatively small mass ratio μ_{TMD} can lead to a high total TMD mass for modes with a large modal mass. TMDs of large size are often split into multiple smaller units. For footbridges, the total TMD mass generally can reach several hundreds or thousands kilograms [76, 126]. The frequency of commercial TMDs generally lies in the range between 0.3 Hz and 40 Hz [76] and a tolerance of the TMD frequency tuning op to 0.05 Hz is reported in [129]. Practical limitations for the TMD stiffness k_{TMD} can then be calculated from the TMD mass and frequency. For the TMD damping ratio ξ_{TMD}, values up to 20% are obtained from the case studies of footbridges provided in [126]. Higher

values are seldom reported in literature. The corresponding damping constant c_{TMD} from the case studies in [126] goes over 6000 Ns/m and even higher values (9000 Ns/m) are reported in [34]. Higher values of the damping constant imply larger devices.

To ensure an activation of the TMD, the acceleration amplitudes must be sufficiently high such that the TMD starts oscillating relative to the bridge deck motion. For vibrations with small amplitudes, the TMD is ineffective [232]. This is especially important for horizontally moving TMDs since the minimum required frictional force must already be exceeded below the trigger for the lock-in effect of 0.10 m/s^2 [34, 232]. For perfectly levelled rods of the sliding TMD, the force only depends on the static frictional force. The actual friction coefficient has been experimentally verified in [232] for horizontally moving TMDs and it is found that the acceleration level at which the TMDs are activated is twice as high for poorly levelled rods. As acceleration levels are a trigger for the activation of the TMD, the velocity is the limiting factor for the effective working of the damper component.

4.2.3 Positioning

The TMD is mostly tuned to reduce vibrations dominated by one specific mode. Therefore, TMDs are often designed by simplifying the dynamic behaviour of the main structure as an equivalent SDOF system in the frequency range around the natural frequency of the selected mode. Then it is implicitly assumed that the TMD is attached to the most effective position, corresponding to the antinode of the mode at which the TMD is tuned. In that case, the equivalent mass (equation (4.1)) equals the modal mass resulting in the highest possible mass ratio μ_{TMD}. However, if the contribution of multiple modes is accounted for (MDOF system), the installation of multiple TMDs can be required. The TMDs are installed at the antinodes of the corresponding modes. Examples of footbridges where multiple TMDs are considered in the design are given in [34, 210, 232].

Alternatively, the positioning of the TMD(s) can be part of the design problem. Daniel et al. in [48] propose a strategy to determine the TMD properties for a multi-mode vibration problem considering the first harmonic of the walking loading. In first instance, a TMD is considered at the antinode of each mode. The mass of each TMD then is determined recursively based on the absolute acceleration levels of the bridge deck at the corresponding position of the TMD. Similarly, a problem for the optimal placement of the damping devices is defined in [131] where a meta-heuristic firefly algorithm is used to solve the problem in which the location of the dampers are discrete numbers while

the damping constants are continuous variables. Constraints are added for both the damper characteristics and available (predefined) positions while the maximal acceleration is minimised. Two examples are given for the design and placement of friction dampers for truss footbridges subjected to walking loading described by the model of Bachmann [12]. Other design methodologies are given in [193, 201, 202] for multi-storey buildings. The performance of the TMDs is evaluated by considering the sum of the amplitudes of the transfer function of the uncontrolled structure for a number of preselected locations.

Nevertheless, even for these more advanced design strategies, a number of locations for the damping devices is preselected. This positioning is often based on engineering judgement. In practice, a maximum TMD efficiency is desired and the TMD is therefore always positioned as close as possible to (one of) the antinode(s) of the mode at which the TMD is tuned.

4.2.4 Effect of detuning

The TMD parameters have to be tuned to the dynamic behaviour of the structure to which they are attached. The tuning of the TMD natural frequency is of major importance for its performance. However, small shifts in the natural frequency of the structure during its lifetime or due to human occupancy can adversely affect the TMD performance [31]. This effect of detuning was studied by Rana and Soong [168] and Werkle et al. [233]. In [149, 168], it is concluded that the optimal TMD parameters are more sensitive to uncertainties in the natural frequency than to uncertainties in the modal damping ratio. A design considering MTMDs is less sensitive to detuning compared to a single TMD since the units have slightly different parameters and the frequencies are distributed covering a broader range around the natural frequency [178, 241].

In figure 4.11, the effect of a detuned TMD is given considering the conventional design method from equation (4.4). It is seen that the effect of detuning increases for lower mass ratios and that uncertainty in the structural damping ξ_j does not significantly affect the performance corresponding to the findings in [149, 168]. It is therefore recommended in [230] to determine the natural frequency of the footbridge in situ for the effective tuning of the TMD. Minor adjustments of the TMD properties are possible (on-site) after fabrication [76]. However, next to shifts in the natural frequency of the footbridge, also changes in the stiffness of the TMD k_{TMD} can result in detuning (e.g. fatigue behaviour due to the relative displacements [230]). The considered range of variation in figure 4.11 corresponds to the largest range of uncertainty in the natural frequency as proposed in section 3.2 and to the range of variation on the TMD stiffness k_{TMD} as proposed in [233]. The effect of an uncertain TMD damping ratio ξ_{TMD} on

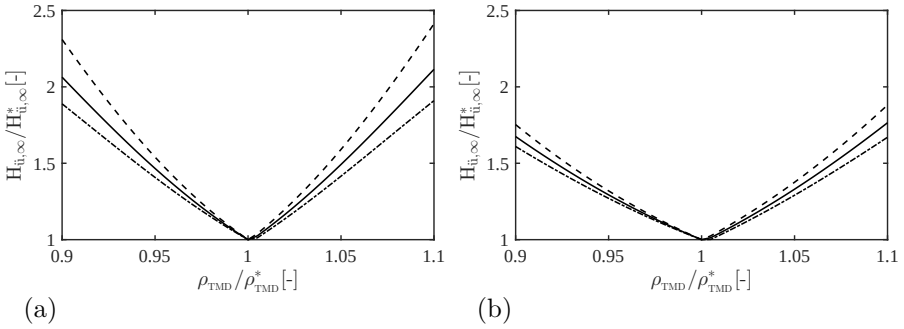

Figure 4.11: Effect of detuning on TMD performance given as the ratio of the H_∞-norm for TMD with detuned frequency ratio ρ_{TMD} and with optimal frequency ratio ρ^*_{TMD} according to equation (4.4) for TMD with mass ratio (a) $\mu_{\text{TMD}} = 2\%$ and (b) $\mu_{\text{TMD}} = 5\%$. Effect of structural damping given for $\xi_j = 0.5\%$ (– –), $\xi_j = 1.0\%$ (–) and $\xi_j = 1.5\%$ (–·).

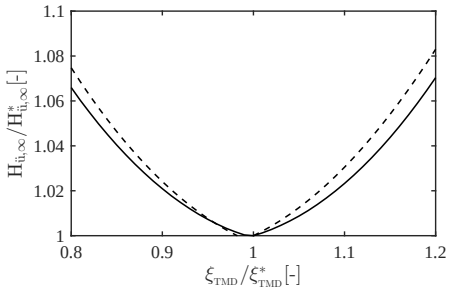

Figure 4.12: Effect of detuning on TMD performance given as the ratio of the H_∞-norm for TMD with detuned damping ratio ξ_{TMD} and with optimal damping ratio ξ^*_{TMD} according to equation (4.4) for an undamped main system $\xi_j = 0\%$. TMD with mass ratio $\mu_{\text{TMD}} = 2\%$ (–) and $\mu_{\text{TMD}} = 5\%$ (– –).

the performance is much smaller (see figure 4.12), corresponding to the findings in [233]. The effect is smaller for lower mass ratios.

4.3 Robust design optimisation

Two types of measures for the robustness of a system have been discussed in section 3.1.4 to evaluate the effect of uncertainties. It is desired to account for these uncertainties in the design. The present section first discusses possible formulations of the robust optimisation problem where the effect of uncertainties is directly included in the performance evaluation or as constraints (section 4.3.1). Second, solution techniques and optimisation algorithms are summarised in section 4.3.2.

4.3.1 Problem formulation

The typical mathematical formulation of a constrained optimisation problem is given as:

$$\begin{aligned} \underset{\mathbf{x}}{\text{minimise}} \quad & f(\mathbf{x}) \\ \text{subject to} \quad & g(\mathbf{x}) = 0 \\ & h(\mathbf{x}) \leq 0 \\ & \underline{\mathbf{x}} \leq \mathbf{x} \leq \bar{\mathbf{x}} \end{aligned} \tag{4.7}$$

with $\mathbf{x} \in \mathbb{R}^n$ the vector of n design variables of the problem, $f(\mathbf{x}) : \mathbb{R}^n \to \mathbb{R}$ the objective function, $g(\mathbf{x}) : \mathbb{R}^n \to \mathbb{R}^v$ the vector of v equality constraints and $h(\mathbf{x}) : \mathbb{R}^n \to \mathbb{R}^w$ the vector of w inequality constraints. Additional constraints are added for the lower and upper bounds of the design variables, $\underline{\mathbf{x}}$ and $\bar{\mathbf{x}}$ respectively. The optimisation is solved by finding the values for the decision variables in the vector of design variables such that the objective function is minimised and such that the constraints are satisfied. In the formulation of the optimisation problem above, the design variables are found for a deterministic problem.

By considering uncertainty on one or more of the design variables, the optimisation problem can be formulated alternatively to ensure robustness of the design. The effect of uncertainties can be included in two ways [107]. In a first way, the effect of uncertainties is considered in the objective function where one (single-objective) or multiple (multi-objective) functions are simultaneously minimised. If uncertainties are treated probabilistically, the cost function can be formulated in terms of the expected value, the standard deviation, percentile values, etc. of an output function. For non-probabilistic approaches, the objective function is defined as a worst case design. In a second way, the

effect of uncertainties is included in the constraints of the optimisation problem. Similarly, statistical moments or failure probabilities may not exceed a threshold value and are here implemented as (non-linear) design constraints.

Several formulations of the robust optimisation problem are defined in literature [59, 226]. Below, a selection is given of widely applied general optimisation problems that deal with the effect of uncertainty. The formulation of each problem corresponds with one or a combination of the measures for robustness as presented in section 3.1.4. For the sake of simplicity, only inequality constraints are considered below. However, a similar approach can be used for equality constraints.

Reliability based design optimisation (RBDO)

For reliability based design optimisations, the targeted reliability index (probability of failure) is typically included as design constraint [5, 226] while the objective function is modelled deterministically. The optimisation problem can be written as:

$$\begin{aligned} &\underset{\mathbf{x}}{\text{minimise}} \quad f(\mathbf{x}) \\ &\text{subject to} \quad p_F\left(h(\mathbf{x})\right) \leq p_F^t \end{aligned} \tag{4.8}$$

with p_F^t the maximum allowed probability of failure of the design constraint $h(\mathbf{x})$. In comparison with conventional designs where constraints are added deterministically, probabilistic constraints are implemented for RBDO [59]. An extensive overview and comparison of different calculation techniques for RBDO designs is given in [5]. Generally, two approaches are considered. First, in double loop approaches, the reliability analysis is performed in a separate loop from the optimisation loop. Due to the large number of calculations for the reliability analysis in the inner loop of the optimisation problem, RBDO methods are generally computationally expensive [11]. To tackle this difficulty, single loop approaches are given in [5] and the probabilistic constraints are interpreted as equivalent deterministic constraints. Other example applications are elaborated in [59, 167].

Robust design optimisation (RDO)

In robust design optimisation, the variability of the objective function is considered. A trade-off between performance and robustness is targeted using Pareto optimality [59, 226] and formulating the objective function as

a weighted sum of the expected value $\mu_{f(\mathbf{x})}$ and the standard deviation $\sigma_{f(\mathbf{x})}$ of the performance. The optimisation problem is defined as:

$$\begin{aligned} \underset{\mathbf{x}}{\text{minimise}} \quad & W\frac{\mu_{f(\mathbf{x})}}{\mu^0_{f(\mathbf{x})}} + (1-W)\frac{\sigma_{f(\mathbf{x})}}{\sigma^0_{f(\mathbf{x})}} \\ \text{subject to} \quad & h(\mathbf{x}) \leq 0 \end{aligned} \tag{4.9}$$

with $W \in [0;1]$ a weighting factor for the trade-off between performance and robustness. $\mu^0_{f(\mathbf{x})}$ and $\sigma^0_{f(\mathbf{x})}$ represent the mean value and standard deviation of the performance function for solving the optimisation problem with $W = 1$ and $W = 0$ respectively. The utopia point is defined by $[\mu^0_{f(\mathbf{x})}, \sigma^0_{f(\mathbf{x})}]$ but is not feasible since the trade-off must be considered [127]. An overview of different methods to solve robust optimisation problems is discussed in [150, 157].

Reliability based robust design optimisation (RBRDO)

The advantages of both previous types of optimisation problems are combined in the reliability based robust design optimisation. The objective function is formulated for performance and robustness while constraints are added for reliability [99, 184] as follows:

$$\begin{aligned} \underset{\mathbf{x}}{\text{minimise}} \quad & W\frac{\mu_{f(\mathbf{x})}}{\mu^0_{f(\mathbf{x})}} + (1-W)\frac{\sigma_{f(\mathbf{x})}}{\sigma^0_{f(\mathbf{x})}} \\ \text{subject to} \quad & p_F(h(\mathbf{x})) \leq p^t_F \end{aligned} \tag{4.10}$$

Different algorithms are proposed in literature to efficiently solve the RBRDO problem. In [99], a probability based robustness index is therefore defined. The algorithm in [137] tries to shorten the computational time for multi-objective optimisation problems accounting for probability based constraints. Similarly, in [243], an equivalent deterministic constraint replaces the probabilistic constraints to speed up the calculation time.

Worst case robust design optimisation

For problems where the uncertainty of the design variables is modelled using (fuzzy) intervals, an alternative formulation of the optimisation problem is proposed. Similar to the worst case measure for robustness from section 3.1.4, the optimisation problem is defined to satisfy the worst case situation. If multiple objective functions are considered, the value which has to be minimised is found by solving a sub-problem where the maximum value (worst case) is

retained. Alternatively, the worst case value can be calculated as the infinity norm of all objective functions. Constraints can be added similarly by finding the worst possible value of the constraints. Then, the optimal solution is found by solving following problem:

$$\begin{aligned} \underset{\mathbf{x}}{\text{minimise}} \quad & \|f(\mathbf{x})\|_\infty \qquad \forall x_i \in [\underline{x}_i, \bar{x}_i] \\ \text{subject to} \quad & \|h(\mathbf{x})\|_\infty \leq 0 \quad \forall x_i \in [\underline{x}_i, \bar{x}_i] \end{aligned} \tag{4.11}$$

The constraints of the optimisation problem (4.11) can also be implemented alternatively by defining a separate constraint for each combination of possible values of the uncertain values x_i in their corresponding intervals. Specific algorithms to solve interval optimisation problems are proposed in [19, 44, 80].

4.3.2 Solution techniques and optimisation algorithms

To solve the design problems defined in the previous section 4.3.1, optimisation algorithms are used. In this section, the basic working principle of a selection of optimisation algorithms needed in this thesis is given. First, the distinction between algorithms for local and global optimisation is made. Gradient-based algorithms will be selected for local optimisation. Second, optimality conditions are summarised to verify whether the solution is an optimiser or not. Third, a selection of algorithms to deal with non-linear constraints is described.

Local and global optimum

To solve an optimisation problem, such as the one defined in its general formulation in equation (4.7), two types of optimisation methods are distinguished. First, local optimisation methods will find a local optimum in the neighbourhood of the initial point. Second, global optimisation methods are targeting the global minimum.

Local optimisation algorithms aim to find the local optimum in the neighbourhood of the starting point. In each iteration, a better estimate for the optimum is found and optimality criteria are verified to identify whether the estimate is an optimiser or not. A gradient-based evaluation of the sensitivities of the objective and constraints function is often made. The main advantage of gradient-based methods is that they converge relatively fast to the optimal solution. The gradient and Hessian are often approximated with finite difference calculations. Alternatively, the derivatives are calculated analytically when possible or for functions composed of multiple consecutive operations, the chain

rule is applied in algorithmic differentiation (forward or backward calculation). An extensive overview of numerical algorithms for local optimisation is given in [142]. For gradient-based optimisation methods, two strategies are generally distinguished. First, in the line search algorithm, a direction $\mathbf{r}_k$ is determined per iteration k and the step size t_k in that direction is calculated to obtain a lower function value. This results in a new point and the algorithm is repeated until the optimality conditions are satisfied. The total number of iterations is thus not known in advance and depends on the initial point. The second algorithm (trust region) defines an approximating quadratic model function for the objective function in a region around the current estimate. Then, the argument (direction and step size) of the minimum value of the model function is used for the next iteration. Again, optimality conditions are verified to check whether the solution is an optimiser or not. Since the obtained solution could be a local optimum depending on the choice of the initial point, it is recommended to solve the problem for different starting points in the feasible range of the design variables. Multiple local optima can potentially be detected leading to a more reliable (global) solution. For convex functions (e.g. the quadratic model function), however, the obtained local optimiser is also the global solution.

For global optimisation, evolutionary algorithms are widely used since they work with a population of possible solutions. Genetic algorithms (GA) are often used to solve multi-objective optimisation problems since they consider a set of solutions. An initial population of solutions is selected and tested to a fitness function. To obtain the next population of solutions, previous populations are combined leading to a better fitness (*crossover*). Randomness can be applied to the previous set of solutions (*mutation*) aiming at the global optimum. In contrast with gradient-based methods, the total number of iterations is predefined in advance assuming that the global optimum is sufficiently well approximated for the selected number of iterations. The disadvantage is the high computational effort since a large number of function evaluations is needed for the effective exploration of the design space, especially when a reliability approach is considered. For more information about evolutionary algorithms, the reader is referred to [50, 192] where an overview of algorithms is given.

Optimality conditions

For gradient-based optimisation algorithms, optimality conditions are formulated to check whether $\mathbf{x}$ is a local optimum. The conditions can be verified for continuous objective functions which are at least twice differentiable. For an unconstrained problem, a first order necessary condition (FONC) is that the local optima $\mathbf{x}^*$ are characterised by a zero gradient $\nabla f(\mathbf{x}^*) = 0$. If a non-zero gradient is found in the local optima, there is at least one descent direction

leading to lower function values. For constrained optimisation problems, the objective function is replaced by the Lagrangian function $\mathcal{L}(\mathbf{x}, \boldsymbol{\lambda}, \boldsymbol{\nu})$ combining the objective function with the equality and inequality constraints as follows:

$$\mathcal{L}(\mathbf{x}, \boldsymbol{\lambda}, \boldsymbol{\nu}) = f(\mathbf{x}) + \sum_{i=1}^{v} \lambda_i g_i(\mathbf{x}) + \sum_{j=1}^{w} \nu_j h_j(\mathbf{x}) \tag{4.12}$$

with $\boldsymbol{\lambda} \in \mathbb{R}^v$ and $\boldsymbol{\nu} \in \mathbb{R}^w$ the Lagrange multipliers. The FONCs for constrained problems are defined by the Karush-Kuhn-Tucker (KKT) conditions as:

FONC (constrained):

$$\nabla \mathcal{L}(\mathbf{x}^*, \boldsymbol{\lambda}, \boldsymbol{\nu}) = 0 \tag{4.13}$$

$$g_i(\mathbf{x}^*) = 0 \quad i = 1, ..., v \tag{4.14}$$

$$h_j(\mathbf{x}^*) \leq 0 \quad j = 1, ..., w \tag{4.15}$$

$$\nu_j \geq 0 \quad j = 1, ..., w \tag{4.16}$$

$$\nu_j h_j(\mathbf{x}^*) = 0 \quad j = 1, ..., w \tag{4.17}$$

These conditions are not sufficient for optimality since $\mathbf{x}^*$ can also be a maximiser. From the second order necessary conditions (SONCs), it follows that the local minima of an unconstrained problem require a positive semi-definite Hessian matrix ($\nabla^2 f(\mathbf{x}^*) \geq 0$). For a constrained optimisation problem, a set of feasible directions $\mathbf{r}$ is defined in which the derivative is zero ($\nabla f(\mathbf{x}^*)^\mathsf{T} \mathbf{r} = 0$) and the SONCs are defined as:

SONC (constrained): If $\mathbf{x}^*$ is a local minimiser, then there is a $\boldsymbol{\lambda} \in \mathbb{R}^v$ and $\boldsymbol{\nu} \in \mathbb{R}^w$ for which the KKT conditions hold and $\mathbf{r}^\mathsf{T} \nabla^2_\mathbf{x} \mathcal{L}(\mathbf{x}^*, \boldsymbol{\lambda}, \boldsymbol{\nu}) \mathbf{r} \geq 0$.

The conditions above are necessary for optimality but not sufficient (e.g. saddle points can also satisfy these conditions, without being a minimiser). Second order sufficient conditions (SOSCs) are imposed to ensure $\mathbf{x}^*$ is a local minimiser: $\nabla f(\mathbf{x}^*) = 0$ and $\nabla^2 f(\mathbf{x}^*) > 0$ (for unconstrained problems). For constrained optimisation problems, SOSCs are defined similarly to ensure optimality as:

SOSC (constrained): If there is a $\boldsymbol{\lambda} \in \mathbb{R}^v$ and $\boldsymbol{\nu} \in \mathbb{R}^w$ for which the KKT conditions hold and if ($\mathbf{r}^\mathsf{T} \nabla^2_\mathbf{x} \mathcal{L}(\mathbf{x}^*, \boldsymbol{\lambda}, \boldsymbol{\nu}) \mathbf{r} > 0$), then $\mathbf{x}^*$ is a local minimiser.

These conditions allow to mathematically determine whether a point is a local minimiser and are verified in each iteration of gradient-based optimisation algorithms.

Selected algorithms for gradient-based optimisation

Optimality conditions have been defined to check whether a point is an optimiser. Algorithms are developed to iteratively search for an estimation closer to the local optimum. The line search strategy is used for globalisation aiming at determining a sufficiently large step length in the descent direction per iteration. A selection of gradient-based algorithms that will be used in this thesis to determine the step direction is summarised below.

Newton type methods can be considered to find the descent direction. In each iteration step, the FONC is linearised to determine the step direction $\mathbf{r}_k$. For an unconstrained problem, this results in following equation:

$$\nabla f(\mathbf{x}_k) + \mathbf{B}\mathbf{r}_k = 0 \tag{4.18}$$

with $\mathbf{B}$ the (approximated) Hessian of the objective function. Note that equation (4.18) also corresponds to the gradient of a model function $\nabla_{\mathbf{r}} m_k$ which quadratically approximates the objective function at step k. The step direction is found by minimising the model function m_k:

$$\mathbf{r}_k = \arg\min_{\mathbf{r}} \left(m_k(\mathbf{x}+\mathbf{r}) = f(\mathbf{x}_k) + \nabla f(\mathbf{x}_k)^\mathsf{T}\mathbf{r} + \frac{1}{2}\mathbf{r}^\mathsf{T}\mathbf{B}_k\mathbf{r} \right) \tag{4.19}$$

By solving equation (4.18) for $\mathbf{r}_k$ (or by minimising the model function m_k), the next step is obtained as $\mathbf{x}_{k+1} = \mathbf{x}_k + t_k\mathbf{r}_k$ with t_k the step length as determined by line search to ensure a sufficiently decrease of the objective function. When the exact Hessian is considered ($\mathbf{B}_k = \nabla^2 f(\mathbf{x}_k)$), the exact Newton method is used. However, other approximations for $\mathbf{B}$ are recommended for computational reasons and to ensure a descent direction (positive definite, $\mathbf{B} \succ 0$). A computationally efficient updating procedure for $\mathbf{B}$ is defined by Broyden–Fletcher–Goldfarb–Shanno (BFGS) and leads to fast convergence of the optimisation problem. Then, $\mathbf{B}$ is updated as follows:

$$\mathbf{B}_{k+1} = \mathbf{B}_k - \frac{\mathbf{B}_k\mathbf{s}_k\mathbf{s}_k^\mathsf{T}\mathbf{B}_k}{\mathbf{s}_k^\mathsf{T}\mathbf{B}_k\mathbf{s}_k} + \frac{\mathbf{z}_k\mathbf{z}_k^\mathsf{T}}{\mathbf{z}_k^\mathsf{T}\mathbf{s}_k} \tag{4.20}$$

with $\mathbf{z}_k = \nabla f(\mathbf{x}_{k+1}) - \nabla f(\mathbf{x}_k)$ and $\mathbf{s}_k = \mathbf{x}_{k+1} - \mathbf{x}_k$. In the first step, $\mathbf{B}$ is initialised as an identity matrix. The BFGS approximation for the Hessian is used by default in the Matlab *fmincon* algorithm.

For constrained optimisation problems, equation (4.18) does not hold since constraint functions must be considered. However, for equality constrained problems, Newton's method can be applied to the KKT conditions and the next iteration step is determined by solving these linearised equations for $\mathbf{r}_k$ and $\boldsymbol{\lambda}$ (see eq. (4.21) and (4.22)). To deal with inequality constraints in the

optimisation problem, two algorithms are considered in this thesis. In the first algorithm, **sequential quadratic programming (SQP)**, a quadratic model function of the Lagrangian is minimised in each iteration, as previously done for the unconstrained problem. Since the quadratic model is convex, the FONCs are sufficient for optimality. For inequality constrained problems, the quadratic problem is solved for a selected set of constraints for which holds $h_j(\mathbf{x}) + \nabla h_j(\mathbf{x})^\mathsf{T}\mathbf{r}_k = 0$ with $j \in \mathcal{A}$ (*active set* $\mathcal{A}$) while other constraints are verified afterwards. After each iteration, the set of active constraints is updated and the next iteration is calculated as for equality constrained problems by solving eq. (4.21)-(4.23) finding $\mathbf{r}_k$, $\boldsymbol{\lambda}$ and $\boldsymbol{\mu}$. The Newton-based linearisation of the KKT conditions is given as follows:

$$\nabla f(\mathbf{x}) + \mathbf{B}\mathbf{r}_k + \sum_{i=1}^{k} \lambda_i \nabla g_i(\mathbf{x}) + \sum_{j=1}^{l} \nu_j \nabla h_j(\mathbf{x}) = 0 \tag{4.21}$$

$$g_i(\mathbf{x}) + \nabla g_i(\mathbf{x})^\mathsf{T}\mathbf{r}_k = 0 \quad i = 1, ..., k \tag{4.22}$$

$$h_j(\mathbf{x}) + \nabla h_j(\mathbf{x})^\mathsf{T}\mathbf{r}_k = 0 \quad j \in \mathcal{A} \tag{4.23}$$

$$h_j(\mathbf{x}) + \nabla h_j(\mathbf{x})^\mathsf{T}\mathbf{r}_k < 0 \quad j \notin \mathcal{A} \tag{4.24}$$

$$\nu_j \geq 0 \quad j = 1, ..., l \quad j \in \mathcal{A} \tag{4.25}$$

with $\mathcal{A}$ the set of active constraints. Note that the KKT condition (4.17) is trivial since for inactive constraints ($j \notin \mathcal{A}$) the condition holds that $\nu_j = 0$. In the BFGS-updating of the matrix $\mathbf{B}$, the Lagrangian is considered such that $\mathbf{z}_k = \nabla\mathcal{L}(\mathbf{x}_{k+1}, \boldsymbol{\lambda}_{k+1}, \boldsymbol{\nu}_{k+1}) - \nabla\mathcal{L}(\mathbf{x}_k, \boldsymbol{\lambda}_{k+1}, \boldsymbol{\nu}_{k+1})$. A second method to deal with constraints in the optimisation problem is the **interior point** algorithm. The KKT conditions for the inequality constraints (eq. (4.15)-(4.17)) are replaced by a smooth constraint such that $\nu_j h_j(\mathbf{x}^*) = \tau$ with τ sufficiently small. Together with the linearised equations (4.21) and (4.22), these conditions can be solved. Both algorithms (SQP with active set and interior point) are implemented in the Matlab function *fmincon*.

4.4 Robust TMD design

The aim of this chapter is to achieve a robust performance of the TMD. In this section, the design problem is formulated by discussing different parts of the optimisation problem. The assumptions made are situated to other TMD design problems found in literature. The distinction between the decision variables of the optimisation problem and other design variables is made first.

Second, the objective function is defined, followed by the constraints to ensure robustness. Then, the mathematical formulation of the optimisation problem is given considering the approach for the robust vibration serviceability assessment from chapter 3. Finally, it is indicated how to account for additional variation on the TMD parameters to evaluate detuning effects.

Design variables

In equation (4.7), the general mathematical formulation of an optimisation problem is given in which $\mathbf{x}$ represents the vector of design variables. In the proposed TMD design problem, the vector of design variables $\mathbf{x}$ is split for clarity in multiple components as:

$$\mathbf{x} = [\mathbf{y}, \mathbf{b}, \boldsymbol{\beta}, \mathbf{l}] \tag{4.26}$$

with $\mathbf{y}$ the vector of decision variables that have to be tuned, $\mathbf{b}$ the parameters describing the structural (dynamic) behaviour, $\boldsymbol{\beta}$ the parameters to characterise the considered uncertainty in the modal parameters and $\mathbf{l}$ the parameters to define the loading.

In many conventional designs, only the TMD frequency ratio ρ_{TMD} and damping ratio ξ_{TMD} are considered as decision variables [138], sometimes computed from a preselected mass ratio [7, 8, 52, 228]. Alternatively, all TMD parameters can be considered as design parameters [118, 246]. In this thesis, the vector of decision variables $\mathbf{y}$ is composed of all TMD parameters:

$$\mathbf{y} = [m_{\text{TMD}}, k_{\text{TMD}}, c_{\text{TMD}}] \tag{4.27}$$

For the structural parameters, the vector $\mathbf{b}$ is composed of the modal parameters of the footbridge ($\mathbf{f}$,$\boldsymbol{\xi}$,$\boldsymbol{\Phi}$) but also of the geometrical properties of the bridge, needed for the simulation of pedestrian traffic. The multiplication factors which account for uncertainties in the modal parameters (section 3.5.1) are represented by $\boldsymbol{\beta}$ and the parameters required to describe the walking loading (step frequency, walking velocity, load model, etc.) are considered in $\mathbf{l}$.

Objective function

In literature, several formulations of the objective function for the (robust) TMD parameter tuning problem are found. In conventional methods, the maximum amplitude of the response in frequency domain (H_∞-norm) is often minimised [7, 8, 52, 228]. In other designs, the response is explicitly calculated and the objective function is defined by an efficiency factor relating the response

of the structure with TMD to the response of the structure without TMD, while accounting for uncertain structural parameters [119, 169]. Similar, different levels of uncertainty for the modal parameters are considered and the expected value of the objective function is minimised [98]. Alternatively, a linear combination of the mean value and the standard deviation of the peak response can be minimised [246]. A reliability based TMD design is performed in [42] accounting for a small range of uncertainties in the modal parameters for the TMD tuning. In [109, 211, 240], designs are given where human-induced excitation is considered in the objective function.

In this thesis, the design of the TMD encompasses a trade-off between performance and cost-efficiency. The design can be described as an optimisation problem where a cost function is minimised satisfying a set of constraints. Here, the total mass of the TMD(s) m_{TMD} is taken as a measure of its cost. A similar approach is proposed in [48]. Using gradient-based optimisation algorithms, the derivatives of the objective function can easily be calculated since only the TMD mass is considered.

Constraints for robustness

The proposed TMD design aims at a robust performance with respect to uncertainties in the modal parameters of the structure and variability in the loading. Aspects for the design of TMDs are discussed in section 4.2. To ensure performance, constraints for vibration serviceability and for operability can be added to the optimisation problem. Several examples for the implementation of constraints under variability in the human-induced loading frequency are found (e.g. constraints for the relative TMD displacement in [240] or constraints for the maximum acceleration in [48]). In [120], constraints are added for a linear combination of the expected value and the standard deviation of the relative TMD displacement considering uncertainty on the structural and loading parameters. Below, it is indicated how design constraints are added in this thesis, accounting for the effect of uncertainties in the modal parameters and for variability in the loading.

The constraints are formulated in terms of responses and therefore the effect of human-induced walking loading is explicitly accounted for. To ensure performance (vibration comfort) under uncertain circumstances, the robust vibration serviceability approach proposed in chapter 3 is used. For a selected level of uncertainty α, constraints are implemented for all combinations of possible values of the mean step frequency of the flow μ_{f_s} in the predefined interval (eq. (3.16)), and all possible values in the intervals of the multiplication factor of the uncertain modal parameters ($\beta_f(\alpha)$, $\beta_\xi(\alpha)$ and $\beta_m(\alpha)$). This

results in a large number of constraints, corresponding to the dimensions of the hypercube described in section 3.4. For vibration serviceability, the instantaneous peak response is evaluated and a criterion for vibration comfort $\ddot{u}_{\text{comfort}}$ is imposed by the designer. The relative TMD displacement $\Delta_{\text{rel}} = |u_{\text{TMD}} - u_{\text{B}}|$ can be limited similarly to a tolerance value Δ_{tol}. The constraints are non-linear and the gradient is here calculated using finite difference methods. Additional constraints are added for the lower and upper bound of the TMD parameters to ensure constructibility. Limits for the TMD parameters have been given in section 4.2.2.

TMD problem definition

In section 4.3, several formulations of robust optimisation problems have been summarised. Since no probabilistic analysis is made in the proposed TMD design strategy, the worst case definition is selected to define the problem. The effect of uncertainties is included in the constraints. A similar strategy has been proposed in [48] to minimise the TMD mass under criteria for vibration comfort. The proposed TMD design optimisation problem thus can be summarised as follows. To minimise the total TMD mass, taken as a measure for the cost, the vector of decision variables $\mathbf{y}$ consisting of the TMD mass m_{TMD}, stiffness k_{TMD} and damping c_{TMD}, is tuned. Constraints for vibration serviceability ($\ddot{u}_{\text{comfort}}$) and operability ($\Delta_{\text{tol}}$) are added to ensure performance under uncertain circumstances for a selected level of uncertainty α. Uncertainties in the modal parameters ($\beta_f(\alpha)$, $\beta_\xi(\alpha)$ and $\beta_m(\alpha)$) and variability in the loading (μ_{f_s}) are considered. Then, the parameter tuning problem for a single TMD can be mathematically written as follows:

$$
\begin{aligned}
\underset{\mathbf{y}}{\text{minimise}} \quad & m_{\text{TMD}} \\
\text{subject to} \quad & \ddot{u}_{\max}(\mathbf{y}, \mathbf{b}, \boldsymbol{\beta}(\alpha), \mathbf{l}, T) \leq \ddot{u}_{\text{comfort}} \quad \forall \beta_f(\alpha), \forall \beta_\xi(\alpha), \forall \beta_m(\alpha), \forall \mu_{\text{fs}} \\
& \Delta_{\text{rel}}(\mathbf{y}, \mathbf{b}, \boldsymbol{\beta}(\alpha), \mathbf{l}, T) \leq \Delta_{\text{tol}} \quad \forall \beta_f(\alpha), \forall \beta_\xi(\alpha), \forall \beta_m(\alpha), \forall \mu_{\text{fs}} \\
& \underline{\mathbf{y}} \leq \mathbf{y} \leq \bar{\mathbf{y}}
\end{aligned}
\tag{4.28}
$$

with T the length of the time window in which the response is evaluated and $\underline{\mathbf{y}}$ and $\bar{\mathbf{y}}$ representing the lower and upper bound, respectively of the decision variables.

In the proposed TMD parameter tuning problem, it is assumed that all TMD constants are tuned independently. However, conventional relations relating the TMD mass to an optimal frequency ratio and damping ratio can also be used (e.g. using equations (4.3) or (4.4)).

Trade-off between total cost and robust design

The proposed methodology allows to investigate the trade-off between the cost of the TMD and the level of robustness, i.e. for what deviations from the nominal values of the modal parameters vibration serviceability is still guaranteed.

When there is insufficient time for designing and installing the TMD based on measurements in between the construction of the bridge and before it is put into service, the largest level of uncertainties in the modal parameters ($\alpha = 0.0$) is considered to estimate the required TMD. When only seasonal variations of the modal parameters need to be accounted for, a higher α-level can be selected leading to a smaller TMD mass and a more cost-effective design. In addition, the problem can be solved considering the nominal values of the modal parameters for $\alpha = 1.0$. Then, only variability in the loading is accounted for.

The trade-off thus encompasses the total cost, containing the cost for measurements and/or TMD units, and the timing of the design process. A comparison between designs at different levels of uncertainty allows to gradually evaluate the effect of uncertainties on the TMD design.

Accounting for variations on TMD parameters

In section 4.2.4, the effect of detuning is discussed. The proposed methodology accounts for the effect of uncertainties in the modal parameters and for variability in the loading. In this way, detuning is implicitly considered since uncertainty in the natural frequency is accounted for.

The proposed approach can be extended to also consider additional uncertainty on the TMD parameters, including the TMD stiffness k_{TMD} and damping c_{TMD}. This can be modelled using multiplication factors as for the modal parameters (section 3.2). In [233], a similar approach is used to investigate the effect of detuning. Up to 20% variation is considered for the TMD stiffness k_{TMD} leading to significant detuning. The effect of uncertainty on the TMD damping c_{TMD} is rather small considering a variation of 0.5 to 1.5 times the nominal value [233]. In [182], an approach to evaluate the TMD efficiency considering uncertainty in the TMD frequency f_{TMD} and damping ξ_{TMD}, is proposed.

4.5 Effect of uncertainties on a conventional and a robust TMD design

The effect of detuned TMD parameters on the performance has been shown in section 4.2.4. To account for uncertainties in the modal parameters of the footbridge, a robust approach is proposed in section 4.4.

In this section, two designs of a TMD for the Phénix footbridge (example 2.3) are elaborated. It is investigated how the TMD performance is affected by detuning to evaluate its robustness. The effect of uncertainties in the modal parameters of the footbridge is evaluated gradually following the procedure proposed in section 3.2. The TMDs are tuned considering human-induced loading. A response calculation following the HiVoSS guideline [170] is considered (section 2.3.3). For both designs, criteria for vibration comfort and operability are imposed by limiting the maximum allowed acceleration and relative TMD displacement, respectively.

First, a conventional TMD design is elaborated in which the TMD is tuned to the nominal values of the modal parameters. Afterwards, the effects of detuning are investigated to evaluate the robust performance. Second, a robust design of the TMD is discussed. Multiple designs, performed for different levels of uncertainty, are compared to investigate the trade-off between cost and robustness.

4.5.1 Effects of detuning for a conventional TMD design

Conventional TMD design procedures are summarised in section 4.1.3 and rely on the nominal values of the modal parameters of the footbridge. The TMD frequency ratio ρ_{TMD} and damping ratio ξ_{TMD} are calculated as a function of the mass ratio μ_{TMD}, for example using equations (4.3) or (4.4). The design then consists of determining the minimally required mass ratio such that a sufficient reduction in the response is obtained and that the relative TMD displacement is feasible in the working space. In example 4.1, a conventional design procedure [222] is applied for the Phénix footbridge. It is indicated how the minimally required mass ratio is selected satisfying design constraints for different pedestrian densities. Afterwards, the effect of uncertainties on the TMD performance is investigated and shortcomings of these conventional methods are listed.

Example 4.1. Effect of detuning for a conventional TMD design for the Phénix footbridge

In this example, a conventional TMD design is elaborated for the Phénix footbridge. The effect of human-induced loading is accounted for following the procedure proposed in the HiVoSS guideline (section 2.3.3). The five pedestrian densities from table 2.5 are therefore considered. As shown in example 2.3, resonance with the first mode is expected leading to high acceleration levels. The TMD is added in the midpoint of the footbridge corresponding to the location with the largest modal displacement for the first mode.

First, the TMD design is discussed following a conventional design procedure. Second, detuning effects are investigated by considering uncertainties in the modal parameters of the structure.

TMD parameter tuning

Two design constraints are imposed to the TMD tuning problem. First, a maximum allowed (vertical) acceleration $\ddot{u}_{\text{comfort}}$ of 1 m/s^2 is imposed. Second, a constraint is added for the relative TMD displacement ($\Delta_{\text{tol}} = 45$ mm). Both constraints must be satisfied for all pedestrian densities considered in the analysis.

The TMD parameters are tuned following equation (4.4) to minimise the acceleration peak response. Then, the optimal TMD frequency ratio ρ^*_{TMD} and optimal TMD damping ratio ξ^*_{TMD} are given for a selected value of the mass ratio μ_{TMD}. The minimally required mass ratio can be determined based on an evaluation of both constraints (e.g. following the graphs proposed in figure 4.3).

The effect of human-induced walking loading is considered and the response is calculated following equations (2.63)–(2.66). For a selected pedestrian density, following relations between the maximum acceleration $\ddot{u}_{1,\max}$ and the modal damping ratio of the first mode ξ_1 hold:

$$\begin{aligned} \ddot{u}_{1,\max} &\sim \frac{\sqrt{\xi_1}}{\xi_1} \quad \text{for } d < 1\,\text{pers./m}^2 \\ \ddot{u}_{1,\max} &\sim \frac{1}{\xi_1} \quad \text{for } d \geq 1\,\text{pers./m}^2 \end{aligned} \tag{4.29}$$

where the difference for low and high pedestrian densities originates from the different equivalent numbers of pedestrians according to the guidelines

(eq. (2.63)). The effective damping ξ_{eff} thus can be calculated as follows:

$$\begin{aligned} \xi_{\text{eff}} &= \left(\frac{\ddot{u}_{1,\max}}{\ddot{u}_{\text{comfort}}} \right)^2 \xi_1 \quad \text{for } d < 1\,\text{pers./m}^2 \\ \xi_{\text{eff}} &= \left(\frac{\ddot{u}_{1,\max}}{\ddot{u}_{\text{comfort}}} \right) \xi_1 \quad \text{for } d \geq 1\,\text{pers./m}^2 \end{aligned} \tag{4.30}$$

This effective damping equals the value obtained by equation (4.6) in which ξ_{eff}^0 is related to the height of the frequency response function (eq. (4.5)). Since in the considered TMD design, the optimal parameters are found using equation (4.4), a relation between the effective damping and the mass ratio of the TMD is obtained (see figure 4.13(a)). A modal damping ratio of $\xi_1 = 0.4\%$ is assumed for the first mode. The minimally required mass ratio is retained for each pedestrian density d to satisfy the constraints. Following parameters are summarised in table 4.1: the nominal value of the natural frequency accounting for the added mass (f_1), the maximum acceleration response of the footbridge without TMD according to equation (2.66) ($\ddot{u}_{1,\max}$), the effective damping ratio prescribed by equation (4.30) (ξ_{eff}) and the minimally required mass ratio to obtain the effective damping ratio with equation (4.6). To satisfy criteria for vibration comfort (acceleration constraint), a rather low TMD mass ratio is needed. More specifically, the minimally required mass ratio to satisfy constraints for accelerations equals 0.13% and is determined by the pedestrian density of 1 pers./m^2. The proposed method is based on the simplified loading model of the guidelines to calculate the effective damping ratio (eq.(4.30)) and to evaluate the TMD performance. It is shown in [222] that this assumption is only valid for relatively low effective damping ratios, which is the case here.

The constraint for the relative TMD displacement is evaluated similarly. Figure 4.13(b) shows the ratio of the relative TMD displacement to the static deflection as a function of the mass ratio, obtained considering the footbridge and the TMD as two coupled SDOF systems. For each pedestrian density, the constraint is evaluated and the minimally required mass ratio is retained. Numerical values are given in table 4.1. A large discrepancy is found between the minimally required mass ratios for different densities due to the amplitude of the equivalent force (eq. (2.64)-(2.65)).

From table 4.1, it can be seen that the minimally required mass ratio is determined by the constraints for the relative TMD displacement for the highest pedestrian density ($\mu_{\text{TMD}} = 0.89\%$). Considering the modified values of the modal parameters accounting for the added mass of the pedestrians, the TMD constants can be calculated from the dimensionless values through equation (4.4).

The optimal TMD parameters are summarised in table 4.2 in absolute terms as well as in dimensionless values.

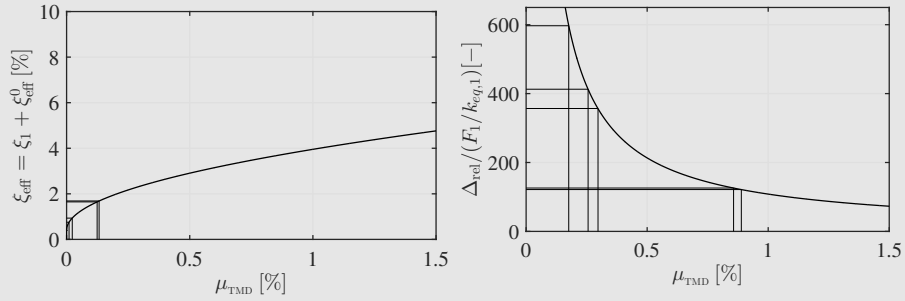

(a) (b)

Figure 4.13: Conventional TMD design for the Phénix footbridge following eq. (4.4). (a) Effective damping ξ_{eff} and (b) ratio of the relative displacement and static deflection of the footbridge with a modal damping ratio of $\xi_1 = 0.4\%$ for different values of the mass ratio μ_{TMD}. Indication of the minimally required mass ratio μ_{TMD} for different pedestrian densities.

Pedestrian density d	[pers./m^2]	0.2	0.5	0.8	1.0	1.5
Natural frequency f_1	[Hz]	1.63	1.60	1.57	1.55	1.50
$\ddot{u}_{1,\max}$	[m/s^2]	0.99	1.37	1.53	4.22	4.12
ξ_{eff} (equation (4.30))	[%]	0.39	0.75	0.93	1.69	1.65
μ_{TMD}	[%]	0.00	0.01	0.02	0.13	0.12
$\Delta_{\text{tol}}/(F_1/k_{eq,1})$	[-]	597	422	357	126	122
μ_{TMD}	[%]	0.18	0.26	0.30	0.86	**0.89**

Table 4.1: Conventional TMD design for the Phénix footbridge. Evaluation of design constraints to obtain the minimally required mass ratio.

μ_{TMD} [%]	ρ_{TMD} [-]	ξ_{TMD} [%]	m_{TMD} [kg]	k_{TMD} [N/m]	c_{TMD} [Ns/m]
0.89	0.996	5.77	1402	123515	1519

Table 4.2: Conventional TMD design for the Phénix footbridge. Optimal TMD parameters according to eq. (4.4). Values are derived considering the modified value of the modal parameters accounting for the added mass.

Effect of detuning

The effect of detuning on the TMD performance is investigated by considering uncertainty in the modal parameters of the footbridge. The approach proposed in section 3.2 is followed. Multiplication factors for the natural frequency (β_{f_1}) and the modal damping ratio (β_{ξ_1}) of the first mode are considered. No uncertainty in the modal mass is accounted for here ($\beta_m = 1$). Since resonance is assumed with the uncertain value of the natural frequency ($\beta_{f_1} \times f_1$), the amplitude of the loading varies as well and can be determined according to the HiVoSS guideline [170] as given in figure 2.10.

For different levels of uncertainty α, the maximum acceleration response and relative TMD displacement for the footbridge equipped with TMD are calculated. The results are summarised in figure 4.14(a) and (b) for the acceleration and relative displacement, respectively. The effect of added mass due to the pedestrians on the natural frequencies is accounted for in the response. The assessment at $\alpha = 1.0$ (darkest range) is for the nominal values of the natural frequency and modal damping ratio. For all pedestrian densities, the acceleration levels meet the criterion imposed for vibration comfort. The maximum acceleration is obtained for the density of 1 pers./m^2. The acceleration levels are below the value of 1 m/s^2 since the TMD mass ratio is determined by the constraint for relative displacements. For higher levels of uncertainty (dark to light), the range of accelerations increases and unacceptable levels for vibration comfort are reached (see table 2.11 for the comfort scales). For the higher pedestrian densities, a large range of responses is found at the upper bound. This is explained by the wide range of the value for the reduction coefficient when uncertainty in the natural frequency is considered. In figure 4.14(b), a similar analysis is made for the relative TMD displacement. At $\alpha = 1.0$, considering the nominal values of the modal parameters, it is expected that the calculated maximum relative displacement reaches the tolerable value of $\Delta_{\text{tol}} = 45$ mm. The resulting maximum value is slightly below the limit, however, which can be explained as follows. The TMD parameters are given by equation (4.4) assuming no modal damping while in the analysis afterwards, the value of $\xi_1 = 0.4\%$ is considered. Alternatively, the serial solution according to Asami [8] can be used to tune the TMD parameters for lightly damped structures. Again, considering the effect of uncertainties in the modal parameters, the range of calculated relative displacements strongly increases for higher levels of uncertainty.

These results clearly show how the analytical expressions from equation (4.4) allow the designer to optimally tune a damper device for a given structure with known modal parameters. However, it does not provide any robustness with respect to uncertainties in the modal parameters of the structure, which are

unavoidable in the design stage.

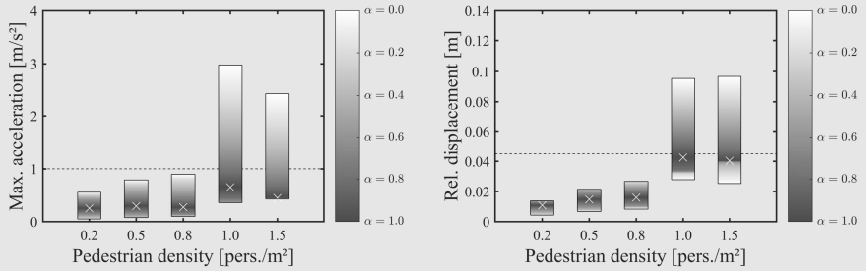

(a) (b)

Figure 4.14: Robust vibration serviceability assessment for the Phénix footbridge with TMD tuned according to equation (4.4). (a) Acceleration response, (b) Relative TMD displacement. Possible range of response for increasing levels of uncertainty for the natural frequency and the modal damping ratio (dark to light) and indication of the response at nominal conditions (×).

4.5.2 Trade-off between cost and robustness in a robust TMD design

In example 4.1, no uncertainty in the modal parameters of the footbridge is assumed for the tuning of the TMD parameters. The strategy that is followed ensures performance for the nominal values of the modal parameters. However, a strong effect of detuning is observed. In example 4.2, the robust TMD design procedure from section 4.4 is applied for the Phénix footbridge, directly accounting for the effect of uncertainty in the TMD design. A comparison is made between TMD designs at different levels of uncertainty, as also described in [110].

Example 4.2. Trade-off between TMD cost and robustness applied for the Phénix footbridge

In this example, the trade-off between the TMD cost and the degree of robustness is illustrated. As in example 4.1, the TMD is tuned to reduce vibrations of the Phénix footbridge under human-induced walking loading assuming resonance with the first mode. The effect of human-induced walking loading is explicitly considered in the TMD parameter tuning following the procedure proposed

in the HiVoSS guidelines (see section 2.3.3). First, the TMD optimisation problem is defined and the results are discussed. Second, the obtained results are evaluated with respect to the imposed design constraints.

TMD parameter tuning

The procedure proposed in section 3.2 is used to account for uncertainty in the natural frequency (β_{f_1}) and the modal damping ratio (β_{ξ_1}) of the first mode. Since resonance is assumed [170], no additional variability on the step frequency is considered.

As proposed in section 4.4, the objective is to minimise the TMD mass, taken as a measure for its cost. For each pedestrian density, the limit value for vibration comfort $\ddot{u}_{\text{comfort}}$ is set to 1 m/s^2 and the maximally allowed relative displacement Δ_{tol} is 45 mm. Both requirements are imposed as design constraints and must be satisfied for all values of the natural frequency and the modal damping ratio in their corresponding range determined by the level of uncertainty α (see section 3.2). All TMD parameters (m_{TMD}, k_{TMD}, c_{TMD}) are tuned independently from each other as decision variables. This leads to the following formulation of the optimisation problem:

$$\begin{aligned} &\underset{m_{\text{TMD}},k_{\text{TMD}},c_{\text{TMD}}}{\text{minimise}} && m_{\text{TMD}} && && \\ &\text{subject to} && \ddot{u}_{1,\max} && \leq \ddot{u}_{\text{comfort}} && \forall\beta_{f_1}(\alpha), \forall\beta_{\xi_1}(\alpha), \forall d \\ &&& \Delta_{\text{rel}} && \leq \Delta_{\text{tol}} && \forall\beta_{f_1}(\alpha), \forall\beta_{\xi_1}(\alpha), \forall d \end{aligned} \tag{4.31}$$

The optimisation problem is solved using a sequential quadratic programming (SQP) algorithm as implemented in the Matlab function *fmincon*. Constraints have been defined for each combination of the discretised intervals for β_{f_1} and β_{ξ_1} and for each density d. The optimisation problem is solved for different levels of uncertainty α to investigate the trade-off between performance and cost. For each level of uncertainty, the optimiser converges after less than 50 iterations in a few seconds of wall-clock time on a computer with an Intel Core i5-4300U @ 1.90 GHz dual core processor (4 logical processors) using Windows 7 Professional x64 in combination with 8 Gb of RAM.

The solutions of the optimisation problem (4.31) for different α-levels are given in table 4.3. The optimised TMD parameters are given both in absolute terms and in dimensionless values. To evaluate the design constraints, the range of maximum peak accelerations and the range of relative displacements is given for the pedestrian density for which the constraints are active. The values for μ_{TMD},

ρ_{TMD} and ξ_{TMD} are calculated using eq. (4.2) considering the nominal values of f_1 and ξ_1.

The results at the level $\alpha = 1.0$ correspond to a design where no uncertainties in the modal parameters are considered. Compared to the results obtained by the conventional design (table 4.2), a lower TMD mass is found but a higher damping is obtained. For a decreasing value of α, the level of uncertainty increases and the minimally required TMD mass increases illustrating the trade-off between cost and robustness. A strong increase of m_{TMD} is found from $\alpha = 0.4 \rightarrow 0.2$ and from $\alpha = 0.2 \rightarrow 0.0$ where the limit on the acceleration response for a density of 1 pers./m^2 becomes active for the highest value of the natural frequency that is possible in the interval of β_{f_1}. The TMD damping c_{TMD} increases in absolute terms with the level of uncertainty but the corresponding dimensionless value ξ_{TMD} slightly decreases. The range of peak accelerations and relative displacements also increases for a lower value of α. This is due to the wider range for $\beta_{\xi_1}(\alpha)$ and due to the strong increase of the reduction coefficient of the loading ψ (see figure 2.10), which is affected by the value of $\beta_{f_1}(\alpha)$. An overall decrease of the TMD relative displacement is also found for a larger TMD mass, corresponding to the findings in [230].

α	m_{TMD} [kg]	k_{TMD} [N/m]	c_{TMD} [Ns/m]	d [p./ m^2]	μ_{TMD} [%]	ρ_{TMD} [-]	ξ_{TMD} [%]	$\ddot{u}_{1,\max}$ [m/s^2]	Δ_{rel} [mm]
1.0	989	87821	2340	1.5	0.63	1.00	12.55	1.00-1.00	45-45
0.8	1133	104005	2628	1.5	0.72	1.02	12.11	0.86-1.00	38-45
0.6	1265	120503	2880	1.5	0.80	1.04	11.66	0.84-1.00	33-45
0.4	1396	136515	2964	1.5	0.88	1.05	10.74	0.81-1.00	28-45
0.2	1656	164717	3334	1.0	1.11	1.03	10.10	0.59-1.00	23-40
0.0	1976	201694	4366	1.0	1.33	1.04	10.94	0.57-1.00	17-36

Table 4.3: Optimised TMD parameters as a solution of eq. (4.31) for the Phénix footbridge and constraint evaluation at different α-levels.

Evaluation of TMD performance

The (robust) performance of the TMD is evaluated by verifying the constraints at each level of uncertainty α. Both the acceleration response and the relative TMD displacement are evaluated for all possible combinations of the uncertain variables $\beta_{f_1}(\alpha)$ and $\beta_{\xi_1}(\alpha)$. To illustrate the effectiveness of the TMD, the results for two TMD designs are given. The first considers the largest level of uncertainty ($\alpha = 0.0$) and the second considers a moderate level of uncertainty ($\alpha = 0.6$).

The first type of design constraints is imposed to limit the acceleration response.

At all α-levels, the acceleration constraint is active for the pedestrian densities of 1.0 and 1.5 pers./m^2 (see table 4.3). The vibration serviceability assessment for a structure with TMD is given in figure 4.15 for different α-levels. Figure 4.15(a) shows the assessment for the structure with TMD designed at $\alpha = 0.0$. It can be seen that for larger levels of uncertainty, the range of responses strongly increases. The maximum allowed acceleration level is guaranteed for each pedestrian density considering the largest range of uncertainties. In figure 4.15(b), the assessment is given for the structure with TMD tuned at $\alpha = 0.6$. The acceleration constraint is satisfied for the levels in the range $\alpha = 0.6 - 1.0$ while for higher levels of uncertainty, the maximum allowed acceleration is exceeded.

A similar evaluation is made for the relative TMD displacement (see figure 4.16). For the TMD designed at $\alpha = 0.0$, the constraint is not active as is also indicated in table 4.3. The opposite holds for the TMD designed at $\alpha = 0.6$ (figure 4.16(b)) where the relative TMD displacement is below the tolerance value for all cases in the range of $\alpha = 0.6 - 1.0$.

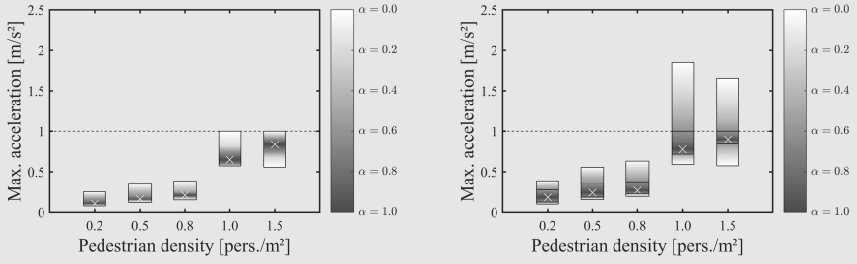

(a) (b)

Figure 4.15: Robust vibration serviceability assessment for the Phénix footbridge with TMD tuned for worst case response (a) at $\alpha = 0.0$ considering the largest range of uncertainty, (b) at $\alpha = 0.6$ considering a smaller range of uncertainty, indicated with (–). Possible range of acceleration levels for increasing levels of uncertainty for the natural frequency and the modal damping ratio (dark to light) and indication of the response at nominal conditions (×).

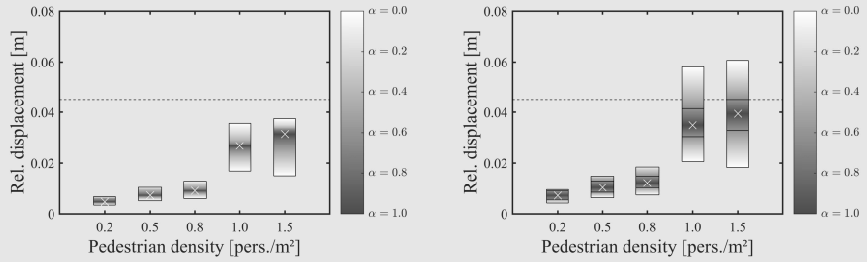

Figure 4.16: Robust evaluation of the relative TMD displacement for the Phénix footbridge with TMD tuned for worst case response (a) at $\alpha = 0.0$ considering the largest range of uncertainty, (b) at $\alpha = 0.6$ considering a smaller range of uncertainty, indicated with (–). Possible range of relative TMD displacement for increasing levels of uncertainty for the natural frequency and the modal damping ratio (dark to light) and indication of the response at nominal conditions (×).

4.6 Conclusion

In this chapter, a procedure for the robust design of TMDs has been elaborated. The procedure is developed to account for the effect of uncertainties in the modal parameters ensuring the TMD performance. An optimisation problem is defined to minimise the TMD mass, taken as a measure of its cost, by tuning the TMD mass, stiffness and damping. Design constraints are implemented for operability and vibration serviceability considering human-induced walking loading. To deal with the effect of uncertainties in the modal parameters and variability in the walking loading, the procedure proposed in chapter 3 is applied. Robustness is ensured through the implementation of the constraints. Gradient-based optimisation algorithms are used for a faster convergence to an optimised solution. The proposed procedure is generic however and can be applied for other types of vibration absorbers.

For the case study of the Phénix footbridge, two TMD designs have been elaborated to illustrate the procedure. A simplified response calculation following conventional guidelines is considered assuming resonance with the mode to which the TMD is tuned. Design constraints are added to limit the relative TMD displacement and the bridge deck acceleration. First, a conventional TMD design is discussed where the TMD parameters are tuned considering the nominal

values of the modal parameters. It is shown that the effect of uncertainties in the modal parameters strongly affects the functioning of the TMD leading to a suboptimal performance. Both constraints for the relative displacement and the acceleration are violated when detuning effects are considered. Second, the proposed robust TMD design is applied. For the considered level of uncertainty in the design, the constraints are now satisfied. The sensitivity of the TMD design to the effect of uncertainties is verified by solving the optimisation problem for different levels of uncertainty. The trade-off between cost and robustness is investigated and it is found that a design with higher robustness is characterised by an increased TMD mass and damping.

For the TMD design elaborated in the example, a simplified response calculation is considered. Resonance with the mode to which the TMD is tuned is considered and it is assumed that the amplitude of the equivalent loading is the same as in the case without TMD. In the next chapter, the proposed method for the assessment and TMD design is elaborated considering detailed load models in the simulations of pedestrian traffic. Multiple harmonic components of the loading and all modes of the structure then are considered.

Chapter 5

Case study of the Avelgem footbridge

In this chapter, the proposed methodologies for the robust vibration serviceability assessment and the robust design of a TMD for footbridges are applied in a case study. In addition to the examples given in chapter 3 and 4, the present application is elaborated more deeply to illustrate how the methodologies could be integrated in the whole construction process of a footbridge from design to completion. Simulations of pedestrian flows are considered using a detailed load model. First, the Avelgem footbridge and its dynamic behaviour are discussed in section 5.1. Second, the robust vibration serviceability assessment is presented in section 5.2 for different levels of uncertainty and for multiple pedestrian densities. It is investigated which modes are governing the response and vibration levels are evaluated with respect to vibration comfort. Third, several TMD designs are elaborated. A comparison is made to evaluate the cost-efficiency with respect to the robustness of the performance to uncertainties.

5.1 The Avelgem footbridge

The case study concerns a tied arch footbridge located in Avelgem, Belgium (see figure 5.1(a)). The footbridge is a steel box girder structure with a cross section as given in figure 5.1(b). The section is stiffened by longitudinal and transversal stiffeners. The latter are placed at regular distances over the length of the bridge. The bridge is symmetric with respect to the longitudinal and the lateral axis. The structure has one main span of 70 m and two smaller side spans of

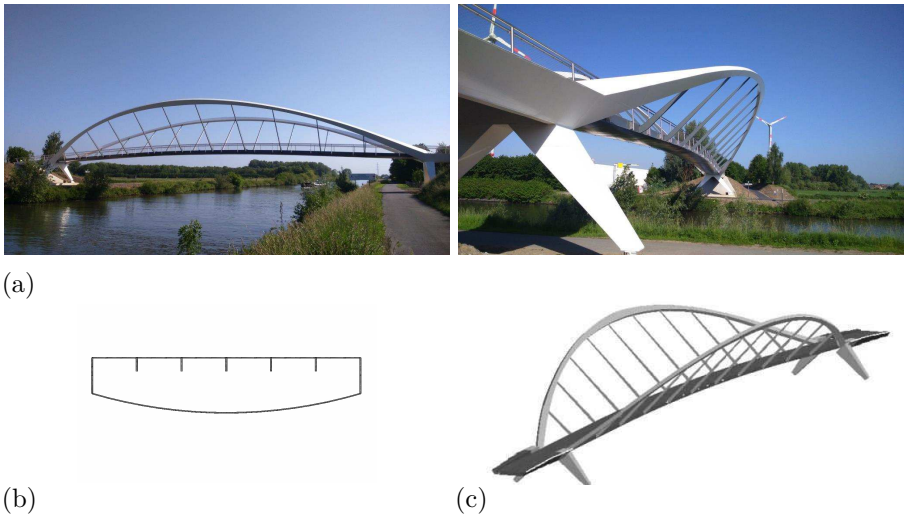

(a) (b) (c)

Figure 5.1: The Avelgem footbridge: (a) Global views, (b) cross section and (c) full view of the FEM with the bridge deck, arches, tension bars and pillars.

11 m. The total width of the deck is 3 m. The bridge has a mass of 197 ton and is simply supported at the end abutments while translations are fixed at the bottom of the pillars. A FEM in ANSYS ® [4] (see figure 5.1(c)) is used to compute the modal parameters. The arches, tension bars, stiffeners and pillars are modelled using 824 beam elements (Timoshenko beam theory) while the steel box girder section is modelled with 81410 shell elements (Mindlin-Reissner shell theory). This results in a system with a total number of 481998 DOFs.

Only the contribution of modes of the bridge deck with a frequency lower than 10 Hz, which are in the range of the harmonic components of the walking loading, will be considered. Figure 5.2 shows 10 mode shapes as computed by the FEM. The modal parameters are summarised in table 5.1. The minimum value of the equivalent mass is provided considering the maximum modal displacements of the bridge deck in longitudinal ($m_{\mathrm{eq},j,\mathrm{min,lon}}$), lateral ($m_{\mathrm{eq},j,\mathrm{min,lat}}$) and vertical ($m_{\mathrm{eq},j,\mathrm{min,ver}}$) direction and considering the maximum vector sum of all directions, corresponding to the modal mass m_j (equations (2.30) and (2.7)). High values of the equivalent mass in a direction indicate that the contribution of the mode in that direction is small. From table 5.1 and figure 5.2 it follows that modes 1, 3, 6, 8 and 9 are clear vertical bending modes while modes 2 and 5 are lateral bending modes. For modes 4, 7 and 10, both a strong vertical and lateral component is found in the torsional shape. A modal damping of 0.4% is assumed for all modes as prescribed in [9, 170] for steel footbridges.

j [-]	f_j [Hz]	ξ_j [%]	$m_{\mathrm{eq},j,\mathrm{min,lon}}$ [$\times 10^2$ ton]	$m_{\mathrm{eq},j,\mathrm{min,lat}}$ [ton]	$m_{\mathrm{eq},j,\mathrm{min,ver}}$ [ton]	m_j [ton]
1	2.02	0.4	217.0	3478.9 $\times 10^4$	47.6	47.5
2	3.54	0.4	188.0	111.7	606.5	110.3
3	3.66	0.4	148.0	1047.1$\times 10^2$	25.6	25.6
4	4.03	0.4	100.1	156.1	534.0	137.5
5	4.59	0.4	148.9	248.2	1470.0	230.6
6	4.88	0.4	174.7	3023.3$\times 10^3$	56.5	56.5
7	5.47	0.4	201.0	43.4	59.0	25.0
8	6.37	0.4	71.0	3558.7 $\times 10^6$	47.6	47.6
9	9.35	0.4	72.2	492.8 $\times 10^3$	59.3	59.1
10	9.79	0.4	51.3	138.6	367.4	121.8

Table 5.1: Modal parameters of the Avelgem footbridge as calculated by the FEM in ANSYS ® [4].

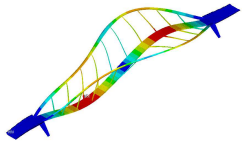

(Mode 1 - $f_1 = 2.02$ Hz)

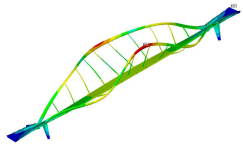

(Mode 2 - $f_2 = 3.54$ Hz)

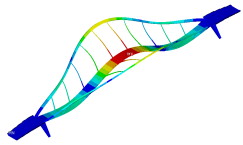

(Mode 3 - $f_3 = 3.66$ Hz)

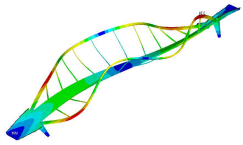

(Mode 4 - $f_4 = 4.03$ Hz)

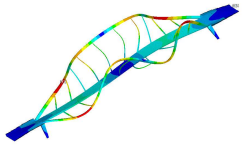

(Mode 5 - $f_5 = 4.59$ Hz)

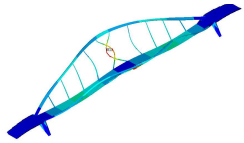

(Mode 6 - $f_6 = 4.88$ Hz)

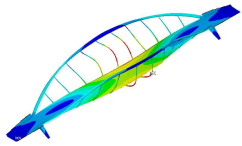

(Mode 7 - $f_7 = 5.47$ Hz)

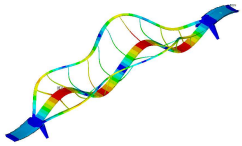

(Mode 8 - $f_8 = 6.37$ Hz)

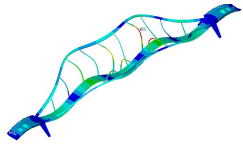

(Mode 9 - $f_9 = 9.35$ Hz)

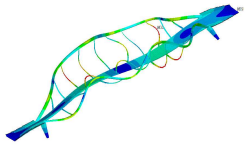

(Mode 10 - $f_{10} = 9.79$ Hz)

Table 5.2: Results of the FEM of the Avelgem footbridge: 3D view of the first 10 mode shapes.

5.2 Robust vibration serviceability assessment

A robust vibration serviceability assessment of the Avelgem footbridge is discussed in this section. The methodology proposed in chapter 3 is followed. The effect of uncertainties in the modal parameters and variability in the loading is accounted for. First, the effect of human-structure interaction on the modal parameters is investigated. The equations of motion for the coupled crowd-structure system have been derived in section 2.3.2. Second, scenarios for the simulations of moving pedestrian traffic are given. Third, the results of the robust vibration serviceability assessment are discussed. The analysis is performed for five different pedestrian densities as previously introduced in example 2.2 (see table 2.5).

5.2.1 Effect of human-structure interaction on the modal parameters

The effect of HSI on the dynamic behaviour of the structure is investigated in nominal conditions first. The transfer function for accelerations is given in figure 5.2 for the empty structure and for the coupled crowd-structure system considering HSI for the pedestrian densities of 0.2, 0.5, 0.8, 1.0 and 1.5 pers/m^2. The nominal values of the human body characteristics are considered. In figure 5.2(a), the input and output point for the transfer function are the antinode of the first mode (point A, figure 5.3). The first peak of the transfer function corresponds to the first mode and is found at 2.02 Hz for the empty structure. The other peaks represent the contribution of the third, fourth, sixth, seventh and ninth mode. In figure 5.2(b), the input and output point correspond to the point at midspan of the footbridge (point B, figure 5.3). The contribution of the third, sixth, seventh and ninth mode are visible. Considering the coupled crowd-structure system, slightly different transfer functions are obtained. Shifted values of the natural frequencies and an increased effective damping ratio are observed.

The effect of HSI on the modal parameters is given in table 5.3 for three selected modes by summarising the modified value of the natural frequency, the ratio of the added modal mass of the crowd to the modal mass of the considered mode and the effective damping ratio following equation (3.21). First, the values are given for the first mode for which the natural frequency is lower than the human body frequency ($f_1 < f_{\text{H}}$). Second, the effect of HSI on the third mode is investigated which has a natural frequency relatively close to the human body frequency ($f_3 \approx f_{\text{H}}$). Third, the ninth mode is considered for which the natural frequency is far above the human body frequency ($f_9 \gg f_{\text{H}}$).

Pedestrian density d	[pers./m^2]	0.2	0.5	0.8	1.0	1.5
Natural frequency f_1	[Hz]	1.98	1.92	1.87	1.84	1.78
Mass ratio $m_{1,\text{crowd}}/m_1$	[%]	3.31	8.28	13.25	16.56	24.84
Effective damping $\xi_{\text{eff},1}$	[%]	0.77	1.21	1.57	1.77	2.16
Natural frequency f_3	[Hz]	3.64	3.61	3.55	3.54	3.05
Mass ratio $m_{3,\text{crowd}}/m_3$	[%]	3.38	8.46	13.53	16.91	25.37
Effective damping $\xi_{\text{eff},3}$	[%]	2.76	6.36	9.95	12.36	17.55
Natural frequency f_9	[Hz]	9.36	9.38	9.40	9.42	9.46
Mass ratio $m_{9,\text{crowd}}/m_9$	[%]	2.90	7.25	11.60	14.50	21.75
Effective damping $\xi_{\text{eff},9}$	[%]	0.70	1.15	1.59	1.87	2.55

Table 5.3: Effect of human-structure interaction on the modal parameters of the first, third and ninth mode of the Avelgem footbridge.

The natural frequency of the first mode decreases for higher pedestrian densities since the crowd is stiffer than the footbridge and mainly acts as added mass [219]. The effective damping is affected and increases for higher pedestrian densities, as is also concluded for the Phénix footbridge in example 3.2. For natural frequencies of the bridge close to the human body frequencies (e.g. $f_3 = 3.66$ Hz), it is more difficult to distinguish the modified values of the natural frequency. Generally, a decrease is found for values close to the human body frequency. The maximum value in the neighbourhood of the original frequency is retained and is given in table 5.3. The effect of HSI on the effective damping is much more significant. Substantially increased values are found for both low and high pedestrian densities (see table 5.3). For higher modes ($f_j \gg f_{\text{H}}$), the pedestrians are more flexible than the structure and the natural frequency remains close to that of the empty structure. An increase of the effective damping is noticed as well, illustrated in table 5.3 for the ninth mode.

5.2.2 Scenarios for the simulations

For each pedestrian density, simulations of moving pedestrian traffic are performed considering variability in the average step frequency μ_{f_s} and uncertainties in the modal parameters (see section 3.2). Since the uncertainties are of a general nature, the multiplication factors are applied to the properties of all modes simultaneously as proposed in section 3.2.3. Variations in the loading are dealt with as discussed in section 3.3. Continuous flows of pedestrians are composed for each pedestrian density and for each value of μ_{f_s} in the interval (see section 3.3.2). To account for inter-subject variability, the step frequencies

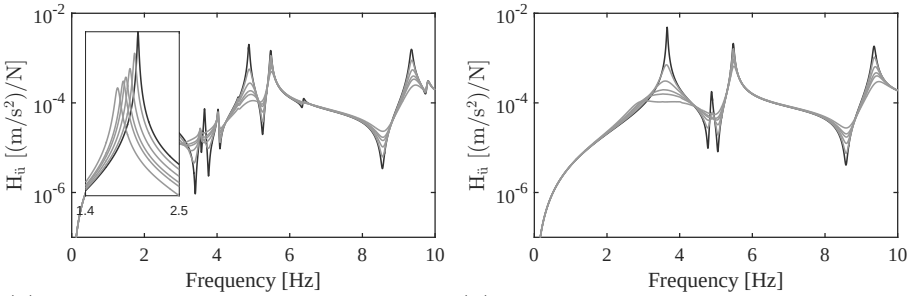

Figure 5.2: Transfer function for vertical accelerations of the empty structure (dark) and the coupled crowd-structure system for different pedestrian densities (light). Input and output point at the antinode of (a) mode 1 (b) mode 3 (midspan).

of the pedestrians are sampled from following distribution: $f_s \sim \mathcal{N}(\mu_{f_s}, \sigma_{f_s})$ with σ_{f_s} depending on the pedestrian density. The assumptions made for the simulations at nominal conditions are summarised in table 3.1. The longitudinal position of the pedestrians is determined by their walking velocity while the lateral position is sampled from five possible walking paths, equally spaced along the width of the bridge (see figure 5.3). HSI effects are accounted for considering the human body parameters from table 3.1.

As can be seen from table 5.3 and figure 5.2, a considerable increase of the effective damping is obtained by HSI for almost all modes. The effect increases for higher pedestrian densities and is larger for higher crowd-bridge modal mass ratios [219]. For higher pedestrian densities, the effective damping is much higher than that of the empty footbridge and a rather minor influence of uncertainty in the modal damping is therefore expected in the vibration serviceability assessment. For lower pedestrian densities, however, a larger effect is expected and uncertainty in the modal damping ratio is relevant. The uncertainty in the modal mass affects the amplitudes of the steady-state response, related to the height of the peaks, as well. The responses are mainly determined by an increased effective damping due to HSI. It has been verified that uncertainty in the modal mass has only small effects on the response for both low and high crowd-structure modal mass ratios. Therefore, no uncertainty in the modal mass is accounted for in the vibration serviceability assessment. Uncertainty in the natural frequency and variability on the average step frequency are important to evaluate if resonance can occur which is determining for the vibration serviceability assessment as has been concluded in section 3.5.

In the simulations, the interval of the average step frequency is discretised with

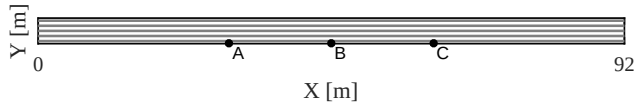

Figure 5.3: Top view of the Avelgem footbridge with indication of the five possible walking paths.

a fixed absolute value of 0.01 Hz while the intervals of the multiplication factors β_f and β_ξ were discretised with a fixed number of 21 uniformly distributed values. No additional uncertainty in the modal mass is considered for the reasons stated above. The computing time for the full analysis (considering all pedestrian densities and all uncertainties) is approximately 300 minutes on a desktop computer with an Intel Xeon E5-2630 @ 2.40 GHz quad core processor (32 logical processors) using Windows 10 Enterprise x64 in combination with 144 Gb of RAM.

The response is calculated for the coupled crowd-structure system (see section 2.3.2 for the equations of motion) and is evaluated by calculating the 95th percentile of the instantaneous peak value obtained in a time window of $2 \times \frac{92 \text{ m}}{1.34 \text{ m/s}} \approx 137$ s corresponding to twice the time pedestrians need to cross the bridge as suggested in [9, 170, 251]. The instantaneous peak value of the response is approximated as $\mu_{\ddot{u}_{\max}(T)} + 2\sigma_{\ddot{u}_{\max}(T)}$ using equations (2.67)–(2.69). The focus is on the assessment of vertical vibrations, but the same methodology can be followed for lateral vibrations. The response is calculated at all locations of the bridge deck and the overall maximum value over all bridge deck points is retained in the final assessment.

5.2.3 Discussion

An extensive discussion of the results is given below. It is indicated which modes are governing the response and how the response is affected by the considered ranges of uncertainties. Vibration levels are evaluated with respect to comfort criteria and it is shown for which locations of the bridge the maximum response is obtained.

Evaluation at nominal conditions

The robust vibration serviceability assessment of the Avelgem footbridge is given in figure 5.4(a) as a function of the level of uncertainty in the modal parameters α for five pedestrian densities. The contribution of all modes is considered

(left bars). The level $\alpha = 1.0$ (darkest) does not consider uncertainty in the modal parameters and represents the possible acceleration levels considering only variability in the average step frequency. For higher levels of uncertainty (dark to light), the minimal and maximal possible value of the instantaneous peak acceleration account for both variability in the loading and uncertainty in the modal parameters. The values of the instantaneous peak acceleration corresponding to the nominal values of the modal parameters and the average value of μ_{f_s} for each pedestrian density are indicated by cross markers. An indication of the level of vibration comfort (maximum, medium, minimum or unacceptable) according to [9] is added.

For nominal conditions of the flow and disregarding uncertainty in the modal parameters, the response slightly increases for densities up to 0.8 pers./m^2 and then strongly reduces for the higher densities (see figure 5.4(a)). The reduction in the walking speed for an increasing pedestrian density drives the values of the average step frequency (table 2.5) further away from the dominant natural frequency of the footbridge in this particular case (here $f_1 = 2.02$ Hz for the empty footbridge). Then, no resonance is expected. However, due the added mass effect of the pedestrians, the value of the first natural frequency also decreases for increasing pedestrian densities (see table 5.3). For these higher densities, the added damping effect of HSI increases leading to a significant reduction of the response [219].

A similar analysis is made considering only the contribution of the first mode in the response. In figure 5.4(a) (right bars), the results are compared to those obtained considering all modes. It can be seen that in this particular case, the response is mainly governed by the contribution of the first mode since the additional effects of other modes are relatively small.

Modes contributing to the response

To interpret the results from figure 5.4, the shifted value of the natural frequencies relative to the average value of μ_{f_s} are considered (see table 2.5). This information is given for two pedestrian densities (0.2 and 1.5 pers./m^2) in figure 5.5, which shows the acceleration PSD function of the vertical acceleration at point A from figure 5.3, corresponding to the antinode of mode 1. Here, the nominal values of the modal parameters and the nominal conditions for the flow are considered.

For the pedestrian density of 0.2 pers./m^2, a first peak is found around 1.95 Hz. The average value of the first harmonic component of the walking loading ($\mu_{f_s} = 1.89$ Hz) and deviating values ($\sigma_{f_s} = 0.10$ Hz) of the step frequencies for which resonance occurs with the natural frequency of the first mode (at

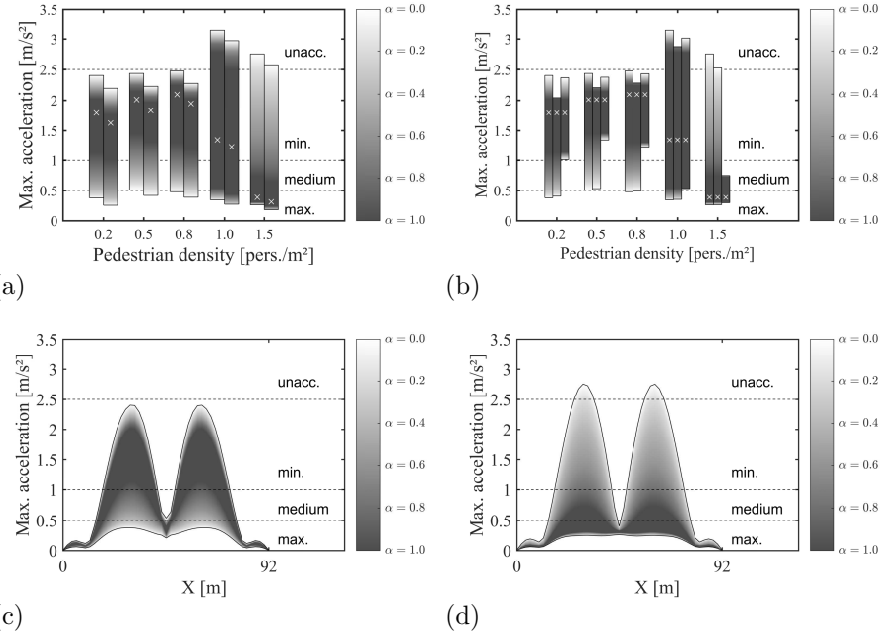

Figure 5.4: Robust vibration serviceability assessment for the Avelgem footbridge: possible range of the 95th percentile of the instantaneous peak response accounting for variability in the loading and for uncertain modal parameters of the structure, indicated by increasing levels of uncertainty in the natural frequency and modal damping ratio (dark to light) and indication of the response at nominal conditions (×). Comfort criteria according to [9]. Overall maximum of all locations of the bridge deck for different pedestrian densities: (a) considering the contribution of all modes (left bars) and the first mode only (right bars). (b) effect of uncertainties of β_f and β_ξ combined (left bars), β_f only (middle bars) and β_ξ only (right bars). Maximum response along the length of the bridge for (c) 0.2 pers./m^2 and (d) 1.5 pers./m^2.

1.98 Hz for $d = 0.2$ pers./m^2, see table 5.3) are contributing to the peak. If only the first mode is accounted for in the calculation (dashed line in fig. 5.5), the contribution due to higher harmonic loading components is clearly observed at 3.78 Hz, 5.67 Hz and 7.56 Hz for the second, third and fourth harmonic component respectively. If the PSD of the acceleration response considering all modes contributing to the response is evaluated, more peaks are found representing the contribution of other modes due to higher harmonic loading components. For example, for a density $d = 0.2$ pers./m^2, additional peaks are found around 4.9 Hz, 5.5 Hz, and 9.3 Hz corresponding to contributions of the sixth, seventh and ninth mode, respectively. However, their contribution to the total response is rather small as can be seen from figure 5.4(a).

For higher densities, the natural frequencies shift further from the nominal values due to HSI-effects. For the highest pedestrian density of $d = 1.5$ pers./m^2, it is observed that the first natural frequency of the footbridge is significantly influenced by the pedestrians (see table 5.3). The first peak of the PSD at point A is relatively broad and is found in a frequency range around 1.56 Hz for $d = 1.5$ pers./m^2 (figure 5.5(b)). This is due to the contribution of the first harmonic component of the loading with $\mu_{f_s} = 1.51$ Hz and for deviating values for which near-resonance occurs with the shifted value of the natural frequency of the first mode (1.78 Hz). The contribution of other modes is found at 5.57 Hz and 9.38 Hz for the seventh and ninth mode respectively. The contribution of the sixth mode is very small as could also be concluded from the transfer function from figure 5.2(a) (highest density). If only the contribution of the first mode is accounted for, the contribution due to the second, third and fourth harmonic component of the loading is clearly observed at 3.02 Hz, 4.53 Hz and 6.04 Hz respectively.

Effect of uncertainties

Figure 5.4(a) illustrates how a wider range of uncertainties in the modal parameters leads to a larger interval of the instantaneous peak response. The effect of uncertainties on the calculated acceleration levels is further discussed below for different pedestrian densities. In figure 5.4(b), the particular effect of uncertainty in the natural frequency and modal damping ratio on the vibration serviceability assessment is given assuming the contribution of all modes. A comparison is made between the assessment considering all uncertainties (left bars), considering only uncertainty in natural frequencies (middle bars) and considering only uncertainty in modal damping ratios (right bars). Variability on the average step frequency is considered in all analyses.

For pedestrian densities up to 0.8 pers./m^2, (near-)resonance can occur for the

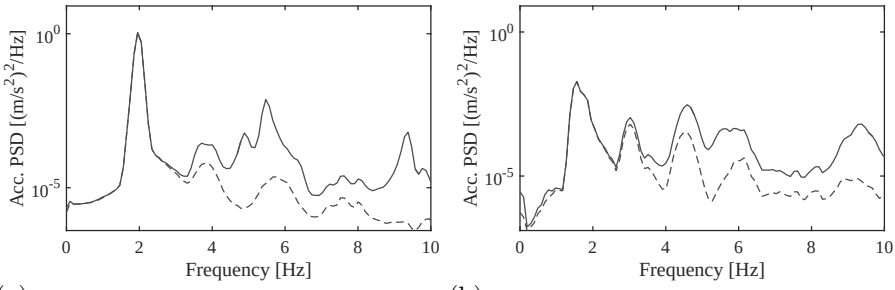

Figure 5.5: PSD of the acceleration response at point A assuming nominal conditions ($\beta_f = 1$, $\beta_\xi = 1$ and $\mu_{f_s} = \bar{f}_s$) and considering the contribution of all modes (–) and the first mode only (– –) to the response for a pedestrian density of (a) $d = 0.2$ pers./m^2 and (b) $d = 1.5$ pers./m^2.

loading frequency $\mu_{f_s} \in [\bar{f}_s - 0.1, \bar{f}_s + 0.1]$ and the natural frequency of the first mode, resulting in a range of relatively high responses for the nominal conditions. Considering uncertainties in the natural frequency leads to non-resonant cases, resulting in a strongly decreased response which explains the wide range of responses at the lower bound. On the contrary, the intervals at the upper bound are much smaller since resonance is already possible for the nominal conditions. This is clearly seen in figure 5.4(b) where the effect of uncertainty in the natural frequency only is visualised separately (middle bars). The effect of uncertainty in the modal damping ratio is visualised similarly (right bars) and is larger for the range at the upper bound when compared to that at the lower bound. The range of responses of the right bars is mainly determined by the considered variation on the average step frequency.

A similar interpretation holds for the pedestrian density of 1 pers./m^2. However, the range of responses at nominal conditions is now much larger since both near-resonance and off-resonance is possible between the average step frequency $\mu_{f_s} \in [1.73 - 0.1, 1.73 + 0.1]$ Hz and the shifted value of the natural frequency (1.84 Hz). The effect of uncertainties is therefore smaller for the range at both the upper and lower bound. The effect of β_ξ results in slightly higher response values but remains rather small due to the relatively high effective damping ratio that substantially increases by the added damping of the human bodies.

For the highest pedestrian density, i.e. for 1.5 pers./m^2, no resonance for $\mu_{f_s} \in [1.51 - 0.1, 1.51 + 0.1]$ Hz and the shifted value of the natural frequency of the first mode (around 1.78 Hz) is expected which explains the small range of relatively low response levels at nominal conditions. For this density, the effect of human-structure interaction leads to a significant reduction of the

response. If additional uncertainty in the natural frequency is considered, the effect on the response is relatively small at the lower bound since off-resonance is already the case at nominal conditions resulting in low vibration levels. The effect of uncertainty in the natural frequency at the upper bound of the range is much larger since (near-)resonance can occur between the natural frequency and step frequency, resulting in higher vibration levels (see also figure 5.4(b)). The additional effect of β_ξ here is very low since the added damping due to the human bodies already results in a strongly increased effective damping ratio.

For this particular footbridge, it can thus be concluded that the additional effect of variability on the average step frequency is determining for the vibration serviceability assessment for pedestrian densities $d \leq 1$ pers./m^2. By considering the effect of uncertainty in the modal damping ratio, the ranges of responses slightly increase. The effect of uncertainty in the natural frequency is rather low since resonance between the loading and the first mode is possible at nominal conditions. For the highest density of 1.5 pers./m^2, the effect of uncertainty in the natural frequency is determining since resonance cannot occur at the nominal situation. The effect of uncertainty in the modal damping ratio is rather small due to the relatively high effective damping determined by the added damping of the human bodies.

Response evaluation at different locations on the bridge deck

Figure 5.4(a) only shows the overall maximum response along the bridge deck for different pedestrian densities. A closer look at the response for different locations along the length of the bridge deck is given in figure 5.4(c) and (d) for the pedestrian densities of 0.2 and 1.5 pers./m^2 respectively. Figure 5.4(a) is a summary of the results from figure 5.4(c) and (d). For example, the upper and lower bound of the range of responses at $\alpha = 0.0$ in figure 5.4(a) correspond to the maximum values of the upper and lower bound given for $\alpha = 0.0$ for different locations along the length of the bridge in figure 5.4(c) and (d). For the pedestrian densities of 0.2 and 1.5 pers./m^2, the small and large range, respectively, at the upper bound is clearly visible. As already concluded, the contribution of the first mode is governing the response and the maximum accelerations are obtained at the antinodes of that mode (point A and C in figure 5.3).

Vibration comfort

A minimum level of vibration comfort is predicted at the level $\alpha = 1.0$ for all pedestrian densities up to 0.8 pers./m^2 while unacceptable levels are reached

for 1 pers./m^2. For the highest density, a maximum level of vibration comfort is predicted for $\alpha = 1.0$. When uncertainty in the natural frequency and modal damping ratio is considered, it is found that the level of comfort becomes unacceptable for the highest densities of 1 and 1.5 pers./m^2 for some values of the parameters. For all other pedestrian densities, a minimum level for vibration comfort is predicted. Similar levels of vibration comfort are found when only the contribution of the first mode is considered.

5.3 Cost-effective TMD design for the Avelgem footbridge

From section 5.2, it follows that the response of the Avelgem footbridge is governed by the contribution of the first mode while only a small contribution of other modes is found, both for nominal and deviating conditions. Minimum to unacceptable levels for vibration comfort are found. To ensure vibration comfort, a TMD is designed. For an optimal performance of the TMD, the device is preferably installed close to the antinodes of the mode to which it is tuned (see section 4.1.3). In this case, two locations are possible which both correspond to antinodes of the first mode (point A and C in figure 5.3). If these locations are not feasible, e.g. due to practical limitations, this lead to a suboptimal performance.

In this section, different design scenarios of the TMD are elaborated and compared to each other to find the most cost-effective solution while ensuring robustness with respect to uncertainties. First, a single TMD at one of the antinodes of the first mode is considered (Case A). The minimally required mass is determined such that design criteria are satisfied and the TMD parameters are tuned independently from each other. From [178, 241], it is concluded that the robustness can be increased by considering multiple TMDs and it is interesting to investigate if the cost can be reduced by considering multiple TMDs. In this application, this is investigated considering two TMDs, one at each antinode of the first mode. In the second case (Case B), two identical TMDs are considered. Third, it is investigated if the cost can be further reduced by two independently tuned TMDs (Case C). A fourth TMD design is considered where two TMDs are tuned independently following the conventional tuning from equation (4.4) (Case D). A comparison is made between the different cases and criteria for vibration comfort are evaluated for different levels of uncertainty. The contribution of all modes is accounted for in the TMD design.

First, the TMD design problem as introduced in chapter 4 is applied for the Avelgem footbridge. The equations of motion for the coupled crowd-structure-

TMD system are given as well. Second, the results of the optimisation problem are discussed for all TMD design cases. Third, the TMD performance is evaluated considering the vibration serviceability assessment for the structure with TMD(s). Afterwards, the additional effect of variation in the optimised TMD characteristics on the performance is investigated.

5.3.1 TMD design problem for the Avelgem footbridge

Problem formulation

The general TMD parameter tuning problem (4.28) is rewritten in equation (5.1) to account for multiple TMDs. As decision variables, the TMD mass m_{TMD}, stiffness k_{TMD} and damping c_{TMD} of the different TMDs are considered. The aim is to minimise the TMD mass as a measure for its cost while meeting the vibration serviceability criteria. Below, the optimisation problem is defined for the Avelgem footbridge for the tuning of n TMDs (with $n = 1$ or $n = 2$ depending on the considered design case).

$$\begin{aligned} &\underset{\mathbf{y}}{\text{minimise}} \quad C^T\mathbf{y} \\ &\text{subject to} \qquad \underset{\forall\beta_f(\alpha),\forall\beta_\xi(\alpha),\forall\mu_{f_s}}{\mu_{\ddot{u}_{\max}(T)} + 2\sigma_{\ddot{u}_{\max}(T)}} \leq \ddot{u}_{\text{comfort}} \end{aligned} \tag{5.1}$$

$$\text{with } \mathbf{y} = \begin{bmatrix} m_{\text{TMD},1} \\ k_{\text{TMD},1} \\ c_{\text{TMD},1} \\ \vdots \\ m_{\text{TMD},n} \\ k_{\text{TMD},n} \\ c_{\text{TMD},n} \end{bmatrix} \text{ and the selected cost function } C = \begin{bmatrix} 1 \\ 0 \\ 0 \\ \vdots \\ 1 \\ 0 \\ 0 \end{bmatrix}.$$

In this case, the limit for vertical vibrations is $\ddot{u}_{\text{comfort}} = 0.5\ \text{m/s}^2$, corresponding to a maximum level of vibration comfort [9]. Since the footbridge is located in a rural environment, unrestricted pedestrian traffic is expected. The TMD is designed such that all design criteria are satisfied for a pedestrian density up to 0.5 pers./m^2. No limits for relative TMD displacements are considered.

Non-linear constraints are implemented for all combinations of the mean step frequency of the flow μ_{f_s}, and all values of the multiplication factor of the uncertain frequency β_f and modal damping β_ξ at the level α as proposed for a worst case design in section 4.3.1.

The proposed methodology for the TMD design allows to investigate the trade-off between the cost of the TMDs and the level of robustness, i.e. for what deviations from the nominal values of the modal parameters vibration serviceability is still guaranteed [111]. To illustrate the trade-off, the problem for the Avelgem footbridge is solved three times for each of the cases. First, the largest level of uncertainties in the modal parameters is considered corresponding to $\alpha = 0.0$. Second, the problem is solved for a higher α-level ($\alpha = 0.6$). In addition, the problem is solved a third time considering the nominal values of the modal parameters for $\alpha = 1.0$ where only variability in the loading is accounted for. The trade-off thus encompasses the total cost, containing the cost for measurements and/or TMD units, and the timing of the construction process that can be related to the selected α-level.

The optimisation problem defined in equation (5.1) is solved using a gradient based method with an interior-point approach for handling the constraints as implemented in Matlab (*fmincon* function) [204]. In order to reduce the computational effort, a coarser discretisation of the intervals of the multiplication factors is considered. The interval for β_f contains six values and for β_ξ, only the lowest possible value is considered assuming this situation as the most disadvantageous. The interval of the average step frequency contains eleven values. Afterwards, the solution is verified considering the finer discretisation for μ_{f_s}, β_f and β_ξ.

Coupled crowd-structure-TMD system

The interaction forces between the TMD, modelled as a SDOF system, and the structure can be derived similarly as for the human bodies (see section 2.3.2). The equations of motion for the coupled crowd-structure-TMD system are now defined as:

$$\bar{\mathbf{M}}_{\text{TOT}} \begin{bmatrix} \ddot{\mathbf{z}}(t) \\ \ddot{\mathbf{u}}_{\text{H}}(t) \\ \ddot{\mathbf{u}}_{\text{TMD}}(t) \end{bmatrix} + \bar{\mathbf{C}}_{\text{TOT}} \begin{bmatrix} \dot{\mathbf{z}}(t) \\ \dot{\mathbf{u}}_{\text{H}}(t) \\ \dot{\mathbf{u}}_{\text{TMD}}(t) \end{bmatrix} + \bar{\mathbf{K}}_{\text{TOT}} \begin{bmatrix} \mathbf{z}(t) \\ \mathbf{u}_{\text{H}}(t) \\ \mathbf{u}_{\text{TMD}}(t) \end{bmatrix} = \begin{pmatrix} \boldsymbol{\Phi}^{\mathsf{T}} \mathbf{S}_{\text{H}}(t) \mathbf{p}_s(t) \\ \mathbf{0} \\ \mathbf{0} \end{pmatrix} \quad (5.2)$$

with $\mathbf{u}_{\text{TMD}}$ referring to the displacement of the bridge deck at the DOFs of the FEM corresponding to the location of TMDs. $\bar{\mathbf{M}}_{\text{TOT}} \in \mathbb{R}^{\frac{n_s}{2} \times \frac{n_s}{2}}$, $\bar{\mathbf{C}}_{\text{TOT}} \in \mathbb{R}^{\frac{n_s}{2} \times \frac{n_s}{2}}$ and $\bar{\mathbf{K}}_{\text{TOT}} \in \mathbb{R}^{\frac{n_s}{2} \times \frac{n_s}{2}}$ are the total mass, damping and stiffness matrix

respectively, with $n_{\mathrm{s}} = 2(n_{\mathrm{dof}} + n_{\mathrm{H}} + n_{\mathrm{TMD}})$ and are composed as follows:

$$\bar{\mathbf{M}}_{\mathrm{TOT}} = \begin{bmatrix} \bar{\mathbf{M}} & \mathbf{0} & \mathbf{0} \\ \mathbf{0} & \mathbf{M}_{\mathrm{H}} & \mathbf{0} \\ \mathbf{0} & \mathbf{0} & \mathbf{M}_{\mathrm{TMD}} \end{bmatrix} \tag{5.3}$$

$$\bar{\mathbf{C}}_{\mathrm{TOT}} = \begin{bmatrix} \bar{\mathbf{C}} & -\boldsymbol{\Phi}^{\mathsf{T}}\mathbf{S}_{\mathrm{H}}(t)\mathbf{C}_{\mathrm{H}} & -\boldsymbol{\Phi}^{\mathsf{T}}\mathbf{S}_{\mathrm{TMD}}\mathbf{C}_{\mathrm{TMD}} \\ -\mathbf{C}_{\mathrm{H}}\mathbf{S}_{\mathrm{H}}^{\mathsf{T}}(t)\boldsymbol{\Phi} & \mathbf{C}_{\mathrm{H}} & \mathbf{0} \\ -\mathbf{C}_{\mathrm{TMD}}\mathbf{S}_{\mathrm{TMD}}^{\mathsf{T}}\boldsymbol{\Phi} & \mathbf{0} & \mathbf{C}_{\mathrm{TMD}} \end{bmatrix} \tag{5.4}$$

$$\bar{\mathbf{K}}_{\mathrm{TOT}} = \begin{bmatrix} \bar{\mathbf{K}} & -\boldsymbol{\Phi}^{\mathsf{T}}\mathbf{S}_{\mathrm{H}}(t)\mathbf{K}_{\mathrm{H}} & -\boldsymbol{\Phi}^{\mathsf{T}}\mathbf{S}_{\mathrm{TMD}}\mathbf{K}_{\mathrm{TMD}} \\ -\mathbf{K}_{\mathrm{H}}\mathbf{S}_{\mathrm{H}}^{\mathsf{T}}(t)\boldsymbol{\Phi} & \mathbf{K}_{\mathrm{H}} & \mathbf{0} \\ -\mathbf{K}_{\mathrm{TMD}}\mathbf{S}_{\mathrm{TMD}}^{\mathsf{T}}\boldsymbol{\Phi} & \mathbf{0} & \mathbf{K}_{\mathrm{TMD}} \end{bmatrix} \tag{5.5}$$

with $\mathbf{M}_{\mathrm{TMD}} = \mathrm{diag}\{m_{\mathrm{TMD},n}\}$ and $\mathbf{S}_{\mathrm{TMD}} \in \mathbb{R}^{n_{\mathrm{dof}} \times n_{\mathrm{TMD}}}$ a time-invariant selection matrix transferring the forces of the TMD to the corresponding DOFs of the FEM of the bridge. The state-space equation now reads as:

$$\dot{\mathbf{x}}(t) = \mathbf{A}_c(t)\mathbf{x}(t) + \mathbf{B}_c \begin{pmatrix} \boldsymbol{\Phi}^{\mathsf{T}}\mathbf{S}_{\mathrm{H}}(t)\mathbf{p}_s(t) \\ \mathbf{0} \\ \mathbf{0} \end{pmatrix} \tag{5.6}$$

with $\mathbf{x}(t) \in \mathbb{R}^{n_{\mathrm{s}}}$ the state vector that contains the modal displacement and modal velocities of all nodes and the displacements and velocities of each human body and each TMD:

$$\mathbf{x}(t) = \begin{bmatrix} \mathbf{z}(t) \\ \mathbf{u}_{\mathrm{H}}(t) \\ \mathbf{u}_{\mathrm{TMD}}(t) \\ \dot{\mathbf{z}}(t) \\ \dot{\mathbf{u}}_{\mathrm{H}}(t) \\ \dot{\mathbf{u}}_{\mathrm{TMD}}(t) \end{bmatrix} \tag{5.7}$$

The continuous time system matrix $\mathbf{B}_c \in \mathbb{R}^{n_{\mathrm{s}} \times \frac{n_{\mathrm{s}}}{2}}$ is defined as:

$$\mathbf{B}_c = \begin{bmatrix} \mathbf{0} \\ \bar{\mathbf{M}}_{\mathrm{TOT}}^{-1} \end{bmatrix} \tag{5.8}$$

5.3.2 Results

The solution of the optimisation problem defined by equation (5.1) (TMD parameters) is summarised in table 5.4 for the three considered values of α and for the different design cases (A-B-C-D). Both absolute values and dimensionless

parameters corresponding to the TMD characteristics are given considering the nominal values of the modal mass and natural frequency of the first mode of the footbridge (see table 5.1). Below, the results of the different designs are discussed and a comparison of the cost-efficiency is made.

Single TMD (Case A)

In case A, a single TMD at position A (figure 5.3) is considered. The TMD parameters are tuned independently from each other for the considered levels of uncertainty and are summarised in table 5.4. For decreasing levels of uncertainty, the total TMD mass and damping decreases. The TMD frequency is slightly below the natural frequency of the first mode and a relatively high TMD mass ratio μ_{TMD} is obtained (7–9%).

Two identical TMDs (Case B)

The TMD design is now repeated considering two identical TMDs, each positioned at one antinode of the first mode (point A and C in figure 5.3). The TMD mass, stiffness and damping are the same for both TMDs and are independently tuned. As for the case of the single TMD, the total TMD mass increases for higher levels of uncertainty and the TMD frequencies are slightly below the nominal value of the natural frequency at which they are tuned. Two identical TMDs are obtained, each with a mass ratio below 5%. When compared to the case of a single TMD (Case A), the total TMD mass has been decreased.

Two independently tuned TMDs (Case C)

In the third design, two different TMDs are considered for which the parameters are tuned independently from each other. As for cases A and B, a lower total TMD mass and damping are found at a lower level of uncertainty ($\alpha = 0.0 \rightarrow \alpha = 1.0$). A considerable difference is found between the masses of the TMDs at both locations (point A and C in figure 5.3) but with a smaller total mass compared to the cases of a single TMD (Case A) and two identical TMDs (Case B). In this particular case, all modes of the footbridges are symmetrical so that the positioning of the TMDs can switch without loss of effectiveness. For the TMDs tuned at $\alpha = 0.6$ and $\alpha = 1.0$, a strong decrease of the TMD damping c_{TMD} is obtained as well.

The frequency of the TMDs is close to the natural frequency of the first mode of the footbridge in the range between $\beta_f^-(\alpha) \times 2.02$ Hz and $\beta_f^+(\alpha) \times 2.02$ Hz, as

was expected for the given TMD positions. The frequencies of both TMDs tuned a level α are different due to the simultaneous tuning for multiple combinations considering the intervals for $\beta_f(\alpha)$, $\beta_\xi(\alpha)$ and μ_{f_s}. Each TMD is thus tuned specifically for a particular combination of the average step frequency and the uncertain modal parameters resulting in a worst case response.

Two independently but conventionally tuned TMDs (Case D)

In addition, the TMDs are tuned considering the conventional methodology following equation (4.4). The TMD stiffness and damping are calculated as a function of the TMD mass (ratio). Two TMDs are considered (position A and C from figure 5.3) and tuned independently. In comparison with the previous designs, a strongly increased TMD mass and damping is now required. Again, the total TMD mass increases for higher levels of uncertainty. The TMD stiffness and damping are given in a grey font colour in table 5.4 to indicate that they are tuned as a function of the TMD mass (ratio).

Evaluation of cost-efficiency

From the results in table 5.4, it follows that a TMD tuned in Case C is the most cost-effective design. The minimally required mass for the conventionally tuned TMDs (Case D) is 24%, 34% and 49% higher when compared to that of Case C for the different designs at the level $\alpha = 0.0$, $\alpha = 0.6$ and $\alpha = 1.0$ respectively. Similar, for Case A and Case B, an increase of the total mass of 4%, 15%, 20% and 1%, 9%, 14% respectively, is obtained when compared to Case C for the different designs at $\alpha = 0.0$, $\alpha = 0.6$ and $\alpha = 1.0$.

Computational effort

The optimisation problem defined in equation (5.1) is solved using the interior-point algorithm of *fmincon* in Matlab. The calculations are performed on a desktop computer with an Intel Xeon E5-2630 @ 2.40 GHz quad core processor (32 logical processors) using Windows 10 Enterprise x64 in combination with 144 Gb of RAM. The problem is solved treating twelve groups of constraints simultaneously (parallel computing). Each group consists of one combination of the average step frequencies and the modal parameters and contains the response of 29 points on the bridge deck. Using the discretisation of the intervals for the average step frequency and the uncertain modal parameters as given in section 5.3.1, a function evaluation at the level of uncertainty $\alpha = 1.0/0.6/0$ consists of 11/55/121 groups of constraints for each pedestrian density. This

results in 638/3190/7018 actual constraints, respectively, for each function evaluation (two considered pedestrian densities and 29 points on the bridge deck).

For the case of two independently tuned TMDs (case C) and considering the largest range of uncertainty ($\alpha = 0.0$), the algorithm converged after 85 iterations resulting in 725 function evaluations. The required wall-clock time for the calculation is approximately 2650 minutes. For lower levels of uncertainty ($\alpha = 0.6/1.0$), convergence is obtained after 75/77 iterations resulting in 645/608 function evaluations. The computational time is approximately 990/240 minutes. The number of iterations for convergence depends on the initial point. The optimised solution can be used as the initial point for the underlying problem where a larger range of uncertainties is considered. The number of function evaluations is considerably lower in the case where only one TMD is considered (Case A) or when two identical TMDs are assumed (Case B). For these cases, three decision variables are used instead of six.

5.3.3 Evaluation of TMD performance

Vibration serviceability assessment with TMD

The vibration serviceability assessment for the structure equipped with TMD(s) is now performed to verify their effectiveness. The results are given in figure 5.6 (left bars) for different TMD configurations and the considered levels of uncertainty. For all pedestrian densities, a strong reduction of the response is found compared to the results in figure 5.4. It can be seen that for the TMDs designed at lower levels of uncertainty ($\alpha = 0.6$ and $\alpha = 1.0$), the range of responses becomes larger and that higher vibration levels are reached compared to the designs at $\alpha = 0.0$. The assessment for nominal values ($\alpha = 1.0$) results in the smallest range of accelerations since only the effect of variability in the loading is present (figure 5.6).

For a pedestrian density of 0.2 and 0.5 pers./m^2 and a TMD design at a level of uncertainty $\alpha = 0.0$, the maximum acceleration equals 0.5 m/s^2, satisfying the design constraint (figure 5.6(a,d,g,j)). Similarly, for the TMD(s) designed for $\alpha = 0.6$ and $\alpha = 1.0$, the maximum acceleration equals 0.5 m/s^2 at the level $\alpha = 0.6$ and $\alpha = 1.0$ respectively, for $d \leq 0.5$ pers./m^2 (figure 5.6(b,e,h,k) and 5.6(c,f,i,l) respectively). For higher densities, no constraints are added for vibration comfort and acceleration levels above 0.5 m/s^2 are obtained. However, a strong reduction is found compared to the case without TMD (figure 5.4). For the conventionally tuned TMDs (Case D), the ranges of responses are lower

		$\alpha = 0.0$		$\alpha = 0.6$		$\alpha = 1.0$	
		TMD 1	TMD 2	TMD 1	TMD 2	TMD 1	TMD 2
Case A	m_{TMD} [kg]	4348	–	4077	–	3726	–
	Σm_{TMD} [kg]	4348		4077		3726	
	k_{TMD} [N/m]	648582	–	605890	–	548599	–
	c_{TMD} [Ns/m]	8241	–	7790	–	7738	–
	f_{TMD} [Hz]	1.94	–	1.94	–	1.93	–
	μ_{TMD} [%]	9.14	–	8.57	–	7.83	–
	ρ_{TMD} [-]	0.96	–	0.96	–	0.96	–
	ξ_{TMD} [%]	7.76	–	7.84	–	8.56	–
Case B	m_{TMD} [kg]	2124	2124	1934	1934	1770	1770
	Σm_{TMD} [kg]	4248		3868		3540	
	k_{TMD} [N/m]	313327	313327	281777	281777	256780	256780
	c_{TMD} [Ns/m]	4182	4182	3269	3269	3224	3224
	f_{TMD} [Hz]	1.93	1.93	1.92	1.92	1.92	1.92
	μ_{TMD} [%]	4.46	4.46	4.07	4.07	3.72	3.72
	ρ_{TMD} [-]	0.96	0.96	0.95	0.95	0.95	0.95
	ξ_{TMD} [%]	8.10	8.10	7.00	7.00	7.56	7.56
Case C	m_{TMD} [kg]	1415	2778	1523	2013	1572	1531
	Σm_{TMD} [kg]	4193		3535		3103	
	k_{TMD} [N/m]	220746	389656	194863	323336	203396	248526
	c_{TMD} [Ns/m]	1333	7075	1715	2151	1767	1614
	f_{TMD} [Hz]	1.99	1.88	1.80	2.02	1.81	2.03
	μ_{TMD} [%]	2.97	5.83	3.20	4.23	3.30	3.22
	ρ_{TMD} [-]	0.99	0.94	0.89	1.00	0.90	1.01
	ξ_{TMD} [%]	3.77	10.75	4.98	4.22	4.94	4.14
Case D	m_{TMD} [kg]	2679	2513	2146	2586	2155	2463
	Σm_{TMD} [kg]	5192		4732		4618	
	k_{TMD} [N/m]	406905	382854	329380	393454	330737	375698
	c_{TMD} [Ns/m]	9566	8692	6892	9067	6935	8441
	f_{TMD} [Hz]	1.96	1.96	1.97	1.96	1.97	1.97
	μ_{TMD} [%]	5.63	5.28	4.51	5.43	4.53	5.17
	ρ_{TMD} [-]	0.97	0.97	0.98	0.97	0.98	0.98
	ξ_{TMD} [%]	14.47	14.01	12.96	14.21	12.99	13.87

Table 5.4: Optimised values of the parameters of the four different TMD designs and for the three considered values of the parameter α which defines the range of uncertainties in the modal parameters.

for higher densities when compared to the other designs which is due to the fact that a higher TMD mass was required.

The effect of variation on the average step frequency and uncertainty in the natural frequency or modal damping ratio individually, is given in the middle and right bars respectively. As for the structure without TMD, the effect of uncertainty in the natural frequency is important. Only a small additional effect of uncertainty in the modal damping ratio is obtained since the effective damping is mainly determined by the TMD and the human bodies.

The performance of the two independently tuned TMDs (Case C) is selected for a more detailed discussion. The ranges of accelerations of the structure with TMDs are given in table 5.5 for different levels of uncertainty α and for the pedestrian densities for which the constraints are imposed (0.2 and 0.5 pers/m^2). The constraints that are active are indicated in a bold font. For the designs at the levels $\alpha = 0.6$ and $\alpha = 1.0$, constraints for vibration serviceability are only active for a pedestrian density of 0.5 pers./m^2. For higher levels of uncertainty, the maximum comfort level is not met for the densities of 0.2 and 0.5 pers./m^2.

In figure 5.6, the performance is also evaluated for higher pedestrian densities. For a density of 1.5 pers./m^2, the TMD seems not to be effective at nominal conditions when compared to the structure without TMD (figure 5.4(a)). When the effect of uncertainties is considered, however, an overall reduction of the range of responses is observed (figure 5.6 versus figure 5.4(a) for 1.5 pers./m^2).

It was verified that the vibration comfort criteria are also satisfied when the TMDs switch positions due to symmetry of the modes. In problem (5.1), no constraints are added for the relative TMD displacements. For the different TMD designs, the relative TMD displacements are verified afterwards and maximum values up to 15 mm are found which are in the feasible range (see section 4.2.2).

Modes contributing to the response for the structure with TMD

To investigate the modal contribution to the response of the structure with TMD, the design of two independently tuned TMDs at $\alpha = 0.0$ (Case C) is selected for further discussion.

The acceleration PSD is given in figure 5.7(a) and (b) for the pedestrian densities of 0.2 and 1.5 pers/m^2 respectively. The nominal conditions of the modal parameters are considered in the response calculation ($\alpha = 1.0$ and $\mu_{f_s} = \bar{f}_s$). A strong decrease of the first peak value is now obtained for the density of 0.2 pers./m^2 when compared to the case without TMD. For the highest density of $d = 1.5$ pers./m^2, the peak is only slightly affected. This

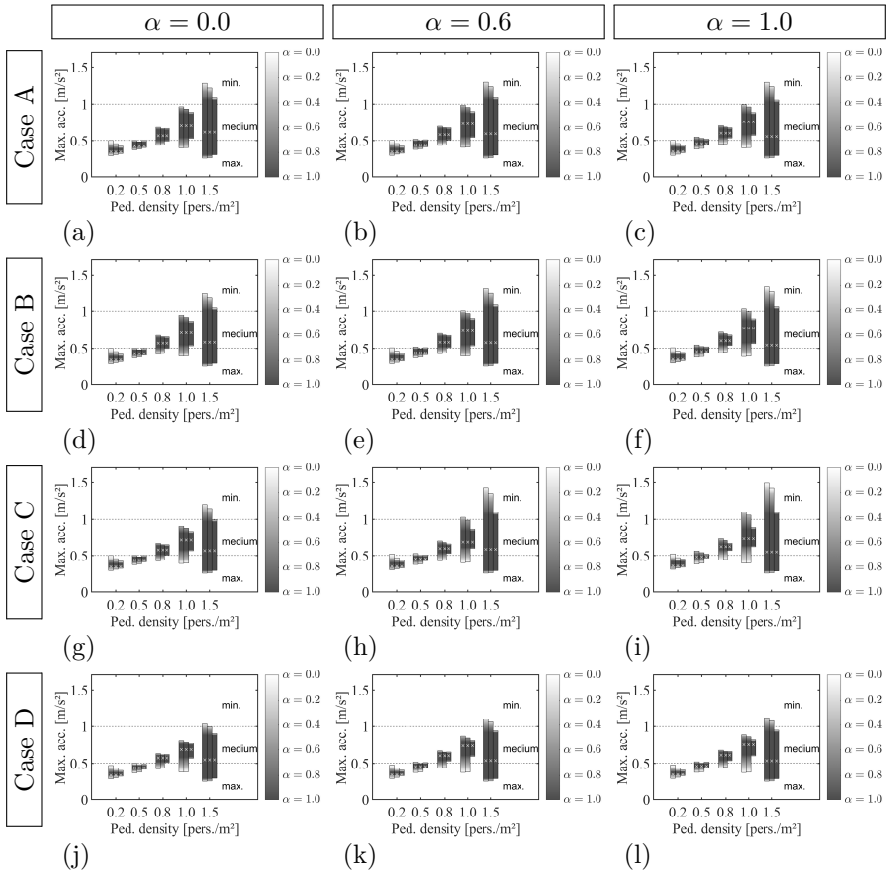

Figure 5.6: Robust vibration serviceability assessment for the Avelgem footbridge for different TMD designs. Possible range of the 95th percentile of the instantaneous peak response accounting for variability in the loading and for β_f and β_ξ combined (left bars), β_f (middle bars) and β_ξ (right bars), indicated by increasing levels of uncertainty in the modal parameters (dark to light) and indication of the response at nominal conditions ($\times$). Comfort criteria according to [9]. (a)-(c) Single TMD (Case A), (d)-(f) Two identical TMDs (Case B), (g)-(i) Two independently tuned TMDs (Case C) and (j)-(l) Two independently but conventionally tuned TMDs (Case D).

means that in this specific case the response for the higher density is less influenced by the TMDs than for the lower pedestrian density ($\beta_f = 1$, $\beta_\xi = 1$ and $\mu_{f_s} = \bar{f}_s$). The contribution of the higher modes is similar to the case without TMDs. It can be seen that the contribution of mode 7 (peak around

	TMD $\alpha = 0.0$		TMD $\alpha = 0.6$		TMD $\alpha = 1.0$	
d	0.2 p./m^2	0.5 p./m^2	0.2 p./m^2	0.5 p./m^2	0.2 p./m^2	0.5 p./m^2
α	$\mu_{\ddot{u}_{\max(T)}} + 2\sigma_{\ddot{u}_{\max(T)}}$ [m/s^2]					
1.0	0.35-0.39	0.43-0.48	0.35-0.40	0.44-0.49	0.36-0.42	0.48-**0.50**
0.8	0.34-0.41	0.41-0.48	0.34-0.42	0.43-0.50	0.35-0.43	0.46-0.52
0.6	0.33-0.44	0.40-0.49	0.33-0.45	0.41-**0.50**	0.34-0.45	0.44-0.54
0.4	0.32-0.45	0.39-0.49	0.33-0.46	0.40-0.51	0.33-0.46	0.42-0.55
0.2	0.31-0.46	0.39-0.50	0.32-0.47	0.39-0.52	0.32-0.47	0.41-0.56
0.0	0.31-**0.50**	0.38-**0.50**	0.32-0.52	0.38-0.53	0.32-0.52	0.40-0.56

Table 5.5: Range of instantaneous peak acceleration of the Avelgem footbridge equipped with two independently tuned TMDs with parameters according to Case C (table 5.4). Evaluation at different α-levels for a density of 0.2 and 0.5 pers./m^2.

5.47 Hz) and mode 9 (peak around 9.35 Hz) are not affected by the TMD.

The maximum acceleration levels along the length of the bridge are given in figure 5.7(c) and (d) for a pedestrian density of 0.2 and 1.5 pers./m^2. The contribution of all modes is accounted for. For the lowest density, the effect of the TMD is clearly visible. The maximum response is now found at midspan and is mainly due to the contribution of the seventh mode. The response at the antinodes of the first mode strongly decreased compared to the case without TMD (see figure 5.4).

Effect of detuned TMD parameters

The proposed robust design optimisation accounts for uncertainty in the modal parameters of the structure and variability in the walking characteristics (average step frequency). In section 4.2.4, it is shown that detuning strongly affects the performance of the TMDs. The effect of a detuned frequency ratio is directly considered in the TMD design by assuming variation in the natural frequency of the structure, implicitly considering that detuning is caused by uncertainty in the main structure. However, additional variation on the TMD parameters can be considered too. Below, the additional effect of variation on the TMD stiffness and TMD damping is investigated for the Avelgem footbridge. The effect is illustrated for a pedestrian density of 0.5 pers./m^2, the case of two independently tuned TMDs (Case C) and two levels of uncertainty ($\alpha = 0.0$ and $\alpha = 1.0$).

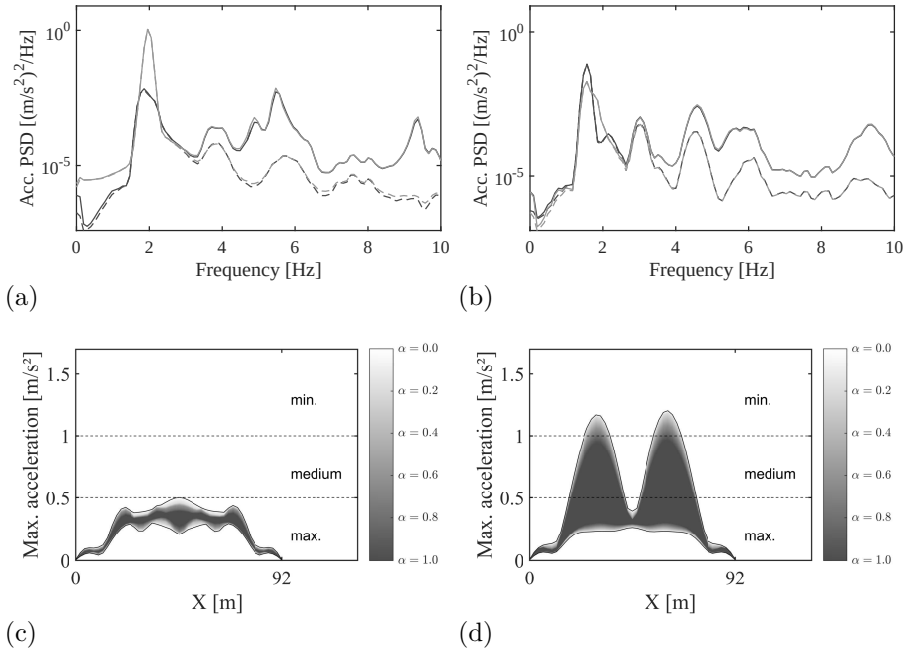

Figure 5.7: Structure with two independently tuned TMDs (Case C) at $\alpha = 0.0$. PSD of the acceleration response at point A assuming nominal conditions ($\beta_f = 1$, $\beta_\xi = 1$ and $\mu_{f_s} = \bar{f}_s$) and considering the contribution of all modes (–) and only the first mode (– –) in the response. PSD for the structure without TMDs (light) and with TMDs (dark) for a pedestrian density of (a) $d = 0.2$ pers./m^2 and (b) $d = 1.5$ pers./m^2. Maximum response along the length of the bridge for different levels of uncertainty for (c) 0.2 pers./m^2 and (d) 1.5 pers./m^2.

Figure 5.8(a) shows the effect of uncertainty in the TMD stiffness on the responses, given as a function of the ratio of the actual TMD stiffness $k_{\text{TMD}}^{\text{actual}}$ to the optimised value k_{TMD} from table 5.4. First, the effect is shown considering the nominal values of the modal parameters and the nominal conditions of the flow (dark). It is seen that the TMD ensures performance and only small deviations in the maximum response are observed. The TMDs designed at $\alpha = 0.0$ satisfy performance considering additional detuning effects while the TMDs designed at $\alpha = 1.0$ only satisfy performance when the optimised value of k_{TMD} is considered. Second, the combined effect of uncertainty in the TMD stiffness ($k_{\text{TMD}}^{\text{actual}}$), uncertainty in the natural frequency and modal damping ratio of the footbridge and variability in the average step frequency is considered. The worst case value is retained for different values of the actual TMD stiffness.

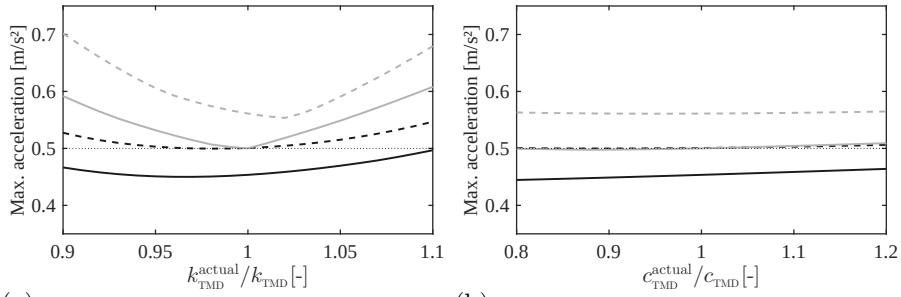

Figure 5.8: Effect of detuned TMD parameters on the maximum response for two independently tuned TMDs (Case C) at $\alpha = 0.0$ (–) and at $\alpha = 1.0$ (– –). Maximum response for a pedestrian density of 0.5 pers./m^2 considering nominal conditions of the flow and no uncertainty in the modal parameters (dark) and worst case value of the response considering variation on the average step frequency and uncertainty in the natural frequency (light). Effect of (a) detuned TMD stiffness (frequency ratio) and (b) detuned TMD damping (ratio).

The effect is now larger since high levels of off-tuning are considered (for both the natural frequency and the TMD frequency). The TMD performance is now only ensured when no additional variation on the TMD stiffness is considered ($k_{\mathrm{TMD}}^{\mathrm{actual}}/k_{\mathrm{TMD}} = 1$). A significant response reduction is guaranteed with the TMD, however, unless the strong off-tuning considered in the analysis. This is especially the case for the design at $\alpha = 0.0$.

A similar analysis is made for uncertainty in the TMD damping (figure 5.8(b)). The effect is smaller than for the detuned frequency ratio from figure 5.8(a), as was also concluded in section 4.2.4. Again, the TMD designed for $\alpha = 0.0$ is more robust to the effect of uncertainties and additional variation on the TMD damping.

5.4 Conclusion

The proposed methodologies for the robust vibration serviceability assessment of footbridges (chapter 3) and the robust design of a TMD for footbridges (chapter 4) have been applied in a case study. A detailed load model is used for the pedestrian walking forces and simulations of moving pedestrian traffic are considered accounting for human-structure interaction effects.

First, it is illustrated how the dynamic behaviour of the structure is affected by human occupancy. The transfer function of the coupled crowd-structure system is calculated for different pedestrian densities. For the natural frequencies below (above) the human body frequencies, a decreases (increase) of the natural frequency is obtained. The effective damping increases in both cases. For frequencies close to the human body frequency, a small shift in the frequency is obtained but a substantial increase of the modal damping is obtained.

The robust vibration serviceability assessment is performed for different levels of uncertainty. The range of responses is tested and minimal levels for vibration comfort are found for low pedestrian densities. For high densities, the maximum acceleration exceed the minimal level for vibration comfort. It is found that the total response is dominated by the first mode and that uncertainty in the natural frequency has a larger effect on the response when compared to the effect of uncertainty in the modal damping ratio. This is explained by HSI effects leading to a high effective damping ratio. Additional changes in the modal damping ratio than become less important, especially for higher pedestrian densities.

A TMD is selected to reduce the vibration levels. A comparison is made between different configurations and the trade-off between cost and robustness is investigated. It is assumed that the cost of the TMD is determined by the total mass. The obtained results show that the total TMD mass can be reduced by considering two TMDs instead of one. The mass can be further reduced if both TMDs are tuned independently. When compared to a conventional TMD design, a strong reduction of the total TMD mass and damping is obtained. The total TMD mass increases if a higher level of uncertainty is considered for the design, illustrating the trade-off between cost and robustness. However, it should be noted that in real applications the total TMD cost not depends solely on its mass and that a single TMD can be preferred to two TMDs due to e.g. the manufacturing cost.

The performance of the TMD is guaranteed for all levels of uncertainty accounted for in the design. The additional effect of detuned values of the TMD stiffness and damping has also been investigated. If this variation on the TMD parameters is considered together with uncertainty in the modal parameters and variability in the loading, wider ranges of responses are obtained, exceeding predefined levels for vibration comfort. A sufficiently large response reduction by the TMD can be ensured after evaluating the effect of additional variation on the TMD parameters. Alternatively, this additional variation can be directly included in the design problem.

Chapter 6

Conclusions and recommendations for further research

For lightweight and slender footbridges, a high sensitivity to human-induced loading is often expected such that vibration serviceability is the governing criterion in the design. The evaluation of the dynamic behaviour requires assumptions on the human-induced loading and the modal parameters of the structure. If predefined criteria for vibration comfort are not met, TMDs are opted. Their performance strongly depends on an accurate knowledge of the modal parameters of the main structure.

In this research, the concept of robustness is introduced to account for the effect of uncertainties in the modal parameters and for variability in the loading. Two major objectives are distinguished. First, the development of an approach for the robust vibration serviceability assessment of footbridges is aimed. Second, the focus is on the robust design of TMDs for vibration serviceability of footbridges.

In this final chapter, the main conclusions of the research are summarised first. Some recommendations for future research and steps for further valorisation of the proposed methodologies are suggested afterwards.

6.1 Main conclusions of the research

Robust vibration serviceability assessment

For the vibration serviceability assessment of footbridges, both an adequate description of the modal parameters, describing the dynamic behaviour of the structure, and sufficiently accurate models for the human-induced loading are required. The natural frequency and modes can be calculated by a FEM while the modal damping is estimated based on experience with similar structures. After construction, measurements can provide more accurate information. The assumptions made in the model or temporary and seasonal changes cause uncertainty sometimes resulting in significant discrepancies between the assumed and actual values of the modal parameters. The considered type of human-induced excitation in this thesis is walking loading. Assumptions are made for the inherent variation in the walking characteristics (inter- and intra-subject variability) and a mathematical model is to be selected to describe the walking force. A recommended method to obtain the pedestrian walking force is based on the combination of single foot step forces. Simulations of moving pedestrian traffic using a detailed model of the human-induced walking loading, including interaction effects between pedestrians mutually and between crowd and structure, are performed. For the case of the Phénix footbridge, it is demonstrated that HSI effects lead to an increase of the effective damping ratio, strongly affecting the response. In alternative, simplified methods for the response calculation (e.g. existing guidelines), the contribution of only one mode is accounted for and resonance with that mode is assumed while HSI effects are disregarded. A reduction coefficient is introduced for natural frequencies outside the range of the expected loading frequencies for walking. Its value depends on the natural frequency, resulting in a high sensitivity to uncertainties. For both the detailed simulations and the simplified methods, uncertainties in the dynamic behaviour of the structure and the assumptions made for the walking loading strongly affect the vibration serviceability assessment. A methodology for the robust vibration serviceability assessment of footbridges is therefore proposed.

To account for uncertainties in the modal parameters of the structure, multiplication factors are used which are modelled as fuzzy numbers. A selected value of the membership function corresponds to a range of uncertainty. In the design stage, the largest level of uncertainty can be selected. After construction and if measurements are available, only temporary variations in the modal parameters need to be accounted for and the level of uncertainty can be reduced. Alternatively, in a multi-level evaluation, the gradual effect of uncertainties for multiple values of the membership function is considered. Additional variability

on stochastically modelled walking characteristics is also accounted for. In particular, a range is defined in which the average step frequency may vary. A similar approach can be used for other parameters such as for the human body parameters considering HSI.

The intervals for the multiplication factors at a selected level of uncertainty have to be discretised and combined with the interval of possible values for the average step frequency, resulting in a number of deterministic response calculations. A range of responses is obtained, laying between the best and worst case value for the selected level of uncertainty. The range is tested to criteria for vibration comfort rather than a single value. The multi-level assessment provides a measure for the sensitivity of the response of the footbridge to the effect of uncertainties. A well-thought-out discretisation of the intervals helps to reduce the total number of combinations between the intervals for the modal parameters and the average step frequency. For example, the lower (upper) bound value of the interval for the modal damping ratio always results in the worst (best) case response at the selected level of uncertainty such that the calculations assuming intermediate values of the modal damping ratios do not provide additional relevant information. For frequencies, a precision up to 0.01 Hz is recommended. For the case study of the Phénix footbridge, it is shown that uncertainty in the natural frequency and variability on the average step frequency strongly affect the response since both variables are determining for the occurrence of resonance. The effect of uncertainty in the modal damping ratio and the modal mass is smaller.

Robust vibration serviceability design of TMDs

If predefined limits for vibration comfort are exceeded, TMDs can be installed to reduce vibration levels. Since the TMD mass, stiffness and damping are tuned to the modal characteristics of one particular mode, an accurate description of the dynamic characteristics of the footbridge is required. Deviations in the modal parameters lead to a strongly detuned TMD resulting in a suboptimal performance. A procedure for the robust design of TMDs has therefore been elaborated. Compared to conventional methods where the contribution of only one mode and a harmonic loading is assumed in frequency domain, the proposed method directly considers the walking loading in the design by means of time-domain simulations of more realistic loading scenarios. The proposed procedure is generic and can also be applied for other types of vibration absorbers.

A robust optimisation problem has been defined to tune the TMD. A cost function, determined by the total TMD mass, is to be minimised. Design constraints are added for operability and for vibration serviceability. The effect

of uncertainties in the modal parameters and variability in the walking loading is implemented in the design constraints following the procedure proposed in chapter 3. A constraint is added for each combination and robustness is ensured since for the optimised solution, the constraint leading to the worst case satisfies the predefined criteria. The problem can be solved for a selected level of uncertainty or alternatively, for different levels of uncertainty which allows to gradually investigate the sensitivity of the TMD design to the effect of uncertainties as a trade-off between cost and robustness.

The procedure for the robust design of a TMD is illustrated for the Phénix footbridge where design constraints are implemented considering a simplified response calculation following design guides. It is shown that a TMD tuned following conventional methods does not satisfy performance when uncertainties in the modal parameters are considered. Afterwards, the robust optimisation problem is solved for different levels of uncertainty. The trade-off between the total cost and the considered level of uncertainty (robustness) is illustrated. For larger levels of uncertainty, the total TMD mass, related to its cost, and the TMD damping increase. The TMD performance now is ensured since the design constraints are satisfied for the considered level of uncertainty.

Full-scale applicability

In chapter 5, the proposed methodology for the robust vibration serviceability assessment and robust design of a TMD is applied in a case study. The response of the Avelgem footbridge is computed by means of simulations of moving pedestrian traffic considering a detailed load model.

It is shown that HSI significantly affects the dynamic behaviour of the structure, mainly due to the strongly increased effective damping. A significant effect of uncertainty in the natural frequency of the footbridge on the vibration serviceability assessment is found. The effect of uncertainty in the modal damping ratio or modal mass is of less importance since the effective damping strongly increased due to the human bodies when considering HSI effects. A minimal level of vibration comfort is found for low pedestrian densities and for different levels of uncertainty. Since the response is dominated by the contribution of the first mode, a TMD is tuned to that mode to reduce the vibration levels.

Aiming at a cost-efficient TMD design, a comparison has been made between different TMD configurations. Constraints have been implemented to ensure vibration serviceability while the total mass of the TMD(s) is minimised. For this particular case study, it is concluded that the total TMD mass is reduced by considering two TMDs instead of one, one at each antinode of the first

mode. The mass can be further reduced if both TMDs are tuned independently from each other. By tuning the TMD parameters independently from each other, a strong reduction of the total TMD mass and damping is obtained when compared to a conventional design where the TMD stiffness and damping are given as a function of its mass. The obtained results clearly illustrate the trade-off between cost and robustness. A higher level of uncertainty considered for the design results in a higher total mass. In real designs, the total TMD cost not only depends on its mass, however, and other aspects contribute to the total cost. The insensitivity (robustness) of the design to the considered range of uncertainties is guaranteed. The TMD performance has also been evaluated for an additional variation on the TMD parameters. Higher ranges of responses are obtained, exceeding the levels for vibration comfort as imposed in the design constraint. However, a sufficiently large response reduction is ensured. Alternatively, the additional variation on the TMD parameters can be directly included in the design problem.

The procedure has been elaborated for a specific case study where the response is governed by the contribution of one mode. The methodology for the vibration serviceability assessment and the robust design of a TMD is general, however, and is applicable for other structures since simulations of moving pedestrian traffic are performed directly for the considered footbridge.

6.2 Recommendations for further research and valorisation

Based on the results of this work, recommendations for further research can be made. Below, suggestions are given for future research topics and for further valorisation of the proposed methodologies in an industrial context.

General robust design

The design procedure for robustness proposed in this research is applied for the vibration comfort of footbridges. The robust optimisation problem can be formulated more generally however. For example, the design variables can consist of structural parameters in dimensioning problems [59, 99, 107]. The methodology to gradually account for uncertainty can be directly applied to the calculated modal parameters or can be applied similarly to other properties of the footbridge (e.g. material properties, stiffness of the boundary conditions, etc.). To ensure a cost-efficient design, the objective function of the general robust design problem can be defined similarly as for the TMD by relating the

level of robustness to the total cost. The cost function can be interpreted as a dimensioning problem (material cost) where additional installation costs can be implemented. Constraints for vibration serviceability and for static design requirements are added for a selected level of uncertainty to ensure performance and robustness. A (sizing) problem is solved by determining the dimensions of the structure. Alternatively, the decision variables can be selected from a set of possible values (discrete integer optimisation [166, 247]) or values from catalogues are opted for predefined solutions of the individual components (e.g. steel beams), which is often beneficial for the total cost.

In addition, a comparison can be made between the total cost of the design where robustness is obtained by the design of a TMD and where a general robust design is considered.

Verification of the load model

In the performed simulations of pedestrian traffic, a simplified model to account for HHI is considered and the pedestrian characteristics are sampled based on information given in literature. Until now, that input for the load models has not been validated in situ for real pedestrian traffic, especially for high-density crowds. To verify the assumptions made, a full-scale observation and identification of the walking behaviour of pedestrians is required. In [215], a methodology is proposed to identify the pedestrian trajectory using video-based motion tracking. In combination with inertial tracking at the lower back of the pedestrians [220], the step frequency and walking velocity can be derived and used as input for the load models.

Steps for practical implementation and further valorisation

Suggestions for further improvements of the considered load model and the proposed methodology for the assessment and TMD tuning are given below.

- *Vibration serviceability assessment in lateral direction.* For some footbridges, lateral vibrations are the governing criterion for vibration comfort, especially when lock-in can occur [47, 140]. This interaction phenomenon between human and structure is not implemented in the considered load model. However, for a reliable vibration serviceability assessment of lateral vibrations, it is recommended to account for the effect. The models proposed in [39, 96] can be used for this application.
- *Extension to other types of human-induced loading.* The proposed methodology focusses on robustness for vibration serviceability of

footbridges under walking loading. However, the approach is generic and can be applied to other types of (human-induced) loading. In particular, running and jogging loading are of interest for vibration serviceability. Since the range of loading frequencies of running is much larger than for walking, resonance with other modes is possible. Furthermore, the amplitudes of the harmonic components of the running force are significantly higher than those of walking [144, 163]. Up to now, the effect of running is not considered in the vibration serviceability assessment of footbridges. More research first has to be performed to better characterise this type of loading, especially for groups of running persons (synchronisation, inter- and intra-subject variability, interaction with the structure, etc.). It is expected that the vibration serviceability assessment considering running loading significantly differs from that considering walking loading. Consequently, if TMDs are required, the modes that are sensitive to running are generally not affected by a TMD designed for walking (and vice versa) [144]. Including the effect of walking and running loading in the response calculation should result in a more comprehensive vibration serviceability assessment and TMD design.

- *Selected variations and level of uncertainty.* In this research, it is found that uncertainty in the natural frequency and variability in the average step frequency are the most determining parameters for the robust vibration serviceability assessment. Critical hereby is the selection of the range of variation in the modal parameters, often based on values found in literature or obtained from long-term measurements. Alternatively, if more information is known about the distribution of e.g. material properties, propagation of the uncertainty in the analysis of the FEM is useful to investigate the effect on the modal parameters. Furthermore, additional variability on the human body parameters or other parameters characterising the walking loading can be considered in a similar way as for the average step frequency.

- *Practical TMD design issues.* For the TMD design, it is assumed that the TMD mass is the only factor determining its cost. However, in practice, the total cost often consists of multiple factors: design and manufacturing costs (e.g. engineering, materials, manufacturing time, etc.), installation costs (e.g. transportation, tuning, etc.) and maintenance cost (e.g. retuning, periodic inspection, etc.). An alternative objective function thus can be selected including multiple aspects of the total cost such as proposed in [207] or considering a life cycle cost analysis for the structure equipped with TMD [125]. Furthermore, a linear behaviour of the TMD stiffness and damping constant is assumed in this thesis while non-linearities can be expected in certain circumstances, for example for

higher vibration amplitudes [75, 177]. A viscous power law damping [177] and/or cubic stiffness non-linearity [75] can be considered in the TMD parameter tuning.

Suggestions for further steps in the valorisation and practical implementation of the developed methodology are given below.

- *Implementation of the methodology for practical use.* Matlab code is developed for the robust vibration serviceability assessment of pedestrian traffic and the TMD optimisation. Toolboxes with predefined functions are used for basic operations. As Matlab is not commonly used in design offices, conversion of the code is recommended. The procedure for the robust assessment following simplified methods (e.g. guidelines) is relatively easy to implement using spreadsheets (e.g. Microsoft Excel). More difficulties are expected for the simulations of moving pedestrian traffic and the optimisation of the TMD parameters. The methodologies can be reimplemented in simulation software that is more common in industry (e.g. as an additional type of loading). For the TMD tuning problem in particular, special attention must be given to optimisation algorithms provided by the software package.
- *Reduction of the computational cost.* The proposed methodology for the robust vibration serviceability assessment requires a large number of response calculations especially if the intervals for multiple uncertain variables are combined. The number of uncertain variables can be reduced based on engineering judgement by selecting the variables that are governing the assessment. However, for the TMD design, the computational effort can be quite high since a nested response calculation is performed in each loop of the optimisation routine to calculate the constraints. To reduce the computational effort for each response calculation, the crowd-structure(-TMD) system order can be reduced. The aim is to find an equivalent load that replaces the effect of the SDOF systems representing human bodies. The number of states for the calculations then considerably decreases resulting in a lower computational effort.

Bibliography

[1] Abe, M., and Fujino, Y. Dynamic characterization of multiple tuned mass dampers and some design formulas. *Earthquake Engineering & Structural Dynamics (EESD) 23*, 8 (1993), 813–835.

[2] Agu, E., and Kasperski, M. Influence of the random dynamic parameters of the human body on the dynamic characteristics of the coupled system of structure-crowd. *Journal of Sound and Vibration 330*, 3 (2011), 431–444.

[3] Alampalli, S. Influence of in-service environment on modal parameters. In *Proceedings-SPIE The International Society For Optical Engineering* (1998), vol. 1, Citeseer, pp. 111–116.

[4] Ansys. *ANSYS® Mechanical APDL Academic Research, Release 16.2*. Canonsburg, Pennsylvania.

[5] Aoues, Y., and Chateauneuf, A. Benchmark study of numerical methods for reliability-based design optimization. *Structural and Multidisciplinary Optimization 41*, 2 (2010), 277–294.

[6] Araújo, J., Carlos, M., Brito, H. M. B. F., and Pimentel, R. L. Experimental evaluation of synchronisation in footbridges due to crowd density. *Structural Engineering International 19*, 3 (2009), 298–303.

[7] Asami, T., and Nishihara, O. Closed-Form Exact Solution to H∞ Optimization of Dynamic Vibration Absorbers (Application to Different Transfer Functions and Damping Systems). *Journal of Vibration and Acoustics 125*, 3 (2003), 398–405.

[8] Asami, T., Nishihara, O., and Baz, A. M. Analytical Solutions to H∞ and H2 Optimization of Dynamic Vibration Absorbers Attached to Damped Linear Systems. *Journal of Vibration and Acoustics 124*, 2 (2002), 284–295.

[9] Association Française de Génie Civil, Sétra/AFGC. *Sétra: Evaluation du comportement vibratoire des passerelles piétonnes sous l'action des piétons*, 2006.

[10] Avci, O. Amplitude-Dependent Damping in Vibration Serviceability: Case of a Laboratory Footbridge. *Journal of Architectural Engineering 22*, 3 (2016), 04016005.

[11] Awad, Z. K., Aravinthan, T., Zhuge, Y., and Gonzalez, F. A review of optimization techniques used in the design of fibre composite structures for civil engineering applications. *Materials and Design 33*, 1 (2012), 534–544.

[12] Bachmann, H., and Ammann, W. *Vibrations in Structures: Induced by Man and Machines*. Structural engineering documents. IABSE, 1987.

[13] Bachmann, H., Pretlove, A., and Rainer, J. Vibrations induced by people. In *Vibration Problems in Structures*. Springer, 1995, pp. 1–28.

[14] Bachmann, H., and Weber, B. Tuned vibration absorbers for "lively" structures. *Structural Engineering International 5*, 1 (1995), 31–36.

[15] Barton, J., Tedesco, S., Healy, T., and O'Flynn, B. Potential for new smart knee device to cut down on knee surgery recovery time. *Engineers Journal* (2017).

[16] Bäumer, R., and Starossek, U. Closed-Form Steady-State Response Solution of the Twin Rotor Damper and Experimental Validation. *Journal of Vibration and Acoustics, Transactions of the ASME 139*, 2 (2017), 021017.

[17] Bertram, J. E. A., and Ruina, A. Multiple Walking Speed-frequency Relations are Predicted by Constrained Optimization. *Journal of Theoretical Biology 209*, 4 (2001), 445–453.

[18] Beyer, H.-G., and Sendhoff, B. Robust optimization–a comprehensive survey. *Computer Methods in Applied Mechanics and Engineering 196*, 33 (2007), 3190–3218.

[19] Bhurjee, A. K., and Panda, G. Efficient solution of interval optimization problem. *Mathematical Methods of Operations Research 76*, 3 (2012), 273–288.

[20] British Standard Institution. *BS 5400-2:1978 Steel, concrete and composite bridges - Part 2: Specification for loads*, 1978.

[21] British Standard Institution. *ISO 2631-2:1989 Evaluation of human exposure to whole body vibration - Part 2: human exposure to continuous and shock-induced vibration in buildings (1 to 80 Hz)*, 1989.

[22] British Standard Institution. *BS 6472:1992 Guide to evaluation of human exposure to vibration in buildings (1Hz to 80 Hz)*, 1992.

[23] British Standard Institution. *NA to BS EN 1991-2:2003, UK National Annex to Eurocode 1: Actions on structures - Part 2: Traffic loads on bridges*, 2008.

[24] Brownjohn, J., Dumanoglu, A., and Taylor, C. Dynamic investigation of a suspension footbridge. *Engineering Structures 16*, 6 (1994), 395–406.

[25] Brownjohn, J., and Pavić, A. Experimental methods for estimating modal mass in footbridges using human-induced dynamic excitation. *Engineering Structures 29*, 11 (2007), 2833–2843.

[26] Brownjohn, J. M., Pavić, A., and Omenzetter, P. A spectral density approach for modelling continuous vertical forces on pedestrian structures due to walking. *Canadian Journal of Civil Engineering 31*, 1 (2004), 65–77.

[27] Bruno, L., and Corbetta, A. Uncertainties in crowd dynamic loading of footbridges: A novel multi-scale model of pedestrian traffic. *Engineering Structures 147* (2017), 545–566.

[28] Bujňák, J., Hlinka, R., Odrobiňák, J., and Vičan, J. Diagnostics and evaluation of footbridges. *Procedia Engineering 40* (2012), 56–61.

[29] Bulleit, W. Uncertainty in Structural Engineering. *Practice Periodical on Structural Design and Construction 13*, 1 (2008), 24–30.

[30] Butz, C. *Beutrag zur Berechnung Fußgängerinduzierter Brückenschwingungen - Shaker Verlag.* PhD thesis, RWTH Aachen, 2006.

[31] Butz, C., Feldmann, M., Heinemeyer, C., Sedlacek, G., Charbrolin, B., Lemaire, A., Lukic, M., Martin, P.-O., Caetano, E., Cunha, Á., Goldack, A., Keil, A., and Schlaich, M. SYNPEX: Advanced load models for synchronous pedestrian excitation and optimised design guidelines for steel footbridges. Report, Research Fund for Coal and Steel, 2008.

[32] Butz, C., Schuermann, C., and Benicke, O. Tuned mass dampers for the footbridge of VW Autostadt in Wolfsburg, Germany. In *Proceedings*

of the 4th International Footbridge Conference (Wroclaw, Poland, July 2011).

[33] Caetano, E., Cunha, Á., Magalhães, F., and Moutinho, C. Studies for controlling human-induced vibration of the Pedro e Inês footbridge, Portugal. Part 1: Assessment of dynamic behaviour. *Engineering Structures 32* (2010), 1069–1081.

[34] Caetano, E., Cunha, Á., Magalhães, F., and Moutinho, C. Studies for controlling human-induced vibration of the Pedro e Inês footbridge, Portugal. Part 2: Implementation of tuned mass dampers. *Engineering Structures 32* (2010), 1082–1091.

[35] Caprani, C. C. Application of the pseudo-excitation method to assessment of walking variability on footbridge vibration. *Computers and Structures 132* (2014), 43–54.

[36] Caprani, C. C., and Ahmadi, E. Formulation of human–structure interaction system models for vertical vibration. *Journal of Sound and Vibration 377* (2016), 346–367.

[37] Cara, J. Computing the modal mass from the state space model in combined experimental – operational modal analysis. *Journal of Sound and Vibration 370* (2016), 94–110.

[38] Carpineto, N., Lacarbonara, W., and Vestroni, F. Mitigation of Pedestrian-induced Vibrations in Suspension Footbridges via Multiple Tuned Mass Dampers. *Journal of Vibration and Control 16*, 5 (2010), 749–776.

[39] Carroll, S., Owen, J., and Hussein, M. Experimental identification of the lateral human–structure interaction mechanism and assessment of the inverted-pendulum biomechanical model. *Journal of Sound and Vibration 333*, 22 (2014), 5865–5884.

[40] Casado, C. M., Díaz, I. M., De Sebastian, J., Poncela, A. V., and Lorenzana, A. Implementation of passive and active vibration control on an in-service footbridge. *Structural Control and Health Monitoring 20*, 1 (2013), 70–87.

[41] Casciati, F., Rodellar, J., and Yildirim, U. Active and semi-active control of structures – theory and applications: A review of recent advances. *Journal of Intelligent Material Systems and Structures 23*, 11 (2012), 1181–1195.

[42] Chakraborty, S., and Roy, B. K. Reliability based optimum design of Tuned Mass Damper in seismic vibration control of structures with bounded uncertain parameters. *Probabilistic Engineering Mechanics 26*, 2 (2011), 215–221.

[43] Charles, P., and Bui, V. Transversal dynamic actions of pedestrians and synchronisation. In *Proceedings of the 2nd International Footbridge Conference (Footbridge 2005)* (6-8 December 2005).

[44] Chen, S. H., Wu, J., and Chen, Y. D. Interval optimization for uncertain structures. *Finite elements in analysis and design 40* (2004), 1379–1398.

[45] Coscia, V., and Canavesio, C. First-order macroscopic modelling of human crowd dynamics. *Mathematical Models and Methods in Applied Sciences 18* (2008), 1217–1247.

[46] Dallard, P., Fitzpatrick, A. J., Flint, A., Le Bourva, S., Low, A., Smith, R. M. R., and Willford, M. The London Millenium Footbridge. *The Structural Engineer 79*, 22 (2001), 17–35.

[47] Dallard, P., Fitzpatrick, T., Flint, A., Low, A., Smith, R., Willford, M., and Roche, M. The London Millennium footbridge: Pedestrian-Induced Lateral Vibration. *Journal of Bridge Engineering 6* (2001), 412–417.

[48] Daniel, Y., Lavan, O., and Levy, R. Multiple-Tuned Mass Dampers for Multimodal Control of Pedestrian Bridges. *Journal of Structural Engineering 138*, 9 (2012), 1173–1178.

[49] Davenport, A. G. Note on the distribution of the largest value of a random function with application to gust loading. In *ICE Proceedings* (1964), vol. 28, Thomas Telford, pp. 187–196.

[50] Deb, K. *Multi-Objective Optimization using Evolutionary Algorithms*. John Wiley & Sons, 2001.

[51] Degrauwe, D. *Uncertainty propagation in structural analysis by fuzzy numbers*. PhD thesis, KU Leuven, 2007.

[52] Den Hartog, J. *Mechanical Vibrations*. Dover, 1985.

[53] Departement Mobiliteit en Openbare Werken Expertise Beton en Staal. Overzicht voetbruggen en fietsbruggen, November 2017.

[54] Der Kiureghian, A. Structural response to stationary excitation. *Journal of the Engineering Mechanics Division 106*, 6 (1980), 1195–1213.

[55] Detroux, T., Habib, G., Masset, L., and Kerschen, G. Performance, robustness and sensitivity analysis of the nonlinear tuned vibration absorber. *Mechanical Systems and Signal Processing 60* (2015), 799–809.

[56] Díaz, I. M., Pereira, E., Hudson, M. J., and Reynolds, P. Enhancing active vibration control of pedestrian structures using inertial actuators with local feedback control. *Engineering Structures 41* (2012), 157–166.

[57] Dietrich, F., and Köster, G. Gradient navigation model for pedestrian dynamics. *Physical Review E - Statistical, Nonlinear, and Soft Matter Physics 89*, 6 (2014), 1–8.

[58] Ding, Y. L., and Li, A. Q. Temperature-induced variations of measured modal frequencies of steel box girder for a long-span suspension bridge. *International Journal of Steel Structures 11*, 2 (2011), 145–155.

[59] Doltsinis, I., and Kang, Z. Robust design of structures using optimization methods. *Computer Methods in Applied Mechanics and Engineering 193*, 23 (2004), 2221–2237.

[60] Donders, S., Vandepitte, D., Van De Peer, J., and Desmet, W. Assessment of uncertainty on structural dynamic responses with the short transformation method. *Journal of Sound and Vibration 288*, 3 (2005), 523–549.

[61] Dong, W., and Shah, H. C. Vertex method for computing functions of fuzzy variables. *Fuzzy Sets and Systems 24*, 1 (1987), 65–78.

[62] Du, X. P., and Chen, W. Towards a better understanding of modeling feasibility robustness in engineering design. *Journal of Mechanical Design 122*, 4 (2000), 385–394.

[63] Dziuba, P., Grillaud, G., Flamand, O., Sanquier, S., and Tétard, Y. La passerelle Solférino comportement dynamique (dynamic behaviour of the Solférino bridge). *Bulletin Ouvrages Métalliques 1* (2001), 34–57.

[64] Ebrahimpour, A., Hamam, A., Sack, R. L., and Patten, W. N. Measuring and modeling dynamic loads imposed by moving crowds. *Journal of Structural Engineering 122*, 12 (1996), 1468–1474.

[65] Elias, S., and Matsagar, V. Research developments in vibration control of structures using passive tuned mass dampers. *Annual Reviews in Control 44* (2017), 129–156.

[66] Elishakoff, I. *Probabilistic Theory of Structures*. Dover, 1998.

[67] Elishakoff, I. Possible limitations of probabilistic methods in engineering. *Applied Mechanics Reviews 53*, 2 (2000), 19–36.

[68] Ellis, B. R. On the response of long-span floors to walking loads generated by individual and crowds. *The Structural Engineer 78* (2000), 1–25.

[69] European Committee for Standardisation. *EN 1998-2 Eurocode 8: Design of structures for earthquake resistance - Part 2: Bridges*, 2003.

[70] European Committee for Standardisation. *NBN EN 1995-2 Eurocode 5: Design of timber structures - Part 2: Bridges*, 2005.

[71] European Committee for Standardisation. *NBN EN 1995-2 ANB Eurocode 1: Actions on Structures - Part 2: Traffic loads on bridges*, 2011.

[72] Ferrarotti, A., and Tubino, F. Generalized Equivalent Spectral Model for Serviceability Analysis of Footbridges. *Journal of Bridge Engineering 21*, 12 (2016), 1–9.

[73] Field, A. One Way Independent ANOVA by Hand. *Research Methods in Psychology C8057* (2008), 1–13.

[74] Fisco, N. R., and Adeli, H. Smart structures: Part I - Active and semi-active control. *Scientia Iranica 18*, 3 A (2011), 275–284.

[75] Gatti, G. Fundamental insight on the performance of a nonlinear tuned mass damper. *Meccanica 53*, 1-2 (2018), 111–123.

[76] GERB Vibration Control Systems. Vibration protection for structures, buildings, machinery and other equipment with tuned mass dampers. Reference list, 2007.

[77] Ghosh, A., and Basu, B. A closed-form optimal tuning criterion for TMD in damped structures. *Structural Control and Health Monitoring 14*, 4 (2007), 681–692.

[78] Glanville, M., Kwok, K., and Denoon, R. Full-scale damping measurements of structures in Australia. *Journal of Wind Engineering and Industrial Aerodynamics 59*, 2-3 (1996), 349–364.

[79] Gutierrez Soto, M., and Adeli, H. Tuned Mass Dampers. *Archives of Computational Methods in Engineering 20*, 4 (2013), 419–431.

[80] Hansen, E., and Walster, G. W. *Global Optimization Using Interval Analysis*. Marcel Dekker Inc, New York, 2004.

[81] Hanss, M. The transformation method for the simulation and analysis of systems with uncertain parameters. *Fuzzy Sets and Systems 130*, 3 (2002), 277–289.

[82] Hanss, M., and Mäck, M. Certainly uncertain - the charm of fuzzy predictions. *Procedia Engineering 199* (2017), 48–55.

[83] Hanss, M., and Turrin, S. A fuzzy-based approach to comprehensive modeling and analysis of systems with epistemic uncertainties. *Structural Safety 32*, 6 (2010), 433–441.

[84] Hasofer, A. M., and Lind, N. C. Exact and invariant second moment code format. *Journal of the Engineering Mechanics Division 100*, 1 (1974), 111–121.

[85] Heinemeyer, C., Butz, C., Keil, A., Schlaich, M., Goldack, A., Trometor, S., Lukic, M., Chabrolin, B., Lemaire, A., Martin, P.-O., Cunha, Á., and Caetano, E. Design of lightweight Footbridges for Human Induced Vibrations: Background document in support to the implementation, harmonization and further development of the eurocodes. Tech. rep., JRC Scientific and Technical Reports - European Commission, 2009.

[86] Helbing, D., Buzna, L., Johansson, A., and Werner, T. Self-organized pedestrian crowd dynamics: Experiments, simulations, and design solutions. *Transportation Science 39*, 1 (2005), 1–24.

[87] Helbing, D., and Molnar, P. Social force model for pedestrian dynamics. *Physical Review E 51*, 5 (1995), 4282.

[88] Heylen, W., Lammens, S., and Sas, P. *Modal Analysis Theory and Testing*. Katholieke Universiteit Leuven, Faculty of Engineering, Department of Mechanical Engineering, Division of Production Engineering, Machine Design and Automation, 1998.

[89] Hu, W.-H., Caetano, E., and Cunha, A. Structural health monitoring of a stress-ribbon footbridge. *Engineering Structures 57* (2013), 578 – 593.

[90] Hu, W.-H., Moutinho, C., Caetano, E., Magalhães, F., and Cunha, Á. Continuous dynamic monitoring of a lively footbridge for serviceability assessment and damage detection. *Mechanical Systems and Signal Processing 33* (2012), 38 – 55.

[91] Hughes, R. L. A continuum theory for the flow of pedestrians. *Transportation Research Part B: Methodological 36*, 6 (2002), 507–535.

[92] Huth, O., and Khbeis, H. Pot bearings behavior after 32 years of service: In situ and laboratory tests. *Engineering Structures 29*, 12 (2007), 3352–3363.

[93] Hwang, J. S., Lee, S. H., and Kareem, A. Estimation of modal masses of a structure with a mass-type damping device. *Engineering Structures 99* (2015), 149–156.

[94] Ibrahim, R. A. Recent advances in nonlinear passive vibration isolators. *Journal of Sound and Vibration 314*, 3-5 (2008), 371–452.

[95] Igusa, T., and Der Kiureghian, A. Response of uncertain systems to stochastic excitation. *Journal of Engineering Mechanics 114*, 5 (1988), 812–832.

[96] Ingólfsson, E. T., and Georgakis, C. T. A stochastic load model for pedestrian-induced lateral forces on footbridges. *Engineering Structures 33*, 12 (2011), 3454–3470.

[97] International Organization for Standardization. *ISO/DIS 10137:2007 Bases for design of structures - Serviceability of buildings and walkways against vibration*, 2007.

[98] Jensen, H., Setareh, M., and Peek, R. TMDs for Vibration Control of systems with Uncertain Properties. *Journal of Structural Engineering 118*, 12 (1992), 3285–3296.

[99] Jeong, S., and Park, G. Reliability-based robust design optimization using the probabilistic robustness index and the enhanced single loop single vector approach. In *10th World Congress on Structural and Multidisciplinary Optimization* (2013), pp. 19–24.

[100] Ji, T., and Ellis, B. R. Human-Structure Interaction in Vertical Vibrations. *Proceedings of the ICE - Structures and Buildings 122*, 1 (1997), 1–9.

[101] Kang, Z. *Robust design optimization of structures under uncertainties*. PhD thesis, Universität Stuttgart, 2005.

[102] Kasperski, M., and Sahnaci, C. Serviceability of pedestrian structures. In *Conference Proceedings of the Society for Experimental Mechanics Series* (2007).

[103] Kerr, S. C. *Human Induced Loading on Staircases.* PhD thesis, University College of London, Mechanical Engineering Department, 1998.

[104] Knoll, F., and Vogel, T. *Design for Robustness.* Structural Engineering Documents. IABSE, 2009.

[105] Krenk, S. Dynamic response to pedestrian loads with statistical frequency distribution. *Journal of Engineering Mechanics 138*, 10 (2012), 1275–1281.

[106] Kwok, K., and Samali, B. Performance of tuned mass dampers under wind loads. *Engineering Structures 17*, 9 (1995), 655–667.

[107] Lee, K. H., and Park, G.-J. Robust optimization considering tolerances of design variables. *Computers and Structures 79* (2001), 77–86.

[108] Li, H. N., and Ni, X. L. Optimization of non-uniformly distributed multiple tuned mass damper. *Journal of Sound and Vibration 308*, 1-2 (2007), 80–97.

[109] Li, Q., Fan, J., Nie, J., Li, Q., and Chen, Y. Crowd-induced random vibration of footbridge and vibration control using multiple tuned mass dampers. *Journal of Sound and Vibration 329*, 19 (2010), 4068–4092.

[110] Lievens, K., Lombaert, G., De Roeck, G., and Van den Broeck, P. Robust design of a TMD for the vibration serviceability of a footbridge. *Engineering Structures 123* (2016), 408–418.

[111] Lievens, K., Lombaert, G., Van Nimmen, K., De Roeck, G., and Van den Broeck, P. Robust vibration serviceability assessment of footbridges subjected to pedestrian excitation: strategy and applications. *Engineering Structures 171* (2018), 236–246.

[112] Lievens, K., Van Nimmen, K., Lombaert, G., De Roeck, G., and Van den Broeck, P. Prediction of peak response values of structures with and without tmd subjected to random pedestrian flows. In *Journal of Physics: Conference Series* (2016), vol. 744, IOP Publishing, p. 012227.

[113] Lorenzana, A., Poncela, A. V., Sebastián, J., Ibán, N., Istrate, M. V., Vasallo, A., Pereda, J., Díaz, I. M., Casado, C. M., and Castaño, J. One year of the structural health monitoring of Pedro Gómez Bosque footbridge. In *6th World Conference on Structural Control and Monitoring, (Barcelona, Spain), July* (2014), pp. 344–353.

[114] Maes, K. *Filtering techniques for force identification and response estimation in structural dynamics.* PhD thesis, KU Leuven, 2016.

[115] Magalhães, F., Cunha, A., Caetano, E., and Brincker, R. Damping estimation using free decays and ambient vibration tests. *Mechanical Systems and Signal Processing 24* (2010), 1274–1290.

[116] Mallie, M., Ney, L., Bols, B., Van Nimmen, K., Van den Broeck, P., and De Roeck, G. Two mass-tuned footbridges, Belgium. In *Proceedings of the 5th International Footbridge Conference* (London, England, July 2014).

[117] Marano, G. C., and Greco, R. Robust optimization for TMD with uncertain bounded system parameters and stochastic excitation. *Asian Journal of Civil Engineering (Building and Housing) 9*, 5 (2008), 433–455.

[118] Marano, G. C., and Greco, R. Optimization criteria for tuned mass dampers for structural vibration control under stochastic excitation. *Journal of Vibration and Control 17* (2011), 679–688.

[119] Marano, G. C., Greco, R., and Sgobba, S. A comparison between different robust optimum design approaches: application to tuned mass dampers. *Probabilistic Engineering Mechanics 25*, 1 (2010), 108–118.

[120] Marano, G. C., and Quaranta, G. Robust optimum criteria for tuned mass dampers in fuzzy environments. *Applied Soft Computing 9*, 4 (2009), 1232–1243.

[121] Matsumoto, Y., and Griffin, M. Dynamic response of the standing human body exposed to vertical vibration: influence of posture and vibration magnitude. *Journal of Sound and Vibration 212*, 1 (1998), 85–107.

[122] Matsumoto, Y., and Griffin, M. J. Mathematical models for the apparent masses of standing subjects exposed to vertical whole-body vibration. *Journal of Sound and Vibration 260* (2003), 431–451.

[123] Matsumoto, Y., Nishioka, T., Shiojiri, H., and Matsuzaki, K. Dynamic design of footbridges. In *Proceedings of the International Association for Bridge and Structural Engineering* (1978), vol. 2, IABSE, pp. 1–15.

[124] Matsumoto, Y., Sato, S., Nishioka, T., and Shiojiri, H. A study on dynamic design of pedetrian over-bridges in consideration of characteristics of pedestrians. In *Proceedings of the Japan Society of Civil Engineers* (1972), vol. 205, Japan Society of Civil Engineers, pp. 63–70.

[125] Matta, E. Lifecycle cost optimization of tuned mass dampers for the seismic improvement of inelastic structures. *Earthquake Engineering and Structural Dynamics 47*, 3 (2018), 714–737.

[126] Maurer Söhne. Tuned mass and viscous dampers - technical information and products. Reference list, 2011.

[127] Medina, J. C., and Taflanidis, A. Probabilistic measures for assessing appropriateness of robust design optimization solutions. *Structural and Multidisciplinary Optimization 51*, 4 (2015), 813–834.

[128] Meinhardt, C. Einsatz von multiplen Schwingungstilger-Systemen an schlanken Fußgängerbrücken. *Stahlbau 86*, 4 (2017), 366–372.

[129] Meinhardt, C., Dressen, O., and Dalmer, F. Increase of the structural damping due to the application of tuned mass dampers TMD subject to the footbridge construction. In *Third International Conference, Footbridge* (2008).

[130] Mendes, P. J., Barros, J. A., Sena-Cruz, J. M., and Taheri, M. Development of a pedestrian bridge with GFRP profiles and fiber reinforced self-compacting concrete deck. *Composite Structures 93*, 11 (2011), 2969–2982.

[131] Miguel, L. F. F., Miguel, L. F. F., and Lopez, R. H. A firefly algorithm for the design of force and placement of friction dampers for control of man-induced vibrations in footbridges. *Optimization and Engineering 16*, 3 (2015), 633–661.

[132] Moens, D., and Hanss, M. Non-probabilistic finite element analysis for parametric uncertainty treatment in applied mechanics: Recent advances. *Finite Elements in Analysis and Design 47*, 1 (2011), 4–16.

[133] Moens, D., and Vandepitte, D. A survey of non-probabilistic uncertainty treatment in finite element analysis. *Computer Methods in Applied Mechanics and Engineering 194* (2005), 1527–1555.

[134] Moens, D., and Vandepitte, D. Recent advances in non-probabilistic approaches for non-deterministic dynamic finite element analysis. *Archives of Computational Methods in Engineering 13*, 3 (2006), 389–464.

[135] Möller, B., Graf, W., and Beer, M. Fuzzy structural analysis using α-level optimization. *Computational Mechanics 26*, 6 (2000), 547–565.

[136] Moser, P., and Moaveni, B. Environmental effects on the identified natural frequencies of the Dowling Hall Footbridge. *Mechanical Systems and Signal Processing 25*, 7 (2011), 2336 – 2357.

[137] Motta, R. d. S., and Afonso, S. M. An efficient procedure for structural reliability-based robust design optimization. *Structural and Multidisciplinary Optimization 54*, 3 (2016), 511–530.

[138] Mrabet, E., Guedri, M., Ichchou, M., and Ghanmi, S. New approaches in reliability based optimization of tuned mass damper in presence of uncertain bounded parameters. *Journal of Sound and Vibration 355* (2015), 93–116.

[139] Murray, T. M., Allen, D. E., and Ungar, E. E. *Floor vibrations due to human activity - Steel design guide series 11.* American Institute of Steel Construction, Canadian Institute of Steel Construction, 1997.

[140] Nakamura, S.-i., and Kawasaki, T. Lateral vibration of footbridges by synchronous walking. *Journal of Constructional Steel Research 62*, 11 (2006), 1148–1160.

[141] Niu, S., Wang, C., and Gao, S. A novel crowd random loads model for pedestrians walking on footbridge. *Archive of Applied Mechanics 86*, 7 (2016), 1369–1381.

[142] Nocedal, J., and Wright, S. J. *Numerical Optimization.* Springer, 1999.

[143] Oberkampf, W., DeLand, S., Rutherford, B., Diegert, K., and Alvin, K. A new methodology for the estimation of total uncertainty in computational simulation. In *Proceedings of the 40th AIAA/ASME/ASCE/AHS/ASC Structures, Structural Dynamics and Materials Conference* (1999), AIAA-99-1612, pp. 3061–3083.

[144] Occhiuzzi, A., Spizzuoco, M., and Ricciardelli, F. Loading models and response control of footbridges excited by running pedestrians. *Structural Control and Health Monitoring 15* (2008), 349–368.

[145] Oeding, D. *Verkehrsbelastung und Dimensionierung von Gehwegen und anderen Anlagen des Fußgängerverkehrs.* PhD thesis, Technische Hochschule Carolo-Wilhelmina zu Braunschweig, 1963.

[146] Ontario Government. *Ontario Highway Bridge Design Code ONT83.* Ontario, Canada, 2000.

[147] Pachi, A., and Ji, T. Frequency and velocity of people walking. *Structural Engineer 83*, 3 (2005), 36–40.

[148] Pańtak, M., Jarek, B., and Średniawa, W. Application of EN 1990/A1 Vibration Serviceability Limit State Requirements for Steel Footbridges. *Procedia Engineering 40* (2012), 345–350.

[149] Papadimitriou, C., Katafygiotis, L. S., and Au, S.-K. Structural Uncertainties on TMD Design: A Reliability-Based Approach C. *Journal of Structural Control 4*, 1 (1997), 65–88.

[150] Park, G.-J., Lee, T.-H., Lee, K. H., and Hwang, K.-H. Robust Design : An Overview. *AIAA Journal 44*, 1 (2006), 181–191.

[151] Pavić, A. *Vibration serviceability of long-span cast in-situ concrete floors.* PhD thesis, Department of Civil and Structural Engineering, University of Sheffield, 1999.

[152] Pedersen, L., and Frier, C. Sensitivity of footbridge vibrations to stochastic walking parameters. *Journal of Sound and Vibration 329*, 13 (2010), 2683 – 2701.

[153] Peeters, B., and De Roeck, G. Reference-based stochastic subspace identification for output-only modal analysis. *Mechanical Systems and Signal Processing 13*, 6 (1999), 855–878.

[154] Peeters, B., and De Roeck, G. One-year monitoring of the Z24-bridge: environmental effects versus damage events. *Earthquake Engineering & Structural Dynamics 30*, 2 (2001), 149–171.

[155] Pereira, E., Díaz, I. M., Hudson, E. J., and Reynolds, P. Optimal control-based methodology for active vibration control of pedestrian structures. *Engineering Structures 80* (2014), 153–162.

[156] Pernica, G. Dynamic load factors for pedestrian movements and rhythmic exercises. *Canadian Acoustics 18*, 2 (1990), 3.

[157] Persson, J. A., and Ölvander, J. How to compare performance of robust design optimization algorithms, including a novel method. *Artificial Intelligence for Engineering Design, Analysis and Manufacturing 31*, 03 (2017), 286–297.

[158] Petersen, C. *Dynamik der Baukonstruktionen.* Vieweg und Teubner Verlag, 2000.

[159] Piccardo, G., and Tubino, F. Equivalent spectral model and maximum dynamic response for the serviceability analysis of footbridges. *Engineering Structures 40* (2012), 445–456.

[160] Poovarodom, N., Kanchanosot, S., and Warnitchai, P. Application of non-linear multiple tuned mass dampers to suppress man-induced vibrations of a pedestrian bridge. *Earthquake Engineering and Structural Dynamics 32*, 7 (2003), 1117–1131.

[161] Preumont, A. On the peak factor of stationary Gaussian processes. *Journal of Sound and Vibration 100*, 1 (1985), 15–34.

[162] Racic, V., and Brownjohn, J. M. W. Stochastic model of near-periodic vertical loads due to humans walking. *Advanced Engineering Informatics 25*, 2 (2011), 259–275.

[163] Racic, V., and Morin, J. B. Data-driven modelling of vertical dynamic excitation of bridges induced by people running. *Mechanical Systems and Signal Processing 43*, 1-2 (2014), 153–170.

[164] Racić, V., Pavić, A., and Brownjohn, J. M. W. Experimental identification and analytical modelling of walking forces: a literature review. *Journal of Sound and Vibration 326* (2009), 1–49.

[165] Rainer, J., Pernica, G., and Allen, D. E. Dynamic loading and response of footbridges. *Canadian Journal of Civil Engineering 15*, 1 (1988), 66–71.

[166] Rajeev, S., and Krishnamoorthy, C. S. Discrete optimization of structures using genetic algorithms. *Journal of Structural Engineering 118*, 5 (1992), 1233–1250.

[167] Ramu, P., Qu, X., Youn, B. D., Haftka, R. T., and Choi, K. K. Inverse reliability measures and reliability-based design optimisation. *International Journal of Reliability and Safety 1*, 1/2 (2006), 187.

[168] Rana, R., and Soong, T. T. Parametric study and simplified design of tuned mass dampers. *Engineering Structures 20*, 3 (1998), 193–204.

[169] Rathi, A. K., and Chakraborty, A. Reliability-based performance optimization of TMD for vibration control of structures with uncertainty in parameters and excitation. *Structural Control and Health Monitoring 24*, 1 (2017).

[170] Research Fund for Coal and Steel. *HiVoSS: Design of Footbridges*, 2008.

[171] Reynders, E. *System identification and modal analysis in structural mechanics*. PhD thesis, KU Leuven, 2009.

[172] Reynders, E., and De Roeck, G. Reference-based combined deterministic-stochastic subspace identification for experimental and operational modal analysis. *Mechanical Systems and Signal Processing 22*, 3 (2008), 617–637.

[173] Reynolds, P., Wright, J., Pavić, A., and Armitage, T. Methodology for modal testing of the Millennium Bridge, London. In *Proceedings of the ICE - Structures and Buildings* (2002), vol. 152, pp. 111–121.

[174] Ricciardelli, F., Briatico, C., Ingólfsson, E. T., and Georgakis, C. Experimental validation and calibration of pedestrian loading models for footbridges. In *Proccedings of the second edition of the international conference EVACES* (October 2007), pp. 189–199.

[175] Ricciardelli, F., and Demartino, C. Design of Footbridges against Pedestrian-Induced Vibrations. *Journal of Bridge Engineering 21*, 8 (2007), 1–13.

[176] Ricciardelli, F., and Pizzimenti, A. D. Lateral Walking-Induced Forces on Footbridges. *Journal of Bridge Engineering 12*, December (2007), 677–688.

[177] Rüdinger, F. Optimal Vibration Absorber with Nonlinear Viscous Power Law Damping and White Noise Excitation. *Journal of Engineering Mechanics 132*, 1 (2006), 46–53.

[178] Sahnaci, C., Meinhardt, C., and Krampe, T. Performance of MTMD systems based on realistic load contributions due to walking. In *Proceedings of the 6th International Footbridge Conference* (Berlin, Germany, September 2017).

[179] Salyards, K. A., and Noss, N. C. Experimental evaluation of the influence of human-structure interaction for vibration serviceability. *Journal of Performance of Constructed Facilities 28*, 3 (2014), 458–465.

[180] SBR. *SBR Richtlijn: Trillingen van vloeren door lopen - Richtlijn voor het voorspellen, meten en beoordelen*, 2005.

[181] Scheller, J., and Starossek, U. Design and experimental verification of a new active mass damper for control of pedestrian-induced bridge vibrations. In *Proceedings of the 4th International Footbridge Conference* (Wroclaw, Poland, July 2011).

[182] Schmelzer, B., Oberguggenberger, M., and Adam, C. Efficiency of tuned mass dampers with uncertain parameters on the performance of structures under stochastic excitation. *Proceedings of the Institution of Mechanical Engineers, Part O: Journal of Risk and Reliability 224* (2010), 297–308.

[183] Schuëller, G. I. On the treatment of uncertainties in structural mechanics and analysis. *Computers and Structures 85*, 5-6 (2007), 235–243.

[184] Schuëller, G. I., and Jensen, H. A. Computational methods in optimization considering uncertainties – an overview. *Computer Methods in Applied Mechanics and Engineering 198*, 1 (2008), 2–13.

[185] Sedlacek, G. *Generalisation of criteria for floor vibrations for industrial, office, residential and public building and gymnastic halls : contract no. 7210-PR/314, 1 July 2001 to 30 June 2004 ; final report.* EUR / European Commission. Office f. Official Publ. of the Europ. Communities, 2006.

[186] Setareh, M., ASCE, M., Ritchey, J. K., Murray, T. M., and Koo, J.-h. Semiactive Tuned Mass Damper for Floor Vibration Control. *Journal of Structural Engineering 133*, 2 (2007), 242–250.

[187] Setareh, M., Ritchey, J. K., Baxter, A. J., and Murray, T. M. Pendulum Tuned Mass Dampers for Floor Vibration Control. *Journal of Performance of Constructed Facilities 20*, 1 (2006), 64–73.

[188] Shahabpoor, E., Pavić, A., and Racić, V. Identification of mass-spring-damper model of walking humans. *Structures 5* (2016), 233–246.

[189] Shahabpoor, E., Pavić, A., and Racić, V. Structural vibration serviceability: New design framework featuring human-structure interaction. *Engineering Structures 136* (2017), 295–311.

[190] Shahabpoor, E., Pavić, A., Racić, V., and Živanović, S. Effect of group walking traffic on dynamic properties of pedestrian structures. *Journal of Sound and Vibration 287* (2017), 207 – 225.

[191] Shum, K. Closed form optimal solution of a tuned liquid column damper for suppressing harmonic vibration of structures. *Engineering Structures 31*, 1 (2009), 84 – 92.

[192] Simon, D. *Evolutionary optimization algorithms.* John Wiley & Sons, 2013.

[193] Singh, M. P., and Moreschi, L. M. Optimal placement of dampers for passive response control. *Earthquake Engineering & Structural Dynamics 31*, 4 (2002), 955–976.

[194] Sohn, H. Effects of environmental and operational variability on structural health monitoring. *Philosophical Transactions of the Royal Society A: Mathematical, Physical and Engineering Sciences 365*, 1851 (2007), 539–560.

[195] Soize, C. Stochastic modeling of uncertainties in computational structural dynamics - Recent theoretical advances. *Journal of Sound and Vibration 332*, 10 (2013), 2379–2395.

[196] Soong, T. T., and Spencer, B. F. Supplemental energy dissipation: state-of-the-art and state-of-the-practice. *Engineering Structures 24*, 3 (2002), 243–259.

[197] Soria, J. M., Díaz, I. M., García-palacios, J. H., and Ibán, N. Vibration Monitoring of a Steel-Plated Stress-Ribbon Footbridge: Uncertainties in the Modal Estimation. *Journal of Bridge Engineering 21*, 8 (2016), 1–13.

[198] Spencer, B., and Nagarajah, S. State of the Art of Structural Control. *Journal of Structural Engineering*, 129 (2003), 845–856.

[199] Sundaresan, S., Ishii, K., and Houser, D. R. A robust optimization procedure with variations on design variables and constraints. *Advances in design automation 69*, 1 (1993), 379–386.

[200] Tait, M. J. Modelling and preliminary design of a structure-TLD system. *Engineering Structures 30*, 10 (2008), 2644–2655.

[201] Takewaki, I. Optimal Damper Placement for Minimum Transfer Functions. *Earthquake Engineering and Structural Dynamics 26* (1997), 1113–1124.

[202] Takewaki, I., Yoshitomi, S., Uetani, K., and Tsuji, M. Non-monotonic optimal damper placement via steepest direction search. *Earthquake Engineering & Structural Dynamics 28*, 6 (1999), 655–670.

[203] Taylor, D. P. History, design, and applications of fluid dampers in structural engineering. `http://taylordevices.com/papers/history/design.htm`. [Online; accessed 27-February-2018].

[204] The Mathworks Inc. *MATLAB version 8.6.0 (R2015b)*. Natick, Massachusetts, 2015.

[205] Toso, M. A., Gomes, H. M., Da Silva, F. T., and Pimentel, R. L. Experimentally fitted biodynamic models for pedestrian-structure interaction in walking situations. *Mechanical Systems and Signal Processing 72-73* (2016), 590–606.

[206] Tsai, H.-C., and Lin, G.-C. Explicit formulae for optimum absorber parameters for force-excited and viscously damped systems. *Journal of Sound and Vibration 176*, 5 (1994), 585–596.

[207] Tse, K. T., Kwok, K. C. S., and Tamura, Y. Performance and Cost Evaluation of a Smart Tuned Mass Damper for Suppressing Wind-Induced Lateral-Torsional Motion of Tall Structures. *Journal of Structural Engineering 138* (2012), 514–525.

[208] Tsui, K.-L. An overview of Taguchi method and newly developed statistical methods for robust design. *IIE Transactions 24*, 5 (1992), 44–57.

[209] Tubino, F. Probabilistic assessment of the dynamic interaction between multiple pedestrians and vertical vibrations of footbridges. *Journal of Sound and Vibration 417* (2018), 80–96.

[210] Tubino, F., Carassale, L., and Piccardo, G. Human-Induced Vibrations on Two Lively Footbridges in Milan. *Journal of Bridge Engineering 21*, 8 (2015).

[211] Tubino, F., and Piccardo, G. Tuned mass damper optimization for the mitigation of human-induced vibrations of pedestrian bridges. *Meccanica 50* (2015), 809–824.

[212] Tubino, F., and Piccardo, G. Serviceability assessment of footbridges in unrestricted pedestrian traffic conditions. *Structure and Infrastructure Engineering 12*, 12 (2016), 1650–1660.

[213] Van den Broeck, P., and De Roeck, G. *TRICON: Prediction and control of human-induced vibrations of civil engineering structures.* financed by the Flemish government: IWT, agency for Innovation by Science and Technology, 2012.

[214] Van den Broeck, P., and De Roeck, G. *Trillingsreducerende maatregelen voor vloeren en voetgangersbruggen onder mens-geïnduceerde belasting.* Tetra OPTRIS, 2014.

[215] Van Hauwermeiren, J., Van Nimmen, K., Vergauwen, M., and Van den Broeck, P. Vision-based methodology for characterizing the flow of a high-density crowd. In *Maintenance, Safety, Risk, Management and Life-Cycle Performance of Bridges: Proceedings of the Ninth International Conference on Bridge Maintenance, Safety and Management (IABMAS 2018)* (Melbourne, Australia, July 2018), N. Powers, D. M. Frangopol, R. Al-Mahaidi, and C. Caprani, Eds., Taylor and Francis Group, London, p. 169.

[216] Van Nimmen, K. *Numerical and experimental study of human-induced vibrations of footbridges.* PhD thesis, KU Leuven, 2015.

[217] Van Nimmen, K., Lombaert, G., De Roeck, G., and Van den Broeck, P. Vibration serviceability of footbridges: Evaluation of the current codes of practice. *Engineering Structures 59* (2014), 448–461.

[218] Van Nimmen, K., Lombaert, G., De Roeck, G., and Van den Broeck, P. Human-induced vibrations of footbridges: The effect of vertical human-structure interaction. In *Proceedings of the 34th International Modal Analysis Conference Series* (Orlando, FL, February 2016).

[219] Van Nimmen, K., Lombaert, G., De Roeck, G., and Van den Broeck, P. The impact of vertical human-structure interaction on the response of footbridges to pedestrian excitation. *Journal of Sound and Vibration 402* (2017), 104–121.

[220] Van Nimmen, K., Lombaert, G., Jonkers, I., De Roeck, G., and Van den Broeck, P. Characterisation of walking loads by 3D inertial motion tracking. *Journal of Sound and Vibration 333*, 20 (2014), 5212–5226.

[221] Van Nimmen, K., Van den Broeck, P., Verbeke, P., Schauvliege, C., Mallié, M., Ney, L., and De Roeck, G. Numerical and experimental analysis of the vibration serviceability of the Bears' Cage footbridge. *Structure and Infrastructure Engineering 13*, 3 (2016), 390–400.

[222] Van Nimmen, K., Verbeke, P., Lombaert, G., De Roeck, G., and Van den Broeck, P. Numerical and Experimental Evaluation of the Dynamic Performance of a Footbridge with Tuned Mass Dampers. *Journal of Bridge Engineering 21*, 8 (2016), C4016001.

[223] Venuti, F., and Bruno, L. An interpretative model of the pedestrian fundamental relation. *Comptes Rendus - Mecanique 335*, 4 (2007), 194–200.

[224] Venuti, F., and Bruno, L. Crowd-structure interaction in lively footbridges under synchronous lateral excitation: a literature review. *Physics of Life Reviews 6* (2009), 176–206.

[225] Venuti, F., Racić, V., and Corbetta, A. Modelling framework for dynamic interaction between multiple pedestrians and vertical vibrations of footbridges. *Journal of Sound and Vibration 379* (2016), 245–263.

[226] Wang, S., Li, Q., and Savage, G. J. Reliability-based robust design optimization of structures considering uncertainty in design variables. *Mathematical Problems in Engineering 2015* (2015).

[227] Warburton, G. B. Optimum absorber parameters for various combinations of response and excitation parameters. *Earthquake Engineering & Structural Dynamics 10*, 3 (1982), 381–401.

[228] Warburton, G. B., and Ayorinde, E. O. Optimum absorber parameters for simple systems. *Earthquake Engineering & Structural Dynamics 8* (1980), 197–217.

[229] Weber, B., and Feltrin, G. Assessment of long-term behavior of tuned mass dampers by system identification. *Engineering Structures 32*, 11 (2010), 3670–3682.

[230] Weber, F., Feltrin, G., and Huth, O. SAMCO Final Report - F05 Guidelines for structural control. *Structural Engineering Research Laboratory, Swiss Federal Laboratories for Materials Testing and Research, Dubendorf, Switzerland* (2006).

[231] Weidmann, U. *Transporttechnik der Fussgänger: Transporttechnische Eigenschaften des Fussgängerverkehrs (Literaturauswertung).* ETH, IVT, 1993.

[232] Wen, Q., Hua, X. G., Chen, Z. Q., Yang, Y., and Niu, H. W. Control of Human-Induced Vibrations of a Curved Cable-Stayed Bridge: Design, Implementation, and Field Validation. *Journal of Bridge Engineering 21*, 7 (2016), 04016028.

[233] Werkle, H., Butz, C., and Tatar, R. Effectiveness of "Detuned" TMD's for Beam-Like Footbridges. *Advances in Structural Engineering 16*, 1 (2013), 21–32.

[234] Wheeler, J. E. Prediction and control of pedestrian-induced vibration in footbridges. *Journal of the Structural Division 108* (1982), 2045–2065.

[235] Wieczorek, N., Gerasch, W.-J., Rolfes, R., and Kammerer, H. Semiactive Friction Damper for Lightweight Pedestrian Bridges. *Journal of Structural Engineering 140*, 4 (2014).

[236] Willford, M., Field, C., and Young, P. Improved methodologies for the prediction of footfall-induced vibration. *ASCE - Building Integration Solutions* (2004), 1–15.

[237] Willford, M. R., and Young, P. *A design guide for footfall induced vibration of structures.* Concrete Society for The Concrete Centre, 2006.

[238] Wu, J.-C., Chang, C.-H., and Lin, Y.-Y. Optimal designs for non-uniform tuned liquid column dampers in horizontal motion. *Journal of Sound and Vibration 326*, 1 (2009), 104 – 122.

[239] Xia, Y., Hao, H., Zanardo, G., and Deeks, A. Long term vibration monitoring of an RC-slab: Temperature and humidity effect. *Engineering Structures 28*, 3 (2006), 441 – 452.

[240] Xu, R., Chen, J., and Zhu, X. A hybrid approach for parameter optimization of multiple tuned mass dampers in reducing floor vibrations due to occupant walking: Theory and parametric studies. *Advances in Structural Engineering 20* (2017), 1232–1246.

[241] Yamaguchi, H., and Harnpornchai, N. Fundamental characteristics of Multiple Tuned Mass Dampers for suppressing harmonically forced oscillations. *Earthquake Engineering & Structural Dynamics (EESD) 22*, 1 (1993), 51–62.

[242] Yang, C. Y. *Random vibration of structures*. John Wiley & Sons, 1986.

[243] Yu, H., Gillot, F., and Ichchou, M. Reliability based robust design optimization for tuned mass damper in passive vibration control of deterministic/uncertain structures. *Journal of Sound and Vibration 332*, 9 (2013), 2222–2238.

[244] Zadeh, L. Fuzzy sets as a basis for a theory of possibility. *Fuzzy Sets and Systems 1*, 1 (1978), 3 – 28.

[245] Zadeh, L. A. Fuzzy sets. *Information and control 8*, 3 (1965), 338–353.

[246] Zang, C., Friswell, M., and Mottershead, J. A review of robust optimal design and its application in dynamics. *Computers & Structures 83*, 4 (2005), 315–326.

[247] Zhang, Y., Hou, Y., and Liu, S. A new method of discrete optimization for cross-section selection of truss structures. *Engineering Optimization 46*, 8 (2014), 1052–1073.

[248] Zheng, X., and Brownjohn, J. M. W. Modeling and simulation of human-floor system under vertical vibration. In *Smart Structures and Materials 2001: Smart Structures and Integrated Systems* (2001), vol. 4327, International Society for Optics and Photonics, pp. 513–521.

[249] Zhu, S. J., Zheng, Y. F., and Fu, Y. M. Analysis of non-linear dynamics of a two-degree-of-freedom vibration system with non-linear damping and non-linear spring. *Journal of Sound and Vibration 271*, 1-2 (2004), 15–24.

[250] Živanović, S. *Probability-Based Estimation of Vibration for Pedestrian Structures due to Walking*. PhD thesis, Department of Civil and Structural Engineering, University of Sheffield, 2006.

[251] Živanović, S. Benchmark footbridge for vibration serviceability assessment under the vertical component of pedestrian load. *Journal of Structural Engineering 138*, 10 (2012), 1193–1202.

[252] Živanović, S., Pavić, A., and Ingólfsson, E. T. Modeling spatially unrestricted pedestrian traffic on footbridges. *J. of Struct. Eng. 136*, 10 (2010), 1296–1308.

[253] Živanović, S., Pavić, A., and Reynolds, P. Vibration serviceability of footbridges under human-induced excitation: a literature review. *Journal of Sound and Vibration 279*, 1-2 (2005), 1–74.

[254] Živanović, S., Pavić, A., and Reynolds, P. Modal testing and FE model tuning of a lively footbridge structure. *Engineering Structures 28* (2006), 857–868.

[255] Živanović, S., Pavić, A., and Reynolds, P. Probability-based prediction of multi-mode vibration response to walking excitation. *Engineering Structures 29*, 6 (2007), 942–954.

[256] Živanović, S., Pavić, A., Reynolds, P., and Vujovic, P. Dynamic analysis of lively footbridge under everyday pedestrian traffic. In *Proceedings of the 6th European Conference on Strructural Dynamics (EURODYN 2005)* (4-7 September 2005), pp. 453–459.

Curriculum vitae

Klaus Lievens
°1 April 1991, Tielt, Belgium

Education

PhD in Engineering Technology, Technology Cluster Construction, KU Leuven
September 2013 – December 2018

MSc in Engineering Technology: Civil Engineering, Katholieke Hogeschool Sint-Lieven, Ghent
September 2012 – June 2013

BSc in Industrial Sciences: Construction, Katholieke Hogeschool Sint-Lieven, Ghent
September 2009 – June 2012

Secondary education, De Bron, Tielt
September 2002 – June 2009

Professional experience

Research assistant, Department of Civil Engineering, Technology Cluster Construction, KU Leuven - Technology campus Ghent
September 2013 – December 2018

Teaching assistant, Department of Civil Engineering, Technology Cluster Construction, KU Leuven - Technology campus Ghent
September 2013 – December 2018

Teaching assistant, Department of Civil Engineering, KU Leuven
September 2015 – December 2017

Grants and awards

PhD fellowship of the Flemish government agency for Innovation by Science and Technology (IWT)
January 2015 – December 2018

Travel grant Research Foundation - Flanders (FWO) for participation to IABMAS, 9th International Conference on Bridge Maintenance, Safety and Management. Melbourne, Australia, 9-13 July 2018.
July 2018

Teaching experience

Advisor of 15 MSc theses, Department of Civil Engineering, Technology Cluster Construction, KU Leuven – Technology campus Ghent
September 2013 – June 2018

Teaching assistant
BSc Civil Engineering: Exercises *Strength of materials*
BSc Industrial Science: Exercises *Strength of materials*
BSc Industrial Science: Supervision *Research project*
MSc Industrial Science: Project work *Dynamics of structures*

Workshop STEM: 'Bevende Bruggen en Trillende Torens'

Publications

Papers published or accepted for publication in ISI journals

[1] K. Lievens, G. Lombaert, K. Van Nimmen, G. De Roeck and P. Van den Broeck (2018). Robust vibration serviceability assessment of footbridges subjected to pedestrian excitation: strategy and applications. Engineering Structures, 171, 236-246.

[2] K. Lievens, G. Lombaert, G. De Roeck and P. Van den Broeck (2016). Robust design of a TMD for the vibration serviceability of a footbridge. Engineering Structures, 123, 408-418.

National and international conference papers

[1] K. Lievens, G. Lombaert, G. De Roeck and P. Van den Broeck. Robust vibration serviceability assessment of footbridges for crowd walking excitation. In N. Powers, D. M. Frangopol, R. Al-Mahaidi and C. Caprani, editors, Maintenance, Safety, Risk, Management and Life-Cycle Performance of Bridges - Proceedings of the International Conference on Bridge Maintenance, Safety and Management, IABMAS 2018. Australia, Melbourne, 9-13 July 2018 (pp. 164-164).

[2] K. Lievens, G. Lombaert, G. De Roeck and P. Van den Broeck. (2017). Comparison of TMD designs for a footbridge subjected to human-induced vibrations accounting for structural and load uncertainties. Procedia Engineering: Vol. 199. International Conference on Structural Dynamics, EURODYN 2017. Italy, Rome, 10-13 September 2017 (pp. 1713-1718).

[3] K. Lievens, G. Lombaert, G. De Roeck and P. Van den Broeck. (2016). Robust design of a TMD for vibration serviceability of footbridges accounting for structural and loading uncertainties. In P. Sas, D. Moens and A. van de Walle, editors, Proceedings of ISMA2016 including USD2016. International Conference on Noise and Vibration Engineering, ISMA 2016. Leuven, 19-21 September 2016. International Conference on Uncertainty in Structural Dynamics, USD 2016. Leuven, 19-21 September 2016 (pp. 3699-3710).

[4] K. Lievens, K. Van Nimmen, G. Lombaert, G. De Roeck and P. Van den Broeck. (2016). Prediction of peak response values of structures with and without TMD subjected to random pedestrian flows. Journal of Physics - Conference Series: Vol. 744 (1). International Conference on Recent Advances in Structural Dynamics, RASD, International Conference on Motion and Vibration Control, MOVIC. Southampton, UK, Southampton, UK, 3-6 July 2016, 3-6 July 2016 (art.nr. 012227) Institute of Physics Publishing Ltd.

[5] K. Lievens, P. Van den Broeck, G. De Roeck and G. Lombaert. (2015). Robust vibration serviceability design of a tuned mass damper for the Phénix footbridge. In M. Papadrakakis, V. Papadopoulos and V. Plevris, editors, Proceedings of the 5th International Conference On Computational Methods in Structural Dynamics and Earthquake Engineering, COMPDYN 2015: Vol. 1. International Conference On Computational Methods in Structural Dynamics and Earthquake Engineering, COMPDYN 2015. Crete Island, Greece, 25-27 May 2015 (pp. 2512-2524).

Internal reports

[1] Lievens, K. and Van Nimmen, K. and Van Hauwermeiren, J. Gezels, B. and Van den Broeck, P. Gosseliesbridge Sint-Jans-Molenbeek - Operational modal analysis, Human-induced Vibrations, Report BWM-2018-10 Department of Civil Engineering, Technology Cluster Construction, KU Leuven, October 2018.

[2] Van Hauwermeiren, J. and Lievens, K. and Van Nimmen, K. and Van den Broeck, P. Parkbosbrug (R4) - part II - Operational modal analysis, Human-induced Vibrations, Report BWM-2018-09 Department of Civil Engineering, Technology Cluster Construction, KU Leuven, October 2018.

[3] Lievens, K. and Van Nimmen, K. and Van Hauwermeiren, J. Gezels, B. and Van den Broeck, P. Deerlijk footbridge - Operational modal analysis, Human-induced Vibrations, Report BWM-2018-08 Department of Civil Engineering, Technology Cluster Construction, KU Leuven, October 2018.

[4] Van Hauwermeiren, J. and Lievens, K. and Van Nimmen, K. and Van den Broeck, P. Parkbosbrug (E40) - part II - Operational modal analysis, Human-induced Vibrations, Report BWM-2018-07 Department of Civil Engineering, Technology Cluster Construction, KU Leuven, September 2018.

[5] Van Hauwermeiren, J., Van Nimmen, K., Lievens, K. and Van den Broeck, P. Waalse Krook - bridge North - Operational modal analysis, Human-induced Vibrations, Report BWM-2018-06 Department of Civil Engineering, Technology Cluster Construction, KU Leuven, June 2018.

[6] Van Hauwermeiren, J., Van Nimmen, K., Lievens, K. and Van den Broeck, P. Composite footbridge Puurs, Report BWM-2018-05 Department of Civil Engineering, Technology Cluster Construction, KU Leuven, May 2018.

[7] Van Hauwermeiren, J., Lievens, K., Van Nimmen, K. and Van den Broeck, P. Parkbosbrug (R4) - Operational modal analysis, Human-induced Vibrations, Report BWM-2018-04 Department of Civil Engineering, Technology Cluster Construction, KU Leuven, April 2018.

[8] Lievens, K., Van Nimmen, K., Van Hauwermeiren, J. and Van den Broeck, P. Parkbosbrug (E40) - Operational modal analysis, Human-induced Vibrations, Report BWM-2018-02 Department of Civil Engineering, Technology Cluster Construction, KU Leuven, January 2018.

[9] Lievens, K., Van Nimmen, K., Van Hauwermeiren, J. and Van den Broeck, P. Gymnasium Floor Roosdaal - Operational modal analysis,

Human-induced Vibrations, Report BWM-2018-01 Department of Civil Engineering, Technology Cluster Construction, KU Leuven, January 2018.

[10] Lievens, K., Van Nimmen, K., Gezels, B., Van Hauwermeiren, J., Wei X., Tan, H. and Van den Broeck, P. Gymnasium Floor Roosdaal - Operational modal analysis, Human-induced Vibrations, Vibration serviceability assessment, Report BWM-2017-11 Department of Civil Engineering, Technology Cluster Construction, KU Leuven, November 2017.

[11] Van Hauwermeiren, J., Van Nimmen, K., Lievens, K. and Van den Broeck, P. Large Scale Measurments 26-10-2017 Eeklo Footbrdige (Data management), Report BWM-2017-10 Department of Civil Engineering, Technology Cluster Construction, KU Leuven, November 2017.

[12] Lievens, K., Van Nimmen, K., Van Hauwermeiren, J., Wei X., Tan, H. and Van den Broeck, P. Grandstand Sportief Centrum Neder-Over-Heembeek - Operational modal analysis, Report BWM-2017-07 Department of Civil Engineering, Technology Cluster Construction, KU Leuven, October 2017.

[13] Van Nimmen, K., Lievens, K. and Van den Broeck, P. TU Darmstadt HUMVIB footbridge - Experimental modal analysis, Model calibration, Report BWM-2017-06 Department of Civil Engineering, Technology Cluster Construction, KU Leuven, August 2017.

[14] Lievens, K., Van Nimmen, K., Gezels, B. and Van den Broeck, P. Keizerpark Ghent - Operational modal analysis, Human-induced vibrations, Report BWM-2017-15 Department of Civil Engineering, Technology Cluster Construction, KU Leuven, February 2017.

[15] Van Nimmen, K., Van Hauwermeiren, J., Lievens, K., Gezels B. and Van den Broeck, P. Waalse Krook - Bridge South: Human-induced Vibrations, Experimental study involving high pedestrian densities, Reassessment of the vibration serviceability, Report BWM-2016-09 Department of Civil Engineering, Technology Cluster Construction, KU Leuven, December 2016.

[16] Van Nimmen, K., Lievens, K. and Van den Broeck, P. Moreelsebrug - Analyse efficiëntie TMDs: Operationele modale analyse, Mens-geïnduceerde trillingen, TMD ontwerp, Report BWM-2016-10 Department of Civil Engineering, Technology Cluster Construction, KU Leuven, December 2016.

[17] Van Nimmen, K., Lievens, K., Gezels, B. and Van den Broeck, P. Moreelsebrug - Operationele modale analyse, Mens-geïnduceerde trillingen, TMD ontwerp, Report BWM-2016-08 Department of Civil Engineering, Technology Cluster Construction, KU Leuven, November 2016.

[18] Lievens, K., Van Nimmen, K. and Van den Broeck, P. Poissy footbridge - Vibration serviceability assessment, Report BWM-2016-07 Department of Civil Engineering, Technology Cluster Construction, KU Leuven, November 2016.

[19] Van Nimmen, K., Lievens, K. and Van den Broeck, P. Grobbendonk bridge - Tension bar measurements, Report BWM-2016-06 Department of Civil Engineering, Technology Cluster Construction, KU Leuven, October 2016.

[20] Van Nimmen, K., Lievens, K., Gezels, B., Wei, X. and Van den Broeck, P. Waalse Krook - Bridge South: Operational modal analysis, Human-induced Vibrations, Vibration serviceability assessment, Report BWM-2016-04 Department of Civil Engineering, Technology Cluster Construction, KU Leuven, July 2016.

[21] Van Nimmen, K., Gezels, B., Lievens, K., Wei X., Oliveras, S. and Van den Broeck, P. Park Bridge Spoor Noord - Operational modal analysis, Human-induced vibrations, Vibration serviceability assessment, Report BWM-2016-03 Department of Civil Engineering, Technology Cluster Construction, KU Leuven, July 2016.

[22] Lievens, K., Verbeke, P. and Van den Broeck, P. Knipoog Floor: Vibration serviceability assessment (alternative with 4 additional columns), Report BWM-2015-08c Department of Civil Engineering, Technology Cluster Construction, KU Leuven, August 2015.

[23] Lievens, K., Verbeke, P. and Van den Broeck, P. Knipoog Floor: Vibration serviceability assessment (Span 15.6m), Report BWM-2015-08b Department of Civil Engineering, Technology Cluster Construction, KU Leuven, July 2015.

[24] Lievens, K., Verbeke, P. and Van den Broeck, P. Knipoog Floor: Vibration serviceability assessment (Span 20.34m), Report BWM-2015-08a Department of Civil Engineering, Technology Cluster Construction, KU Leuven, July 2015.

[25] Verbeke, P. Van Nimmen K., Wei X., Lievens, K. Kasapova, K. and Van den Broeck, P. Footbridge Avelgem: Operationnal modal analysis and human-induced vibrations, Report BWM-2015-03 Department of Civil Engineering, Technology Cluster Construction, KU Leuven, March 2015.



FACULTY OF ENGINEERING TECHNOLOGY
DEPARTMENT OF CIVIL ENGINEERING
TECHNOLOGY CLUSTER CONSTRUCTION
STRUCTURAL MECHANICS AND BUILDING MATERIALS
Gebroeders De Smetstraat 1
B-9000 Ghent
klaus.lievens@kuleuven.be
https://iiw.kuleuven.be/onderzoek/structural-mechanics